

p-ISSN 1607-3254  
e-ISSN 2313-690X



Радіоелектроніка  
Інформатика  
Управління

Radio Electronics  
Computer Science  
Control

Радиоэлектроника  
Информатика  
Управление



2024/1



Національний університет «Запорізька політехніка»

## **Радіоелектроніка, інформатика, управління**

Науковий журнал

Виходить чотири рази на рік

№ 1(68) 2024

Заснований у 1998 році, видається з 1999 року.

Засновник і видавець – Національний університет «Запорізька політехніка».

ISSN 1607-3274 (друкований), ISSN 2313-688X (електронний).

Запоріжжя

НУ «Запорізька політехніка»

2024

National University Zaporizhzhia Polytechnic

## **Radio Electronics, Computer Science, Control**

The scientific journal

Published four times per year

№ 1(68) 2024

Founded in 1998, published since 1999.

Founder and publisher – National University Zaporizhzhia Polytechnic.

ISSN 1607-3274 (print), ISSN 2313-688X (on-line).

Zaporizhzhia

NU Zaporizhzhia Polytechnic

2024

Национальный университет «Запорожская политехника»

## **Радиоэлектроника, информатика, управление**

Научный журнал

Выходит четыре раза в год

№ 1(68) 2024

Основан в 1998 году, издается с 1999 года.

Основатель и издатель – Национальный университет «Запорожская политехника».

ISSN 1607-3274 (печатный), ISSN 2313-688X (электронный).

Запорожье

НУ «Запорожская политехника»

2024

**Науковий журнал «Радіоелектроніка, інформатика, управління»** (скорочена назва – РІУ) видається Національним університетом «Запорізька політехніка» (НУ «Запорізька політехніка») з 1999 р. періодичністю чотири номери на рік.

Зареєстровано у Міністерстві юстиції України 19.11.2019 р. (Свідчення про державну реєстрацію друкованого засобу масової інформації серія КВ № 24220-14060 ПР.)

ISSN 1607-3274 (друкований), ISSN 2313-688X (електронний).

Наказом Міністерства освіти і науки України № 409 від 17.03.2020 р. «Про затвердження рішень Атестаційної колегії Міністерства щодо діяльності спеціалізованих вчених рад від 06 березня 2020 року» журнал включений до переліку наукових фахових видань України в категорії «А» (найвищий рівень), в яких можуть публікуватися результати дисертаційних робіт на здобуття наукових ступенів доктора наук і доктора філософії (кандидата наук).

Журнал включений до польського Переліку наукових журналів та рецензованих матеріалів міжнародних конференцій з присвоєною кількістю балів (додаток до оголошення Міністра науки та вищої освіти Республіки Польща від 31 липня 2019 р.: № 16981).

В журналі безкоштовно публікуються наукові статті англійською, російською та українською мовами.

**Правила оформлення статей** подано на сайті: <http://ric.zntu.edu.ua/information/authors>.

Журнал забезпечує **безкоштовний відкритий он-лайн доступ** до повнотекстових публікацій.

Журнал дозволяє авторам мати авторські права і зберігати права на видання без обмежень. Журнал дозволяє користувачам читати, завантажувати, копіювати, поширювати, друкувати, шукати або посилається на повні тексти своїх статей. Журнал дозволяє повторне використання його вмісту у відповідності Creative Commons ліцензією CC BY-SA..

Опублікованим статтям присвоюється унікальний ідентифікатор цифрового об'єкта DOI.

**Журнал входить до наукометричної бази Web of Science.**

**Журнал реферується та індексується** у провідних міжнародних та національних реферативних журналах і наукометричних базах даних, а також розміщується у цифрових архівах та бібліотеках з безкоштовним доступом у режимі on-line, повний перелік яких подано на сайті: <http://ric.zntu.edu.ua/about/editorialPolicies#custom-0>.

**Журнал розповсюджується** за Каталогом періодичних видань України (передплатний індекс – 22914).

**Тематика журналу:** телекомунікації та радіоелектроніка, програмна інженерія (включаючи теорію алгоритмів і програмування), комп'ютерні науки (математичне і комп'ютерне моделювання, оптимізація і дослідження операцій, управління в технічних системах, міжмашинна і людино-машинна взаємодія, штучний інтелект, включаючи системи, засновані на знаннях, і експертні системи, інтелектуальний аналіз даних, розпізнавання образів, штучні нейронні і нейро-нечіткі мережі, нечітку логіку, колективний інтелект і мультиагентні системи, гібридні системи), комп'ютерна інженерія (апаратне забезпечення обчислювальної техніки, комп'ютерні мережі), інформаційні системи та технології (структури та бази даних, системи, засновані на знаннях та експертні системи, обробка даних і сигналів).

Усі статті, пропонувані до публікації, одержують **об'єктивний розгляд**, що оцінюється за суттю без урахування раси, статі, віросповідання, етнічного походження, громадянства або політичної філософії автора(ів).

Усі статті проходять двоступінчасте закриті (анонімне для автора) **рецензування** штатними редакторами і незалежними рецензентами – провідними вченими за профілем журналу.

## РЕДАКЦІЙНА КОЛЕГІЯ

**Головний редактор – Субботін Сергій Олександрович** – доктор технічних наук, професор, завідувач кафедри програмних засобів, Національний університет «Запорізька політехніка», Україна.

**Заступник головного редактора – Піза Дмитро Макарович** – доктор технічних наук, професор, директор інституту інформатики та радіоелектроніки, професор кафедри радіотехніки та телекомунікацій, Національний університет «Запорізька політехніка», Україна.

### Члени редколегії:

**Андрюлідакіс Іосіф** – доктор філософії, голова департаменту телефонії Центру обслуговування мереж, Університет Яніни, Греція;

**Бодянский Євгеній Володимирович** – доктор технічних наук, професор, професор кафедри штучного інтелекту, Харківський національний університет радіоелектроніки, Україна;

**Веннекенс Юст** – доктор філософії, доцент, доцент факультету інженерних технологій (кампус Де Наір), Католицький університет Льовена, Бельгія;

Рекомендовано до видання Вченою радою НУ «Запорізька політехніка», протокол № 7 від 05.03.2024.

Журнал зверстаний редакційно-видавничим відділом НУ «Запорізька політехніка».

**Веб-сайт журналу:** <http://ric.zntu.edu.ua>.

**Адреса редакції:** Редакція журналу «РІУ», Національний університет «Запорізька політехніка», вул. Жуковського, 64, м. Запоріжжя, 69063, Україна.

Тел: (061) 769-82-96 – редакційно-видавничий відділ

E-mail: [rvv@zntu.edu.ua](mailto:rvv@zntu.edu.ua)

**Вольф Карстен** – доктор філософії, професор, професор кафедри технічної інформатики, Дортмундський університет прикладних наук та мистецтв, Німеччина;

**Вуттке Ганс-Дітріх** – доктор філософії, доцент, провідний науковий співробітник інституту технічної інформатики, Технічний університет Льменау, Німеччина;

**Горбань Олександр Миколайович** – доктор фізико-математичних наук, професор, професор факультету математики, Університет Лестера, Велика Британія;

**Городничий Дмитро Олегович** – доктор філософії, кандидат технічних наук, доцент, провідний науковий співробітник Дирекції науки та інженерії, Канадська агенція прикордонної служби, Канада;

**Дробахін Олег Олегович** – доктор фізико-математичних наук, професор, перший проректор, Дніпровський національний університет імені Олеса Гончара, Україна;

**Зайцева Олена Миколаївна** – кандидат фізико-математичних наук, професор, професор кафедри інформатики, Жилінський університет в Жиліні, Словаччина;

**Камеяма Мічітака** – доктор наук, професор, професор факультету науки та інженерії, Університет Ішиномакі Сеншу, Японія;

**Карташов Володимир Михайлович** – доктор технічних наук, професор, завідувач кафедри медіаінженерії та інформаційних радіоелектронних систем, Харківський національний університет радіоелектроніки, Україна;

**Леващенко Віталій Григорович** – кандидат фізико-математичних наук, професор, завідувач кафедри інформатики, Жилінський університет в Жиліні, Словаччина;

**Луенго Давид** – доктор філософії, професор, завідувач кафедри теорії сигналів та комунікацій, Мадридський політехнічний університет, Іспанія;

**Марковска-Качмар Урсула** – доктор технічних наук, професор, професор кафедри обчислювального інтелекту, Вроцлавська політехніка, Польща;

**Олійник Андрій Олександрович** – доктор технічних наук, професор, професор кафедри програмних засобів, Національний університет «Запорізька політехніка», Україна;

**Павліков Володимир Володимирович** – доктор технічних наук, старший науковий співробітник, проректор з наукової роботи, Національний аерокосмічний університет ім. Н.Е. Жуковського «ХАІ», Україна;

**Папшицький Марцін** – доктор наук, професор, професор відділу інтелектуальних систем, Дослідний інститут систем Польської академії наук, м. Варшава, Польща;

**Скруський Степан Юрійович** – кандидат технічних наук, доцент, доцент кафедри комп'ютерних систем і мереж, Національний університет «Запорізька політехніка», Україна;

**Табунчик Галина Володимирівна** – кандидат технічних наук, професор, професор кафедри програмних засобів, Національний університет «Запорізька політехніка», Україна;

**Тригано Томас** – доктор філософії, старший викладач кафедри електричної та електронної інженерії, Інженерний коледж ім. С. Шамон, м. Ашдод, Ізраїль;

**Хенке Карстен** – доктор технічних наук, професор, науковий співробітник факультету інформатики та автоматизації, Технічний університет Льменау, Німеччина;

**Шарпанських Олексій Альбертович** – доктор філософії, доцент, доцент факультету аерокосмічної інженерії, Делфтський технічний університет, Нідерланди.

## РЕДАКЦІЙНО-КОНСУЛЬТАТИВНА РАДА

**Аррас Пітер** – доктор філософії, доцент, доцент факультету інженерних технологій (кампус Де Наір), Католицький університет Льовена, Бельгія;

**Ліснянський Анатолій** – кандидат фізико-математичних наук, головний науковий експерт, Ізраїльська електрична корпорація, Хайфа, Ізраїль;

**Мадрицх Христіан** – доктор філософії, професор факультету інженерії та інформаційних технологій, Університет прикладних наук Каринфії, Австрія;

**Маркосян Мгер Вардкесович** – доктор технічних наук, професор, директор Єреванського науково-дослідного інституту засобів зв'язку, професор кафедри телекомунікацій, Російсько-вірменський університет, м. Єреван, Вірменія;

**Рубель Олег Володимирович** – кандидат технічних наук, доцент факультету інженерії, Університет МакМастера, Гамільтон, Канада;

**Тавхелідзе Автанділ** – кандидат фізико-математичних наук, професор, професор школи бізнесу, технології та освіти, Державний університет ім. Ілії Чавчавадзе, Тбілісі, Грузія;

**Уреутью Дору** – доктор фізико-математичних наук, професор, професор кафедри електроніки та обчислювальної техніки, Трансильванський університет в Брашові, Румунія;

**Шульц Пітер** – доктор технічних наук, професор, професор факультету інженерії та комп'ютерних наук, Гамбургський університет прикладних наук (HAW Hamburg), Гамбург, Німеччина.

The scientific journal **Radio Electronics, Computer Science, Control** is published by the National University «Zaporizhzhia Polytechnic» NU «Zaporizhzhia Polytechnic» since 1999 with periodicity four numbers per year.

The journal is registered by the Ministry of Justice of Ukraine in 19.11.2019. (State Registration Certificate of printed mass media series KB № 24220-14060 IIP).

ISSN 1607-3274 (print), ISSN 2313-688X (on-line).

By the Order of the Ministry of Education and Science of Ukraine from 17.03.2020 № 409 “On approval of the decision of the Certifying Collegium of the Ministry on the activities of the specialized scientific councils dated 06 March 2020” journal is included in the list of scientific specialized periodicals of Ukraine in category “A” (highest level), where the results of dissertations for Doctor of Science and Doctor of Philosophy may be published.

The journal is included to the Polish List of scientific journals and peer-reviewed materials from international conferences with assigned number of points (Annex to the announcement of the Minister of Science and Higher Education of Poland from July 31, 2019: Lp. 16981).

The journal publishes scientific articles in English, Russian, and Ukrainian free of charge.

The article formatting rules are presented on the site: <http://ric.zntu.edu.ua/information/authors>.

The journal provides policy of on-line open (free of charge) access for full-text publications. The journal allow the authors to hold the copyright without restrictions and to retain publishing rights without restrictions. The journal allow readers to read, download, copy, distribute, print, search, or link to the full texts of its articles. The journal allow reuse and remixing of its content, in accordance with Creative Commons license CC BY-SA.

Published articles have a unique digital object identifier (DOI).

The journal is included into Web of Science.

The journal is abstracted and indexed in leading international and national abstracting journals and scientometric databases, and also placed to the digital archives and libraries with a free on-line access, full list of which is presented at the site: <http://ric.zntu.edu.ua/about/editorialPolicies#custom-0>.

The journal is distributed by the Catalogue of Ukrainian periodicals (the catalog number is 22914).

The journal scope: telecommunications and radio electronics, software engineering (including algorithm and programming theory), computer science (mathematical modeling and computer simulation, optimization and operations research, control in technical systems, machine-machine and man-machine interfacing, artificial intelligence, including data mining, pattern recognition, artificial neural and neuro-fuzzy networks, fuzzy logic, swarm intelligence and multiagent systems, hybrid systems), computer engineering (computer hardware, computer networks), information systems and technologies (data structures and bases, knowledge-based and expert systems, data and signal processing methods).

All articles proposed for publication receive an objective review that evaluates substantially without regard to race, sex, religion, ethnic origin, nationality, or political philosophy of the author(s).

All articles undergo a two-stage blind peer review by the editorial staff and independent reviewers – the leading scientists on the profile of the journal.

## EDITORIAL BOARD

**Editor-in-Chief** – **Sergey Subbotin** – Dr. Sc., Professor, Head of Software Tools Department, National University “Zaporizhzhia Polytechnic”, Ukraine.

**Deputy Editor-in-Chief** – **Dmytro Piza** – Dr. Sc., Professor, Director of the Institute of Informatics and Radio Electronics, Professor of the Department of Radio Engineering and Telecommunications, National University “Zaporizhzhia Polytechnic”, Ukraine.

### Members of the Editorial Board:

**Iosif Androulidakis** – PhD, Head of Telephony Department, Network Operation Center, University of Ioannina, Greece;

**Evgeniy Bodyanskiy** – Dr. Sc., Professor, Professor of the Department of Artificial Intelligence, Kharkiv National University of Radio Electronics, Ukraine;

**Oleg Drobakhin** – Dr. Sc., Professor, First Vice-Rector, Oles Honchar Dnipro National University, Ukraine;

**Alexander Gorban** – PhD, Professor, Professor of the Faculty of Mathematics, University of Leicester, United Kingdom;

**Dmitry Gorodnichy** – PhD, Associate Professor, Leading Research Fellow at the Directorate of Science and Engineering, Canada Border Services Agency, Ottawa, Canada;

**Karsten Henke** – Dr. Sc., Professor, Research Fellow, Faculty of Informatics and Automation, Technical University of Ilmenau, Germany;

**Michitaka Kameyama** – Dr. Sc., Professor, Professor of the Faculty of Science and Engineering, Ishinomaki Senshu University, Japan;

**Volodymyr Kartashov** – Dr. Sc., Professor, Head of the Department of Media Engineering and Information Radio Electronic Systems, Kharkiv National University of Radio Electronics, Ukraine;

**Vitaly Levashenko** – PhD, Professor, Head of Department of Informatics, University of Žilina, Slovakia;

**David Luengo** – PhD, Professor, Head of the Department of Signal Theory and Communication, Madrid Polytechnic University, Spain;

**Ursula Markowska-Kaczmar** – Dr. Sc., Professor, Professor of the Department of Computational Intelligence, Wrocław University of Technology, Poland;

**Andrii Oliinyk** – Dr. Sc., Professor, Professor of the Department of Software Tools, National University “Zaporizhzhia Polytechnic”, Ukraine;

**Marcin Paprzycki** – Dr. Sc., Professor, Professor of the Department of Intelligent Systems, Systems Research Institute, Polish Academy of Sciences, Warsaw, Poland;

**Volodymyr Pavlikov** – Dr. Sc., Senior Researcher, Vice-Rector for Research, N. E. Zhukovsky National Aerospace University “KhAI”, Ukraine;

**Alexei Sharpanskykh** – PhD, Associate Professor, Associate Professor of Aerospace Engineering Faculty, Delft University of Technology, Netherlands;

**Stepan Skrupsky** – PhD, Associate Professor, Associate Professor of the Department of Computer Systems and Networks, National University “Zaporizhzhia Polytechnic”, Ukraine;

**Galyna Tabunshchyk** – PhD, Professor, Professor of the Department of Software Tools, National University “Zaporizhzhia Polytechnic”, Ukraine;

**Thomas (Tom) Trigano** – PhD, Senior Lecturer of the Department of Electrical and Electronic Engineering, Sami Shamoon College of Engineering, Ashdod, Israel;

**Joost Vennekens** – PhD, Associate Professor, Associate Professor, Faculty of Engineering (Campus de Nair), Katholieke Universiteit Leuven, Belgium;

**Carsten Wolff** – PhD, Professor, Professor of the Department of Technical Informatics, Dortmund University of Applied Sciences and Arts, Germany;

**Heinz-Dietrich Wuttke** – PhD, Associate Professor, Leading Researcher at the Institute of Technical Informatics, Technical University of Ilmenau, Germany;

**Elena Zaitseva** – PhD, Professor, Professor, Department of Informatics, University of Žilina, Slovakia.

## EDITORIAL-ADVISORY COUNCIL

**Peter Arras** – PhD, Associate Professor, Associate Professor, Faculty of Engineering (Campus De Nair), Katholieke Universiteit Leuven, Belgium;

**Anatoly Lisnianski** – PhD, Chief Scientific Expert, Israel Electric Corporation Ltd., Haifa, Israel;

**Christian Madritsch** – PhD, Professor of the Faculty of Engineering and Information Technology, Carinthia University of Applied Sciences, Austria;

**Mher Markosyan** – Dr. Sc., Professor, Director of the Yerevan Research Institute of Communications, Professor of the Department of Telecommunications, Russian-Armenian University, Yerevan, Armenia;

**Oleg Rubel** – PhD, Associate Professor, Faculty of Engineering, McMaster University, Hamilton, Canada;

**Peter Schulz** – Dr. Sc., Professor, Professor, Faculty of Engineering and Computer Science, Hamburg University of Applied Sciences (HAW Hamburg), Hamburg, Germany;

**Avtandil Tavkhelidze** – PhD, Professor, Professor of the School of Business, Technology and Education, Ilia State University, Tbilisi, Georgia;

**Doru Ursuțiu** – Dr. Sc., Professor, Professor, Department of Electronics and Computer Engineering, University of Transylvania at Brasov, Romania.

Recommended for publication by the Academic Council of NU «Zaporizhzhia Polytechnic», protocol № 7 dated 05.03.2024.

The journal is imposed by the editorial-publishing department of NU Zaporizhzhia Polytechnic.

The journal web-site is <http://ric.zntu.edu.ua>.

The address of the editorial office: Editorial office of the journal Radio Electronics, Computer Science, Control, National University Zaporizhzhia Polytechnic, Zhukovskiy street, 64, Zaporizhzhia, 69063, Ukraine.

Tel.: +38-061-769-82-96 – the editorial-publishing department.

E-mail: [rvv@zntu.edu.ua](mailto:rvv@zntu.edu.ua)

Fax: +38-061-764-46-62

© National University «Zaporizhzhia Polytechnic», 2024

## ЗМІСТ

<b>РАДІОЕЛЕКТРОНІКА ТА ТЕЛЕКОМУНІКАЦІЇ.....</b>	<b>6</b>
<i>Bondarenko O. V., Stepanov D. M., Verbytskyi O. O., Siden S. V.</i> METHOD OF EVALUATION THE EFFICIENCY OF FIBER-OPTIC CABLES MODELS WITH MULTI-MODULAR DESIGN BASED ON MASS AND DIMENSIONAL INDICATORS.....	6
<i>Kostyria O. O., Hryzo A. A., Khudov H. V., Dodukh O. M., Lisohorskyi B. A.</i> TWO-FRAGMENT NON-LINEAR-FREQUENCY MODULATED SIGNALS WITH ROOTS OF QUADRATIC AND LINEAR LAWS FREQUENCY CHANGES.....	17
<i>Magro V. I., Panfilov O. G.</i> RESEARCH OF THE FEATURES OF DIGITAL SIGNAL FORMATION IN SATELLITE COMMUNICATION LINES..	28
<i>Vanin V. A., Pershyna I. I.</i> SCATTERING OF ELECTROMAGNETIC WAVES ON FLAT GRID TWO-PERIODIC STRUCTURES.....	41
<b>МАТЕМАТИЧНЕ ТА КОМП'ЮТЕРНЕ МОДЕЛЮВАННЯ.....</b>	<b>51</b>
<i>Bashkatov A. M., Yuldashova O. A.</i> DECISION-MAKING MODELS AND THEIR APPLICATION IN TRANSPORT DELIVERY OF BUILDING MATERIALS.....	51
<i>Larchenko L. V., Parkhomenko A. V., Larchenko B. D., Korniienko V. R.</i> DESIGN MODELS OF BIT-STREAM ONLINE-COMPUTERS FOR SENSOR COMPONENTS.....	62
<i>Perederyi V. I., Borchik E. Y., Zosimov V. V., Bulgakova O. S.</i> EVALUATION OF THE INFLUENCE OF ENVIRONMENTAL FACTORS AND COGNITIVE PARAMETERS ON THE DECISION-MAKING PROCESS IN HUMAN-MACHINE SYSTEMS OF CRITICAL APPLICATION.....	76
<i>Prykhodko S. B., Prykhodko N. V., Koltsov A. V.</i> A NONLINEAR REGRESSION MODEL FOR EARLY LOC ESTIMATION OF OPEN-SOURCE KOTLIN-BASED APPLICATIONS.....	85
<b>НЕЙРОІНФОРМАТИКА ТА ІНТЕЛЕКТУАЛЬНІ СИСТЕМИ.....</b>	<b>96</b>
<i>Brychkovskiy O. D.</i> REFINEMENT AND ACCURACY CONTROL OF THE SOLUTION METHOD FOR THE DURABILITY PROBLEM OF A CORRODING STRUCTURE USING NEURAL NETWORK.....	96
<i>Berezsky O. M., Liashchynskiy P. B.</i> METHOD OF GENERATIVE-ADVERSARIAL NETWORKS SEARCHING ARCHITECTURES FOR BIOMEDICAL IMAGES SYNTHESIS.....	104
<i>Kashan V. Yu., Hnatushenko V. V.</i> MACHINE LEARNING FOR AUTOMATIC EXTRACTION OF WATER BODIES USING SENTINEL-2 IMAGERY...118	118
<i>Kovalenko S. M., Kutsenko O. S., Kovalenko S. V., Kovalenko A. S.</i> APPROACH TO THE AUTOMATIC CREATION OF AN ANNOTATED DATASET FOR THE DETECTION, LOCALIZATION AND CLASSIFICATION OF BLOOD CELLS IN AN IMAGE.....	128
<i>Lysechko V. P., Sadovnykov B. I., Komar O. M., Zhuchenko O. S.</i> A RESEARCH OF THE LATEST APPROACHES TO VISUAL IMAGE RECOGNITION AND CLASSIFICATION.....	140
<i>Syromiatnikov M. V., Ruvinskaya V. M.</i> UA-LLM: ADVANCING CONTEXT-BASED QUESTION ANSWERING IN UKRAINIAN THROUGH LARGE LANGUAGE MODELS.....	147
<i>Хаханов В. І., Абдуллаєв В. Х., Чумаченко С. В., Литвинова Є. І., Хаханова І. В.</i> ІНТЕЛЕКТУАЛЬНИЙ КОМП'ЮТИНГ В ПАМ'ЯТІ.....	161
<b>ПРОГРЕСИВНІ ІНФОРМАЦІЙНІ ТЕХНОЛОГІЇ.....</b>	<b>175</b>
<i>Batiuk T., Dosyn D.</i> REALIZATION OF THE DECISION-MAKING SUPPORT SYSTEM FOR TWITTER USERS' PUBLICATIONS ANALYSIS.....	175
<i>Batsamut V. M., Hodlevsky S. O., Babkov Yu. P., Morkvin D. A.</i> METHOD OF CREATING A MINIMAL SPANNING TREE ON AN ARBITRARY SUBSET OF VERTICES OF A WEIGHTED UNDIRECTED GRAPH.....	188
<i>Ваєрук Є. Я., Махров В. В., Гедеон Г. О.</i> ПРОЄКТУВАННЯ КОНВЕЄРНОГО ПРОЦЕСОРА RISC-V АРХІТЕКТУРИ З АПАРАТНИМ СПІВПРОЦЕСОРОМ ЦИФРОВОЇ ОБРОБКИ СИГНАЛІВ.....	197
<i>Kolodochka D. O., Polyakova M. V.</i> LAMA-WAVELET: IMAGE IMPAINTING WITH HIGH QUALITY OF FINE DETAILS AND OBJECT EDGES.....	208
<i>Rolik O. I., Omelchenko V. V.</i> PROACTIVE HORIZONTAL SCALING METHOD FOR KUBERNETES.....	221
<i>Yanko A. S., Krasnobayev V. A., Nikolsky S. B., Kruk O. O.</i> METHOD FOR DETERMINING THE BIT GRID OVERFLOW OF A COMPUTER SYSTEM OPERATING IN THE SYSTEM OF RESIDUAL CLASSES.....	228
<b>УПРАВЛІННЯ У ТЕХНІЧНИХ СИСТЕМАХ.....</b>	<b>242</b>
<i>Zozulya V. A., Osadchy S. I., Nedilko S. N.</i> STEWART PLATFORM DYNAMICS MODEL IDENTIFICATION.....	242

# CONTENTS

<b>RADIO ELECTRONICS AND TELECOMMUNICATIONS.....</b>	<b>6</b>
<i>Bondarenko O. V., Stepanov D. M., Verbytskyi O. O., Siden S. V.</i>	
METHOD OF EVALUATION THE EFFICIENCY OF FIBER-OPTIC CABLES MODELS WITH MULTI-MODULAR DESIGN BASED ON MASS AND DIMENSIONAL INDICATORS.....	6
<i>Kostyria O. O., Hryzo A. A., Khudov H. V., Dodukh O. M., Lisohorskyi B. A.</i>	
TWO-FRAGMENT NON-LINEAR-FREQUENCY MODULATED SIGNALS WITH ROOTS OF QUADRATIC AND LINEAR LAWS FREQUENCY CHANGES.....	17
<i>Magro V. I., Panfilov O. G.</i>	
RESEARCH OF THE FEATURES OF DIGITAL SIGNAL FORMATION IN SATELLITE COMMUNICATION LINES..	28
<i>Vanin V. A., Pershyna I. I.</i>	
SCATTERING OF ELECTROMAGNETIC WAVES ON FLAT GRID TWO-PERIODIC STRUCTURES.....	41
<b>MATHEMATICAL AND COMPUTER MODELING.....</b>	<b>51</b>
<i>Bashkatov A. M., Yuldashova O. A.</i>	
DECISION-MAKING MODELS AND THEIR APPLICATION IN TRANSPORT DELIVERY OF BUILDING MATERIALS.....	51
<i>Larchenko L. V., Parkhomenko A. V., Larchenko B. D., Korniienko V. R.</i>	
DESIGN MODELS OF BIT-STREAM ONLINE-COMPUTERS FOR SENSOR COMPONENTS.....	62
<i>Perederyi V. I., Borchik E. Y., Zosimov V. V., Bulgakova O. S.</i>	
EVALUATION OF THE INFLUENCE OF ENVIRONMENTAL FACTORS AND COGNITIVE PARAMETERS ON THE DECISION-MAKING PROCESS IN HUMAN-MACHINE SYSTEMS OF CRITICAL APPLICATION.....	76
<i>Prykhodko S. B., Prykhodko N. V., Koltsov A. V.</i>	
A NONLINEAR REGRESSION MODEL FOR EARLY LOC ESTIMATION OF OPEN-SOURCE KOTLIN-BASED APPLICATIONS.....	85
<b>NEUROINFORMATICS AND INTELLIGENT SYSTEMS.....</b>	<b>96</b>
<i>Brychkovskiy O. D.</i>	
REFINEMENT AND ACCURACY CONTROL OF THE SOLUTION METHOD FOR THE DURABILITY PROBLEM OF A CORRODING STRUCTURE USING NEURAL NETWORK.....	96
<i>Berezsky O. M., Liashchynskiy P. B.</i>	
METHOD OF GENERATIVE-ADVERSARIAL NETWORKS SEARCHING ARCHITECTURES FOR BIOMEDICAL IMAGES SYNTHESIS.....	104
<i>Kashan V. Yu., Hnatushenko V. V.</i>	
MACHINE LEARNING FOR AUTOMATIC EXTRACTION OF WATER BODIES USING SENTINEL-2 IMAGERY...118	
<i>Kovalenko S. M., Kutsenko O. S., Kovalenko S. V., Kovalenko A. S.</i>	
APPROACH TO THE AUTOMATIC CREATION OF AN ANNOTATED DATASET FOR THE DETECTION, LOCALIZATION AND CLASSIFICATION OF BLOOD CELLS IN AN IMAGE.....	128
<i>Lysechko V. P., Sadovnykov B. I., Komar O. M., Zhuchenko O. S.</i>	
A RESEARCH OF THE LATEST APPROACHES TO VISUAL IMAGE RECOGNITION AND CLASSIFICATION.....	140
<i>Syromiatnikov M. V., Ruvinskaya V. M.</i>	
UA-LLM: ADVANCING CONTEXT-BASED QUESTION ANSWERING IN UKRAINIAN THROUGH LARGE LANGUAGE MODELS.....	147
<i>Hahanov V. I., Abdullayev V. H., Chumachenko S. V., Lytvynova E. I., Hahanova I. V.</i>	
IN-MEMORY INTELLIGENT COMPUTING.....	161
<b>PROGRESSIVE INFORMATION TECHNOLOGIES.....</b>	<b>175</b>
<i>Batiuk T., Dosyn D.</i>	
REALIZATION OF THE DECISION-MAKING SUPPORT SYSTEM FOR TWITTER USERS' PUBLICATIONS ANALYSIS.....	175
<i>Batsamut V. M., Hodlevsky S. O., Babkov Yu. P., Morkvin D. A.</i>	
METHOD OF CREATING A MINIMAL SPANNING TREE ON AN ARBITRARY SUBSET OF VERTICES OF A WEIGHTED UNDIRECTED GRAPH.....	188
<i>Vavruk Y. Y., Makhrov V. V., Hedeon H. O.</i>	
THE DESIGN OF THE PIPELINED RISC-V PROCESSOR WITH THE HARDWARE COPROCESSOR OF DIGITAL SIGNAL PROCESSING.....	197
<i>Kolodochka D. O., Polyakova M. V.</i>	
LAMA-WAVELET: IMAGE IMPAINTING WITH HIGH QUALITY OF FINE DETAILS AND OBJECT EDGES.....	208
<i>Rolik O. I., Omelchenko V. V.</i>	
PROACTIVE HORIZONTAL SCALING METHOD FOR KUBERNETES.....	221
<i>Yanko A. S., Krasnobayev V. A., Nikolsky S. B., Kruk O. O.</i>	
METHOD FOR DETERMINING THE BIT GRID OVERFLOW OF A COMPUTER SYSTEM OPERATING IN THE SYSTEM OF RESIDUAL CLASSES.....	228
<b>CONTROL IN TECHNICAL SYSTEMS.....</b>	<b>242</b>
<i>Zozulya V. A., Osadchy S. I., Nedilko S. N.</i>	
STEWART PLATFORM DYNAMICS MODEL IDENTIFICATION.....	242

# РАДІОЕЛЕКТРОНІКА ТА ТЕЛЕКОМУНІКАЦІЇ

## RADIO ELECTRONICS AND TELECOMMUNICATIONS

UDC 681.7.068

### METHOD OF EVALUATION THE EFFICIENCY OF FIBER-OPTIC CABLES MODELS WITH MULTI-MODULAR DESIGN BASED ON MASS AND DIMENSIONAL INDICATORS

**Bondarenko O. V.** – Dr. Sc., Professor, Laureate of the State Prize in Science and Technology, Head of the Department of fiber-optic lines of electronic communications, State University of Intelligent Technologies and Communication, Odesa, Ukraine.

**Stepanov D. M.** – PhD, Associate professor, Associate professor of the Department of Switching Systems of Electronic Communications, State University of Intelligent Technologies and Telecommunication, Odesa, Ukraine.

**Verbytskyi O. O.** – Director of LLC “Projectbudalliance”, Odesa, Ukraine.

**Siden S. V.** – PhD, Acting Head of the Department of Radioelectronic Systems and Technologies, State University of Intelligent Technologies and Telecommunication, Odesa, Ukraine.

#### ABSTRACT

**Context.** Today, the leading cable production plants in many countries of the world manufacture single- and multi-module designs of fiber-optic cables (FOC) with different protective covers and the number of fibers. This creates a wide range of possible FOC models for different consumer (buyer) requirements. However, the lack of openness of prices for FOC for the consumer, in particular for the project organization, and the desire of the manufacturer to save on production creates a need for the development and research of a method for evaluating the effectiveness of FOC of a multi-module design. In the work, it is proposed to do this by analyzing a number of optical cable models according to parameters-criteria – the compactness coefficient and the economic efficiency coefficient of the FOC by diameter.

**Objective.** To develop a method of evaluation the efficiency of fiber-optic cables models with multi-modular design based on mass-dimensional indicators, which will allow to quickly choose an appropriate model of the FOC with the given initial data.

**Method.** A method of evaluating the efficiency of the FOC modular design has been developed and proposed. It is based on the comparison of cable models and the selection of the most appropriate of them at given initial data. The paper proposed and introduced parameters-criteria for this – the compactness coefficient  $\nu$  and the efficiency coefficient according to the diameter of the cable  $E_0$  – which show the connection of the design characteristics of the FOC to a certain parameter of its structure. At the same time, the most effective model (design) of the FOC compared to the basic models in terms of technical conditions, both from the point of view of the manufacturer and the customer, consists in lower material costs for its production while simultaneously ensuring the specified requirements for the cable (first of all, number of fibers and mechanical strength). This will allow, at the stage of cable design, to make an appropriate choice of its model with given initial parameters and to develop such a design of the FOC, which will allow to minimize the dimensions (and therefore the material capacity and cost) of the model without losing its quantitative and qualitative characteristics.

**Results.** The paper presents the results of the development and research of the method of evaluating the efficiency of the FOC with multi-module structure based on mass and dimensional indicators. For example, using the developed method, it is shown that it is possible to choose a FOC model with a diameter smaller by 10.9% and save 15.5% of the cable cost for each kilometer of the fiber optic communication line while ensuring the initial requirements for the cable.

**Conclusions.** The scientific novelty of the work results is that, method of evaluation the efficiency of a modular FOC design has been first developed, which allows at the cable design stage to compare the model with the cable design according to the technical conditions (TC) and the appropriate choice of this model with the given initial parameters. The practical significance lies in the possibility of using this method to make an accelerated selection of the cable model at the stage of its design, while simultaneously providing the necessary capacity of the FOC with optical fibers and minimizing the cost of its materials and dimensions.

**KEYWORDS:** fiber-optic cable, cable design, geometric dimensions, mass-dimensional indicators, cost of cable materials.

#### ABBREVIATIONS

AON is an all optical network  
FOC is a fiber optic cable;  
FOCL is a fiber-optic communication line;  
FE is a filling element;  
FTTB is a Fiber To The Build;

FTTH is a Fiber To The Home;  
HF is a hydrophobic filler;  
OM is an optical module;  
OF is an optical fiber;  
CSE is a central strength element;  
PSE is a peripheral strength element.

## NOMENCLATURE

$\nu$  is a coefficient of FOC compactness;  
 $E_0$  is a coefficient of economic efficiency of the FOC by diameter;  
 $d_{OM}$  is a diameter of the optical module tube;  
 $D_c$  is an outer diameter of the cable;  
 $n$  is a number of twisted elements in the cable core;  
 $\theta$  is an angle of spiral twisting of the elements in the cable core;  
 $m$  is a number of layers in the cable core;  
 $\Delta t_{wb}$  is a radial thickness of the water-blocking tape;  
 $\Delta t_{ph}$  is a radial thickness of protective hose;  
 $V_c$  is a the volume of fiber optic cable;  
 $P_c$  is a mass of fiber optic cable;  
 $P_{OF}$  is a mass of optical fiber;  
 $P_{CSE}$  is a mass of the central strength element;  
 $P_{OM}$  is an optical module mass;  
 $P_{hf1}$  is a mass of hydrophobic filler inside optical module;  
 $P_{hf2}$  is a mass of hydrophobic filler between optical modules;  
 $P_{ph}$  is a mass of the protective hose;  
 $P_{wb}$  is a mass of water-blocking tape;  
 $P_{PSE}$  is a mass of the peripheral strength element;  
 $d$  is a diameter of solid element;  
 $D_{av}$  is an average diameter of the tubular element, mm;  
 $\delta$  is a wall thickness of the tubular element, mm;  
 $l$  is a length of the element of the cable, km;  
 $\gamma$  is a density of the material of structural element;  
 $K$  is a structural or technological coefficients (twisting, helicity, corrugation, etc.);  
 $E_0$  is a parameter-criterion of the economic efficiency of the cable, UAH/(km·mm);  
 $C_c$  is a full cost of materials of cable, UAH/km;  
 $N$  is a number of cable design elements.  
 $C_{el}$  is a cost of the cable element, UAH/km;  
 $C_1$  is a cost of one kilometer or unit of cable element material, UAH/kg;  
 $M$  is a mass of the volume element of the FOC, kg/km;  
 $K_w$  is a rate of waste in the manufacture of the FOC element, %;  
 $LD$  is a linear density of aramid threads, dtex;  
 $n_{at}$  is a number of aramid threads in PSE layer;  
 $P_{ha}$  is a mass of hydrophobic aggregate in all OM, kg;  
 $D_{inOM}$  is an inner diameter of the tube OM, mm;  
 $d_{OF}$  is a diameter of one OF, mm;  
 $K_h$  is a coefficient of helical stacking of fiber;  
 $n_{OF}$  is a number of fiber in one module tube;  
 $\gamma_{gz}$  is a material density of hydrophobic aggregate, kg/mm<sup>3</sup>;  
 $K_{OM}$  is a constructive and technological coefficient that takes into account the spiral stacking of OM around the CSE;  
 $n_{OM}$  is a number of OM in the core of the OC;  
 $d_{out}$  is an outer diameter of the tubular element of the FOC, mm;  
 $d_{in}$  is an inner diameter of the tubular element of the FOC, mm.

## INTRODUCTION

Modern society in the conditions of rapid technical progress requires providing the increasing number of telecommunication services and services, the implementation of which occurs due to the use of various means of telecommunications. The steady increasing the number of users of telecommunication services and their requirements leads to an increase in the volume of information transmitted in the communication network. And it determines the expansion of the transport telecommunications network and the subscriber access network. In addition, one of the main trends is the introduction of 5th generation (5G) mobile communication networks, which provide high data transfer rates and low delay. Future mobile communication networks place high demands not only on quality characteristics, but also on the efficiency of the infrastructure on which communication provision is based [1]. In this context, the design of optical cables becomes a main element, providing an extremely important foundation for the transmission of data in huge volumes.

In many countries of the world, the communication network today has a two-level hierarchical structure (transport telecommunication network and subscriber access network) using both copper and fiber optic communication cables. High-speed mutual exchange of information (audio, video, various types of data) between the devices of nodes of the transport telecommunication network is carried out exclusively on the basis of fiber-optic cables of various designs. On the subscriber access networks the FOCs are increasingly being replaced the traditional electrical cables with copper cores due to the possibility of simultaneously receiving integrated services of the Internet, television and telephony, which will also ensure a certain network energy independence during the provision of services. This is achieved by the creation of appropriate constructions of FOC and the building of new high-speed fiber optic communication lines. For this purpose, factories are actively working in cable production (PJSC “Odeskabel”, PJSC “Zavod ‘Pivdenkabel’” and others).

Factories producing cable products, guided by their own scientific developments, design and manufacture an increasingly large and wide range of FOC of various designs for certain operating conditions (in soil, cable ducts, underwater, for suspension, in mines, subchannels, collectors, etc.). At the same time, in order to achieve significant profitability of production and ensure the technical efficiency of the cable, cable production plants try to choose the appropriate design of the FOC (size and number of structural elements, their materials, manufacturing technology, weight and cost of the cable) according to the criterion “technical ability/cost of the cable”. At the same time, the organization (customer) that performs the design and/or building of FOCL needs such a brand of cable for certain laying conditions, which would at the same time ensure minimum costs for its purchase and compliance with the requirements for the technical ability of the ca-

ble. That is, the customer of cable products chooses the FOC brand on the basis of requirements from: the specified number of optical fibers and the operating conditions of the cable, which determines the type of its protective coatings, mechanical strength, mass, dimensions, etc. That is why the manufacturing plants provide a wide range of cable products for the needs of the customer. Such a task of choosing the optimal cable laying for the given conditions is very large in scope of work and duration in time. Therefore, the cable production plant designs, calculates, develops and tests only the basic prototypes of FOC brands. And variations of the basic FOC model create a wide range of brands of this cable. The task of choosing an effective (expedient) sample of the FOC during the design falls on the manufacturer, and during the construction of the FOC – on the design organization.

Currently, there is no publicly available regulatory documentation on the development of FOC, and known sources provide only individual details about the calculation of their structures. Therefore, it requires the creation of new, improvement of existing methods of design, calculation and development, evaluation of cable structures for given operating conditions.

Today, the leading cable production plants mostly manufacture single- and multi-module FOC designs with different protective covers and number of fibers. At the same time, within the framework of one brand of cable, the same FOC design has a different number of OF. This leads to the complication of choosing an appropriate design of the FOC, and sometimes to its impracticality in certain operating conditions, reducing its technical capability. And the development of a method for evaluating the effectiveness of FOC models based on mass-dimensional indicators will allow to make an appropriate choice of cable design with a given number of optical fibers, as well as with the possibility of reducing the cost of materials for production.

**The object of study** is the evaluation of the effectiveness of models of fiber-optic cables with multi-module design by mass and dimensional indicators.

**The subject of study** is the model of a multi-module fiber optic cable design.

**The purpose of the work** is to develop a method of evaluating the efficiency of models of fiber-optic cables with multi-module design based on mass-dimensional indicators, which will allow to quickly choose an appropriate (better) model of the FOC with the given initial data. This approach is universal when creating a wide range of cable products and selecting a cable based on the “quality/price” criterion for specific operating conditions.

## 1 PROBLEM STATEMENT

Suppose there are  $m$  models of FOC with modular design, each of which has a certain number of optical fibers and other technical characteristics, which in practice depend on the technological capabilities of production. First of all, the number of optical fibers  $n_{OF}$ , © Bondarenko O. V., Stepanov D. M., Verbytskyi O. O. Siden S. V., 2024  
DOI 10.15588/1607-3274-2024-1-1

the number  $N$  and the dimensions ( $d, \Delta t$ ) of the structural elements, their materials, the mass  $P_c$ , the price  $C_1$  and the volume  $V_c$  determine the full cost of the FOC  $C_c$ , which can be represented as a function  $C_c = f(n, N, P_c, V_c, K, \gamma, C_1)$ .

The task of finding an effective FOC model consists in finding such a cable model  $x$  with the minimum total cost of materials  $C_x = \min[C_{c1}, C_{c2}, \dots, C_{cm}]$  and the number of fibers, which is greater than the required  $N_{OF} > N_{OFneed}$ .

In turn, the problem of finding an effective FOC model is to find such a set of mass-dimensional parameters of the cable design ( $n, N, d, P_c, V_c$ ) in which  $C_c \rightarrow \min$ . For this purpose, it is proposed to introduce criteria-parameters: cable compactness coefficient  $\nu$  and economic efficiency coefficient by diameter  $E_0$ .

## 2 REVIEW OF THE LITERATURE

Analysis of the works of well-known authors in the field of fiber-optic communication, in particular, design, development and production of FOC – Malke G., Hessing P., Kanamori H., Beyer G., Bailey D., Wright E., Bondarenko O.V., Katok V.B. etc. [2 – 12] showed the lack of completeness of research in this direction. In particular, these works show approaches to the calculation and design of modular structures of cables according to tensile load [2, 3, 5, 7, 12], features of the use of different materials for structural elements of cables [4], consideration of metrological standards during the production of FOC [6], features of the construction of a modular type FOC [8], interrelations of the sizes of the structural elements of the FOC and methods of determining the cost of the cable [8, 10, 11]. However, the assessment of the effectiveness of modular constructions of the FOC based on mass-dimensional indicators, which would allow choosing the appropriate cable structure for the given initial data (conditions), remained out of the authors’ attention.

## 3 MATERIALS AND METHODS

Currently, in the conditions of the market economy, there are a lot of different telecommunication companies (telecommunication operators) that are engaged the providing telecommunication needs of consumers within the limits of a settlement or district. Network construction technologies such as Fiber to the Build and Fiber to the Home, which are built on the basis of FOCL, have become especially popular for use. They make it possible to implement the AON optical information transmission technology. For this, communication operator companies use FOC with different amount of OF (for laying in the ground, cable duct, low-current channels, hanging between buildings or on network poles for various purposes).

To ensure the necessary bandwidth of communication lines and networks, FOCs with a certain number (from 4 and more) of single-mode optical fibers with low attenuation are used. In some countries, FOCs as a rule with modular design are manufactured and used on communi-

cation networks. Modular designs of the FOC core can have a different structure, i.e. different number and sizes of twisting elements (tubes of optical modules, filling elements, layers, etc.), which determines the difference in their geometrical and dimensional parameters. Fibers in FOC are placed inside the tube of optical modules with different diameters, which are filled with hydrophobic filler. In such FOC the core contains, as a rule, from 2 to 12 OM tubes in the first layer or OM and a certain number of filling elements, which are spirally arranged around the central strength element. As a rule, the CSE is made of a fiberglass rod or a steel rope with a polyethylene sheath. The diameter of the CSE depends on the number of elements in the first layer of the cable core. The size of the CSE, in turn, is decisive when calculating the value of the maximum permissible tensile load of the FOC, the value of which is used to estimate the long-term mechanical strength of the cable and to conduct its development [2, 8, 11].

The choice of the FOC core structure, materials and sizes of the structural elements of the cable determines its technical indicators, including weight and dimensions.

Therefore, FOC designers solve the task of developing a cable design that would allow minimizing the dimensions (which means the material capacity and cost) of the models without losing their quantitative and qualitative characteristics. At the same time, the design of a certain brand of FOC can have several options for the core and the number of OF in it. This requires the selection of the optimal design of the FOC for the given operating conditions. At the same time, the effectiveness of the FOC model (construction) compared to the basic models according to the technical specifications, both from the point of view of the manufacturer and the customer, consists in lower material costs for its production while simultaneously ensuring the specified requirements for the cable (primarily, in terms of the number of fibers and mechanical strength). The choice of a modular design of the FOC with OF freely located inside determines the absence of mechanical stresses in the fibers and ensures their integrity during operation [11].

The efficiency of the FOC design in terms of mass and dimensions compared to the basic models according to the technical conditions consists in the lower material consumption of its structural elements while ensuring the proper level of its technical ability. The solution to this problem is based on the definition and study, first of all, of the FOC cores, which are difference between cable models. This will make it possible to compare FOC models with each other according to the criteria of constructive efficiency and to choose the most appropriate one of them at the given initial data.

In order to evaluate the effectiveness of fiber-optic cable models based on mass-dimensional indicators, it is necessary to introduce parameters-criteria that would show the connection of the characteristics of the FOC design to a certain parameter of its structure. Therefore, it

is proposed to introduce the following parameters-criteria in the work:

- cable compactness coefficient, which shows the relationship with the volume of the FOC and its mass;
- coefficient of economic efficiency of the FOC by diameter, which characterizes the part of the cable cost per unit of its diameter.

In a general view, the structure of the core of an optical cable with a single-layer multi-module unarmored design is presented in Fig. 1 [2, 3, 6, 8, 10].

First of all, it is necessary to show the relation between the outer diameter of the FOC structure and the number of layers, the number and sizes of elements (OM or FE) in the layers, the radial thicknesses of the protective layers of the cable, etc.

Taking into account [2, 8, 9, 10], the outer diameter of the FOC of the multi-module design according to Fig. 1 can be determined by the expression:

$$D_c = d_{OM} \left( \sqrt{1 + \frac{1}{\sin^2 \theta} \left[ \frac{1}{\sin^2 \frac{\pi}{n}} - 1 \right]} + 1 \right) + 2(m-1)d_{OM} + 2\Delta t_{wb} + 2\Delta t_{ph}. \quad (1)$$

For a generalized assessment of FOC models, we will calculate the parameters of their technical and economic group. As you know, the technical and economic group includes three main parameters, namely: product cost (UAH/km), dimensions or volume  $V$  (dm<sup>3</sup>) and mass  $P_c$  (kg/km) [7, 13, 14].

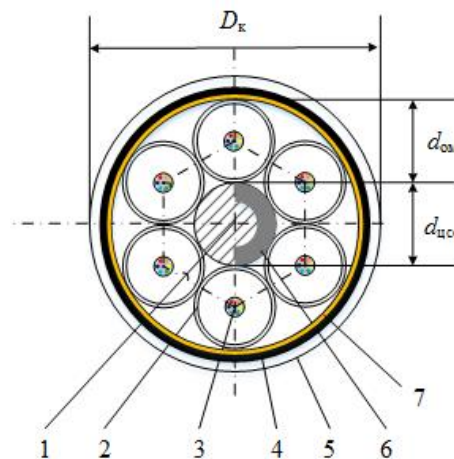


Figure 1 – Cross-section of a model of a single-layer construction of FOC: 1 – CSE; 2 – OM tube; 3 – OF; 4 – water-blocking layer; 5 – protective hose; 6 – polyethylene coating (in the case of metal TSE); 7 – peripheral strength element

According to [2], the product of the volume and mass of the cable model under investigation will allow to obtain the parameter-criterion – the compactness coefficient of the FOC  $\nu$  (dm<sup>3</sup>·kg):

$$\nu = V_c \cdot P_c. \quad (2)$$

By the value of the parameter-criterion of the compactness coefficient, it is possible to compare the material consumption of the cable with the material consumption of the basic design according to the technical specifications and, thus, determine the efficiency of its model based on mass-dimensional indicators. The smaller the value of the compactness factor, the smaller its weight and material consumption.

The volume of the cable  $V_c$  is defined as the sum of the volumes of all its structural elements (solid or tubular) and their fillings. Expressions for calculating the volumes of solid and tubular structural elements of the FOC are presented as:

- for solid element  $V_c = \pi d_{el}^2 \cdot l \cdot K / 4$  ;
- for tubular element  $V_c = \pi(d_{out}^2 - d_{in}^2) \cdot l \cdot K / 4$  .

The mass of the FOC is the sum of the masses of all its elements and their fillings. The mass of FOC can be calculated using the following expression:

$$P_c = \sum_{i=1}^N P_i = P_{OF} + P_{CSE} + P_{OM} + P_{hf1} + P_{hf2} + P_{wb} + P_{PSE} + P_{ph} . \quad (3)$$

Most cable construction elements are solid (optical fibers, CSE or PSE fiberglass rods, filling elements, etc.) or tubular (OM tube, protective hose, etc.). According to [7, 8, 10], the expressions for calculating the mass of solid and tubular structural elements of the FOC are generally presented as:

- for a solid element

$$P = \frac{\pi d^2}{4} \gamma l(k, K) ; \quad (4)$$

- for a tubular element

$$P = \pi D_{av} \delta \gamma l(k, K) . \quad (5)$$

In formulas (4) and (5), the nominal dimensions of the elements are substituted (without taking into account tolerances) and the nominal mass is calculated (without taking into account waste).

The mass of the hydrophobic filler of the OM cable tubes is determined by the expression [9]:

$$P_{hf} = \frac{\pi}{4} (D_{inOM}^2 - d_{OF}^2 K n_{OF}) \gamma_{hf} l K_{OM} n_{OM} . \quad (6)$$

The mass of aramid threads, kg, can be calculated by the expression [9]:

$$P_{PSE} = LD \cdot n_{at} 10^{-4} . \quad (7)$$

Establishing a relation between the compactness coefficient of the FOC, in particular, from its core structure

(the number of OM tubes, fibers, etc.) will allow choosing a less material-consuming cable model while providing a given amount of OF.

It is possible to calculate the cost of materials of individual elements and the total cost of materials of all elements of the FOC based on the determined masses of the cable elements and the prices of their materials.

It is obvious that each model of FOC, due to its different diameter, volume (material consumption), has a corresponding cost price. Therefore, in order to quantitatively compare the efficiency of the designs of these models, in this work it is proposed to introduce a parameter-criterion of the economic efficiency of the FOC by the diameter  $E_0$ , which will characterize the cost of the cable materials per unit of its diameter, i.e.:

$$E_0 = \frac{C_c}{D_c} . \quad (8)$$

The total cost of materials of all elements of the FOC is determined by the expression [9]:

$$C_c = \sum_{i=1}^N C_{eli} . \quad (9)$$

The cost of materials for a separate element of the cable is calculated according to the expression [9]:

$$C_{el} = C_1 M \left( \frac{100 + K_w}{100} \right) . \quad (10)$$

According to the value of the parameter-criterion – coefficient of economic efficiency of the FOC by diameter, it is possible to compare the cost of materials of different cables models and, thus, determine its more efficient design. The lower the value of the coefficient of economic efficiency of the FOC, the lower the cost of the part of the cost of the cable materials per unit of its diameter. Thus, lower costs for cable materials as a whole.

#### 4 EXPERIMENTS

A multi-module FOC design without armor was chosen as the sample for the research (Fig. 1). It can contain several (1, 2 and 3) concentric layers of OM around the CSE. The number of elements in the first layer used in practice are in ranges from 3 to 12 [2, 5, 10, 11].

In the investigated FOC models, the following were adopted: the diameter of the OM tube (element in layer)  $d_{OM} = 2.3$  mm with the maximum number of OF in each module  $N_{OF} = 12$ , the fiber diameter in the primary protective coating  $d_{OM} = 0.255$  mm, the step of the spiral arrangement of the layer elements around the CSE  $h = 90$  mm. The densities of materials and semi-finished products used in the calculations for the structural elements of the FOC and their cost are taken according to [2, 10].

In this work, the assumptions are:

1. All elements of the layer are OM tubes with optical fibers. All OM tubes in FOC design are completely filled by fibers, that is, they contain 12 fibers in each.

2. OM tubes, which have a spiral arrangement around the CSE with a certain angle, in the cross-section of the cable were considered as circles, not an ellipse.

Calculations of data arrays of FOC models were performed in the MathCad 14 software environment using expressions (1)–(10) and known geometry formulas.

### 5 RESULTS

Using expression (1), calculations of the outer diameters of the intended models of the FOC were performed in

the paper. At the same time, taking into account the rule of “correct twisting”, at twisting the elements of the cable core in a spiral layer, their number in each subsequent layer increases by six compared to the previous one. And their variety is determined by the possible number of elements of a layer from 3 to 12 and layers from 1 to 3 [10]. The results of the calculations of the outer diameters of the FOC models are presented in the Table 1.

For a visual representation and better understanding, the results of the calculations of the outer diameters of the FOC models are presented in Fig. 2.

Table 1 – The results of the calculations of the diameters of the FOC models

Number of layers in FOC design	Number of elements in the first layer									
	3	4	5	6	7	8	9	10	11	12
I	8.5	9.1	9.7	10.4	11.1	11.8	12.5	13.2	14	14.7
II	13.1	13.7	14.3	15	15.7	16.4	17.1	17.8	18.6	19.3
III	17.7	18.3	18.9	19.6	20.3	21	21.7	22.4	23.2	23.9

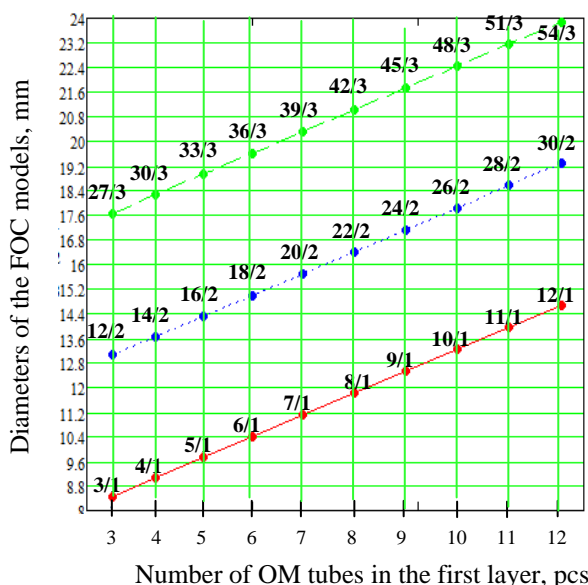


Figure 2 – Dependences of the outer diameter of FOC models on the number of OMs in the first cable layer for one-, two- and three-layers core designs ( $m/n$  FOC model number, where  $m$  is the total number of OMs;  $n$  is the number of layers)

Three dependencies are shown in Fig. 2 show the connection between the number of OM in the first, second, and third layers and the outer diameter of the FOC. Fig. 2 shows that with an increase of the number of OM in the first FOC layer from 3 to 12 in the one-, two- and three-layers structure of the cable core, its outer diameter will increase linearly. It can also be seen that some models of FOC with the same number of OM tubes can be obtained using a different number of layers and provide the same cable capacity (or even more), but with a smaller diame-

ter. This fact makes it possible to obtain a given capacity of OF in the cable when using a larger number of layers, while achieving smaller dimensions (material consumption) of the FOC. The smaller dimensions of the FOC lead to a decrease in the material capacity of the cable and, as a result, to a decrease in the cost of its materials during manufacture.

In order to quantitatively verify this statement, it is necessary to carry out a generalized assessment of the effectiveness of each presented model of the FOC according to the criteria outlined in the work.

According to expressions (2) – (7), the calculations of the mass of structural elements of the FOC were performed. All calculations of the coefficient of compactness of the FOC models are given in the Table 2 and Fig. 3.

Fig. 3 shows that the dependencies of the compactness coefficient have a parabolic character, that is, a small increase of the number of OM in the first layer leads to a greater increase of the cable compactness coefficient. That is, obtaining a smaller value of the FOC compactness coefficient is achieved when using a smaller number of OM and layers of the cable core. This choice is limited only by the conditions for the total number of optical fibers and the value of the mechanical strength of the cable [11]. This makes it possible to choose a more compact FOC model, which is especially relevant for more efficient use of the space of cable ducts, collectors and other places of cable laying. So, for example, models 12/1 and 12/2 have the same number of OFs in FOC models (144 fibers). According to the dependencies in Fig. 3, by choosing the 12/2 model, it is possible to get a FOC with a lower cost of materials. At the same time, the diameter of the FOC model will decrease by 10.9 %.

Table 2 – The results of calculations the compactness coefficient (dm<sup>3</sup>·kg) of one-, two-, and three-layer FOC designs with different core structures

Number of OM tubes in the first layer	The number of layers of the FOC construction														
	I					II					III				
	Number of OF, $N_{OF}$	Diameter of FOC, mm	Volume of FOC per 1 km, dm <sup>3</sup>	Mass of FOC per 1 km, kg	Compactness coefficient, dm <sup>3</sup> ·kg	Number of OF, $N_{OF}$	Diameter of FOC, mm	Volume of FOC per 1 km, dm <sup>3</sup>	Mass of FOC per 1 km, kg	Compactness coefficient, dm <sup>3</sup> ·kg	Number of OF, $N_{OF}$	Diameter of FOC, mm	Volume of FOC per 1 km, dm <sup>3</sup>	Mass of FOC per 1 km, kg	Compactness coefficient, dm <sup>3</sup> ·kg
3	36	8.5	56.745	150.418	8535.5	144	13.1	134.782	317.830	42837.8	324	17.7	246.057	451.153	111009.4
4	48	9.1	65.039	170.605	11096	168	13.7	147.411	345.018	50859.4	360	18.3	263.022	481.645	126683.2
5	60	9.7	73.898	193.635	14309.2	192	14.3	160.606	375.193	60258.2	396	18.9	280.552	515.222	144546.6
6	72	10.4	84.949	218.876	18593.3	216	15.0	176.715	407.717	72049.7	432	19.6	301.719	551.235	166318.1
7	84	11.1	96.769	246.096	23814.5	240	15.7	193.593	442.363	85638.4	468	20.3	323.655	589.453	190779.4
8	96	11.8	109.359	275.173	30092.6	264	16.4	211.241	479.010	101186.6	504	21.0	346.361	629.756	218122.9
9	108	12.5	122.718	306.163	37571.7	288	17.1	229.658	517.725	118899.7	540	21.7	369.836	672.215	248609.3
10	120	13.2	136.848	338.953	46385	312	17.8	248.846	558.396	138954.6	576	22.4	394.081	716.718	282444.9
11	132	14.0	153.938	373.568	57506.3	336	18.6	271.716	601.055	163316.3	612	23.2	422.733	763.300	322672.1
12	144	14.7	169.717	410.133	69606.5	360	19.3	292.553	645.838	191574.8	648	23.9	448.627	812.103	364331.3

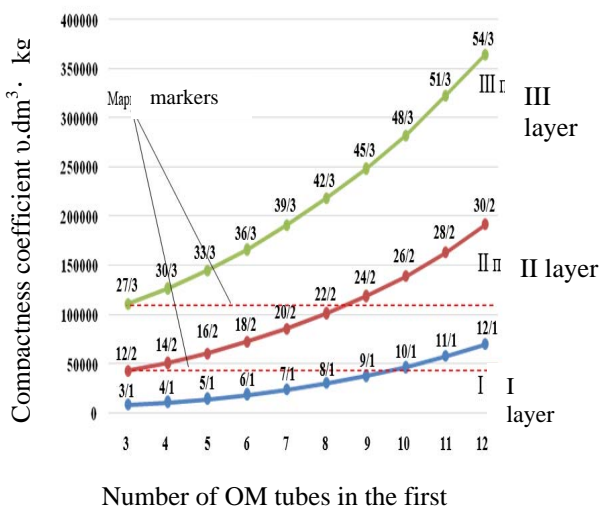


Figure 3 – Dependencies of the compactness coefficient of FOC models on the number of OM in layers ( $m/n$  FOC model number, where  $m$  is the total number of OM;  $n$  is the number of layers)

Using expressions (9), (10), the full cost of FOC materials  $C_c$  (Table 3) for one-, two-, and three-layers cable designs were determined in the work. Fig. 4 makes it possible to establish a visual connection between the cost of materials of the model FOC and the diameter of the cable. This dependence will make it possible to determine the parameter-criterion of economic efficiency of FOC models by diameter.

Fig. 4 shows the dependence of the total cost price of FOC materials on its diameter with different numbers of layers and elements in them. From Fig. 4 and Table 3 it can be seen that some of FOC models have approximately the same cost of materials in the overlapping parts of the graphs. This indicates that it is possible to choose such a

FOC model, which at the same cost of materials will have better indicators of economic efficiency.

It was established that the increase of the cost of FOC materials due to the increase of the number of OM tubes (and therefore the total capacity of the OF inside the cable) from 3 to 12 in the first layer in a single-layer core of the cable is 66.8 %, in a two-layers – 86.6 %, in a three-layers – 87 %. The specified results of the calculation of the increase of the cost price of FOC materials in percent mean that the models of single-layer cables have the smallest cost variation.

According to the expression (8), the parameter-criterion of the economic efficiency of the FOC design by the diameter  $E_0$  is determined. The results of the calculation of  $E_0$  are presented in the Table 4 and Fig. 5.

From the Table 4 and Fig. 5, it can be seen that using more than one layer in the cable core, the value of the parameter-criterion of the coefficient of economic efficiency of the FOC decreases, that is, the expediency of the three-layer design is higher than the others if a large number of OF is needed. But at the same time, it can be seen that in the overlapping parts of the graphs, some FOC models have approximately the same values of the  $E_0$  coefficient. That is, with approximately the same cost of materials of these FOC models, it is advisable to choose the one with a larger number of layers, as this gives a larger number of optical fibers. So, for example, from Fig. 5 models 10/1 and 12/2 have almost identical values of the parameter-criterion of economic efficiency  $E_0$ . However, by choosing the 12/2 model, it will allow us to get a FOC with more optical fibers (144 vs. 120).

On the other hand, for example, the models 12/1 and 12/2 have the same number of optical fibers, but different prices. By choosing the model 12/2 according to the results of this method, it will save 15.5 % of the cost of the cable for each kilometer of FOCL.

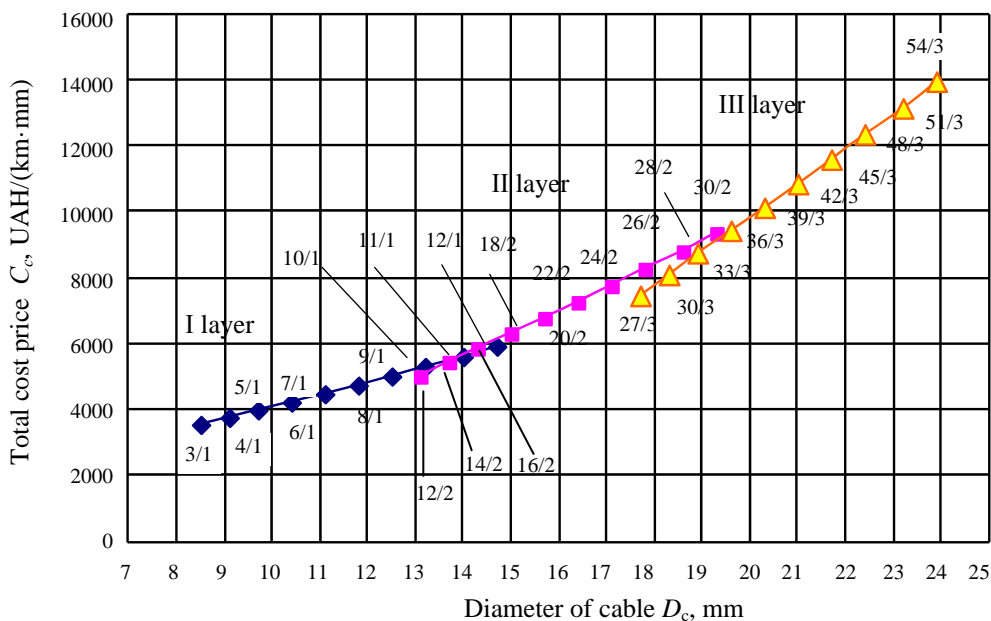


Figure 4 – Dependence of the total cost price of materials of the FOC on its diameter for one-, two- and three-layer designs ( $m/n$  FOC model number, where  $m$  is the total number of OMs;  $n$  is the number of layers)

Table 4 – Results of the calculation of the parameter-criterion of the economic efficiency of the FOC design by diameter

Parameter-criterion of the economic efficiency of the FOC design										
Number of layers in cable core	Number of OM in the first layer									
	3	4	5	6	7	8	9	10	11	12
I	0.416	0.339	0.279	0.227	0.188	0.158	0.134	0.114	0.097	0.085
II	0.117	0.107	0.097	0.088	0.079	0.072	0.065	0.059	0.054	0.049
III	0.067	0.064	0.061	0.057	0.053	0.050	0.047	0.044	0.041	0.038

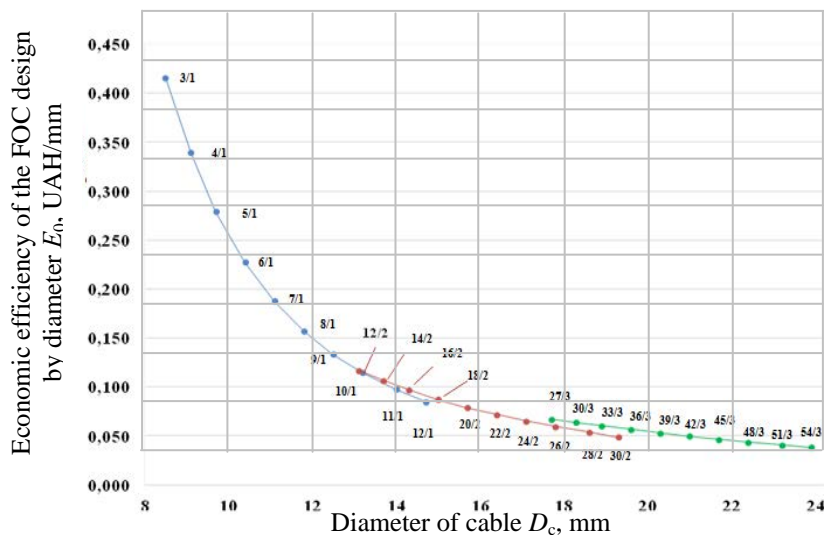


Figure 5 – Dependence of the parameter-criterion of the economic efficiency of the FOC design by the cable diameter ( $m/n$  FOC model number, where  $m$  is the total number of OMs;  $n$  is the number of layers)

## 6 DISCUSSION

The proposed method of evaluating the efficiency of the FOC with a modular design will allow during the cable designing stage to make an appropriate choice of its model with the given initial parameters. The researches presented in this work show a large number of possible models of FOC. This is also confirmed by the variety of cable models that are presented on the official websites of the manufacturers' factories, for example PJSC "Odeskabel" and PJSC "Zavod 'Pivdenkabel'" [13, 14]. Thus, manufacturing plants provide a wide range of cables of the same brand, which differ in the structure of the core and the number of fibers. The consumer, based on his needs, chooses the necessary capacity of the cable. Moreover, a very important point at this stage is the lack of transparency of prices for FOC for the consumer. And the manufacturing plant seeks to save on the cost price of production of the FOC and to reach an agreement on the price through discussion with the buyer. Therefore, this method of evaluating the effectiveness of modular FOC design will allow manufacturing plants to systematize the expediency of manufacturing FOC models, and consumers – without prices, to orient themselves in the expediency of choosing a certain cable model.

The approaches to the creation of multi-layer FOC presented in this work are confirmed by the capabilities of the manufacturing plants according to their prices for cable products [13, 14].

The use of a larger number of layers in a multi-module FOC for reducing the costs of materials is confirmed by the results of work [11].

## CONCLUSIONS

The researches in this work of the effectiveness of the modular FOC design based on mass and dimensional indicators allowed us to do the following conclusions:

1. In the work the method of evaluating the efficiency of the multi-module FOC design based on mass-dimensional indicators by applying to the intended range of cable models the criteria parameters – the cable compactness coefficient and the economic efficiency of the cable by to the diameter  $E_0$  is developed and researched.

2. In the course of researches of FOC models, according to the accepted parameters-criteria, it was established that:

– by changing the number of layer elements and layers, a wide range of FOC models can be obtained to ensure the diversity of cables in terms of the total number of optical fibers;

– the use of the parameter-criterion of compactness is the ability to choose a model of the FOC with a smaller diameter (dimensions) while providing the same amount of OF. In the work, for example, it is shown that using this approach it is possible to choose a FOC model with a diameter smaller by 10.9 %.

– the increase of the cost of the FOC materials due to the increase of the number of OM tubes (and therefore the total capacity of the OF in the cable) from 3 to 12 in the first layer with a single-layer core of the cable is 66.8 %, with a double-layer – 86.6 %, with a three-layer – 87 %.

– the use of a cable with maximally filled by OM tubes in layers with one- and two-layers core is impractical, since the transition to a larger number of layers with a smaller number of OMs will allow to obtain a more compact cable design while simultaneously providing a given number of OFs. Therefore, for example, it is shown in the work that, by selecting the FOC model according to the approaches proposed in the method, it is possible to save 15.5 % of the cost of the cable for each kilometer of the FOCL.

3. The method, results, established facts and statements obtained in this work can be recommended for usage in the process of accelerated selection of a cable model at the stage of its designing, with the simultaneous provision of the necessary capacity of the FOC with optical fibers and the minimization of the cost of its materials and dimensions.

## ACKNOWLEDGEMENTS

The work was carried out at the State University of Intelligent Technologies and Telecommunications (former O.S. Popov Odesa National Academy of Telecommunications) during 2015–2022 y. as part of a number of initiative research works: "Methods and devices for increasing the efficiency of transmission lines. Stage 3 – 5" (state registration number 0117U003419) and "Methods of increasing the reliability and bandwidth of fiber-optic communication lines" (state registration number 0119U103658).

## REFERENCES

1. Chowdhury M. Z., Hossain M. T., Islam A. and Jang Y. M., A Comparative Survey of Optical Wireless Technologies: Architectures and Applications, *IEEE Access*, 2018, Vol. 6, pp. 9819–9840. DOI: 10.1109/ACCESS.2018.2792419.
2. Mahlke G., Gossing P. *Fiber Optic Cables – Fundamentals, Cable Design, System Planning*, 4<sup>th</sup> edition. MCD Corporate Publishing, Munich, 2001, 302 p.
3. Elliott B., Gilmore M. *Fiber optic cabling* (second edition). Newnes, Elsevier, 2002, 318 p. ISBN 978-0-7506-5013-7. DOI: 10.1016/B978-0-7506-5013-7.X5000-4
4. Günter B. *The global cable industry: materials, markets, products*. Sidney, John Wiley & Sons, 2021, 416 p. ISBN: 978-3-527-34627-1. DOI:10.1002/9783527822263
5. Bailey D., Wright E. *Fiber optic cable construction*. Amsterdam, Boston, London, Elsevier, 2003, 288 p. DOI:10.1016/B978-075065800-3/50004-7.
6. Korchevs'kyj O. S. Kolomijec' L. V. *Mehanichni harakterystyky volokonno-optychnyh kabeliv, Zbirnyk naukovyh prac' Odes'koi' derzhavnoi' akademii' tehničnogo reguljuvannja ta jakosti*, 2015, Vyp. 2 (7), pp. 68–72. DOI: 10.32684/2412-5288-2015-2-7-68-72.
7. David Goff. *Fiber Optic Reference Guide*. 3rd edition. New York, 2002, 260 p. DOI: 10.4324/9780080506319
8. Kiforuk S. V. Influence of the ambient temperature on the mechanical tension of the optical cable, *Zbirnik naukovih prac' Odes'koi' derzhavnoi' akademii' tehničnogo reguljuvannâ ta*

- âkosti, 2022, Vyp. 2(21), pp. 20–26. DOI 10.32684/2412-5288-2022-2-21-19-26
9. Bondarenko O. V., Stepanov D. M., Kiforuk S. V., Slobodianiuk I. A. Thermomechanical influence on optical fibers during the production and operation of optical cable, *Naukovi praci ONAZ im. O. S. Popova*. Odesa, 2019, Vyp. № 1, pp. 23–32. DOI:10.33243/2518-7139-2019-1-1-23-32.
10. Bondarenko O. V. Vorobijenko P. P., Koljadenko V. A., Potapova-Sin'ko N. Ju. Metodologichni aspekty rozrahunku povnoi' sobivartosti volokonno-optychnogo kabelju, *Naukovo-teoretychnyj zhurnal Hmel'nyc'kogo ekonomichnogo universytetu "Nauka j ekonomika"*. Hmel'nyc'kyj, 2013, Vyp. № 1 (29), pp. 164–172.
11. Bondarenko O. V., Stepanov D. M., Bagachuk D. G., Romashhenko V. V., Verbyc'kyj O. O. Vybir struktury oserdja optychnyh kabeliv bagatomodul'noi' konstrukcii' za ekonomichnoju efektyvnistju, *Cyfrovi tehnologii': zb. nauk. prac'*. Odesa, 2016, Vyp. № 1, pp. 34–41. Access mode: [http://nbuv.gov.ua/UJRN/ct\\_2016\\_19\\_6](http://nbuv.gov.ua/UJRN/ct_2016_19_6).
12. Tingting Zhan, Minning Ji Optimization of the optical fiber with triple sector stress elements, *Optical Fiber Technology*, 2020, Vol. 57. DOI: 10.1016/j.yofte.2020.102212.
13. Public joint-stock company "Odesa cable works 'Odeskabel'" (2024). Fiber optic cables [Electronic resource]. Access mode: <https://odeskabel.com/en/products/vok-kabeli.html> (accessed 20 January 2024).
14. Private joint-stock company "Yuzhcable works" (2024). Fiber optic cables [Electronic resource]. Access mode: <https://www.yuzhcable.info/index.php?CAT=50&ENG=1> (accessed 20 January 2024).

Received 12.01.2024.  
Accepted 19.02.2024.

УДК 681.7.068

## МЕТОД ОЦІНКИ ЕФЕКТИВНОСТІ МОДЕЛЕЙ ВОЛОКОННО-ОПТИЧНИХ КАБЕЛІВ БАГАТОМОДУЛЬНОЇ КОНСТРУКЦІЇ ЗА МАСО-ГАБАРИТНИМИ ПОКАЗНИКАМИ

**Бондаренко О. В.** – д-р техн. наук, професор, Лауреат Державної Премії в галузі науки і техніки, завідувач кафедри волоконно-оптичних ліній електронних комунікацій, Державний університет інтелектуальних технологій і зв'язку, м. Одеса, Україна.

**Степанов Д. М.** – канд. техн. наук, доцент, доцент кафедри комутаційних систем електронних комунікацій, Державний університет інтелектуальних технологій і зв'язку, Одеса, Україна.

**Вербицький О. О.** – директор ТОВ «Проектбудальянс», Одеса, Україна.

**Сідень С. В.** – канд. техн. наук, в.о. завідувача кафедри радіоелектронних систем і технологій, Державний університет інтелектуальних технологій і зв'язку, Одеса, Україна.

### АНОТАЦІЯ

**Актуальність.** На сьогодні заводи-лідери виробництва кабельної продукції в багатьох країнах світу виготовляють одно- та багатомодульні конструкції волоконно-оптичних кабелів (ВОК) з різними захисними покриттями та кількістю волокон. Це створює широкий ряд можливих моделей ВОК для різних вимог споживача (покупця). Проте відсутність відкритості цін на ВОК для споживача, зокрема для проектною організації, і прагнення виробника зекономити на виробництві створює необхідність в розробці та дослідженні методу оцінки ефективності ВОК багатомодульної конструкції. В роботі запропоновано зробити це шляхом аналізу низки моделей оптичних кабелів за параметрами-критеріями – коефіцієнтом компактності та коефіцієнтом економічної ефективності ВОК за діаметром.

**Мета.** Розробити метод оцінки ефективності моделей волоконно-оптичних кабелів багатомодульної конструкції за масо-габаритними показниками, що дозволить прискорено вибирати доцільну модель ВОК із заданими вихідними даними.

**Метод.** Розроблено і запропоновано метод оцінки ефективності ВОК модульної конструкції, який базується на порівнянні моделей кабелів і виборі найбільш доцільної з них при заданих вихідних даних. В роботі запропоновано та введено для цього параметри-критерії – коефіцієнт компактності  $\nu$  та коефіцієнт ефективності за діаметром кабелю  $E_0$  – які показують зв'язок характеристики конструкції ВОК до певного параметру його структури. При цьому найбільш ефективна модель (конструкція) ВОК порівняно з базовими моделями по технічним умовам, як з точки зору виробника і замовника, полягає в менших матеріаловитратах на його виробництво при одночасному забезпеченні заданих вимог до кабелю (в першу чергу, по кількості волокон та механічній міцності). Це дозволить на етапі проектування кабелю здійснити доцільний вибір його моделі з заданими вихідними параметрами та розробити таку конструкцію ВОК, яка дозволить мінімізувати габарити (а значить матеріалосміність і собівартість) моделі без втрати її кількісних та якісних характеристик.

**Результати.** В роботі приведено результати розробки та дослідження методу оцінки ефективності ВОК багатомодульної конструкції за масо-габаритними показниками. Для прикладу, використовуючи розроблений метод, показано, що можна обрати модель ВОК з діаметром меншим на 10,9 % і зекономити 15,5 % вартості кабелю на кожен кілометр ВОЛЗ при забезпеченні вихідних вимог до кабелю.

**Висновки.** Наукова новизна результатів роботи полягає в тому, що вперше розроблено метод оцінки ефективності ВОК модульної конструкції, який дозволяє на етапі проектування кабелю здійснити порівняння моделі з конструкцією кабелю по технічним умовам (ТУ) та доцільний вибір цієї моделі з заданими вихідними параметрами. Практична значущість полягає в можливості за допомогою даного методу здійснювати прискорений вибір моделі кабелю на етапі його проектування з одночасним забезпеченням необхідної ємності ВОК оптичними волокнами та мінімізації собівартості його матеріалів та габаритів.

**КЛЮЧОВІ СЛОВА:** волоконно-оптичний кабель, конструкція кабелю, геометричні розміри, масо-габаритні показники, собівартість матеріалів кабелю.

#### ЛІТЕРАТУРА

1. A Comparative Survey of Optical Wireless Technologies: Architectures and Applications/ [M. Z. Chowdhury, M. T. Hossan, A. Islam and Y. M. Jang] // IEEE Access. – 2018. – Vol. 6. – P. 9819–9840. DOI: 10.1109/ACCESS.2018.2792419.
2. Mahlke G., Gossing P. Fiber Optic Cables – Fundamentals, Cable Design, System Planning / G. Mahlke, P. Gossing. – 4<sup>th</sup> edition, MCD Corporate Publishing, Munich, 2001. – 302 p.
3. Elliott B. Fiber optic cabling (second edition) / B. Elliott, M. Gilmore. – Newnes, Elsevier, 2002, 318 p. ISBN 978-0-7506-5013-7. DOI: 10.1016/B978-0-7506-5013-7.X5000-4
4. Günter B. The global cable industry: materials, markets, products / B. Günter. – Sidney : John Wiley & Sons, 2021. – 416 p. ISBN: 978-3-527-34627-1. DOI:10.1002/9783527822263
5. Bailey D. Fiber optic cable construction / D. Bailey, E. Wright. – Amsterdam, Boston, London : Elsevier, 2003. – 288 p. DOI:10.1016/B978-075065800-3/50004-7.
6. Корчевський О. С. Механічні характеристики волоконно-оптичних кабелів / О. С. Корчевський, Л. В. Коломієць // Збірник наукових праць Одеської державної академії технічного регулювання та якості. – 2015. – Вип. 2 (7). – С. 68–72. DOI: 10.32684/2412-5288-2015-2-7-68-72.
7. Goff D. Fiber Optic Reference Guide. 3rd edition / D. Goff. – New York, 2002. – 260 p. DOI: 10.4324/9780080506319
8. Kiforuk S. V. Influence of the ambient temperature on the mechanical tension of the optical cable / S. V. Kiforuk // Zbirnik naukovih prac' Odes'koï derzavnoï akademii tehničnogo reguluvannâ ta âkosti. – 2022. – Vyp. 2(21). – P. 20–26. DOI 10.32684/2412-5288-2022-2-21-19-26
9. Thermomechanical influence on optical fibers during the production and operation of optical cable / [O. V. Bondarenko, D. M. Stepanov, S. V. Kiforuk, I. A. Slobodianiuk] // Наукові праці ОНАЗ ім. О. С. Попова. – Одеса. – 2019. – Вип. № 1. – С. 23–32. DOI:10.33243/2518-7139-2019-1-1-23-32.
10. Методологічні аспекти розрахунку повної собівартості волоконно-оптичного кабелю / [О. В. Бондаренко, П. П. Воробієнко, В. А. Коляденко, Н. Ю. Потапова-Сінько] // Науково-теоретичний журнал Хмельницького економічного університету «Наука й економіка». – Хмельницький. – 2013. – Вип. № 1 (29). – С. 164–172.
11. Вибір структури осердя оптичних кабелів багатомодульної конструкції за економічною ефективністю / [О. В. Бондаренко, Д. М. Степанов, Д. Г. Багачук та ін.] // Цифрові технології: зб. наук. праць. – Одеса. – 2016. – Вип. № 1. – С. 34–41.
12. Tingting Zhan Optimization of the optical fiber with triple sector stress elements / Tingting Zhan, Minning Ji // Optical Fiber Technology. – 2020. – Vol. 57. DOI: 10.1016/j.yofte.2020.102212.
13. Public joint-stock company “Odesa cable works ‘Odeskabel’” (2024). Fiber optic cables [Electronic resource]. – Access mode: <https://odeskabel.com/en/products/vok-kabeli.html> (accessed 20 January 2024).
14. Private joint-stock company “Yuzhcable works” (2024). Fiber optic cables [Electronic resource]. – Access mode: <https://www.yuzhcable.info/index.php?CAT=50&ENG=1> (accessed 20 January 2024).

## TWO-FRAGMENT NON-LINEAR-FREQUENCY MODULATED SIGNALS WITH ROOTS OF QUADRATIC AND LINEAR LAWS FREQUENCY CHANGES

**Kostyria O. O.** – Dr. Sc., Senior Research, Leading Research Scientist, Ivan Kozhedub Kharkiv National Air Force University, Kharkiv, Ukraine.

**Hryzo A. A.** – PhD, Associate Professor, Head of the Research Laboratory, Ivan Kozhedub Kharkiv National Air Force University, Kharkiv, Ukraine.

**Khudov H. V.** – Dr. Sc., Professor, Head of Department, Ivan Kozhedub Kharkiv National Air Force University, Kharkiv, Ukraine.

**Dodukh O. M.** – PhD, Leading Research Scientist, Ivan Kozhedub Kharkiv National Air Force University, Kharkiv, Ukraine.

**Lisohorskyi B. A.** – PhD, Senior Researcher, Ivan Kozhedub National Air Force University, Kharkiv, Ukraine.

### ABSTRACT

**Context.** The rapid development of the technology of digital synthesis and processing of radar signals, which has been observed in recent decades, has practically removed restrictions on the possibility of implementing arbitrary laws of frequency modulation of radio oscillations. Along with the traditional use of linearly-frequency-modulated signals, modern radar means use probing signals with non-linear frequency modulation, which provide a lower level of maximum side lobes and a higher rate of their descent. These factors, in turn, contribute to improving the detection characteristics of targets under conditions of passive interference, as well as increasing the probability of detecting small targets against the background of targets with larger effective scattering surfaces. In this regard, a large number of studies are conducted in the direction of further improvement of existing and synthesis of radar signals with new laws of frequency modulation. The use of multifragment nonlinear-frequency-modulated signals, which include fragments with both linear and nonlinear modulation, provides an increase in the number of possible versions of the laws of frequency modulation and synthesis of signals with predicted characteristics. Synthesis of new multifragment signals with a reduced level of side lobes of autocorrelation functions and a higher rate of their descent is an important scientific and technical task, the solution of which is devoted to this article.

**Objective.** The purpose of the work is to develop mathematical models of the current and shifted time of two-fragment nonlinear-frequency modulated signals for the case when the first fragment has a root-quadratic, and the second linear frequency modulation and determine the feasibility of using such a signal in radar applications.

**Method.** The article theoretically confirms that for the mathematical model of the current time, when moving from the first fragment to the second at the junction of fragments, jumps of instantaneous frequency and phase (or only phases for the mathematical model of shifted time) occur, which can significantly distort the resulting signal. Determination of value of frequency-phase jumps for their further elimination is performed by finding difference between value of initial phase of second fragment and final value of phase of first fragment. A distinctive feature of the developed mathematical models is the use of the first fragment of the signal with root-quadratic, and the second – linear frequency modulation.

**Results.** Comparison of the signal, the first fragment of which has root-square frequency modulation, and the signal with two linearly-frequency-modulated fragments, provided that the total duration and frequency deviation are equal, shows that for the new synthesized signal the maximum level of side lobes decreased by 1.5 dB, and their rate of decay increased by 6.5 dB/dec.

**Conclusions.** A new two-fragment signal was synthesized, the first fragment of which has root-quadratic, and the second – linear frequency modulation. Mathematical models of the current time and with a time shift for calculating the values of the instantaneous phase of such a signal have been developed. A distinctive feature of these models is the presence of components to compensate for frequency-phase distortions, taking into account the modulation law of the frequency of the first fragment. The resulting oscillograms, spectra and autocorrelation functions of the synthesized two-fragment signals do not contradict the known theoretical position, which indicates the reliability and adequacy of the proposed mathematical models.

**KEYWORDS:** mathematical model; non-linear frequency modulation; maximum level of side lobes.

### ABBREVIATIONS

ACF is an autocorrelation function;  
SL is a side lobe;  
ML is a main lobe;  
PWM is a pulse-width modulation;  
WP is a weight processing;  
RQFM is a roots of quadratic frequency modulation;  
LFM is a linear frequency modulation;  
MM is a mathematical model;  
MPSLL is a maximum peak side lobe level;  
NLFM is a non-linear frequency modulation;

PSLL is a peak side lobe level;  
REQ is a radio electronic equipment  
RP is a radio pulse;  
FM is a linear frequency modulation;  
FMR is a frequency modulation rate;  
DDS is a digital discrete synthesis;  
DSP is a digital signal processor;  
FPGA is a field-programmable gate array;  
SDR is a software-defined radio;  
PLL is a phase-locked loop.

## NOMENCLATURE

$B_S$  is a time-bandwidth product;  
 $\Delta f_S$  is a frequency deviation of the signal, Hz;  
 $\Delta f_n$  is a frequency deviation of the  $n^{\text{th}}$  signal fragment NLFM, Hz;  
 $T_S$  is a weight of the signal, s;  
 $n=1, 2$  is a serial number signal fragment NLFM;  
 $f_0$  is a initial signal frequency, Hz;  
 $t$  is a current time, s;  
 $T_n$  is a duration of the  $n^{\text{th}}$  signal fragment NLFM, s;  
 $T_{12}$  is a sums of duration of the first and second fragments, s;  
 $\varphi_n(t)$  is a instantaneous phase  $n$ -ro signal fragment NLFM, rad;  
 $\beta_n$  is a FMR  $n^{\text{th}}$  signal fragment NLFM, Hz/s;  
 $\Delta\beta_{21}$  is a difference FMR  $2^{\text{nd}}$  and  $1^{\text{th}}$  fragments, Hz/s;  
 $\beta_{1N}$  is a average FMR  $1^{\text{th}}$  fragment, Hz/s;  
 $\beta_{1E}$  is a ultimate FMR  $1^{\text{th}}$  fragment, Hz/s;  
 $\delta\varphi_{12}$  is a component to compensate for phase jump at fragment junction, rad.

## INTRODUCTION

The widespread use of digital synthesis and radar signal processing due to the introduction of new capabilities of DDS, DSP, FPGA, SDR technologies [1–10] provides the use of signals with various types of PWM [11–16]. Signals with PWM frequency (phase) are called complex signals, among them the most widely used are signals with LFM. Such signals ensure preservation of required distinguishing ability from range in case of increase of radar probing signal duration to increase its energy potential [11–13, 15, 17–22]. Scientific research is actively carried out to improve the technical characteristics of REQ by using complex signals with different types of PWM from LFM, one of the directions is to minimize the value of MPSLL ACF radar signals.

As a rule, this is achieved by selecting the type of modulation of the probe signal [11–24] or by WP of the reflected radio frequency oscillation in the radar receiver [25, 26]. It is also possible to jointly apply the above methods [27–29], which can potentially provide a better result. The effectiveness of the use of WP depends significantly on such a parameter as the rate of decrease in the SL of ACF signals. Therefore, when selecting a probe signal, in addition to the MPSLL, attention should also be paid to the value of the SL descent rate, which should be as achievable as possible.

The choice of the PWM type of the probe signal can be based on the analysis of its spectral characteristics – a sign of a decrease in the ACF MPSLL is the rounding of the signal spectrum, that is, the approximation of its shape to the bell-shaped one. This effect can be achieved by using nonlinear frequency modulation, namely, by in-

creasing the FM, which is a derivative of the instantaneous frequency  $\beta(t) = df(t)/dt$ . In this case, the FM can have both a constant (linear frequency change) and a variable value (non-linear FM). Such signals are related to NLFM signals, they can be formed by sequentially joining fragments in time with linear and nonlinear FM. There are MM two- and three-fragment NLFM signals [30–34]. Single-fragment signals with polynomial, tangential, S-shaped and other types of FM are also known [35–39]. NLFM signals also include phase-manipulated signals [41].

This article is devoted to the consideration of the features of the formation of multi-fragment, namely two-fragment NLFM signals.

There is no doubt that three-fragment NLFM signals provide lower MPSLL compared to two-fragment signals, and therefore their use is more expedient. However, two-fragment signals should not be excluded from consideration, since they are significantly easier to implement, richly illustrative and allow more efficient testing of new theoretical hypotheses and putting into practice the results obtained. Such signals should be used at the initial stage of research to debug MM and develop software products for their practical reproduction.

The research is based on the hypothesis that it is possible to synthesize an NLFM signal with a lower MPSLL and a higher rate of decline of the SL if one of the fragments in the low frequency region has a more rounded shape.

The article considers the case when the first fragment of the NLFM signal has a root-quadratic, and the second – linear FM.

**The object of study** is the process of forming and processing two-fragment NLFM signals.

**The subject of study** are mathematical models of NLFM signals, which consist of two fragments of the RQFM-LFM type.

**The purpose of the work** is to develop the MM of the current and shifted time of the RQFM-LFM signal and determine the feasibility of using such a signal in radar applications.

## 1 PROBLEM STATEMENT

The authors [33], along with NLFM signals, which consist of LFM fragments, consider signals, one of the fragments of which has a nonlinear law of frequency change, for example, exponential. They are also considered as independent tangential, polynomial, S-shaped and other laws of frequency modulation [14, 35–39], which provide two-sided or one-sided rounding of the signal spectrum.

A distinctive feature of the signal with RQFM in comparison with the classical LFM signal is the rounding of the spectrum in the low frequency region, which makes it attractive to use it as one of the fragments for the synthesis of multi-fragment NLFM signals. It is to be expected that the NLFM signals, when included in their composition of the RQFM fragment, will have better

characteristics with MPSLL compared to signals consisting only of LFM fragments.

To determine the features of the synthesis of NLFM signals using RQFM fragments, it is proposed to first consider the option of a two-fragment RQFM-LFM signal with the development of the current and shifted time MM.

The authors of the article propose to consider two-fragment NLFM signals, the first fragment of which has RQFM, that is, its instantaneous frequency changes in accordance with the expression:

$$f_1(t) = f_0 + \beta_{1N} \sqrt{T_1 t}, \quad (1)$$

where  $\beta_{1N} = \frac{\Delta f_1}{T_1}$  – average FMR 1<sup>th</sup> fragment RQFM NLFM signal.

As the initial, let's take the MM of the current time of the NLFM signal with frequency-phase distortion compensation, which consists of two LFM fragments [40]:

$$\varphi(t) = \begin{cases} 2\pi \left[ f_0 t + \frac{\beta_1 t^2}{2} \right], & 0 \leq t \leq T_1; \\ 2\pi \left[ (f_0 - \Delta\beta_{21} T_1) t + \frac{\beta_2 t^2}{2} \right] + \delta\varphi_{12}, & T_1 \leq t \leq T_{12}; \end{cases} \quad (2)$$

where  $\delta\varphi_{12} = \pi T_1^2 \beta_{21}$ ;  $\beta_n = \Delta f_n / T_n$ ;  $\Delta\beta_{21} = \beta_2 - \beta_1$ ;  $T_{12} = T_1 + T_2$ .

The current instantaneous phase component, which compensates for frequency jumps during the transition from the first fragment to the second, is calculated as  $\Delta\beta_{21} T t$ .

As the initial MM shifted time, we also use the NLFM signal with two LFM fragments [41] of the form:

$$\varphi_n(t) = \begin{cases} 2\pi \left[ f_0 t + \frac{\beta_1 t^2}{2} \right], & 0 \leq t \leq T_1; \\ 2\pi \left[ (f_0 + \Delta f_1)(t - T_1) + \beta_2 \left( \frac{t^2}{2} - T_1 t \right) \right] - \delta\varphi_{12}, & T_1 \leq t \leq T_{12} \end{cases} \quad (3)$$

where  $\delta\varphi_{12} = -\pi T_1^2 (\beta_2 + \beta_1)$ .

It is expected that due to the instantaneous change in FMR at the joints of RQFM and LFM fragments, instantaneous frequency and phase jumps (or only phases for MM shifted time) will occur, as is justified in [40, 41], but the expressions for calculating the magnitude of these jumps will be different, and therefore the resulting MM will be new, which is the result research.

The effectiveness of the use of new MMs is evaluated by achievable MPSLL, the rate of reduction of SL

and the width of ML ACF signals, which is measured at 0.707 of the maximum value, compared to the previously obtained in the works [14, 27–41]. Also, when comparing the results obtained, the value of the signal base should be taken into account  $B_S = \Delta f_S T_S$ , that is, the product of the deviation of the signal frequency by its duration, since with a decrease in  $B_S$ , the MPSLL ACF value usually increases.

## 2 REVIEW OF THE LITERATURE

New opportunities for digital synthesis and digital processing of radar signals, which are provided by DDS, DSP, FPGA, SDR technologies, allow to radically revise approaches to the development of a new and improvement of the existing REQ. The stimulator of this process is DDS [1, 2], which provides the development of increasingly high-frequency radio bands. The emergence of such a tool as DSP [3, 4] at one time made a significant improvement in the efficiency of DSP systems in relation to the range of operating frequencies and their band. In the future, the FPGA [5–9] combines DDS with PLL, provides DSP functions, which allows you to quickly change the operating modes of radar equipment by changing the operating frequency, type of probe signal and operating frequency band. SDR technology [10] is now more of a tool for scientific researchers and REQ developers, as due to versatility it can have excessive hardware redundancy.

The above indicates that there is a practical possibility of introducing new types of probing signals with different types of PWM into REQ.

Theoretically, the feasibility of using probing LFM and RQFM signals [11–13, 15, 17–22], which historically were the first among complex signals, has been proved in practice. The authors of these publications define as complex such signals, the base of which, that is, the product of the duration of RP by the width of its frequency band, is more than one. In addition to LFM and RQFM, signals with non-linear PWM frequencies – NLFM signals [11–24, 27–41] are also complex.

The nonlinear PWM frequency allows increasing FRM at the edges of the RP, as a result of which the signal spectrum is rounded, which is equivalent to the WP signal in the time domain [25, 26], but the bypass RP remains rectangular and the energy loss in the radio transmitter does not increase.

Varieties of NLFM signals are widely considered by the authors [14, 27–41], these works are devoted to the problem of improving the characteristics of REQ by reducing MPSLL, which is achieved due to the WP signal in the radio receiver [25, 26], rounding the signal spectrum [14, 30–41] or the simultaneous use of these methods [27–29].

Reduction of MPSLL can be achieved by synthesizing a new type of signal, as described in [33]. The authors proposed a two-fragment NLFM signal, the first fragment of which has an exponential FM.

It is appropriate to clarify the feasibility of using fragments with other non-linear types of FM, which can

also provide rounding of the signal spectrum and reduce MPSLL.

New opportunities for digital synthesis and digital processing of radar signals, which are provided by DDS, DSP, FPGA, SDR technologies, allow to radically revise approaches to the development of a new and improvement of the existing REQ. The stimulator of this process is DDS [1, 2], which provides the development of increasingly high-frequency radio bands. The emergence of such a tool as DSP [3, 4] at one time made a significant improvement in the efficiency of DSP systems in relation to the range of operating frequencies and their band. In the future, the FPGA [5–9] combines DDS with PLL, provides DSP functions, which allows you to quickly change the operating modes of radar equipment by changing the operating frequency, type of probe signal and operating frequency band. SDR technology [10] is now more of a tool for scientific researchers and REQ developers, as due to versatility it can have excessive hardware redundancy.

The above indicates that there is a practical possibility of introducing new types of probing signals with different types of PWM into REQ.

Theoretically, the feasibility of using probing LFM and RQFM signals [11–13, 15, 17–22], which historically were the first among complex signals, has been proved in practice. The authors of these publications define as complex such signals, the base of which, that is, the product of the duration of RP by the width of its frequency band, is more than one. In addition to LFM and RQFM, signals with non-linear PWM frequencies – NLFM signals [11–24, 27–41] are also complex.

The nonlinear PWM frequency allows increasing FRM at the edges of the RP, as a result of which the signal spectrum is rounded, which is equivalent to the WP signal in the time domain [25, 26], but the bypass RP remains rectangular and the energy loss in the radio transmitter does not increase.

Varieties of NLFM signals are widely considered by the authors [14, 27–41], these works are devoted to the problem of improving the characteristics of REQ by reducing MPSLL, which is achieved due to the WP signal in the radio receiver [25, 26], rounding the signal spectrum [14, 30–41] or the simultaneous use of these methods [27–29].

Reduction of MPSLL can be achieved by synthesizing a new type of signal, as described in [33]. The authors proposed a two-fragment NLFM signal, the first fragment of which has an exponential FM.

It is appropriate to clarify the feasibility of using fragments with other non-linear types of FM, which can also provide rounding of the signal spectrum and reduce MPSLL.

### 3 MATERIALS AND METHODS

Using the methods [40] and (1), we determine the final phase of the first fragment and the initial phase of the second fragment of the RQFM-LFM signal for the time  $t=T_1$ . It should be noted that the FMR of a fragment with RQFM is a time variable, its instantaneous value is:

$$\beta_1(t) = \frac{\beta_{1N}}{2} \sqrt{\frac{T_1}{t}}$$

and at time  $t=T_1$ , the final FMR value is:

$$\beta_{1E} = \beta_1(T_1) = \frac{\beta_{1N}}{2}. \quad (4)$$

We have expressions for the final phase of the first and the initial phase of the second fragment:

$$\varphi_{E1} = 2\pi \left( f_0 T_1 + \frac{2}{3} \beta_{1E} T_1^2 \right); \quad (5)$$

$$\varphi_{S2} = 2\pi \left( f_0 T_1 + \frac{1}{2} \beta_{2E} T_1^2 \right) \quad (6)$$

and taking into account (4)–(6) the phase jump at the junction of the fragments is equal to:

$$\delta\varphi_{12} = 2\pi T_1^2 \left( \frac{\beta_2}{2} - \frac{\beta_{1N}}{3} \right). \quad (7)$$

Thus, based on (1), (2) and (7), the MM for calculating the instantaneous phase of the two-fragment NLFM signal in the current time, if the frequency of the first fragment changes according to the root-square law, has the form:

$$\varphi(t) = \begin{cases} 2\pi \left[ f_0 t + \frac{2\beta_{1N} \sqrt{t^3 T_1}}{3} \right], & 0 \leq t \leq T_1; \\ 2\pi \left[ (f_0 - \Delta\beta_{21} T_1) t + \frac{\beta_2 t^2}{2} \right] - \delta\varphi_{12}, & T_1 \leq t \leq T_{12} \end{cases} \quad (8)$$

An MM of the current time of the two-fragment NLFM signal (8) is obtained, which provides determining a frequency jump at the junction of fragments in the case when the first fragment is a signal from RQFM, which, in turn, allows compensating for the corresponding phase jump and taking into account the change in instantaneous frequency when switching to the second fragment.

These results can be applied to the development of an MM shifted time for a similar signal in which the frequency jump at the junction of fragments is compensated automatically.

Using (1), (3), (4) and the results of the studies [41], the phase jump at the fragment junction for MM shifted time is defined as:

$$\delta\varphi_{12} = -\pi T_1^2 \left( \beta_2 + \frac{4\beta_{1N}}{3} \right). \quad (9)$$

Using (1), (3) and (9), we record the MM of the shifted time to calculate the instantaneous phase of the two-fragment NLFM signal, the first fragment of which is the signal from RQFM:

$$\varphi(t) = \begin{cases} 2\pi \left[ f_0 t + \frac{2\beta_{1N} \sqrt{t^3 T_1}}{3} \right], & 0 \leq t \leq T_1 \\ 2\pi \left[ (f_0 + \Delta f_1)(t - T_1) + \frac{\beta_2 (t^2 - T_1 t)}{2} \right] - \delta\varphi_{12}, & T_1 \leq t \leq T_{12} \end{cases} \quad (10)$$

Model (10) differs from (8) in the form of time representation and is fully adequate to it. That is, (8) and (10) allow you to get the same final result in different mathematical ways, which is evidence of their fairness and reliability.

#### 4 EXPERIMENTS

The operability of the two-segment NLFM signals developed by MM, in which the first fragment has RQFM, was checked using the MATLAB application package.

To determine the advantages and disadvantages of the new synthesized RQFM-LFM signal, three more complex signals were simulated: single-fragment (LFM, RQFM) and two-fragment (LFM-LFM) with equivalently identical frequency-time parameters. That is, the total duration and frequency deviation of two-fragment signals is equal to the duration and frequency deviation of single-fragment signals that were taken for research. The following signal characteristics were measured and compared:

- MPSLL value;
- SL descent rate;
- ML ACF signal width at the level of 0.707 of the maximum value.

For a more detailed analysis of RQFM-LFM signals, a group of five signals was studied, for one of which graphic material was provided. Also, for comparison, a graphic material for single-fragment LFM and RQLF signals was obtained, the frequency-time parameters of which coincide with the parameters of one of the RQLF-LFM signals (No. 3, Table 2).

#### 5 RESULTS

The results of studies of single-fragment LFM, RQFM and two-fragment LFM-LFM, RQFM-LFM signals are summarized in Table 1.

Comparison of results for LFM and RQFM signals shows that the RQFM signal has a larger ML ACF width, this is evidence of a decrease in the effective signal spectrum width, which is perfectly logical, since the LFM spectrum of Fig. 1a compared to the RQFM spectrum of Fig. 2b has a more rectangular shape, that is, in the same frequency band, the power spectral density of the RQFM signal is less than that of the LFM signal.

Table 1 – Results of experimental studies of NLFM signals of different types with equivalent frequency-time parameters

Type of signal	$T_1, \mu\text{s}$	$T_2, \mu\text{s}$	$\Delta f_1, \text{kHz}$	$\Delta f_2, \text{kHz}$	MPSLL, dB	Decline of SL, dB/s	ML ACF, $\mu\text{s}$
LFM	120	–	600	–	-13.43	19.65	0.75
RQFM	120	–	600	–	-13.47	19.55	0.92
LFM-LFM	20	100	200	400	-17.31	17.42	0.83
RQFM-LFM	40	80	400	200	-19.0	24.0	1.03

The MPSLL values and the SL decay rates of these signals are virtually indistinguishable.

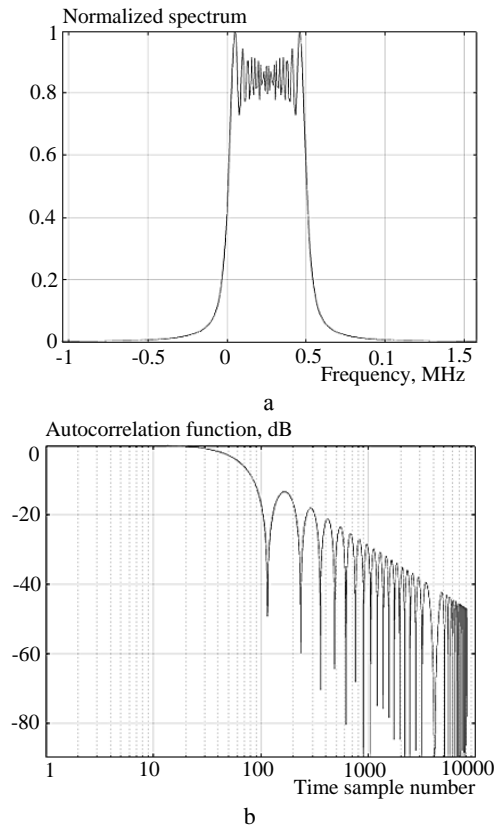


Figure 1 – Spectrum (a), ACF (b) LFM signal

It should be noted that the amplitude of the pulsations of the SL ACF LFM signal (spurious oscillations at the output of the matched filter) exceeds 20 dB (Fig. 1b), for the RQFM signal this value averages 5 dB (Fig. 2c), and therefore the use of WP for such signals should give the best effect.

Table 2 shows the values of frequency-time parameters of the studied two-fragment RQFM-LFM signals calculated in accordance with MM (8). The use of MM (10) provides identical results.

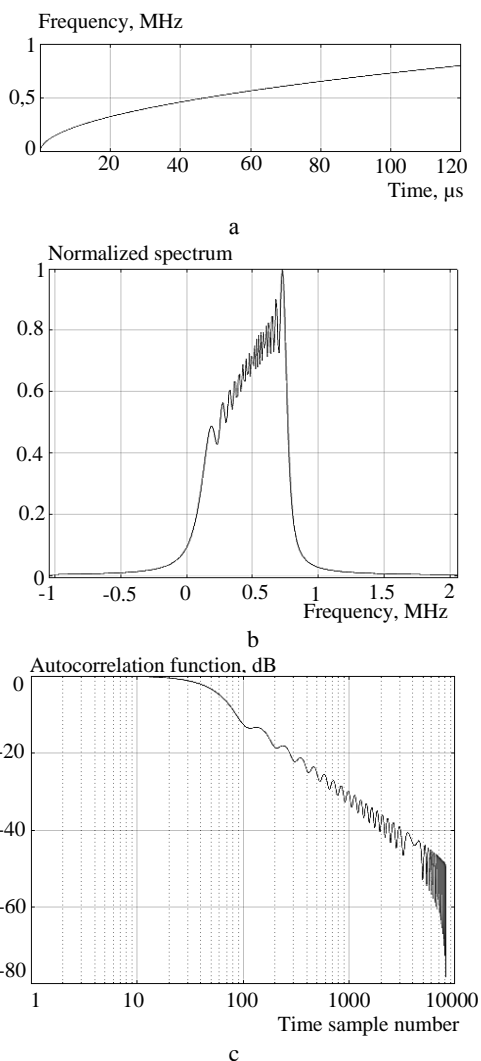


Figure 2 – Frequency change plot (a), spectrum (b), ACF (c) signal with RQFM

Table 2 – Results of experimental studies of two-fragment RQFM-LFM signals

No	$T_1, \mu\text{s}$	$T_2, \mu\text{s}$	$\Delta f_1, \text{kHz}$	$\Delta f_2, \text{kHz}$	MPSLL, dB	Decline of SL, dB/s
1.	20	40	500	300	-20.76	21.5
2.	40	80	500	100	-20.0	26.5
3.	40	80	500	300	-19.71	22.3
4.	80	160	500	300	-19.38	22.6
5.	80	160	600	400	-20.16	20.0

A comparative analysis of the results of Table 1 and Table 2 indicates that, provided the frequency-time parameters of signals such as RQFM-LFM and LFM-LFM are equal, the MPSLL decrease for the new signal is approximately from 1.5 dB to almost 2.7 dB, and the SL decrease rate increase in this case, from 6.6 dB/dec. up to 9.1 dB/dec.

The result of comparing the graphic material for RQFM (Fig. 2) and RQFM-LFM (Fig. 3) signals is interesting. Graphs of the instantaneous frequency change over time in Fig. 2a and Fig. 3a have insignificant differences at the mark of 40  $\mu\text{s}$  – Fig. 3a shows a slight decrease in

the characteristic. In this case, the signal spectra of Fig. 2b and Fig. 3b differ significantly. Figure 3b clearly shows both spectral components of the signal, the transition between them without gaps and differences. That is, there are no frequency and phase jumps at the junction of the fragments.

Based on the results of comparative analysis of ACF signals, the following should be noted. As a result of the combination of two types of FM, the first SL RQFM signal (see. Fig. 2c) on the ACF graph, the RQFM-LFM signal merged with ML (Fig. 3c), as a result of which the width of ML at the minimum level increased, the dip between the first SL and the second SL increased, as a result of which the level of the second SL from -18 dB decreased to -22 dB and the third petal became the maximum at -20 dB. The amplitude of pulsations SL in Fig. 3v compared to Fig. 2b increased by 2–3 dB, but it is significantly less than for the single-fragment LFM signal Fig. 1b. These changes with other digital values are observed in the ACF graphs of RQFM-LFM signals with identical frequency-time parameters, which are included in Table 2.

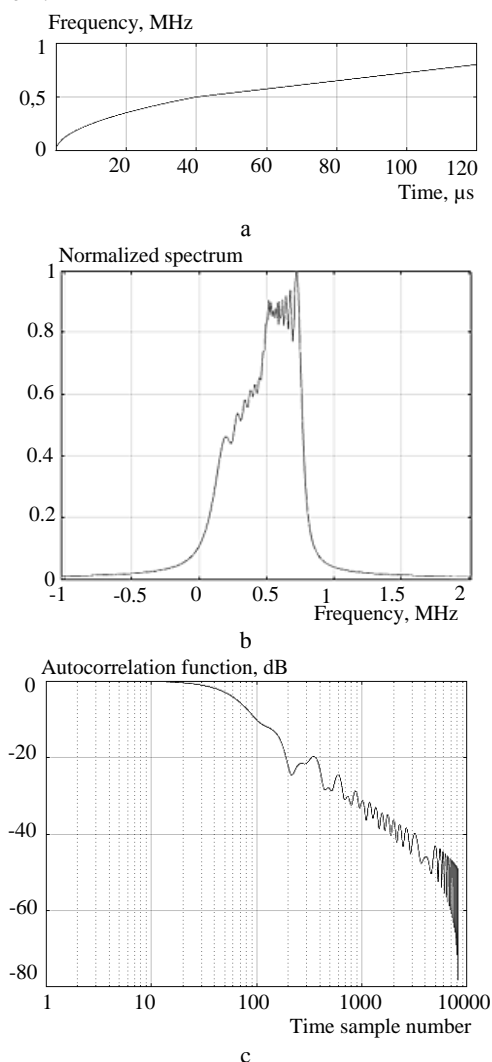


Figure 3 – Frequency change plot (a), spectrum (b), ACF (c) signal from RQFM-LFM

To demonstrate the potentially achievable characteristics, Fig. 4 shows the results of modeling the RQFM-LFM signal with the following parameters:  $f_0 = 0$ ,  $\Delta f_1 = 550$  kHz,  $\Delta f_2 = 100$  kHz,  $T_1 = 20$   $\mu$ s,  $T_2 = 40$   $\mu$ s.

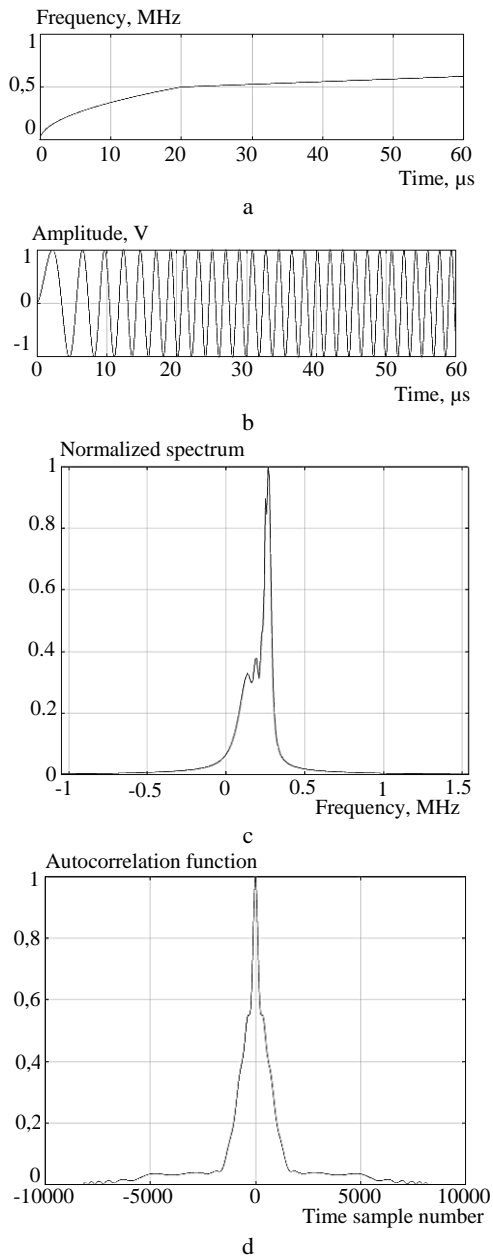


Figure 4 – Frequency change plot (a), oscillogram (b), spectrum (c), ACF (d) RQFM-LFM signal with parameters:  $f_0 = 0$ ,  $\Delta f_1 = 550$  kHz,  $\Delta f_2 = 100$  kHz,  $T_1 = 20$   $\mu$ s,  $T_2 = 40$   $\mu$ s

The frequency change graph of Fig. 4a and the oscillogram of Fig. 4b indicate the absence of abrupt changes in the instantaneous frequency and phase of the signal, which also confirms the appearance of its spectrum of Fig. 4c. For better clarity of the result, the ACF plot is shown on a linear scale. The MPSLL value is  $-26.9$  dB and the SLL decay rate is estimated at 30 dB/dec. ACF

shows the merger of ML with SL, due to which its width at the minimum level has significantly expanded, however, at 0.707 from the maximum value that determines the discriminating ability from the range to the location objects, the ML ACF extension is acceptable.

The ratio of duration and frequency deviations of RQFM and LFM fragments is determined, according to which MMs ensure the absence of frequency and phase jumps (or only phase) at the junction of NLFM signal fragments. For the duration of fragments, the ratio of 1:2 is optimal, that is, the LFM fragment must be twice as long as the RQFM fragment. For frequency deviations, the range of change in the ratio between fragments is significantly larger – from 6:5 to 5:1. If this value is 1:1 and with a subsequent increase in the contribution of the LFM fragment to the ACF of the resulting signal, the RQFM increases and it begins to approach the ACF LFM signal in appearance and characteristics, which is quite logical.

## 6 DISCUSSION

The two-fragment NLFM signals considered in [35] mainly have the form LFM-LFM, the MPSLL obtained for this case is at the level of  $-16.5$  dB, which is a very real result in the absence of phase jump compensation in MM shifted time, which was used. In [33], a two-fragment NLFM signal is proposed, the first fragment of which has an exponential FM, the smallest MPSLL ACF value is  $-25.96$  dB at  $B_S = 200$ . As a result of the studies performed, this result was improved by 0.94 dB with  $B_S = 39$ , that is, such an MPSLL value is obtained for the low-base ( $B_S < 100$ ) signal.

The achieved MRBP level of synthesized RQFM-LFM signals practically reaches (on average, about 1–2 dB worse) MPSLL three-fragment NLFM signals consisting of LFM fragments. However, compared to the latter, the new signals have a wider range of changes in the input frequency parameters and provide a higher SLL decay rate. Therefore, in the case of WP application, an improvement in the results of further MPSLL reduction as compared to the above signals is to be expected.

## CONCLUSIONS

**The scientific novelty.** As a result of the studies, a new two-fragment NLFM signal was synthesized, which consists of RQFM and LFM fragments. Two new MMs (current time and with time shift) have been developed to calculate the instantaneous phase values of such a signal. Studies of MM have demonstrated their mutual compliance and adequacy, which is evidence of their reliability. The combination of RQFM and LFM fragments allows you to get an NLFM signal with a reduced MPSLL level and a higher SLL decay rate. A feature of using RQFM fragments in a two-fragment NLFM signal has been revealed. This feature is that to calculate the frequency parameters of the RQFM fragment, it is necessary to use the average value of FMR  $\beta_{1N}$ , and to determine the components of the frequency-phase correction, take the final

FMR value for the fragment, which is half the average, that is,  $\beta_{1N}/2$ . By mathematical modeling, it is determined that the MPSLL for the studied group of five NLFM signals ranges from  $-19.38$  dB to  $-20.76$  dB, and the SLL decay rate varies from 19 dB/dec to 22 dB/dec, which is on average more than in the case of using only LFM fragments. Comparison with the LFM-LFM type signal for the same frequency-time parameters demonstrates a decrease in MPSLL by 1.5 dB, an increase in the SLL decay rate by 6.5 dB/dec, however, the ML ACF width increased by 24%, which is the price for improving the previous characteristics. Analysis of the obtained oscillograms, spectra and ACF synthesized NLFM signals shows no distortion at the joints of fragments, which indicates that the values of frequency-phase (or only phase) jumps are determined correctly and fully compensated.

**The practical significance** of the obtained results lies in the possibility of using the synthesized NLFM signal for use as a probe in a variety of radar facilities. In addition to the above advantages RQFM-LFM signal is its insensitivity to change the ratio of frequency deviations RQFM and LFM fragments in contrast to LFM-LFM signals. That is, in the case of practical application, the RQFM-LFM type signal will provide greater variability in the frequency parameters of the probe signal without changing the total frequency deviation, which will improve the characteristics of the radar in terms of noise immunity and electronic compatibility.

**Prospects for further research.** In the future, it is planned to develop MM three-fragment NLFM signals that use fragments with a nonlinear law of frequency modulation.

#### ACKNOWLEDGEMENTS

We thank the management of Ivan Kozhedub Kharkiv National Air Force University for the opportunity to conduct scientific research.

#### REFERENCES

1. Lei T., Liang L. Research and design of digital unit for direct digital frequency synthesizer, International Conference on Electronic Materials and Information Engineering (EMIE 2021), *Journal of Physics: Conference Series*, 2021, Vol. 1907, №012004. DOI:10.1088/1742-6596/1907/1/012004.
2. Liu X., Luong H. C. A Fully Integrated 0.27-THz Injection-Locked Frequency Synthesizer With Frequency-Tracking Loop in 65-nm CMOS, *IEEE Journal of Solid-State Circuits*, 2020, Vol. 55, Issue 4, pp. 1051–1063. DOI: 10.1109/JSSC.2019.2954232.
3. Blackledge J. Digital Signal Processing. Dublin, Horwood Publishing, second edition, 2006, 840 p.
4. Li Tan. Digital Signal Processing. Fundamentals and Applications. Georgia, Academic Press, 2008, 816 p.
5. Zhang J., Zhang R., Dai Y. Design and FPGA implementation of DDS based on waveform compression and Taylor series, *2017 29th Chinese Control And Decision Conference (CCDC), 2017, Computer Science, Engineering*, pp. 1301–1306. DOI:10.1109/CCDC.2017.7978718.
6. Genovese M., Napoli E., De Caro D. et al. Analysis and comparison of Direct Digital Frequency Synthesizers implemented on FPGA, *Integration*, 2014, Vol. 47, Issue 2, pp. 261–271.
7. Anil A., Prasad A. FPGA Implementation of DDS for Arbitrary wave generation, *International Journal of Engineering Research and Applications*, 2021, Vol. 11, Issue 7, (Series-II) pp. 56–64. DOI: 10.9790/9622-1107025664.
8. Obadi A. B., Soh P. J., Aldayel O. et al. Detection Using Radar Techniques and Processing With FPGA Implementation, *IEEE Circuits and Systems Magazine*, 2021, Vol. 21, Issue 1, pp. 41–74.
9. Liao X., Zhang L., Hu X. et al. FPGA Implementation of a Higher SFDR Upper DDFS Based on Non-Uniform Piecewise Linear Approximation, *Applied Sciences*, 2023, Vol. 13, Issue 19, №10819. <https://doi.org/10.3390/app131910819>.
10. Vankka J. Digital Synthesizers and Transmitters for Software Radio. New York: Springer, 2005, 359 p. DOI: 10.1007/1-4020-3195-5.
11. Skolnik M. I. Radar Handbook. Editor in Chief. Boston, McGraw-Hill Professional, second edition, 1990, 846 p.
12. Cook C. E., Bernfeld M. Radar Signals: An Introduction to Theory and Application. Boston, Artech House, 1993, 552 p.
13. Levanon N., Mozeson E. Radar Signals. New York, John Wiley & Sons, 2004, 403 p.
14. Saleh M., Omar S.-M., E. Grivel et al. A Variable Chirp Rate Stepped Frequency Linear Frequency Modulation Waveform Designed to Approximate Wideband Non-Linear Radar Waveforms, *Digital Signal Processing*, 2021, Vol. 109, №102884.
15. Van Trees H. L. Detection, Estimation, and Modulation Theory. New York, John Wiley & Sons, 2004, 716 p.
16. Xu Z., Wang X., Wang Y. Nonlinear Frequency-Modulated Waveforms Modeling and Optimization for Radar Applications, *Mathematics*, 2022, Vol. 10, №3939. DOI: 10.3390/math10213939.
17. Meikle H. Modern radar systems. London, Artech House, second edition, 2008, 701 p.
18. Curry G. R. Radar System Performance Modeling. London, Artech House, second edition, 2004, 410 p.
19. Barton D. K. Radar System Analysis and Modeling. London, Artech House, 2005, 545 p.
20. Richards M. A., Scheer J. A., Holm W. A. Principles of modern radar. SciTech Publishing, 2010, 924 p.
21. Mervin C., Budge J., Shawn R. G. Basic Radar Analysis. London, Artech House, 2015, 727 p.
22. Melvin W. L., Scheer J. A. Principles of modern radar. New York, SciTech Publishing, 2013, 846 p.
23. Cook C.E. A class of nonlinear FM pulse compression signals, *Proc. IEEE*, 1964, Vol. 52, pp. 1369 – 1371.
24. Cook C. E, Paolillo J. A pulse compression predistortion function for efficient side lobe reduction in a high-power radar. Proceedings of the IEEE, 1964, Vol. 52(4), pp. 377–389. DOI: 10.1109/proc.1964.2927.
25. Heinzel G., Rüdiger A., Schilling R. Spectrum and spectral density estimation by the Discrete Fourier transform (DFT), including a comprehensive list of window functions and some new flattop windows [Electronic resource]. Access mode: [https://pure.mpg.de/rest/items/item\\_52164\\_1/component/file\\_152163/content](https://pure.mpg.de/rest/items/item_52164_1/component/file_152163/content).
26. Doerry A. W. Catalog of Window Taper Functions for Side lobe Control [Electronic resource]. Access mode:

- [https://www.researchgate.net/publication/316281181\\_Catalog\\_of\\_Window\\_Taper\\_Functions\\_for\\_Sidelobe\\_Control](https://www.researchgate.net/publication/316281181_Catalog_of_Window_Taper_Functions_for_Sidelobe_Control).
27. Ghavamirad R., Sebt M. A. Side Lobe Level Reduction in ACF of NLFM Waveform, *IET Radar, Sonar & Navigation*, 2019, Vol. 13, Issue 1, pp. 74–80.
  28. Chukka A., Krishna B. Peak Side Lobe Reduction analysis of NLFM and Improved NLFM Radar signal, *AIUB Journal of Science and Engineering (AJSE)*, 2022, Vol. 21, Issue 2, pp. 125–131.
  29. Parwana S., Kumar S. Analysis of LFM and NLFM Radar Waveforms and their Performance Analysis, *International Research Journal of Engineering and Technology (IRJET)*, 2015, Vol. 02, Issue 02, pp. 334–339.
  30. Zhao Y., Ritchie M., Lu X. et al. Non-continuous piecewise nonlinear frequency modulation pulse with variable sub-pulse duration in a MIMO SAR Radar System, *Remote Sensing Letters*, 2020, Vol. 11, Issue 3, pp. 283–292.
  31. Jeyanthi J. E., Shenbagavalli A., Mani V.R.S. Study of Different Radar Waveform Generation Techniques for Automatic Air Target Recognition, *International Journal of Engineering Technology Science and Research (IJETSR)*, 2017, Vol. 4, Issue 8, pp. 742–747.
  32. Adithyavalli N. An Algorithm for Computing Side Lobe Values of a Designed NLFM function, *International Journal of Advanced Trends in Computer Science and Engineering*, 2019, Vol. 8, Issue 4, pp. 1026–1031. DOI:10.30534/ijatcse/2019/07842019.
  33. Valli N. A., Rani D. E., Kavitha C. Modified Radar Signal Model using NLFM, *International Journal of Recent Technology and Engineering (IJRTE)*, 2019, Vol. 8, Issue 2S3, pp. 513–516. DOI: 10.35940/ijrte.B1091.0782S319.
  34. Kavitha C., Valli N. A., Dasari M. Optimization of two-stage NLFM signal using Heuristic approach, *Indian Journal of Science and Technology*, 2020, Vol. 13(44), pp. 4465–4473. DOI:10.17485/IJST/v13i44.1841.
  35. Chukka A., Krishna B. Peak Side Lobe Reduction analysis of NLFM and Improved NLFM Radar signal, *AIUB Journal of Science and Engineering (AJSE)*, 2022, Vol. 21, Issue 2, pp. 125–131.
  36. Fan Z., Meng H.-Y. Coded excitation with Nonlinear Frequency Modulation Carrier in Ultrasound Imaging System, *IEEE Far East NDT New Technology & Application Forum (FENDT)*. Kunming, Yunnan province, China, 20–22 November 2020, pp. 31–35.
  37. Song C., Wang Y., Jin G. et al. A Novel Jamming Method against SAR Using Nonlinear Frequency Modulation Waveform with Very High Side Lobes, *Remote Sensing*, 2022, Vol. 14, Issue 21, №5370.
  38. Xu W., Zhang L., Fang C. et al. Staring Spotlight SAR with Nonlinear Frequency Modulation Signal and Azimuth Non Uniform Sampling for Low Side Lobe Imaging, *Sensors*, 2021, Vol. 21, Issue 19, №6487. DOI: 10.3390/s21196487.
  39. Swiercz E., Janczak D., Konopko K. Estimation and Classification of NLFM Signals Based on the Time-Chirp, *Sensors*, 2022, Vol. 22, Issue 21, № 8104. DOI: 10.3390/s22218104.
  40. Kostyria O. O., Hryzo A. A., Dodukh O. M. et al. Mathematical model of a two-fragment signal with a non-linear frequency modulation in the current period of time, *Visnyk NTUU KPI Serii – Radiotekhnika Radioaparaturbuduvannia*, 2023, Vol. 92, pp. 60–67. DOI:10.20535/RADAP.2023.92.60-67.
  41. Kostyria O. O., Hryzo A. A., Dodukh O. M. et al. Improvement of mathematical models with time-shift of two- and tri-fragment signals with non-linear frequency modulation, *Visnyk NTUU KPI Serii – Radiotekhnika Radioaparaturbuduvannia*, 2023, Vol. 93, pp. 22–30. DOI: 10.20535/RADAP.2023.93.22-30.

Received 08.01.2024.  
Accepted 15.02.2024.

УДК 621.396.962

## ДВОФРАГМЕНТНІ НЕЛІНІЙНО-ЧАСТОТНО МОДУЛЬОВАНІ СИГНАЛИ З КОРІНЬ-КВАДРАТИЧНИМ ТА ЛІНІЙНИМ ЗАКОНАМИ ЗМІНИ ЧАСТОТИ

**Костиря О. О.** – д-р техн. наук, с.н.с., пров. наук. співр. Харківського національного університету Повітряних Сил імені Івана Кожедуба, Харків, Україна.

**Гризо А. А.** – канд. техн. наук, доц., начальник НДІ Харківського національного університету Повітряних Сил імені Івана Кожедуба, Харків, Україна.

**Худов Г. В.** – д-р техн. наук, проф., начальник кафедри Харківського національного університету Повітряних Сил імені Івана Кожедуба, Харків, Україна.

**Додух О. М.** – канд. техн. наук, пров. наук. співр. Харківського національного університету Повітряних Сил імені Івана Кожедуба, Харків, Україна.

**Лісогорський Б. А.** – канд. техн. наук, старш. наук. співр. Харківського національного університету Повітряних Сил імені Івана Кожедуба, Харків, Україна.

### АНОТАЦІЯ

**Актуальність.** Бурхливий розвиток техніки цифрового синтезу та обробки радіолокаційних сигналів, який спостерігається у останні десятиліття, практично зняв обмеження щодо можливості реалізації довільних законів частотної модуляції радіоколивань. Поряд з традиційним застосуванням лінійно-частотно-модульованих сигналів в сучасних радіолокаційних засобах використовуються зондувальні сигнали з нелінійною частотною модуляцією, які забезпечують нижчий рівень максимальних бічних пелюсток та більшу швидкість їх спадання. Ці фактори в свою чергу сприяють покращенню характеристик виявлення цілей за умов дії пасивних завад, а також підвищенню ймовірності виявлення малорозмірних цілей на тлі цілей з більшими ефективними поверхнями розсіювання. У зв'язку з цим велика кількість досліджень проводиться у напрямку подальшого удосконалення існуючих та синтезу радіолокаційних сигналів з новими законами частотної модуляції. Використання багатофрагментних нелінійно-частотно-модульованих сигналів, до складу яких входять фрагменти як з лінійною, так і з нелінійною модуляцією забезпечує збільшення кількості можливих варіантів законів частотної модуляції та синтез сигналів з прогнозованими характеристиками. Синтез нових багатофрагментних сигналів зі зниженим рівнем бічних

пелюсток автокореляційних функцій та більшою швидкістю їх спадання є важливою науково-технічною задачею, вирішенню якої присвячено дану статтю.

**Мета роботи** – розробка математичних моделей поточного і зсуненого часу двофрагментних нелінійно-частотно модульованих сигналів для випадку, коли перший фрагмент має корінь-квадратичну, а другий лінійну частотну модуляцію та визначення доцільності використання такого сигналу в радіолокаційних застосуваннях.

**Метод.** В статті теоретично підтверджено, що для математичної моделі поточного часу, при переході від першого фрагменту до другого на стику фрагментів виникають стрибки миттєвої частоти та фази (або тільки фази для математичної моделі зсуненого часу), які можуть суттєво спотворити результуючий сигнал. Визначення величини частотно-фазових стрибків для їх подальшого усунення виконується шляхом знаходження різниці між значенням початкової фази другого фрагменту та кінцевим значенням фази першого. Відмінною особливістю розроблених математичних моделей є використання першого фрагменту сигналу з корінь-квадратичною, а другого – лінійною частотною модуляцією.

**Результати.** Порівняння сигналу, перший фрагмент якого має корінь-квадратичну частотну модуляцію, та сигналу з двома лінійно-частотно модульованими фрагментами за умови рівності сумарної тривалості та девіації частоти показує, що для нового синтезованого сигналу максимальний рівень бічних пелюсток знизився на 1,5 дБ, а швидкість їх спадання збільшилася на 6,5 дБ/дек.

**Висновки.** Синтезовано новий двофрагментний сигнал, перший фрагмент якого має корінь-квадратичну, а другий – лінійну частотну модуляцію. Розроблено математичні моделі поточного часу та зі зсувом часу для розрахунку значень миттєвої фази такого сигналу. Відмінною особливістю цих моделей є наявність складових для компенсації частотно-фазових спотворень з урахуванням закону модуляції частоти першого фрагменту. Отримані осцилограми, спектри та автокореляційні функції синтезованих двофрагментних сигналів не протирічать відомим теоретичним положенням, що свідчить про достовірність та адекватність запропонованих математичних моделей.

**КЛЮЧОВІ СЛОВА:** математична модель; нелінійна частотна модуляція; максимальний рівень бічних пелюсток.

#### ЛІТЕРАТУРА

1. Lei T. Research and design of digital unit for direct digital frequency synthesizer / T. Lei, L. Liang // International Conference on Electronic Materials and Information Engineering (EMIE 2021), Journal of Physics: Conference Series. – 2021, Vol. 1907. – №012004. DOI:10.1088/1742-6596/1907/1/012004.
2. Liu X. A Fully Integrated 0.27-THz Injection-Locked Frequency Synthesizer With Frequency-Tracking Loop in 65-nm CMOS / X. Liu, H. C. Luong // IEEE Journal of Solid-State Circuits. – 2020, Vol. 55, Issue 4. – P. 1051–1063. DOI: 10.1109/JSSC.2019.2954232.
3. Blackledge J. Digital Signal Processing / J. Blackledge – Dublin : Horwood Publishing, second edition, 2006. – 840 p.
4. Tan L. Digital Signal Processing. Fundamentals and Applications / L. Tan. – Georgia : Academic Press, 2008. – 816 p.
5. Zhang J. Design and FPGA implementation of DDS based on waveform compression and Taylor series / J. Zhang, R. Zhang, Y. Dai // 2017 29th Chinese Control And Decision Conference (CCDC), Computer Science, Engineering. – 2017. – P. 1301–1306. DOI:10.1109/CCDC.2017.7978718.
6. Analysis and comparison of Direct Digital Frequency Synthesizers implemented on FPGA / [M. Genovese, E. Napoli, D. De Caro et al.] // Integration. – 2014, Vol. 47, Issue 2. – P. 261–271.
7. Anil A. FPGA Implementation of DDS for Arbitrary wave generation / A. Anil, A. Prasad // International Journal of Engineering Research and Applications. – 2021, Vol. 11, Issue 7. – P. 56–64. DOI: 10.9790/9622-1107025664.
8. Detection Using Radar Techniques and Processing With FPGA Implementation / [A. B. Obadi, P. J. Soh, O. Aldayel et al.] // IEEE Circuits and Systems Magazine. – 2021, Vol. 21, №1. – P. 41–74.
9. FPGA Implementation of a Higher SFDR Upper DDFS Based on Non-Uniform Piecewise Linear Approximation / [X. Liao, L. Zhang, X. Hu et al.] // Applied Sciences. – 2023, Vol. 13, Issue 19. – №10819. https://doi.org/10.3390/app131910819.
10. Vankka J. Digital Synthesizers and Transmitters for Software Radio / J. Vankka – New York : Springer, 2005. – 359 p. DOI: 10.1007/1-4020-3195-5.
11. Skolnik M. I. Radar Handbook. Editor in Chief / M. I. Skolnik. – Boston : McGraw-Hill Professional, second edition, 1990. – 846 p.
12. Cook C. E. Radar Signals: An Introduction to Theory and Application / C. E. Cook, M. Bernfeld. – Boston : Artech House, 1993. – 552 p.
13. Levanon N. Radar Signals / N. Levanon, E. Mozeson. – Hoboken : John Wiley & Sons, 2004. – 403 p.
14. A Variable Chirp Rate Stepped Frequency Linear Frequency Modulation Waveform Designed to Approximate Wideband Non-Linear Radar Waveforms / [M. Saleh, S.-M. Omar, E. Grivel et al.] // Digital Signal Processing. – 2021. – Vol.109. – №102884.
15. Van Trees H. L. Detection, Estimation, and Modulation Theory / H. L. Van Trees. – Edition, reprint : John Wiley & Sons, 2004. – 716 p.
16. Xu Z. Nonlinear Frequency-Modulated Waveforms Modeling and Optimization for Radar Applications / Z. Xu, X. Wang, Y. Wang // Mathematics. – 2022. – Vol. 10, №3939.
17. Meikle H. Modern radar systems / H. Meikle. – London, Artech House, second edition, 2008. – 701 p.
18. Curry G. R. Radar System Performance Modeling / G. R. Curry. – London, Artech House, second edition, 2004. – 410 p.
19. Barton D. K. Radar System Analysis and Modeling / D. K. Barton. – London : Artech House, 2005. – 545 p.
20. Richards M. A. Principles of modern radar / M. A. Richards, J. A. Scheer, W. A. Holm. – SciTech Publishing, 2010. – 924 p.
21. Mervin C. Basic Radar Analysis / C. Mervin, J. Budge, R. G. Shawn. – London, Artech House, 2015. – 727 p.
22. Melvin W. L. Principles of modern radar / W. L. Melvin, J. A. Scheer. – New York: SciTech Publishing, 2013. – 846 p.
23. Cook C. E. A pulse compression predistortion function for efficient side lobe reduction in a high-power radar / C. E. Cook, J. Paolillo // Proceedings of the IEEE. – 1964. – Vol. 52(4). – P. 377–389. DOI: 10.1109/proc.1964.2927.

24. Cook C.E. A class of nonlinear FM pulse compression signals / C. E. Cook // *Proceedings of the IEEE*. – 1964. – Vol. 52(11). – P. 1369–1371.
25. Heinzel G. Spectrum and spectral density estimation by the Discrete Fourier transform (DFT), including a comprehensive list of window functions and some new flat-top windows [Electronic resource] / G. Heinzel, A. Rüdiger, R. Schilling. – Access mode: [https://pure.mpg.de/rest/items/item\\_152164\\_1/component/file\\_152163/content](https://pure.mpg.de/rest/items/item_152164_1/component/file_152163/content).
26. Doerry A. W. Catalog of Window Taper Functions for Side lobe Control [Electronic resource] / A. W. Doerry. – Access mode: [https://www.researchgate.net/publication/316281181\\_Catalog\\_of\\_Window\\_Taper\\_Functions\\_for\\_Side\\_lobes\\_Control](https://www.researchgate.net/publication/316281181_Catalog_of_Window_Taper_Functions_for_Side_lobes_Control).
27. Ghavamirad R. Side Lobe Level Reduction in ACF of NLFM Waveform / R. Ghavamirad, M. A. Sebt // *IET Radar, Sonar & Navigation*. – 2019. – Vol. 13, Issue 1. – P. 74–80.
28. Chukka A. Peak Side Lobe Reduction analysis of NLFM and Improved NLFM Radar signal / A. Chukka, B. Krishna // *AIUB Journal of Science and Engineering (AJSE)*. – 2022. – Vol. 21, Issue 2. – P. 125–131.
29. Parwana S. Analysis of LFM and NLFM Radar Waveforms and their Performance Analysis / S. Parwana, S. Kumar // *International Research Journal of Engineering and Technology (IRJET)*. – 2015. – Vol. 02, Issue 02. – P. 334–339.
30. Non-continuous piecewise nonlinear frequency modulation pulse with variable sub-pulse duration in a MIMO SAR Radar System / [Y. Zhao, M. Ritchie, X. Lu et al.] // *Remote Sensing Letters*. – 2020. – Vol. 11, Issue 3. – P. 283–292.
31. Jeyanthi J. E. Study of Different Radar Waveform Generation Techniques for Automatic Air Target Recognition / J. E. Jeyanthi, A. Shenbagavalli, V.R.S. Mani // *International Journal of Engineering Technology Science and Research (IJETSR)*. – 2017. – Vol. 4, Issue 8. – P. 742–747.
32. Adithyavalli N. An Algorithm for Computing Side Lobe Values of a Designed NLFM function / N. Adithyavalli // *International Journal of Advanced Trends in Computer Science and Engineering*. – 2019. – Vol. 8, Issue 4. – P. 1026–1031. DOI:10.30534/ijatcse/2019/07842019.
33. Valli N. A. Modified Radar Signal Model using NLFM / N. A. Valli, D. E Rani, C. Kavitha // *International Journal of Recent Technology and Engineering (IJRTE)*. – 2019. – Vol. 8, Issue 2S3. – P. 513–516. DOI: 10.35940/ijrte.B1091.0782S319.
34. Kavitha C. Optimization of two-stage NLFM signal using Heuristic approach / C. Kavitha, N. A. Valli, M. Dasari // *Indian Journal of Science and Technology*. – 2020. – Vol. 13(44). – P. 4465–4473. DOI:10.17485/IJST/v13i44.1841.
35. Chukka A. Peak Side Lobe Reduction analysis of NLFM and Improved NLFM Radar signal / A. Chukka, B. Krishna // *AIUB Journal of Science and Engineering (AJSE)*. – 2022. – Vol. 21, Issue 2. – P. 125–131.
36. Fan Z. Coded excitation with Nonlinear Frequency Modulation Carrier in Ultrasound Imaging System / Z. Fan, H.-Y. Meng // *IEEE Far East NDT New Technology & Application Forum (FENDT): Kunming, Yunnan province, China*, – 20–22 Nov. 2020. – P. 31–35.
37. A Novel Jamming Method against SAR Using Nonlinear Frequency Modulation Wave-form with Very High Side Lobes / [C. Song, Y. Wang, G. Jin et al.] // *Remote Sensing*. – 2022. – Vol. 14, Issue 21. – №5370
38. Staring Spotlight SAR with Nonlinear Frequency Modulation Signal and Azimuth Non Uniform Sampling for Low Side Lobe Imaging / [W. Xu, L. Zhang, C. Fang et al.] // *Sensors*. – 2021. – Vol. 21, Issue 19. – №6487. DOI: 10.3390/s21196487.
39. Swiercz E. Estimation and Classification of NLFM Signals Based on the Time-Chirp / E. Swiercz, D. Janczak, K. Konopko // *Sensors*. – 2022. – Vol. 22, Issue 21. – № 8104. DOI: 10.3390/s22218104.
40. Mathematical model of a two-fragment signal with a nonlinear frequency modulation in the current period of time / [O. O. Kostyria, A. A. Hryzo, O. M. Dodukh et al.] // *Visnyk NTUU KPI Serii – Radiotekhnika Radioaparotobuduvannia*. – 2023. – Vol. 92. – P. 60–67. DOI:10.20535/RADAP.2023.92.60-67.
41. Improvement of mathematical models with time-shift of two- and tri-fragment signals with non-linear frequency modulation / [O. O. Kostyria, A. A. Hryzo, O. M. Dodukh et al.] // *Visnyk NTUU KPI Serii – Radiotekhnika Radioaparotobuduvannia*. – 2023. – Vol. 93. – P. 22–30. DOI: 10.20535/RADAP.2023.93.22-30.

## RESEARCH OF THE FEATURES OF DIGITAL SIGNAL FORMATION IN SATELLITE COMMUNICATION LINES

**Magro V. I.** – PhD, Associate Professor, Professor of the Department of Information Security and Telecommunications, Dnipro University of Technology, Dnipro, Ukraine.

**Panfilov O. G.** – Student of the Department of Information Security and Telecommunications, Dnipro University of Technology, Dnipro, Ukraine.

### ABSTRACT

**Context.** Remote sensing of the Earth is now widely used in various fields. One of the challenges of remote sensing is the creation of inexpensive satellite systems operating in polar circular orbits. These systems require the development of a reception-transmission system that allows tens of gigabits of video information to be transmitted to an earth receiving station within ten minutes. That is, there is a need to create a communication system that provides high speed data transmission from small satellites weighing up to 50 kg.

**Objective.** The aim of the work is to study the features of digital signal formation in modern satellite communication lines and to develop a communication system with a high data transfer rate (usually 300 Mbit/s), which can be applied to small Earth Observation satellites.

**Method.** Proposed concept for building a high-speed data transmitter from a remote sensing earth satellite using commercially available off-the-shelf technology. Calculations of the power flow density created at the input of the receiving earth station were performed to find out the possible power of the on-board transmitter.

**Results.** A diagram of a communication system based on the DVB-S standard using the technology of commercially available off-the-shelf products has been developed. The high-speed data transmitter is implemented on a Xilinx® Zynq Ultrascale+™ MPSoC FPGA microchip, which is located on an Enclustra Mercury XU8 module with a high-performance dual 16-bit AD9174 DAC. The on-board transmitter with a power of up to 2 W meets the requirements of the ITU Radio Regulations for the power flux density on the surface of the Earth, which is created by the radiation of the space station EESS in the range 8025–8400 MHz. It is shown that the energy reserve of the communication line of 3 dB is achieved for various commands for coding and modulation changes with an increase in the elevation angle, which allows to increase the speed of information transmission.

**Conclusions.** An original receiving-transmitting system was developed for use in small satellites for remote sensing of the Earth. It is shown that the function of adaptive modeling of ACM of the DVB-S standard allows you to automatically change the transmission parameters in real time depending on the changing conditions of the channel, providing opportunities for more flexible and effective data transmission in various conditions, which will allow to increase the volumes of information transmitted by communication session. The proposed system operates in the X-band and is built using commercially available off-the-shelf products. An antenna with double circular polarization is used as the emitter. Two physical channels represent two polarization modes: right circular polarization and left circular polarization, each of which has three frequency channels.

**KEYWORDS:** small satellite, low Earth orbit, remote sensing of the Earth, power flow density, X-band, DVB-S.

### ABBREVIATIONS

ACM – Adaptive Coding and Modulation;

ADC – Analog-Digital Conversion;

BER – Bit Error Ratio;

CCSDS – Consultative Committee for Space Data Systems;

COTS – Commercially available off-the-shelf;

DAC – Digital-Analog Conversion;

DC – Direct Current;

DVB-S2 – Digital Video Broadcasting – Satellite – Second Generation;

EESS – Earth Exploration Satellite Service;

EO – Earth Observation;

IF – Intermediate Frequency;

ISARA – Integrated Solar Antenna and Reflective Antenna;

ITU – International Telecommunication Union;

FCC – Federal Communications Commission;

FEC – Forward Error Correction;

PFD – Power Flow Density

FFH – Fast Frequency Hopping;

FPGA – Field Programmable Gate Array

HDT – High-speed Data Transmitter;

HSD2 – High Speed Downlink Version 2;

LEO – Low Earth Orbit;

LHCP – Left-Hand Circular Polarization;

MGA – Middle-Gain Antenna;

MIMO – Multiple Input Multiple Output;

MODCOD – changing modulation and coding;

NCO – Numerically-Controlled Oscillator;

NGSO – Non-Geostationary Orbit;

OCSA – Optical Communications and Sensor Demonstration;

OFDM – Orthogonal Frequency Division Multiplexing;

QAM – Quadrature Amplitude Modulation;

RF-DAC – Radio Frequency Digital-Analog Converter;

RHCP – Right-Hand Circular Polarization;

SCSS – Satellite Communication Systems;

SDR – Software Defined Radio;

TT&C – Telemetry, Tracking, and Control;

UHF – Ultra High Frequency.

## NOMENCLATURE

$E_b/N_0$  – signal-to-noise density ratio;  
 $C/N_0$  – carrier-to-noise density ratio;  
 $M_t$  – number of transmitting antennas;  
 $M_r$  – number of receiving antennas.

## INTRODUCTION

The use of small satellites began in the 1980s. Such satellites are usually used in Low Earth Orbits. Explicitly, by the end of 2021, more than 4700 LEO satellites have been successfully launched, accounting for nearly 86% of the total launch volume of all types of satellites [1]. During these years, LEO SCSs have found a plethora of applications, including media broadcasting, backhauling, mobile communication, and broadband Internet [1–6]. In fact, LEO SCS is a supplement to ground systems in areas where there is no coverage. There is now a convergence of ground systems with LEO SCS.

Currently, Earth observation satellite is being widely implemented [7]. In this technological process (EO), satellites are used for non-contact collection of information about objects or phenomena on the Earth's surface. Thanks to EO technology, it is possible to obtain information about changes on the Earth's surface, study climatic and natural phenomena, monitor the use of land plots, detect changes in ecosystems, etc. [8–9]. EO technology is becoming more and more important for monitoring and managing the resources of our planet, as well as for solving various scientific, environmental and economic tasks. Satellites send large volumes of data collected by EO technology to Earth through communications systems. This requires fast and reliable communication systems. The development of advanced data transmission technologies is becoming important to ensure effective information exchange.

Satellite communication systems for EO have specific requirements because their tasks include transmitting and receiving large amounts of real-time data from satellites surveying the Earth's surface. The main requirements for communication systems of EO satellites include:

- wide bandwidth: the system must have a wide enough bandwidth to transmit large volumes of data captured by Earth imaging satellites;
- low signal delay: for additional applications, such as navigation or natural disaster monitoring, low signal delay is important to ensure fast information exchange;
- high bandwidth: the system must have a large bandwidth to process a large flow of data in real time;
- resistance to interference: the satellite system must be resistant to various types of interference, such as atmospheric phenomena, electromagnetic distortions and other interferences;
- global coverage: the system must provide coverage of the entire surface of the Earth in order to have the availability of communication at any point;
- autonomy and reliability: the system must be autonomous and reliable, able to work without human intervention for a long time;

- energy efficiency: the system must be energy efficient, since satellites have limited energy resources;
- compatibility with communication standards: the satellite system must be compatible with communication standards, which ensures its integration with existing networks.

These requirements make it possible to ensure effective operation of EO satellite communication systems and high-quality data collection and transmission for further analysis and use. But there are many technical problems when using near-Earth space. However, the biggest problem is not only the high cost of manufacturing a spacecraft, but also its development and launch into orbit. These problems can be solved with the help of small spacecraft. Their production is cheaper, development takes less time and does not require a large team of specialists.

It is small satellites that have recently begun to play an important role in the EO process. Small satellites include spacecraft with a total mass of 100–500 kg.

In this work, the authors propose an original communication system that provides a high speed of information transmission, and which can be used on small EO satellites.

**The object of study** is satellite communication system.

**The subject of the study** is satellite communication system for EO.

**The purpose of the work** is research into the features of digital signal formation in modern satellite communication lines and the development of a communication system with a high data transfer rate (usually 300 Mbit/s), which can be applied to small EO satellites.

## 1 PROBLEM STATEMENT

It is known that there are several main ways to increase the speed of information transmission in the “satellite-Earth” line [10]. Ka-band bandwidth is many times the available bandwidth compared to X-band, so NASA is moving to Ka-band to increase radio communication speed.

However, the Ka-band has higher attenuation in the atmosphere and clouds, as well as heavy attenuation during rain. For Ka-band, there is limited availability of COTS components such as amplifiers, filters, and mixers compared to X-band [11–12].

Optical communication seems to be a more attractive option for small satellites due to the presence of practically unlimited bandwidth, enormous speed, and the absence of regulations regarding the operation of lasers in comparison with the radio spectrum, which is regulated by the FCC and ITU [13]. However, optical communication terminals are quite expensive, costing about 1 million dollars each. In addition, the availability of optical communication strongly depends on the presence of cloud cover.

The use of hardware or software that can be purchased from commercial suppliers without the need for special

development or modification can significantly reduce the budget of a satellite project. The simultaneous use of several communication channels of the DVB-S2 standard [14] using COTS makes it possible to implement a high-speed data transmitter for small EO satellites.

The purpose of the work is to study the features of digital signal formation in modern satellite communication lines and to develop a communication system with a high data transfer rate (usually 300 Mbit/s), which can be applied to small EO satellites.

## 2 REVIEW OF THE LITERATURE

CCSDS develops standards for various aspects of space communication and data exchange. Here are some recommendations from the CCSDS that may be useful for organizing satellite communications in the context of EO:

- CCSDS Proximity-1 Space Data Link Protocol (CCSDS 211.0-B-3). This standard defines the protocols and services that can be used to exchange data between satellites and ground stations. It provides basic guidelines for the organization of communication [15].

- CCSDS Space Link Extension (CCSDS 232.2-B-1). This standard regulates the extension of the CCSDS protocol to ensure reliable and efficient communication in space. It can be useful for satellite systems that require high reliability [16].

- CCSDS Advanced Orbiting Systems (CCSDS 910.0-M-1). This standard provides guidance on data transmission, and command and control for orbiting satellites. It can be useful for organizing communications and managing satellites in EO systems [17].

- CCSDS File Delivery Protocol (CFDP) (CCSDS 727.0-B-4). This standard defines a protocol for efficient file transfer between different spacecraft. It can be used to transmit data collected by EO satellites to the ground station [18].

- CCSDS Mission Operations (CCSDS 911.0-M-1). This standard provides guidance and principles for mission operations, including mission planning, control, and execution, which may be important for EO satellite missions [19].

These CCSDS recommendations can be used as a basis for the development of satellite EO systems, simplifying the interaction between satellites and other elements of the communication system.

The document [20] contains recommendations on the use of the DVB-S2x standard for space systems. These CCSDS recommendations for the specific application of DVB-S2x for the transmission of information from the EO satellite suggest:

- for the transmission of high-speed EO images, such as high-resolution images, DVB-S2X can be used with QAM modulation with redundancy. This will allow you to achieve high data transfer rates and ensure high image quality;

- for transmission of low-speed data, such as weather and telemetry data, DVB-S2X can be used with amplitude modulation with redundancy. This will make it possible to

achieve acceptable signal quality with a limited channel bandwidth.

It is important to note that choosing a specific application of DVB-S2X for transmitting information from EO satellite is a complex task that requires taking into account a number of factors, such as:

- the data transfer rate that is required for a specific space system;
- channel bandwidth that is available for a specific space system;
- reliability of data transmission, which is required for a specific space system.

To ensure high data transmission reliability, it is recommended to use error control protocols such as FEC. Technologies such as MIMO are recommended to ensure high channel bandwidth utilization. Technologies such as OFDM are recommended to ensure high immunity to interference.

Conventional large satellites are equipped with a downlink system that provides speeds of several hundred Mbps and consumes high DC power of 100–200 W, in some cases more. However, a small satellite can only generate a total power of about 100 W. A high-speed communication system requires about 40 watts for a 10-minute communication session. This limits the use of high data rate communication systems for small satellites.

Thus, a cost-effective approach to increasing the downlink data volume is to increase the downlink data rate to an earth station that has a short communication session with the satellite – about 10 minutes.

Most CubeSat satellite communication systems operate in the UHF, S-band, and X-band [11]. Higher speed commercial X-band radios are capable of speeds of around 50–100 Mbps. Satellites in larger form factors have higher X-band speeds, such as Planet's Skysat satellites with a downlink speed of 480 Mbps and Japan's Hodoshi 4 satellite, which demonstrated an uplink speed of 505 Mbps.

In February 2015, the University of Tokyo published a "record 348 Mbit/s microsatellite downlink event" in a press release [21]. At the ISAS Sagami-hara campus, the 3.8-meter ground station antenna received 348 Mbps data from the Hodoyoshi-4 microsatellite with 16 QAM modulation and successfully demodulated/decoded it without errors. This communication rate is half that of ALOS-2/Daichi-2, a Japanese Earth observation satellite weighing about 2 tons. This result indicates that the data transmission capabilities of a small satellite are approaching those of a large satellite.

Digital Globe's WorldView-2 and Worldview-3 satellites operate at 800 Mbps and 800/1200 Mbps respectively but have a much larger form factor and weigh over 2500 kilograms [22]. The data collected by each satellite's on-board camera is processed, stored, and transmitted together with basic telemetry data in the 8025–8400 MHz band (X-band) to the corresponding ground stations. For TT&C functions, the satellites will receive command communications over the primary uplink using the band

2025–2110 MHz (S-band) which is permitted in the EESS subject to the following conditions.

It is known that the available bandwidth of Ka-band is many times higher than that of X-band. Therefore, NASA is switching to the Ka-band to increase the speed of radio communication. However, the Ka-band has higher attenuation in the atmosphere and clouds, as well as heavy attenuation in rain. For Ka-band devices, there is limited availability of COTS components such as amplifiers, filters, and mixers compared to X-band.

The NASA-sponsored ISARA mission successfully demonstrated the capability of CubeSat communication in the Ka-band at a speed of 100 Mbit/s [23]. This technology uses an antenna that is made in the form of a reflective grid, which is integrated into a modified “Turkey Tail” solar cell that covers the hull of the spacecraft (almost zero volume is required for its placement). Such an antenna has a high gain – 33 dBi. The mass of the ISARA antenna is 0.5 kg and meets the requirements of a 3U spacecraft. This system has demonstrated the ability to transmit data downlink at 100 Mbit/s using a relatively simple ground station with a 70 cm parabolic reflector antenna, enabled by the spacecraft’s ability to precisely point the antenna at the ground station. The most productive commercial Ka-band radio that was used in flight demonstrated a data rate of only 320 Mbit/s on a 6U CubeSat [23]. This station has the following parameters:

- DC power consumption is 20 W;
- the central frequency is 26.8 GHz;
- radio frequency output power – 27 dBm;
- built-in horn antenna with a gain of 23 dBi;
- variable data transfer rate: from 35.3 Mbps to 320.6 Mbps.

Optical communication seems to be an attractive option for small satellites due to the availability of practically unlimited bandwidth, enormous speed and the absence of laser regulations compared to the radio spectrum regulated by the FCC and ITU [24].

In low Earth orbit, the OCS mission addresses two major capabilities of value to many future small spacecraft missions: high-speed optical data transmission and small spacecraft rendezvous operations [25]. The OCS project develops and uses technologies consisting of a low-power laser communication system, proximity sensors and a compact power plant. The second two-satellite OCS mission was launched on November 12, 2017, as part of the Cygnus (OA-8) resupply mission. Modified with lessons learned from the first mission, the two satellites entered the operational phase of the mission in April to demonstrate the world’s first high-speed laser link between a CubeSat and a ground station. This showed the possibility of organizing optical communication. To date, OCS has successfully demonstrated optical communication at 200 megabits per second using a ground-based 30 cm telescope.

The AMS Beacon payload was integrated into the Agile Microsat (AMS) 6U platform built by MIT Lincoln Laboratory to function as a space-based point source for high-speed adaptive optics control [26]. In addition to the

built-in 500 mW laser, this platform is equipped with a reflector and a photodiode with a readout frequency of 1 kHz. The system was successfully launched in May 2022 into low Earth orbit.

However, optical communication terminals are expensive, the availability of optical communication strongly depends on cloud coverage. Considering that about 70% of the Earth’s territory is covered by clouds every day, several terrestrial optical terminals are needed to ensure timely data transmission. However, the process of licensing the radio frequency spectrum is a difficult bureaucratic procedure, which may encourage the transition to the optical spectrum.

The Planet company has achieved good results in the development of HSD2 X-band radio communication [27]. Planet’s HSD2 is a compact, lightweight and low-power next-generation radio that was built and deployed on a 3U CubeSat in December 2018. This system operates in the X-band and is built using COTS parts. It has a dual-polarized antenna. Two physical channels represent two polarization modes: RHCP and LHCP, and each physical channel uses a common bandwidth of 300 MHz. Within each physical channel are three logical channels located between 100 MHz frequency centers. The DVB-S2 commercial digital television broadcasting standard is used for modulation and coding. The ACM scheme is used to dynamically change the modulation and coding for each channel separately based on the available channel set [28].

Currently, the main systems operating high-speed “satellite-Earth” channels are EO systems and satellites-aggregators of information flows from third-party small satellites. The transmission of high-resolution photographs, as well as the ability to receive information by a limited number of ground stations, lead to requests to increase the speed of the space-to-ground channel by more than 1 Gbps in the X- or Ka-band. Currently, the speed of information transmission over X-band radio lines is 300 Mbit/s. The speed of data transmission while maintaining the necessary probability of an error per bit can be increased by increasing the energy of the radio line or by building the receiving and transmitting equipment with better characteristics, which include the quality factor of the receiving system, which depends on the noise temperature, the gain of the antenna, losses that related to antenna guidance, distribution in the antenna-feeder path, signal processing in the modem. According to the recommendation [29], the following modulation methods are proposed in the X-band: phase modulation without GMSK phase break with the break-in filter parameter  $\alpha = 0.25$ ; four-position OQPSK phase modulation with quadrature shift; modulation using 4D-8PSK-TCM convolutional code. Due to the spectral efficiency of no more than 2 bits/(s·Hz) in the selected frequency band (X-band), OQPSK modulation does not reach 1 Gbps even without interference-free coding. Due to the spectral efficiency of no more than 2 bits/(s·Hz) in the selected frequency band (X-band), OQPSK modulation does not reach 1 Gbps even without interference-free coding.

In addition to phase modulations, it is possible to use amplitude-phase methods, such as the DVB-S2 standard [29], which make it possible to achieve a spectral efficiency of up to 4.45 bits/(c·Hz) and a ratio of  $E_b/N_0$  for BER = from  $10^{-7}$  to 15.90dB.

To achieve a bit rate of  $R = 2000$  Mbit/s with a bandwidth of no more than 375 MHz in the X-band, the spectral efficiency of the used signal code scheme is at least 5.33 bit/s·Hz in relation to the final bandwidth of the radio signal. Modulation types widely used in advanced foreign samples do not meet these requirements, and higher-order modulations, such as 64QAM or 64APSK, are unacceptable due to a significant range of variations in the amplitude of the complex envelope. Therefore, it is necessary to switch to the Ka-band due to the much greater availability of this frequency range.

An increase in the speed of information transmission is possible due to adaptive modems, in which the speed of information transmission is adaptively increased when the communication range is reduced during the flight of the satellite. When the spacecraft moves from the edge of the horizon to the zenith, the communication range can change from the maximum value  $d$  to the value of the height of the orbit  $H$  at the zenith, which will lead to an increase in the energy potential due to a decrease in signal losses during its propagation and a decrease in the noise temperature of the receiving system. This feature can be used to increase the speed of information transfer.

Ensuring high data transfer rates can be realized due to the redistribution of the spectrum considering the capabilities of SDR technology, which involves replacing some of the analog components, such as mixers, filters, amplifiers, detectors, with digital processing. With the help of this technology, the received useful signal is fed directly to the ADC or a pre-amplifier located before the ADC. To implement systems based on SDR technology, it is possible to use PLD technology, which allows creating systems on a crystal with many complex digital blocks. The data transmission speed of SDR systems is determined by the capabilities of analog-to-digital and digital-to-analog conversion schemes, as well as the speed of operation of digital units.

For the development and manufacture of faster devices, it is possible to use foreign manufacturers of micro-circuits, such as UMC, TSMC or IHP. TSMC provides the ability to manufacture chips with design standards down to 40nm, a transistor cutoff frequency of  $\approx 400$ GHz, UMC up to 65nm, and a transistor cutoff frequency of  $\approx 360$ GHz. Designing mixed-signal circuits (ADC/DAC) using these technologies is a challenge, as process standards fall below 100 nm, transistors have very low intrinsic gain, which can lead to low effective ADC/DAC bit-rates.

Bandwidth and quality of information transmission can be increased in the case of using MIMO technology, which includes the presence of a certain number of  $M_t$  and  $M_r$ . The high-speed data stream is divided into  $M_t$  independent sequences at a rate of  $1/M_t$ , which are then transmitted simultaneously from several antennas, respec-

tively, using only  $1/M_t$  of their primary frequency band. The data flow converter at the transmitting end of the communication line converts a serial flow into a parallel one and performs the reverse conversion at the receiving end [30]. Implementation of spatio-temporal distribution of signals in MIMO systems allows to increase the bandwidth of communication lines due to the formation of physically different channels. The application of MIMO technology in terrestrial wireless communication systems makes it the most promising for the creation of new high-speed wireless systems. Therefore, the question arises of choosing the type of MIMO technology that can be most rationally used in satellite communication systems that differ from terrestrial systems in terms of coverage area, communication channel topology, propagation delay, and the level of interference in the communication channel. Based on the features of satellite communication, the most promising options for using MIMO systems can be:

- single user transmission scheme using one or two satellites;
- multi-user transmission scheme using one satellite.

The space limitation in a single-satellite system can be negligible when using multiple satellites in single-user communication systems, the so-called orbital diversity. The main disadvantages of orbital separation are the inefficient use of the satellite bandwidth for transmitting the same signal, as well as the need to synchronize transmissions from two independent satellites [30].

### 3 MATERIALS AND METHODS

In the course of the work, an X-band HDT was developed. The transmitter is designed to transmit data from the EO systems to the ground receiving station. The proposed transmitter scheme is based on the industry standard DVB-S2 modulation scheme. However, to reduce costs in this scheme, COTS modulators and demodulators are used. The structural diagram of the HDT is shown in Fig. 1.

The main features of the developed HDT are as follows:

1. The use of a high-speed DAC allows you to implement the entire path of high-frequency modulation in the digital domain. The analog modulation tract is traditionally implemented with discrete components and is difficult to optimize.
2. Parallel use of several DVB-S2 modulators, the outputs of which are divided by frequency and polarization within the permissible bandwidth using RF-DAC. This allows the use of inexpensive COTS demodulators at ground stations. A demodulator for a high data rate Earth observation mission is a very expensive component. In the case of using the 6-channel version, the price of demodulators becomes very high. Whereas standard DVB-S2 COTS demodulators are available at low cost.

3. Using DVB-S2 as a modulation scheme. In the proposed scheme, DVB-S2 was designed in such a way to use any excess of the communication channel by increasing the data throughput. The ability to change the code rate and modulation scheme in real time when the quality

of communication changes allows the DVB-S2 channel to maximize data throughput.

Two physical communication channels implement two polarization modes: RHCP and LHCP, and each physical channel uses a common bandwidth of 300 MHz. Inside each physical channel there are three logical channels, located at 100 MHz from each other between frequency centers. The symbol frequency of a separate channel is 76.8 Msec/s.

Each physical channel has an output RF power of 1 W and is connected to an antenna with a gain of 15 dBi.

Field Programmable Gate Array (FPGA) is widely used in satellite communication [31]. In the developed HDT, an FPGA (Enclustra Mercury XU8) multiplexes the input data into six DVB-S2 cores that modulate and provide FEC. Data packets are encapsulated into DVB-S2 baseband frames with a data transfer rate of 76.8 Msec/s, shifted in frequency, combined into two physical channels, and converted to an analog baseband signal using a high-speed DAC. Two independent superheterodyne transmitters are used to convert baseband signals to X-band signals.

The input data is encoded through several DVB-S2 modulators/encoders. Parallel channels fed to RF-DAC (via high-speed digital interface). RF-DAC mixes different channels to different intermediate frequency (using fully digital control and mixers). Channels are added and fed to two high-speed DACs. The DAC typically outputs the modulated and combined channels at the S-band IF. All the processing done by the RF-DAC (other than the actual DAC output) is done digitally. The IF signals are converted to X-band and amplified by two power amplifiers. The two outputs of the amplifier can be used to forward the signal to the antenna(s) with left and right circular polarization. The earth station receives the radio frequency signal, separates the two polarizations, and transmits the result to the DVB-S2 demodulators, which demodulate the incoming data streams. Data streams are combined to create an output data stream.

During the entire pass, DVB-S2 modulators receive a MODCOD command to ensure the maximum bandwidth of the data channel within the given communication field.

Let's consider in detail the functional architecture of HDT. Fig. 2 shows the physical blocks (PCBs / modules), as well as the interfaces of the external and internal connectors of the HDT scheme.

The power board basically contains the DC-to-DC converter that is required to operate the HDT from the 28V bus. The regulator provides galvanic isolation and provides a fixed 12 V (or 15 V) output from which all internal voltages come. The Power Board also serves as a plinth for the digital board that provides the standard Cubesat form factor. The interface between the two boards is carried out through a standard PC104 connector.

The digital board contains an FPGA module (Enclustra Mercury XU8) and two RF-DACs. The digital card also contains high-speed data transfer interfaces in the form of two GTX links. By default, this interface type uses two SMP connectors per channel. An Enclustra Mer-

cury XU8 digital board and two RF-DACs are connected via the JESD204b interface. Both FPGAs and RF-DACs require an external heatsink to dissipate heat.

The HDT is implemented on the Xilinx® Zynq UltraScale+™ MPSoC FPGA, which is a high-performance system-on-chip device developed by Xilinx. This device combines a programmable logic matrix and ARM Cortex-A53 and Cortex-R5 processor cores, as well as several built-in functions and interfaces. The FPGA is located on the Enclustra Mercury XU8 module (Fig. 3). This is done to save time, cost, and design complexity, as it means that the auxiliary circuitry (SDRAM, flash memory, power supplies, etc.) requires no design effort. The main role of the FPGA is to package the input data stream of the GTX interface into DVB-S2 frames, which are converted into I and Q channels. The values of I and Q are then transmitted to the RF-DAC via the JESD204B interface.

The digital board contains an FPGA module (Enclustra Mercury XU5), as well as an RFDAC and an upconverter of the RFDAC output to S-band. This is done for this board to contain everything needed for use in a CubeSat (that is, it meets the needs of CubeCom). The board form factor is the standard CubeSat form factor. The board contains all the local regulators to allow it to operate from the voltage normally present in the Cubesat (as well as the intermediate voltage provided by the Power Board). The digital board also contains high-speed data transfer interfaces in the form of two GTX channels. By default, two SMP connectors per communication channel are used for this type of interface. The digital board has a heatsink that will cover its top and bottom parts. Both FPGAs and RFDACs need some way to dissipate heat. The transmitter is controlled via the CAN interface.

Consider a digital-to-analog converter. The HDT circuit uses a low-power AD9174 multi-channel dual DAC, which reduces power consumption in high-bandwidth and multi-channel applications while maintaining the required performance. The AD9174 is known to be a high-performance dual 16-bit DAC that supports DAC sampling rates up to 12.6 GSPS (Fig. 4). This device features an 8-lane 15.4Gbps JESD204B data input port, a high-performance on-chip DAC, and digital signal processing capabilities designed for single-band and multi-band direct-to-RF wireless applications.

The AD9174 has three integrated data input channels per RF DAC data channel. Each input channel is fully bypassed. Each data input channel (or channelizer) contains a configurable gain stage, an interpolation filter, and a numerically controlled channel oscillator for flexible multi-band frequency planning. The AD9174 supports input data rates up to 3.08 GSPS complex (in-phase/quadrans (I/Q)) or up to 6.16 GSPS non-complex (real) and can distribute multiple complex input data streams to dedicated channels for individual processing. Each group of three channelizers is summed into a corresponding main data path for additional processing when needed. Each main data channel contains an interpolation filter and one 48-bit main NCO before the RF DAC core.

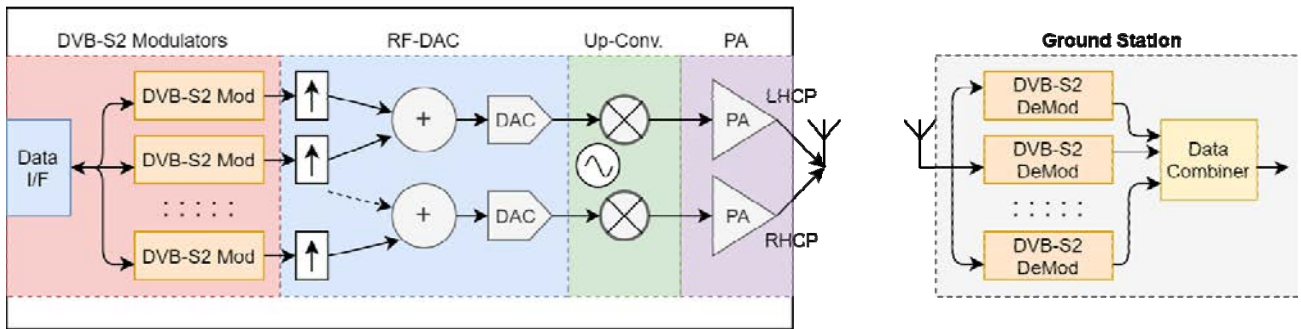


Figure 1 – Structural diagram of the proposed HDT

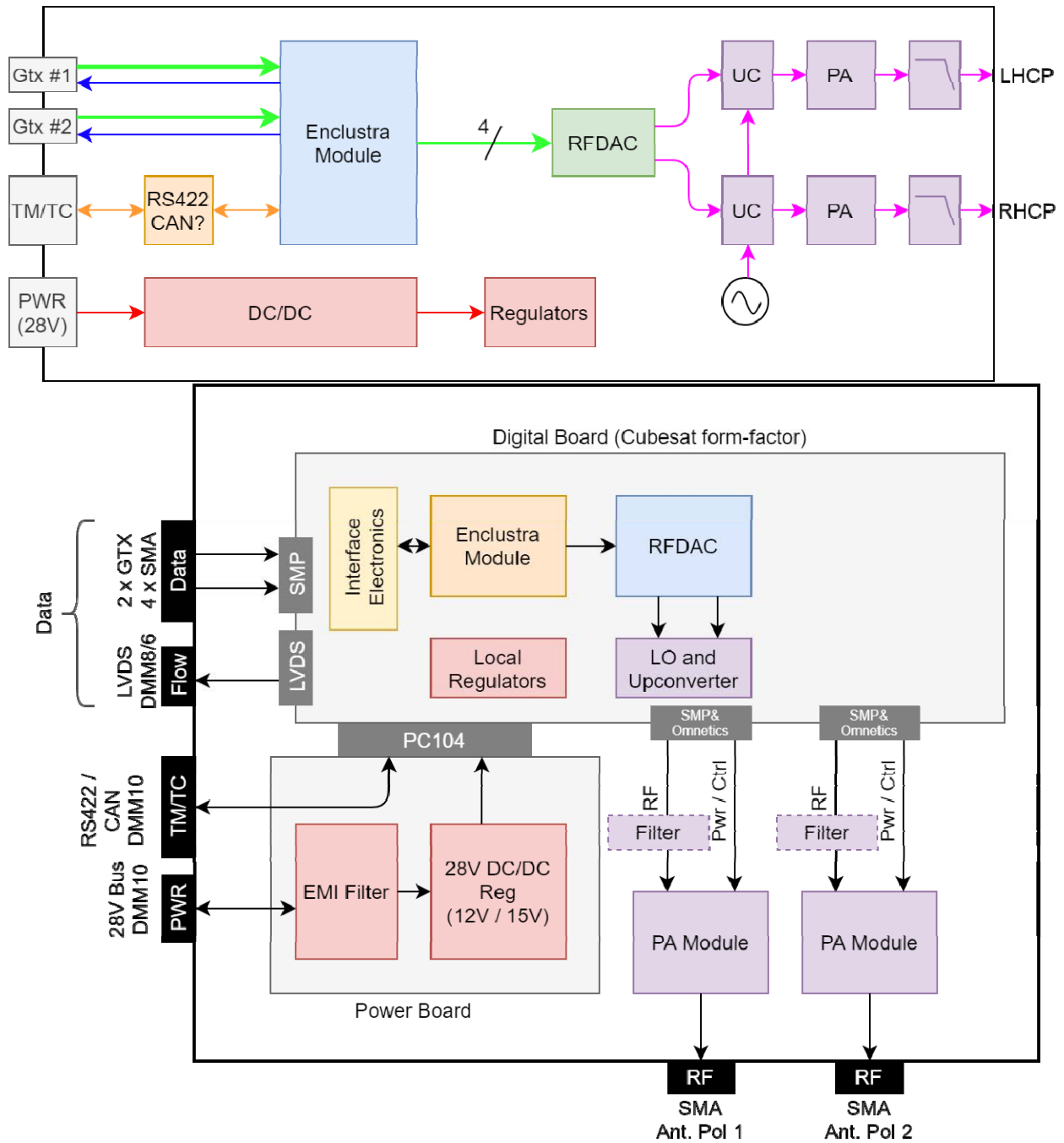


Figure 2 – HDT functional diagram

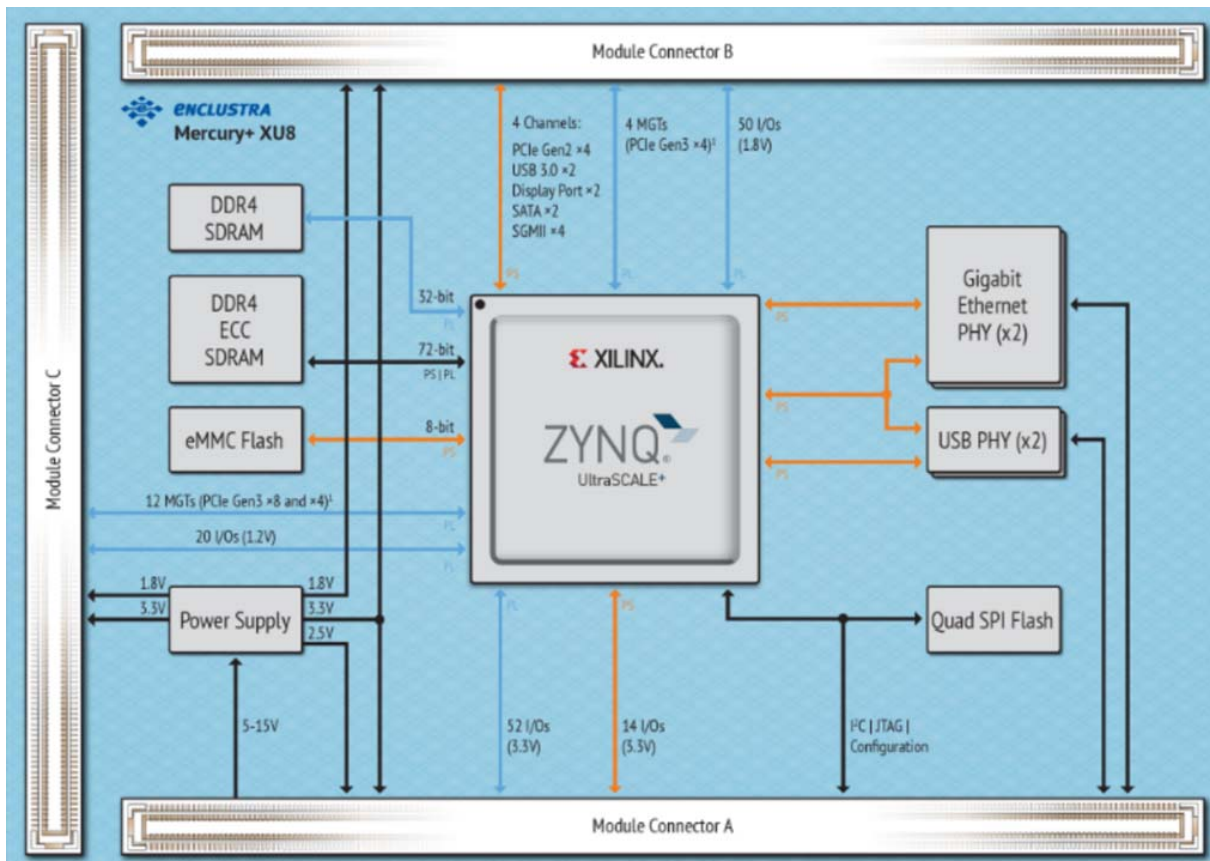


Figure 3 – Block diagram of the Enclustra Mercury XU8 module

## FUNCTIONAL BLOCK DIAGRAM

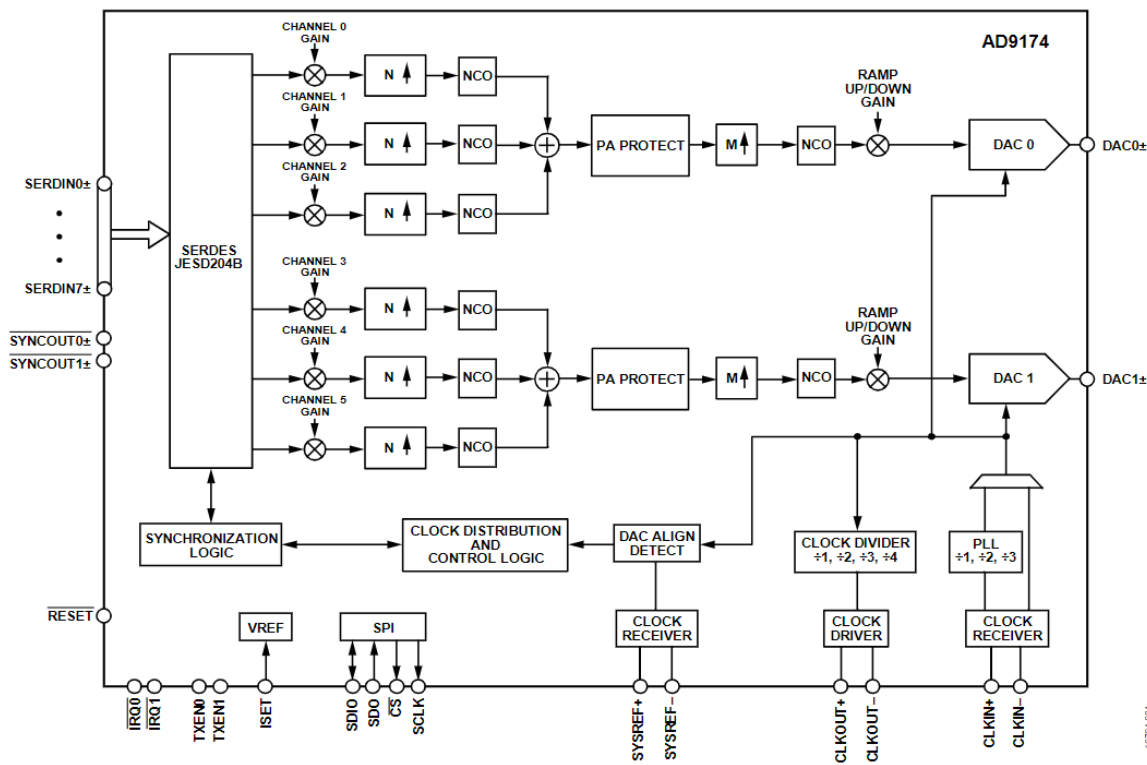


Figure 4 – Functional diagram of AD9174

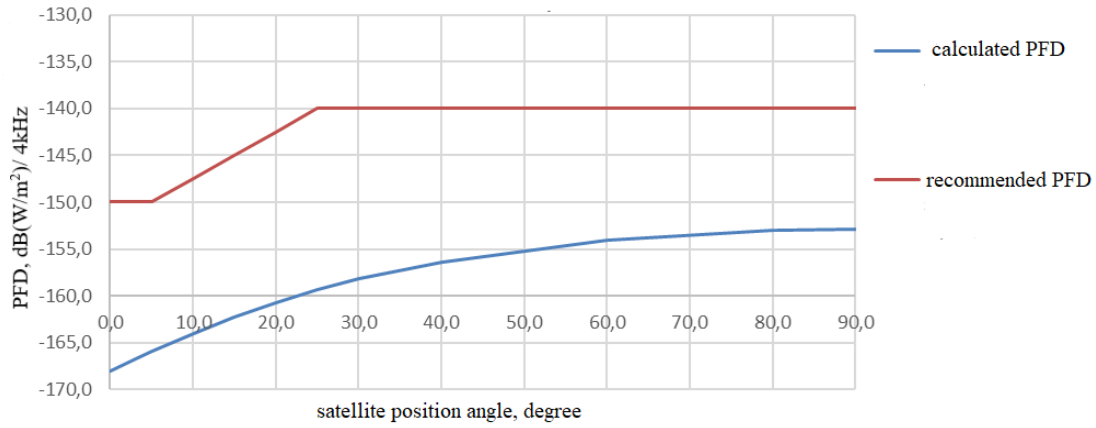


Figure 5 – Dependence of the PFD depending on the angle of the satellite site for the nominal height of the orbit of 400 km, with a transmitter power of 1 W

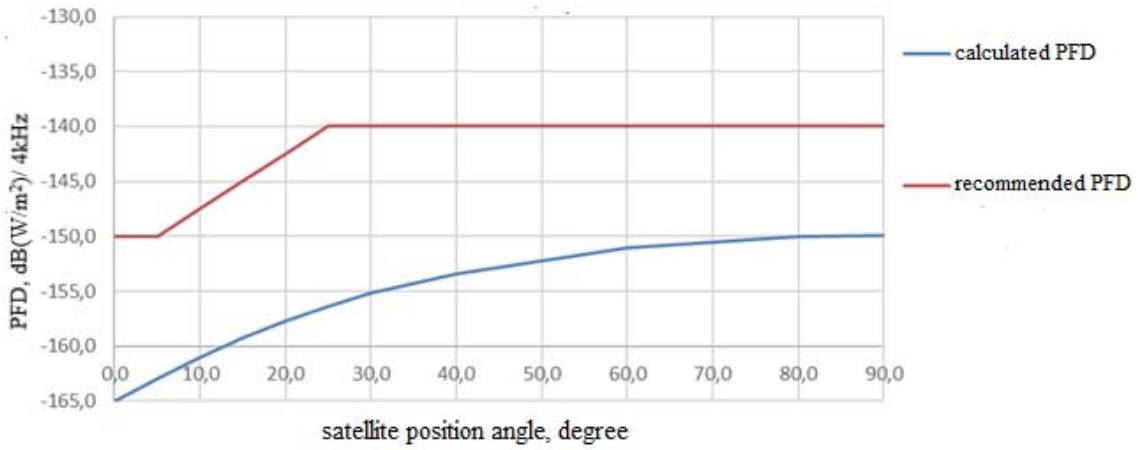


Figure 6 – Dependence of the PFD depending on the angle of the satellite site for the nominal height of the orbit of 400 km, with a transmitter power of 2 W

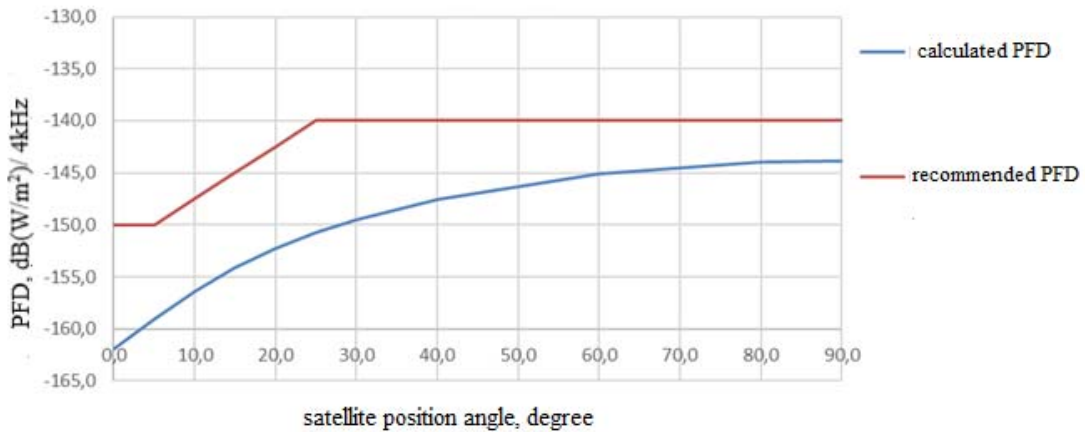


Figure 7 – Dependence of the PFD depending on the angle of the satellite site for the nominal height of the orbit of 200 km, with a transmitter power of 2 W

With a modulator switch, the main data path outputs can be routed to DAC0 alone for single DAC operation, or to both DAC0 and DAC1 for dual IF DAC operation.

The AD9174 also supports Ultra High Data Rate modes, which bypass the channel switch and primary data paths to provide maximum data rates of up to 6.16 GSPS as a single 16-bit DAC, up to 3.08 GSPS as a dual 16-bit DAC. Additionally, the main NCO blocks in the AD9174 contain a bank of 31 32-bit NCOs, each with an independent phase accumulator. Combined with an 80MHz serial peripheral interface for NCO programming, this bank provides phase coherent fast FFH for applications where NCO frequencies are continuously adjustable during operation.

Consider a power amplifier. Two separate PA modules are used to operate the LHCP and RHCP antennas. They consist of an S-band to X-band up-converter and a power amplifier. There are two more separate PAs. They are placed separately and have good thermal contact with the chassis/body. PA modules connect to the digital board via radio frequency communication (using the SMP connector) and the power and control channel (using the Omnetics connector). This is the internal interface. Note that it may be necessary to add additional filters in the RF lines to ensure compliance with ITU standards. Power amplifier modules have a radio frequency output (in the form of an SMA connector). PA modules are connected to the digital board through a radio frequency channel and a power and control channel.

#### 4 EXPERIMENTS

As part of this study, experiments were carried out with a high-speed downlink with 16 QAM: 100 Mbit/s for 237 Mbit/s (ACM13) and 348 Mbit/s (ACM17). During the experiment, an MGA antenna (horn antenna with an average gain of 13.5 dBi, a beam width of 20°) was used to ensure communication. The performance of the proposed system was shown.

In the course of this work, experiments were carried out with the transmission of high-speed data on the downlink, when the satellite passed at an elevation angle of  $>70^\circ$  in the Earth orientation mode. In this state, the earth station was within half the beam width of the on-board antenna. The transmitter retransmitted fixed known data (PN code). The received signals were demodulated and decoded by a software receiver. The calculated  $C/N_0$  ratio obtained based on the adopted IF spectrum was about 9.6 dB/Hz at the ground antenna elevation angle of  $84.5^\circ$  and the tilt range of 622 km. The measured bit error rate was  $1.2 \cdot 10^{-3}$  without error correction. After the turbo decoding process, the measured bit error rate was less than  $1.7 \cdot 10^{-9}$ .

The dependence of the power flux density at the input of the receiving antenna of the earth station, depending on the angle of the satellite at the receiving point, was investigated. A comparison of the calculated PFD for the proposed communication system and the recommended PFD according to the ITU Radio Regulations was made. Calculations were carried out in the Excel program, consider-

ing the typical values of the parameters of the satellite-Earth radio link.

#### 5 RESULTS

In Fig. 5 shows the dependence of the maximum PFD in the 4 kHz band near the Earth's surface depending on the satellite's elevation angle for a nominal orbit height of 400 km, with a transmitter power of 1 W. The blue curve shows the estimated PFD for the developed EO satellite communication system. The red curve corresponds to the recommendations of the ITU Radio Regulations.

In Fig. 6 shows the dependence of the maximum PFD in the 4 kHz band near the Earth's surface depending on the satellite's elevation angle for a nominal orbit height of 400 km, with a transmitter power of 2 W.

In Fig. 7 shows the dependence of the maximum PFD in the 4 kHz band near the Earth's surface depending on the satellite's elevation angle for a nominal orbit height of 200 km, with a transmitter power of 2 W.

#### 6 DISCUSSION

It is known that the ITU Radio Regulations impose a limit on the power flux density on the surface of the Earth for a signal coming from a satellite.

On the other hand, satellite communication systems must ensure very high reliability of reception of transmitted messages. Therefore, the use of multi-level modulation signals ensures high reliability of reception. In addition, reliability can be ensured by increasing the level of the signal arriving at the receiver input, that is, due to the use of sufficiently powerful transmitters, as well as due to receiving and transmitting antennas with a high gain, or due to the use of complex FEC coding.

It should be noted that section 25.208 of the Commission's regulations does not contain limits on the power flux density on the Earth's surface, which is generated by the radiation of NGSO EESS space stations operating in the 8025–8400 MHz range.

However, Table 21–4 of the ITU Radio Regulations states that for Earth Exploration Satellite Service (Space-Earth) and Space Exploration Service (Space-Earth) PFDs on the surface of the Earth generated by EESS space station emissions in the range 8025–8400 MHz, should not exceed the following values:

- 150 dB (W/m<sup>2</sup>) in any range of 4 kHz for angles of incidence from 0 to 5 degrees above the horizontal plane;
- $-150 + 0.5 (d^{-5})$  dB (W/m<sup>2</sup>) in any range of 4 kHz for angles of incidence  $d$  (in degrees) from 5 to 25 degrees above the horizontal plane;
- 140 dB (W/m<sup>2</sup>) in any 4 kHz range for incidence angles from 25 to 90 degrees above the horizontal plane.

These PFD limitations can be compared with the calculated PFD that can be obtained considering the standard conditions of electromagnetic wave propagation in free space, considering the typical losses in the transmission path (filters, power cables, splitters) of the proposed HDT.

From Fig. 5 – 7 the PFD on the surface of the Earth, which is generated by the X-band transmitter, in all

modes of operation and at satellite altitudes of 200 and 400 km corresponds to the PFD limits of the ITU Radio Regulations for all angles of arrival at a transmitter power of up to 2 W.

### CONCLUSIONS

The paper considers the concept of building a high-speed data transmitter using COTS technology and implements a communication system scheme based on the DVB-S standard using COTS. The analysis of the main features of the digital signal formation in the DVB-S standard and the improved DVB-S2X standard was carried out. It was established that even with the use of the DVB-S2X standard, it is impossible to fully reach the Shannon limit.

HDT is implemented on a Xilinx® Zynq Ultrascale+™ MPSoC FPGA, which sits on an Enclustra Mercury XU8 module with a high-performance dual 16-bit AD9174 DAC. It is shown that the function of adaptive modeling of ACM of the DVB-S standard proposed for the communication system allows automatic changes of transmission parameters in real time depending on the changing conditions of the channel. This provides an opportunity for more flexible and effective data transmission in various conditions, which allows to increase the amount of information transmitted during a communication session.

Performed calculations of the power flow density at the receiving location on Earth to find out the possible power of the on-board transmitter. An on-board transmitter of up to 2 W has been shown to meet the requirements of the ITU Radio Regulations for PFDs on the Earth's surface generated by EESS space station radiation in the 8025–8400 MHz range.

**The scientific novelty** of the obtained results lies in the fact that for the first time a scheme of a communication system based on the DVB-S standard using COTS, which can be applied to small EO satellites, is proposed.

**The practical significance** of the obtained results lies in the fact that an original scheme for building a high-speed data transmitter using COTS technology for small EO satellites has been developed. Formulated recommendations for improving the operation of the satellite communication system. It is shown that the use of the ACM adaptive modeling function of the DVB-S standard allows you to automatically change the transmission parameters in real time depending on the changing conditions of the channel. The obtained results can be applied in the construction of small EO satellites.

**Prospects for further research** are the study of OCS systems for EO needs

### ACKNOWLEDGEMENTS

The work was carried out with the assistance of the Department of Information Security and Telecommunications of the Dnipro University of Technology.

### REFERENCES

1. Liu S., Gao Z., Wu Y., Ng D. W. K., Gao X., Wong K.-K., Chatzinotas S., Otterst B. LEO satellite constellations for 5G and beyond: How will they reshape vertical domains? *IEEE Communications Magazine*, 2021, Vol. 59, No. 7, pp. 30–36. <https://doi.org/10.1109/MCOM.001.2001081>
2. Di B., Song L., Li Y., Poor H. V. Ultra-dense LEO: Integration of satellite access networks into 5G and beyond, *IEEE Wireless Communications*, 2019, Vol. 26, No. 2, pp. 62–69. <https://doi.org/10.1109/TWC.2018.2875980>
3. Leyva-Mayorga I., Soret B., Röper M., Wübgen D., Matthiesen B., Dekorsy A., Pop P. LEO small-satellite constellations for 5G and beyond-5G communications, *IEEE Access*, 2020, Vol. 8, pp. 184955–184964. <https://doi.org/10.1109/ACCESS.2020.3029620>
4. Su Y., Liu Y., Zhou Y., Yuan J., Cao H., Shi J. Broadband LEO satellite communications: Architectures and key technologies, *IEEE Wireless Communications*, 2019, Vol. 26, No. 2, pp. 55–61. <https://doi.org/10.1109/MWC.2019.1800299>
5. Xia S., Jiang Q., Zou C., Li G. Beam coverage comparison of LEO satellite systems based on user diversification, *IEEE Access*, 2019, Vol. 7, pp. 181656–181667. <https://doi.org/10.1109/ACCESS.2019.2959824>
6. Chen Q., Giambene G., Yang L., Fan C., Chen X. Analysis of inter-satellite link paths for LEO mega-constellation networks, *IEEE Transaction on Vehicular Technology*, 2021, Vol. 70, No. 3, pp. 2743–2755. <https://doi.org/10.1109/TVT.2021.3058126>
7. Manual of digital Earth. In Huadong G., Michael F. G., Alessandro A. (eds). Singapore, Springer Nature, 2020. 852 p. <https://doi.org/10.1007/978-981-32-9915-3>
8. Cuervo F., Ebert J., Schmidt M., Arapoglou P.-D. Q-Band LEO Earth observation data downlink: radiowave propagation and system performance, *IEEE Access*, 2021, Vol. 9, P. 165611–165617. <https://doi.org/10.1109/ACCESS.2021.3133390>
9. Kimijima S., Nagai M. High spatiotemporal flood monitoring associated with rapid lake shrinkage using planet small-sat and sentinel-1 data, *Remote Sensing*, 2023, No. 15, P. 1099. <https://doi.org/10.3390/rs15041099>
10. Babuscia A. Telecommunication systems for small satellites operating at high frequencies: a review. *Information*, 2020, No. 11, P. 258. <https://doi.org/10.3390/info11050258>
11. Monreal R. M., Alvarez J., Dennis G., Hollen J., Diaz T. Impact of single event effects on key electronic components for COTS-based satellite systems, *Radiation Effects Data Workshop*, 2019, pp. 1–7. <https://doi.org/10.1109/REDW.2019.8906573>
12. Petritoli E., Leccese F. COTS components for space applications: the evaluation of apparent activation energy (E<sub>aa</sub>), *IEEE 9th International Workshop on Metrology for AeroSpace (MetroAeroSpace)*, 2022, pp. 374–378. <https://doi.org/10.1109/MetroAeroSpace54187.2022.9856291>
13. Chaudhry A. U., Yanikomeroğlu H. Laser intersatellite links in a starlink constellation: a classification and analysis. *IEEE Vehicular Technology Magazine*, 2021, Vol. 16, No. 2, pp. 48–56. <https://doi.org/10.1109/MBT.2021.3063706>
14. Pavur J., Moser D., Lenders V., Martinovic I. Secrets in the sky: on privacy and infrastructure security in DVB-S satellite broadband, *Conference on Security and Privacy in Wireless and Mobile Networks*, 2019, pp. 277–284. <https://doi.org/10.1145/3317549.3323418>

15. Recommendation CCSDS 211.1-B-3, *Proximity-1 Space Data Link Protocol – Physical Layer*. Blue book: 2006.
16. Recommendation CCSDS 913.1-B-2, *Space Link Extension – Internet Protocol for Transfer Services*. Blue book: 2015.
17. Recommendation CCSDS 701.0-B-3, *Advanced Orbiting Systems, Networks and Data Links: Architectural Specification*. Blue book: 2001.
18. Recommendation CCSDS 727.0-B-5, *File Delivery Protocol (CFDP)*. Blue book: 2020.
19. Recommendation CCSDS 522.0-B-1, *Mission Operations – Common Services, Recommended Standard*. Blue book: 2020.
20. Recommendation CCSDS 131.0-B-3, *TM synchronization and channel coding*. Blue book, 2017.
21. Satellite missions' catalogue: Hodoyoshi-3 and 4 [Electronic resource]. Access mode: <https://www.eoportal.org/satellite-missions/hodoyoshi-3-4#launch>
22. The European space agency: missions/ WorldView-3 [Electronic resource]. Access mode: <https://earth.esa.int/eogateway/missions/worldview-3>
23. Hodges R. E., Lewis D. K., Radway M. J., Toorian A. S., Aguirre F. H., Hoppe D. J., Shah B. N., Gray A. A. The ISARA mission – flight demonstration of a high gain Ka-band antenna for 100Mbps telecom. *32nd Annual AIAA/USU Conference on Small Satellites*, 2018, pp. 1–5. Access mode: <https://digitalcommons.usu.edu/cgi/viewcontent.cgi?article=4104&context=smallsat>
24. Leveque K., Cuseo Z., King J., Cuseo Z., Babb R. Unlocking the next generation of nano-satellite missions with 320 Mbps Ka-band downlink: on-orbit results. *Small satellite conference*, 2019. Access mode: <https://digitalcommons.usu.edu/smallsat/2019/all2019/110/>
25. Optical Communications and Sensor Demonstration (OCS-D) [Electronic resource]. Access mode: <https://www.nasa.gov/smallspacecraft/ocsd-project/>
26. Sandberg A., Thieu A., Mankame A., Zachary P., Joel K., Mark W., Lulu L.  $\frac{1}{2}$ U low-cost laser guide star payload. *Journal of Astronomical Telescopes, Instruments and Systems*, 2022, Vol. 23, No. 8, pp. 1–17. <https://doi.org/10.1117/1.JATIS.8.3.039003>
27. Devaraj K., Ligon M., Blossom E., Breu J., Klofas B., Colton K., Kingsbury R. Planet high speed radio: crossing gbps from a 3U Cubesat. *Small satellite conference*, 2019. Access mode: <https://digitalcommons.usu.edu/cgi/viewcontent.cgi?article=4405&context=smallsat>
28. Devaraj K., Kingsbury R., Ligon M., Breu J., Vittaldev V., Klofas B., Yeon P., Colton P. Dove high speed downlink system, *31st Annual AIAA/USU Conference on Small Satellites*, 2017, pp. 1–9. Access mode: <https://digitalcommons.usu.edu/cgi/viewcontent.cgi?referer=&httpsredir=1&article=3797&context=smallsat>
29. Recommendation CCSDS 413.0-G-3, *Bandwidth-efficient modulations – summary of definition, implementation, and performance*. Green book, 2009.
30. Addabbo P., Antonacchio F., Beltramonte T., di Bisceglie M., Gerace F., Giangregorio G., Ullo S. L. A review of spectrally efficient modulations for Earth observation data downlink. *IEEE Metrology for aerospace (MetroAeroSpace)*, 2014, pp. 428–432. <https://doi.org/10.1109/MetroAeroSpace.2014.6865963>
31. Gao Z., Zhang L., Han R., Reviriego P., Li Z. Reliability evaluation of Turbo decoders implemented on SRAM-FPGAs, *VLSI Test Symposium*, 2020, pp. 1–6. <https://doi.org/10.1109/VTS48691.2020.9107638>

Received 08.01.2024.

Accepted 28.02.2024.

УДК 621.391.6

## ДОСЛІДЖЕННЯ ОСОБЛИВОСТЕЙ ФОРМУВАННЯ ЦИФРОВОГО СИГНАЛУ В СУПУТНИКОВИХ ЛІНІЯХ ЗВ'ЯЗКУ

**Магро В. І.** – канд. фіз.-мат. наук, доцент, професор кафедри безпеки інформації та телекомунікацій Національного технічного університету «Дніпровська політехніка», Дніпро, Україна.

**Панфілов О. Г.** – студент кафедри безпеки інформації та телекомунікацій Національного технічного університету «Дніпровська політехніка», Дніпро, Україна.

### АНОТАЦІЯ

**Актуальність.** Дистанційне зондування Землі нині знаходить широке застосування в різних галузях. Однією із проблем дистанційного зондування є створення недорогих супутникових систем, що працюють на полярних кругових орбітах. Дані системи потребують розробки прийомо-передавальної системи, що дозволяє передавати десятки гігабіт відеоінформації на земну приймальну станцію протягом десятка хвилин. Тобто існує потреба у створенні системи зв'язку що забезпечує високу швидкість передачі даних з малих супутників, вагою до 50 кг.

**Мета.** Метою роботи є дослідження особливостей формування цифрового сигналу в сучасних супутникових лініях зв'язку та розробка системи зв'язку з високою швидкістю передачі даних (зазвичай 300 Мбіт/с), яка може бути застосована до малих супутників дистанційного зондування Землі.

**Метод.** Запропонована концепція побудови високошвидкісного передавача даних із супутника дистанційного зондування землі із використанням технології комерційно готових або комерційно доступних готових продуктів. Виконані розрахунки щільності потоку потужності для з'ясування можливої потужності бортового передавача. Виконані розрахунки бюджету радіолінії супутник-Земля із застосуванням передбачених режимів команд на зміни кодування та модуляції.

**Результати.** Розроблена схема систему зв'язку на основі стандарту DVB-S з використанням технології комерційно готових продуктів. Високошвидкісний передавач даних реалізовано на FPGA Xilinx® Zynq Ultrascale+™ MPSoC, який розташований на модулі Enclustra Mercury XU8 з високопродуктивним подвійний 16-розрядним DAC AD9174. Бортовий передавач потужністю до 2 Вт задовольняє вимогам Регламенту радіозв'язку ITU до щільності потоку потужності на поверхні Землі, який створюється випромінюванням космічної станції EESS у діапазоні 8025–8400 МГц. Показано, що енергетичний запас лінії зв'язку в 3 дБ досягається для різних команд на зміни кодування та модуляції при збільшенні кута місця, що дозволяє збільшувати швидкість передачі інформації.

**Висновки.** Розроблена оригінальна прийомо-передавальна система для застосування в малих супутниках дистанційного зондування землі. Показано, що саме функція адаптивного моделювання ACM стандарту DVB-S дозволяє автоматично змінювати параметри передачі в реальному часі в залежності від змінюваних умов каналу, надаючи можливості більш гнучкої і

ефективної передачі даних у різних умовах, що дозволить збільшити об'єми інформації, які передаються за сеанс зв'язку. Запропонована система працює в X-діапазоні і побудована з використанням деталей COTS. У якості випромінювачів використовуються антени з двоїною поляризацією. Два фізичні канали представляють два режими поляризації: праву кругову поляризацію і ліву кругову поляризацію, кожна з яких має три частотні канали.

**КЛЮЧОВІ СЛОВА:** малий супутник, низька земна орбіта, дистанційне зондування Землі, густина потоку потужності, X-діапазон, DVB-S.

#### ЛІТЕРАТУРА

1. LEO satellite constellations for 5G and beyond: How will they reshape vertical domains? / [Liu S., Gao Z., Wu Y. et al.] // *IEEE Communications Magazine*. – 2021. – Vol. 59, No. 7. – P. 30–36. <https://doi.org/10.1109/MCOM.001.2001081>
2. Di B. Ultra-dense LEO: Integration of satellite access networks into 5G and beyond / B. Di, L. Song, Y. Li, H. Poor // *IEEE Wireless Communications*. – 2019. – Vol. 26, No. 2. – P. 62–69. <https://doi.org/10.1109/TWC.2018.2875980>
3. LEO small-satellite constellations for 5G and beyond-5G communications / [I. Leyva-Mayorga, B. Soret, M. Röper et al.] // *IEEE Access*. – 2020. – Vol. 8. – P. 184955 – 184964. <https://doi.org/10.1109/ACCESS.2020.3029620>
4. Broadband LEO satellite communications: Architectures and key technologies / [Y. Su, Liu Y., Y. Zhou et al.] // *IEEE Wireless Communications*. – 2019. – Vol. 26, No. 2. – P. 55–61. <https://doi.org/10.1109/MWC.2019.1800299>
5. Beam coverage comparison of LEO satellite systems based on user diversification / [S. Xia, Q. Jiang, C. Zou et al.] // *IEEE Access*. – 2019. – Vol. 7. – P. 181656–181667. <https://doi.org/10.1109/ACCESS.2019.2959824>
6. Analysis of inter-satellite link paths for LEO mega-constellation networks / [Q. Chen, G. Giambene, L. Yang et al.] // *IEEE Transaction on Vehicular Technology*. – 2021. – Vol. 70, No. 3. – P. 2743–2755. <https://doi.org/10.1109/TVT.2021.3058126>
7. Manual of digital Earth / [G. Huadong, F. G. Michael, A. Alessandro (eds)]. – Singapore : Springer Nature, 2020. – 852 p. <https://doi.org/10.1007/978-981-32-9915-3>
8. Q-Band LEO Earth observation data downlink: radiowave propagation and system performance / [F. Cuervo, J. Ebert, M. Schmidt, P.-D. Arapoglou] // *IEEE Access*, 2021. – Vol. 9. – P. 165611–165617. <https://doi.org/10.1109/ACCESS.2021.3133390>
9. Kimijima S. High spatiotemporal flood monitoring associated with rapid lake shrinkage using planet smallsat and sentinel-1 data / S. Kimijima, M. Nagai // *Remote Sensing*. – 2023. – No. 15. – P. 1099. <https://doi.org/10.3390/rs15041099>
10. Babuscia A. Telecommunication systems for small satellites operating at high frequencies: a review / A. Babuscia // *Information*. – 2020. – No. 11. – P. 258. <https://doi.org/10.3390/info11050258>
11. Impact of single event effects on key electronic components for COTS-based satellite systems / [R. M. Monreal, J. Alvarez, G. Dennis et al.] // *Proceeding of the IEEE Radiation Effects Data Workshop*. – 2019. – P. 1–7. <https://doi.org/10.1109/REDW.2019.8906573>
12. Petritoli E. COTS components for space applications: the evaluation of apparent activation energy (E<sub>aa</sub>) / E. Petritoli, F. Leccese // *Proceeding of the IEEE 9th International Workshop on Metrology for AeroSpace (MetroAeroSpace)*. – 2022. – P. 374–378. <https://doi.org/10.1109/MetroAeroSpace54187.2022.9856291>
13. Chaudhry A. U. Laser intersatellite links in a starlink constellation: a classification and analysis / A. U. Chaudhry, H. Yanikomeroğlu // *IEEE Vehicular Technology Magazine*. – 2021. – Vol. 16, No. 2. – P. 48–56. <https://doi.org/10.1109/MBT.2021.3063706>
14. Secrets in the sky: on privacy and infrastructure security in DVB-S satellite broadband / [J. Pavur, D. Moser, V. Lenders, I. Martinovic] // *Proceeding of the Conference on Security and Privacy in Wireless and Mobile Networks*. – 2019. – P. 277–284. <https://doi.org/10.1145/3317549.3323418>
15. Recommendation CCSDS 211.1-B-3. Proximity-1 Space Data Link Protocol – Physical Layer. Blue book. – 2006.
16. Recommendation CCSDS 913.1-B-2. Space Link Extension – Internet Protocol for Transfer Services. Blue book. – 2015.
17. Recommendation CCSDS 701.0-B-3. Advanced Orbiting Systems, Networks and Data Links: Architectural Specification. Blue book. – 2001.
18. Recommendation CCSDS 727.0-B-5. File Delivery Protocol (CFDP). Blue book. – 2020.
19. Recommendation CCSDS 522.0-B-1. Mission Operations – Common Services, Recommended Standard. Blue book. – 2020.
20. Recommendation CCSDS 131.0-B-3. TM synchronization and channel coding. Blue book. – 2017.
21. Satellite missions' catalogue: Hodo-yoshi-3 and 4 [Electronic resource]. – Access mode: <https://www.eoportal.org/satellite-missions/hodoyoshi-3-4#launch>
22. The European space agency: missions/ WorldView-3 [Electronic resource]. – Access mode: <https://earth.esa.int/eogateway/missions/worldview-3>
23. The ISARA mission – flight demonstration of a high gain Ka-band antenna for 100Mbps telecom / [R. E. Hodges, D. K. Lewis, M. J. Radway et al.] // *Proceeding of the 32nd Annual AIAA/USU Conference on Small Satellites*. – 2018. P. 1–5. – Access mode: <https://digitalcommons.usu.edu/cgi/viewcontent.cgi?article=4104&context=smallsat>
24. Unlocking the next generation of nano-satellite missions with 320 Mbps Ka-band downlink: on-orbit results / [K. Leveque, Z. Cuseo, J. King et al.] // *Proceeding of the Small satellite conference*. – 2019. – Access mode: <https://digitalcommons.usu.edu/smallsat/2019/all2019/110/>
25. Optical Communications and Sensor Demonstration (OCS) [Electronic resource]. – Access mode: <https://www.nasa.gov/smallspacecraft/ocsd-project/>
26. ½U low-cost laser guide star payload / [A. Sandberg, A. Thieu, A. Mankame et al.] // *Journal of Astronomical Telescopes, Instruments and Systems*. – 2022. – Vol. 23, No. 8. – P. 1–17. <https://doi.org/10.1117/1.JATIS.8.3.039003>
27. Planet high speed radio: crossing gbps from a 3U Cubesat / [K. Devaraj, M. Ligon, E. Blossom et al.] // *Proceeding of the Small satellite conference*. – 2019. – Access mode: <https://digitalcommons.usu.edu/cgi/viewcontent.cgi?article=4405&context=smallsat>
28. Dove high speed downlink system / [K. Devaraj, R. Kingsbury, M. Ligon et al.] // *Proceeding of the 31st Annual AIAA/USU Conference on Small Satellites*. – 2017. – P. 1–9. – Access mode: <https://digitalcommons.usu.edu/cgi/viewcontent.cgi?referer=&httpsredir=1&article=3797&context=smallsat>
29. Recommendation CCSDS 413.0-G-3. Bandwidth-efficient modulations – summary of definition, implementation, and performance. Green book. – 2009.
30. A review of spectrally efficient modulations for Earth observation data downlink / [P. Addabbo, F. Antonacchio, T. Beltramonte et al.] // *Proceeding of the IEEE Metrology for aerospace (MetroAeroSpace)*. – 2014. – P. 428–432. <https://doi.org/10.1109/MetroAeroSpace.2014.6865963>
31. Reliability evaluation of Turbo decoders implemented on SRAM-FPGAs / [Z. Gao, L. Zhang, R. Han et al.] // *Proceeding of the VLSI Test Symposium*. – 2020. – P. 1–6. <https://doi.org/10.1109/VTS48691.2020.9107638>

## SCATTERING OF ELECTROMAGNETIC WAVES ON FLAT GRID TWO-PERIODIC STRUCTURES

**Vanin V. A.** – Dr. Sc., Professor, Professor of the Department of Higher Mathematics, National Technical University “Kharkiv Polytechnic Institute”, Kharkiv, Ukraine.

**Pershyna I. I.** – Dr. Sc., Professor, Head of the Department of Higher Mathematics, National Technical University “Kharkiv Polytechnic Institute”, Kharkiv, Ukraine.

### ABSTRACT

**Context.** One of the scientific hypotheses for the creation of nonreciprocal optical metasurfaces is based on the use of a wave channel in which rays of the direct and reverse diffraction scenarios are realized on two-periodic flat structures with nonlinear elements. Such processes in the nanometer wavelength range of electronic devices require precise calculations of the interaction of waves and microstructures of devices. It is also important to describe the behavior of antenna devices in mobile communications. Expanding the wavelength range of stable communication is achieved by using prefractal structures in antenna devices in combination with periodic structuring. Similar modeling problems arise when electromagnetic waves penetrate materials with a crystalline structure (radio transparency).

**Objective.** To test this hypothesis, it is necessary to carry out mathematical modeling of the process of scattering of electromagnetic waves by metasurfaces under conditions of excitation of several diffraction orders. It is known that among two-periodic flat lattices of different structures there are five types that fill the plane. These are the Bravais grilles. The problem of scattering of an incident monochromatic TE polarized wave on a metal screen with recesses in two-periodic structures filled with silicon was considered.

**Method.** The paper builds mathematical models for the study of spatial-amplitude spectra of metasurfaces on Bravais lattices and gives some results of their numerical study. The condition for determining the diffraction orders propagating over the grating is proposed. Scattered field amplitudes are from the solution of the boundary value problem for the Helmholtz equation in the COMSOL Multiphysics 5.4 package. Similar problem formulations are possible when studying the penetration of an electromagnetic field into a crystalline substance.

**Results.** Obtained relations for diffraction orders of electromagnetic waves scattered by a diffraction grating. The existence of wavelengths incident on a two-periodic lattice for which there is no reflected wave is shown for different shapes (rectangular, square, hexagonal) of periodic elements in the center of which a depression filled with silicon was made. Distributions of reflection coefficients for different geometric sizes of colored elements and recesses are given. The characteristics of the electric field at resonant modes in the form of modulus isolines show the nature of the interaction of the field over the periodic lattice and the scatterers-depressions. At the resonant wavelengths of the incident waves, standing waves appear in the scatterers.

**Conclusions.** A mathematical model of the set of diffraction orders propagating from a square and hexagonal lattice into half-space is proposed  $z \geq 0$ . It has been shown that flat periodic lattice with square or hexagonal periodicity elements and resonant scatterers in the form of cylindrical recesses filled with silicon can produce a non-mirrored scattered field in metal. The response of the lattices to changes in the wavelength of the incident field by the structure of diffraction orders of the scattered field and high sensitivity to the rotation of the incident plane were revealed. The two-periodic lattices have prospects for creating anti-reflective surfaces of various devices. Two-periodic lattices have prospects for creating anti-reflective surfaces for various devices, laser or sensor electronic devices, antennas in mobile communication elements, and radio transparency elements. They have more advanced manufacturing technologies in relation to spatial crystal structures.

**KEYWORDS:** Maxwell’s equation, periodic lattice elements, diffraction, diffraction orders, non-reciprocity of diffraction spots, numerical tracking methods, resonant metasurface, non-specular reflection.

### NOMENCLATURE

EMW is an electro-magnetic wave;

$\vec{E}(x, y, z, t)$  is a vector of electrical intensity field;

$\vec{H}(x, y, z, t)$  is a vector of magnetic intensity field;

$\rho(x, y, z, t)$  is a density of distribution of electric charges;

$\epsilon_\alpha$  is an absolute electrical permeability of the medium;

$\epsilon_0$  is an electric constant (or vacuum permittivity);

$\mu_\alpha$  is an absolute magnetic permeability of the medium;

$\mu_0$  is a magnetic constant (or vacuum permeability);

$\sigma$  is a conductivity of the medium;

$\omega$  is a cyclic frequency;

$\vec{U}(x, y, z)$  is a total field amplitude;

$S_{mn}$  is a mode (harmonics);

$\Gamma_{mn}$  is a constant spreading for modes  $S_{mn}$ ;

$\theta$  is an EMF incidence angle;

$\varphi$  is an azimuthal angle of the plane of the wave vector of the incident wave;

$\alpha$  is an angle between the coordinate axes;

$\lambda$  is a wavelength;

$l_1, l_2$  are lattice parameters;

$a_1, h_1$  are the radius of the cylinder;

$h_1$  is a parameter of a cylindrical diffuser.

### INTRODUCTION

In cases where the characteristic dimensions of the obstacles to light propagation are proportional to the wavelength, adequate models of light diffraction on them are

based on the Maxwell's system of equations. Problems based on them are solved using the following numerical methods:

- finite and boundary element method for integral equations;
- modal methods for differential and integral equations;
- difference methods for systems of differential and integral equations;
- a method for solving problems on eigenvalues and eigenfunctions for differential and integral operators, which implements the projection method on the basis of the eigenfunctions of the problem operator.

Modal methods have a significant drawback - an increase in numerical complexity with an increase in the number of modes. The time-domain unfolding along orthogonal modes in the time domain for transversely inhomogeneous structures remains problematic.

**The object of study** is the diffraction of electromagnetic waves on biperiodic lattices with recesses.

**The subject of study** is the subject of the study is the conditions on diffraction orders scattered above the lattice and their amplitudes.

**The purpose of the work** is to separate the wavelengths of the incident field at which there is no reflected beam for different forms of periodic elements with a depression on a biperiodic lattice.

### 1 PROBLEM STATEMENT

To study the optical properties of complex periodic structures, it is necessary to overcome the limit of numerical complexity. This is possible when using numerical methods. Variation methods (for example, the Galerkin's method) applied to the Helmholtz equation with respect to the spatial amplitudes of the full field include the choice of the sampling scheme, construction and minimization. The obtained relations are transformed into a system of linear algebraic equations to which discrete analogues of boundary conditions are added.

Maxwell's equations for the electromagnetic field in a conducting medium are as follows:

$$\begin{cases} \varepsilon_\alpha \frac{\partial \vec{E}}{\partial t} + \sigma \vec{E} = \text{rot} \vec{H}, \\ -\mu_\alpha \frac{\partial \vec{H}}{\partial t} = \text{rot} \vec{E}, \\ \text{div} \vec{E} = \frac{\rho}{\varepsilon_\alpha}, \\ \text{div} \vec{H} = 0. \end{cases}$$

The system can be used to obtain wave equations for electric and magnetic tension vectors of field in the space-time representation or frequency range. Thus, for the vector  $\vec{E}(x, y, z, t) = \vec{U}(x, y, z)e^{i\omega t}$ , the amplitude of the total field  $\vec{U}(x, y, z)$  in the frequency domain is obtained from

the solution of the following boundary value problem for the system of equations in a three-dimensional periodic element over the plane of the structure.

$$\text{rot} \left[ \frac{1}{\mu_r} \text{rot} \vec{U} \right] - k_0^2 \left( \varepsilon_r - \frac{i\sigma}{\omega \varepsilon_0} \right) \vec{U} = 0.$$

Substituting the expansion of the field amplitude vector components along the basis from piecewise linear functions into the upper equation, we obtain residual for minimization together with additional boundary conditions on the perfectly conducting basis of the plane structure by projecting it onto the basic elements. We calculate the necessary characteristics of the scattered field above the lattice (for example, reflection coefficients of diffraction modes, intensity of scattered rays (modes), etc.) from the found field parameters.

Let us consider some rectangular and square periodic lattices with scatterers of different depth located in their centers, and forms in the plane, a fragment of which is shown in Fig. 1.

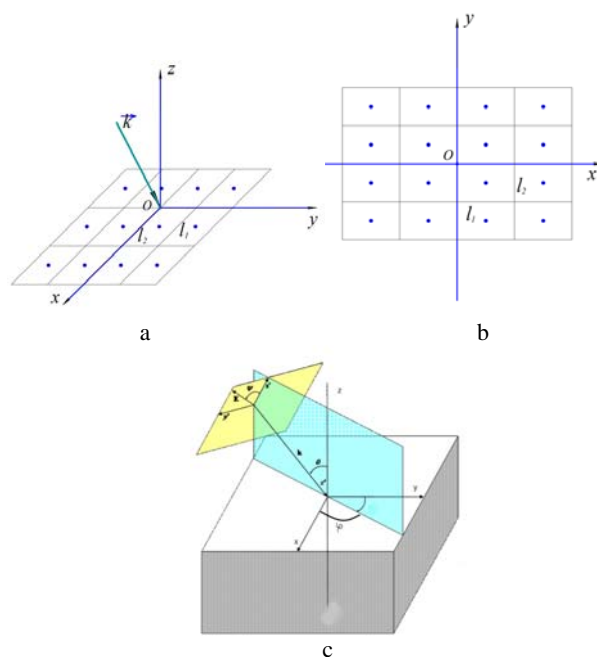


Figure 1 – Rectangular and square ( $l_1 = l_2$ ) lattice: a – spatial position; b – in-plane configuration of the lattice; c – angular characteristics of the falling field

The lattice formed by the periodic translation of the parallelogram ( $l_1 = l_2$ ) are also of practical interest (Fig. 2).

Hexagonal lattices are widely used in antenna technology. For example, the structure of graphene is a periodic combination of hexagonal elements (Fig. 3).

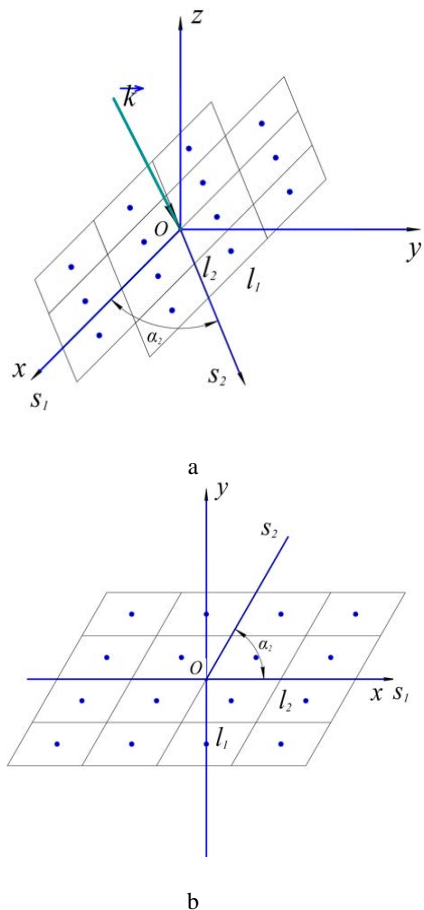


Figure 2 – Lattices made of parallelograms and rhombuses: a – spatial position; b – in-plane configuration of the grating

Fig. 3 shows the hexagonal elements and their associated three sets of rhombuses-shaped elements that fill the unbounded lattice plane and the required coordinate systems ( $xoy$  – the original coordinate system associated with hexagons,  $x'oy'$  – a coordinate system rotated by an angle  $\alpha$ ,  $s_1os_2$  – an oblique coordinate system associated with associates rhombuses, for example, type I).

Transmissive and reflective diffraction gratings are used to spatially separate electromagnetic waves (EMW) into a spectrum. We focus on the study of some of its regularities and methods of controlling the characteristics for two-periodic grilles-screens in the  $xoy$  plane. It is assumed that in the centers of the periodic elements there are depressions – scatterers of various shapes. For the study, we choose the first square grille (Fig. 1) with scatterers in the form of cylindrical recesses with radius  $a_1$  and depth  $h_1$  (Fig. 3b, c) that can be filled with different materials.

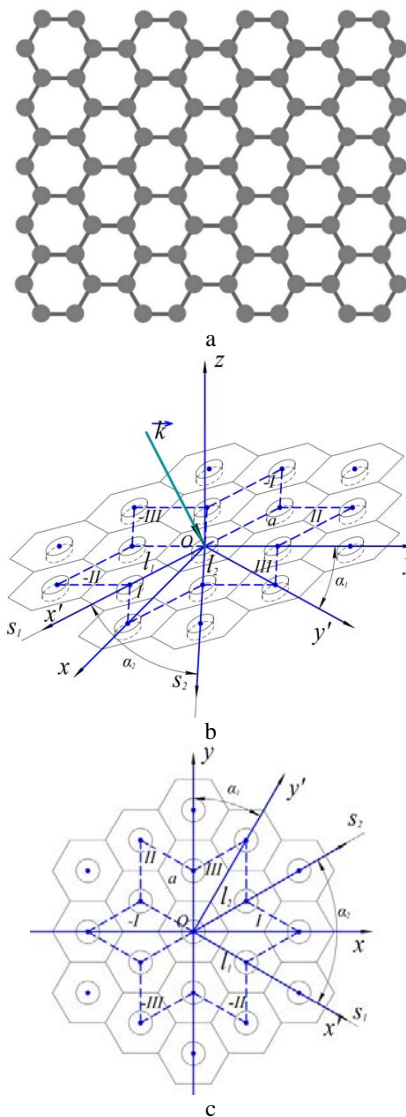


Figure 3 – The structure of grapheme: a – hexagonal lattice of graphene, carbon layer in a honeycomb packing, lattice of regular ( $l_1 = l_2$ ) hexagons; b – spatial position of the hexagonal lattice with cylindrical diffusers; c – a fragment of the lattice in the plane and possible rhombuses to fill it

## 2 REVIEW OF THE LITERATURE

The possibilities of using metamaterials in acoustics, optics and radiophysics are related to the results of research in the theory of electromagnetic wave diffraction on biperiodic flat structures. The characteristic size of the geometric periodicity is of the same order as the wavelength of the incident field. The parameters of dielectric and magnetic permeability also have corresponding periodic changes. Such structures have an advantage over spacious three-period structures in terms of their affordability. Flat biperiodic lattices in the radio and optical wavelength ranges allow obtaining zones of non-reciprocity (absence of reflected rays) in scattered or (deviations in the law of ray direction) penetrating rays (orders) of electromagnetic or sound waves that are not typical for natural materials. The similarity of the mechanisms of nonre-

reciprocal reflection and penetration into the material stimulated the development of their mathematical modeling based on Maxwell's equations. Among them, we note the tasks of studying the practical application of photonic crystals [1–3]. The study of the nonreciprocal scattering and the peculiarities of metamaterials in the form of biperiodic lattices with various shapes (Brave lattices) of a periodic element was performed in [4–7]. The presence of a scattered field without reflected rays is noted for some frequencies of the incident field. Numerical methods are used to study this phenomenon numerically [8–10]. A numerical study of the non-reciprocity phenomenon allows us to obtain detailed information about the polarization features of the scattered field and the diffraction orders of the rays in it.

### 3 MATERIALS AND METHODS

The scatterers can be located on two families of parallel lines with periods  $l_1$  and  $l_2$ . In the lattices plane, we introduce two coordinate systems – a rectangular one with the basis orths  $\overline{e}_x, \overline{e}_y$ , and an oblique one  $s_1os_2$  with the basis orths  $\overline{e}_1, \overline{e}_2$ . The position of the centers of the elements-scattering is determined by the radius-vector

$$\overline{\rho}_{v_1v_2} = v_1 l_1 \overline{e}_1 + v_2 l_2 \overline{e}_2.$$

Then the component of the wave vector incident field  $\overline{k}^I$  in the grille plane is

$$\overline{k}^I = k_1 \overline{e}_1 + k_2 \overline{e}_2, \quad \overline{k}^I = k_x \overline{e}_x + k_y \overline{e}_y.$$

The complete system of solutions of the scalar Helmholtz equation, in accordance with the requirements of Bloch's theorem (known as Floquet's theorem in one-dimensional problems), in the domain  $z > 0$  (over a periodic lattice) can be represented as [9–10].

$$S_{mn} = e^{i\Gamma_{mn}z} e^{i[(k_x - \frac{2\pi m}{l_1})x - \frac{2\pi n}{l_2}s_2]}.$$

Considering the obliquity ( $0 < \alpha \leq \pi/2$ ) of the coordinate system  $s_1os_2$  (Fig. 2) and its connection with the rectangular coordinate system  $xoy$ , where  $\alpha = \alpha_2$

$$\begin{pmatrix} \overline{e}_1 \\ \overline{e}_2 \end{pmatrix} = \begin{pmatrix} 1 & 0 \\ \cos \alpha & \sin \alpha \end{pmatrix} \begin{pmatrix} \overline{e}_x \\ \overline{e}_y \end{pmatrix} = A \begin{pmatrix} \overline{e}_x \\ \overline{e}_y \end{pmatrix},$$

$$\begin{pmatrix} s_1 \\ s_2 \end{pmatrix} = \begin{pmatrix} 1 & -ctg \alpha \\ 0 & 1/\sin \alpha \end{pmatrix} \begin{pmatrix} x \\ y \end{pmatrix} = B \begin{pmatrix} x \\ y \end{pmatrix},$$

then  $B = A^{-1}$  we will get

$$S_{mn} = e^{i\Gamma_{mn}z} e^{i(k_x - \frac{2\pi m}{l_1})x} e^{i(k_y + \frac{2\pi m}{l_1 tg \alpha} - \frac{2\pi n}{l_2 \sin \alpha})y}.$$

For each mode (harmonic)  $S_{mn}$ , the propagation constant along the z-axis is

$$\Gamma_{mn} = \sqrt{k^2 - \chi_x^2 - \chi_y^2},$$

where  $\chi_{x,m,n} = k_x - \frac{2\pi m}{l_1}$ ,  $\chi_{y,m,n} = k_y + \frac{2\pi m}{l_1 tg \alpha} - \frac{2\pi n}{l_2 \sin \alpha}$ ,

$$k_x = k \sin \theta \cos \varphi, k_y = k \sin \theta \sin \varphi, k = \frac{2\pi}{\lambda}.$$

Each spatial mode  $S_{mn}$  for which

$$\text{Im } \Gamma_{mn} \geq 0, \quad (1)$$

meets the condition of energy transfer from the grille plane. The mode ( $m = 0, n = 0$ ) is a mirror-reflected electromagnetic wave. From condition (1) we obtain

$$k^2 - \chi_{x,m,n}^2 - \chi_{y,m,n}^2 \geq 0.$$

We will study the condition for wave propagation in the region above the lattice as a set of admissible parameters of the incident wave and the geometric characteristics of the periodicity element of the lattices.

Let us introduce the characteristic function of parameters of the lattice and incident wave

$$F\left(m, n, \theta, \varphi, \frac{\lambda}{l_1}, \frac{\lambda}{l_2}, \alpha\right) = \left(\sin \theta \cos \varphi - m \frac{\lambda}{l_1}\right)^2 + \left(\sin \theta \sin \varphi - n \frac{\lambda}{l_2 \sin \alpha} + m \frac{\lambda}{l_1} \text{ctg} \alpha\right)^2 - 1,$$

then, the limit of the set of diffraction orders ( $m, n$ ) propagating from the lattice to the region  $z > 0$  is determined by equation.

$$F\left(m, n, \theta, \varphi, \frac{\lambda}{l_1}, \frac{\lambda}{l_2}, \alpha\right) = 0, \quad (2)$$

and the set of orders of propagating modes satisfies the condition

$$F\left(m, n, \theta, \varphi, \frac{\lambda}{l_1}, \frac{\lambda}{l_2}, \alpha\right) \leq 0. \quad (3)$$

In the case of a rectangular coordinate system from (2) with  $\alpha = \pi/2$ , we have

$$F\left(m, n, \theta, \varphi, \frac{\lambda}{\ell_1}, \frac{\lambda}{\ell_2}, \frac{\pi}{2}\right) = \left(\sin \theta \cos \varphi - m \frac{\lambda}{\ell_1}\right)^2 + \left(\sin \theta \sin \varphi - n \frac{\lambda}{\ell_2}\right)^2 - 1 = 0. \quad (4)$$

The region of propagation orders (Fig. 4) at  $\theta = \frac{\pi}{2.5}$ ,  $\varphi = \frac{\pi}{6}$ ,  $\lambda = 400$  nm,  $\ell_1 = 500$  nm,  $\ell_2 = 500$  nm looks like a circle, which includes a certain set of diffraction orders.

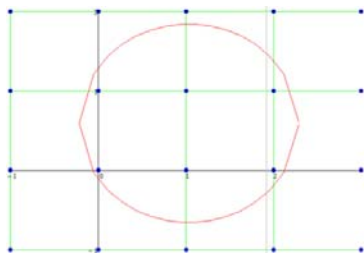


Figure 4 – Scattered diffraction orders for a square grating

$$\theta = \frac{\pi}{2.5}, \varphi = \frac{\pi}{6}, \lambda = 400 \text{ nm}, \ell_1 = 500 \text{ nm}, \ell_2 = 500 \text{ nm}$$

The region of propagation orders in the case  $\theta = \frac{\pi}{3}$ ,  $\varphi = \frac{\pi}{6}$ ,  $\lambda = 500$  nm,  $\ell_1 = 500$  nm,  $\ell_2 = 500$  nm (Fig. 5) includes only four diffraction orders (0, 0), (0, 1), (1, 0), (1, 1)

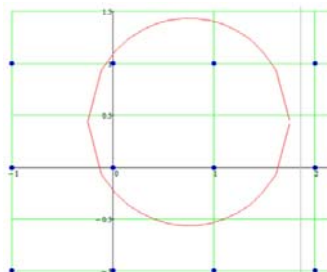


Figure 5 – Scattered diffraction orders for a square grating

$$\theta = \frac{\pi}{3}, \varphi = \frac{\pi}{6}, \lambda = 500 \text{ nm}, \ell_1 = 500 \text{ nm}, \ell_2 = 500 \text{ nm}$$

Parameters at which the two-beam scattering mode (0,0), (1,0) (Fig. 6) is realized, for example, can be  $\theta = \frac{\pi}{3}$ ,  $\varphi = 0$ ,  $\lambda = 500$  nm,  $\ell_1 = 500$  nm,  $\ell_2 = 500$  nm.

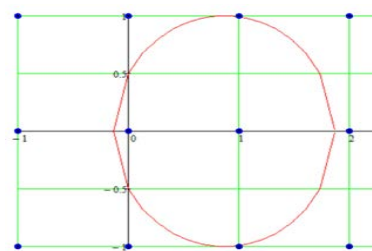


Figure 6 – Scattered diffraction orders for a square grating

$$\theta = \frac{\pi}{3}, \varphi = 0, \lambda = 500 \text{ nm}, \ell_1 = 500 \text{ nm}, \ell_2 = 500 \text{ nm}$$

Choosing the angles  $\theta$ ,  $\varphi$ ,  $\alpha$  and wavelength  $\lambda$  and the lattice parameters  $\ell_1$ ,  $\ell_2$ , we obtain the condition on the diffraction orders ( $m$ ,  $n$ ) of scattered waves in the region  $z > 0$  for parallelogram lattices. Thus, with  $\theta = \frac{\pi}{4.5}$ ,  $\varphi = \frac{\pi}{6}$ ,  $\lambda = 500$  nm,  $\ell_1 = 500$  nm,  $\ell_2 = 500$  nm,  $\alpha = \frac{\pi}{3}$ , we have a set of diffraction orders (Fig. 7a). The two-beam regime of scattering of orders (0, 0) and (1, 1) in such a grille is realized, for example, at  $\theta = \frac{\pi}{4.5}$ ,  $\varphi = 0$ ,

$\lambda = 500$  nm,  $\ell_1 = 500$  nm,  $\ell_2 = 500$  nm,  $\alpha = \frac{\pi}{3}$ , and with a further change of  $\alpha$  to  $\pi/6$ , the diffraction orders are localized (Fig. 7b).

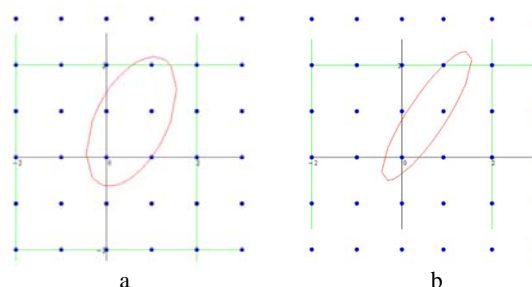


Figure 7 – Diffraction orders of a rhombus grille: a – ion orders

$$\text{for a square grating } \theta = \frac{\pi}{4.5}, \varphi = \frac{\pi}{6}, \lambda = 500 \text{ nm},$$

$$\ell_1 = 500 \text{ nm}, \ell_2 = 500 \text{ nm}, \alpha = \frac{\pi}{3}; \quad \text{b} - \alpha = \frac{\pi}{6}, \varphi = 0$$

In the case of a hexagonal grille (Fig. 3) (side of the hexagon  $a = 500$ nm), the propagation condition for the associated diamond-shaped grille for it

$$\Phi\left(m, n, \theta, \varphi, \frac{\lambda}{\ell_1}, \frac{\lambda}{\ell_2}, \alpha_1, \alpha_2\right) = \left(\sin \theta \cos \varphi - m \frac{\lambda}{\ell_1} \left[\cos(\alpha_1) + \frac{\sin(\alpha_1)}{\text{tg}(\alpha_1)}\right] + n \frac{\lambda}{\ell_2} \frac{\sin(\alpha_1)}{\sin(\alpha_2)}\right)^2 + \left(\sin \theta \cos \varphi - m \frac{\lambda}{\ell_1} \left[\sin(\alpha_1) + \frac{\cos(\alpha_1)}{\text{tg}(\alpha_2)}\right] + n \frac{\lambda}{\ell_2} \frac{\cos(\alpha_1)}{\sin(\alpha_2)}\right)^2 - 1 \leq 0, \quad (5)$$

where  $\alpha_1$  – angle of rotation of the coordinate system relative to the original, orthogonal one;  $\alpha_2$  – the angle between the axes of the oblique coordinate system associated with the rhombus  $\ell_1 = \ell_2$ .

#### 4 EXPERIMENTS

Of practical interest is the problem of increasing the power of some orders in the scattered field and minimizing the intensity of other orders, for example, (0,0). To

investigate this possibility, we performed a comparative analysis of the propagation sets for the studied gratings, controlled the composition of the propagation mode orders by the plane wave incidence angles, and estimated their intensity.

At this stage, we considered the linear problem of the electrodynamics of the incidence of a plane monochromatic wave with TE polarization on a metal screen with periodically arranged scatterers (Fig. 2). The size of the side of the square cell is  $a = 750\text{nm}$ , the dimensions of the cylindrical recess filled with silicon are  $\alpha_1 = 155\text{nm}$  (cylinder radius),  $h_1 = 75\text{nm}$  (depth). The incident wave is characterized by the angles of the wave vector  $\theta = 40^\circ, \varphi = 0^\circ$ . The plane of incidence of the wave, with such data, coincides with the coordinate plane  $xOz$ .

At such values of the interaction parameters, the propagation condition (Fig. 8) gives a two-beam scattering mode  $(0,0), (1,0)$  at a certain range of incident wavelengths. The red curve is the boundary of the region of diffraction orders of propagation. Inside, the dots indicate the orders of modes that propagate from the grille to the region  $z > 0$ .

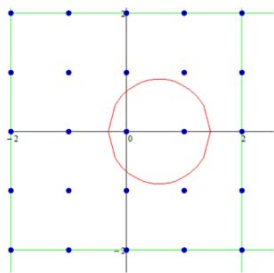


Figure 8 – Diffraction orders of grille with a square-cell at a two-beam composition of the scattered field

A direct numerical study of the diffraction of electromagnetic waves, solving the initial boundary value problem by the finite difference method for unsteady Maxwell's equations on a spatially periodic grille element with C-shaped strips of a given length of perfectly conductive inclusions, was performed in [11].

COMSOL Multiphysics 5.4 provides the ability to create and study various models of the interaction of electromagnetic waves with objects with a periodic structure. The package allows you to supplement the user interface with your own models. With the help of built-in physical interfaces and support from material properties libraries, it is possible to create adequate mathematical models to study the patterns and numerical characteristics of the interaction process.

The research used a section on the physics of beam optics. At the first stage, we considered a linear problem for the wave equations of electrodynamics when a plane monochromatic wave with a given polarization is incident on a two-periodic screen of scatterers (Fig. 2, 3). The problem for system (2) in the region (Fig. 9) is solved by the finite element method.

Fig. 9 shows a periodic fragment of the computational domain over a flat grille (a) and a variant of its discrete elemental breakdown (b) with cylindrical scatterers filled with silicon. The size of the side of the square is  $a = 750\text{nm}$ , the dimensions of the cylinder are  $\alpha_1 = 155\text{nm}, h_1 = 75\text{nm}$ . The incident wave is characterized by the angles of the wave vector  $\theta = 40^\circ, \varphi = 0^\circ$  and the power  $E_0 = 1\text{V/m}, H_0 = 1\text{A/m}$ . The plane of incidence of the wave, with such data, coincides with the coordinate plane  $xOz$ .

A set of input data has been prepared for the calculations

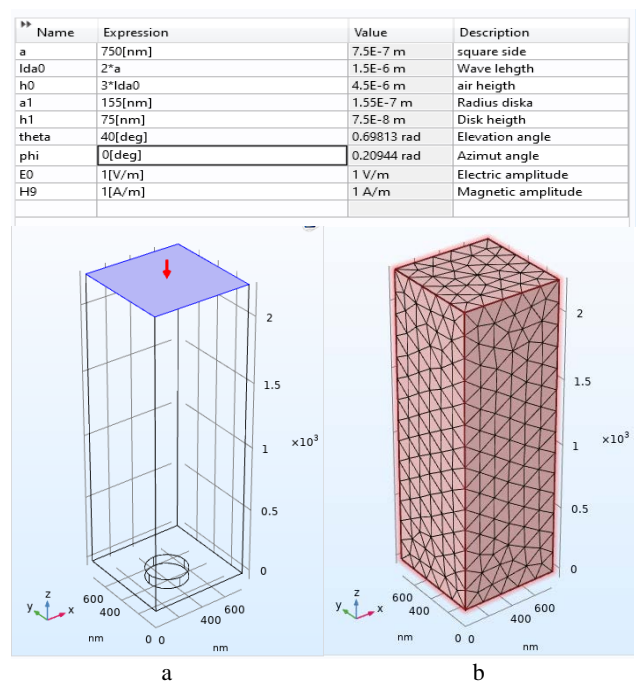


Figure 9 – Periodic element of the computational domain with an input boundary (a) and their finite element partition (b)

Zero amplitude of the mirror wave  $(0, 0)$  is realized by choosing the geometric parameters of a cylindrical diffruser – a recess ( $\alpha_1 = 155\text{nm}$ , and  $h_1 = 75\text{nm}$ ) filled with homogeneous silicon. The search for resonant wavelengths was performed in the range  $\lambda \in [800, 900]\text{nm}$ .

Fig. 10 shows the presence of an incident wavelength at which the reflection coefficient of the reflected wave (curve 1), mode  $(0, 0)$ , is zero, and for the other beam (curve 2), which corresponds to mode  $(1, 0)$ ,  $Kr = 1$ .

Fig. 10 shows that for a wave of  $\lambda^* \cong 848\text{nm}$ , the specular reflection coefficient is zero and the energy is emitted in modes of other orders. The cylindrical recess, which is filled with silicon, works as a waveguide connected to a free half-space and can be resonant. Analysis of the distribution of the modulus of the electric component of the field above the grille shows its moderate interference character. Under resonance conditions, the main field energy is localized in a cylindrical waveguide.

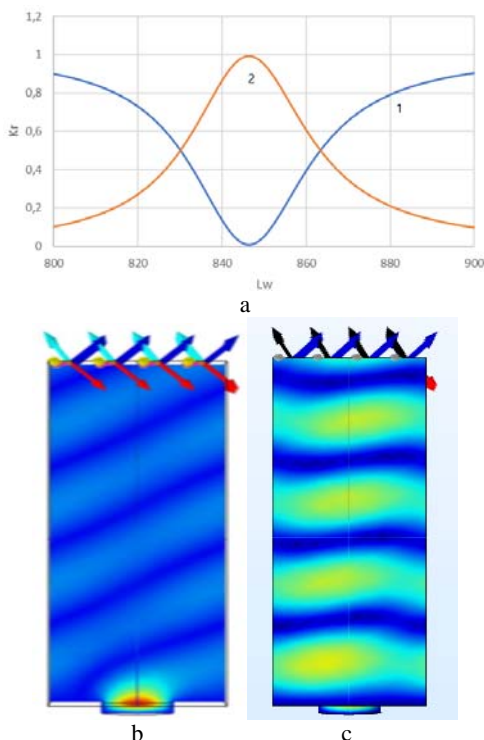


Figure 10 – Full field characteristics over a square lattice:  
 a – reflection coefficient of the incident wavelengths for the following parameters  $\alpha = 750 \text{ nm}$ ;  $\alpha_1 = 155 \text{ nm}$ ,

$h_1 = 75 \text{ nm}$ ;  $\theta = 40^\circ$ ,  $\varphi = 0^\circ$ ; b – isolines of the modulus of the electric field component in the  $xoz$  plane for  $\lambda^* \cong 848 \text{ nm}$ ; c – isolines of the modulus of the electric field component in the  $xoz$  plane for wavelengths other than resonant ones

The choice of the geometric dimensions of the cylindrical recess  $\alpha_1 = 300 \text{ nm}$ ,  $h_1 = 300 \text{ nm}$ , gives rise to a more complex dependence of the reflection coefficients on the incident wavelength (Fig. 11). In a cylindrical deepening-waveguide, a standing wave with two maxima is excited, which gives rise to the shown reflection distribution.

When comparing the isolines of the modulus of the amplitude of the electric component of the field, a change in the polarization of the full-field waves over the periodic grille is noticeable at different wavelengths of the incident field (Fig. 10 b, c).

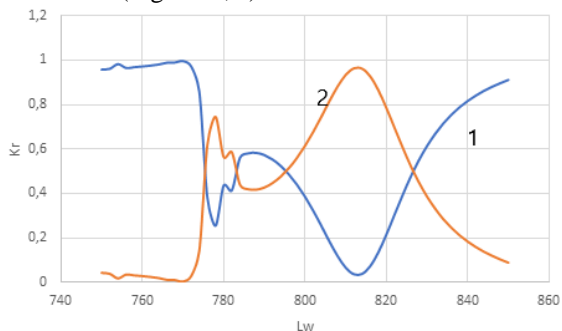


Figure 11 – Reflectance as a function of wavelength for the following parameters  $\alpha = 750 \text{ nm}$ ,  $\alpha_1 = 300 \text{ nm}$ ,  $h_1 = 300 \text{ nm}$ ,  $\theta = 40^\circ$ ,  $\varphi = 0^\circ$

A similar phenomenon of energy redistribution between waves of different orders for a given grille with square cells of periodicity can be found for other sizes of a cylindrical scatterer filled with silicon. Thus, Fig. 12 shows the results of calculations of the reflective properties of a periodic grille at the dimensions of the scatterer  $\alpha_1 = 300 \text{ nm}$ ,  $h_1 = 375 \text{ nm}$ . Resonant complete energy redistribution is realized at  $\lambda^* \cong 998 \text{ nm}$ .

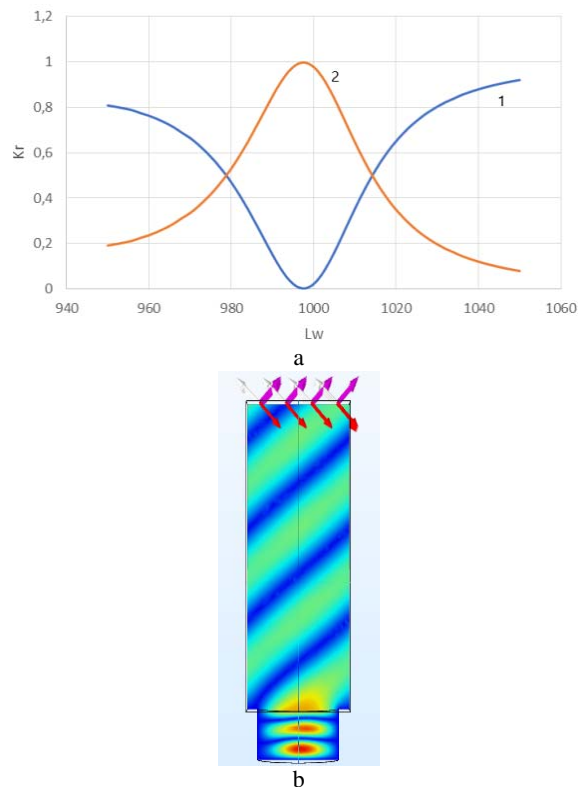


Figure 12 – Full field characteristics over a square lattice:  
 a – distribution of reflection coefficients (1-mirror beam, 2-non-mirror beam) along the incident wave length for parameters  $\alpha = 750 \text{ nm}$ ,  $\alpha_1 = 300 \text{ nm}$ ,  $\theta = 40^\circ$ ,  $\varphi = 0^\circ$ ,  $h_1 = 375 \text{ nm}$ ;  
 b – isolines of the modulus of the electric field component in the  $xoz$  plane for  $\lambda^* \cong 998 \text{ nm}$

More complicated reflection phenomena can be observed when the size of the waveguides or the angle of the wave incidence plane is changed, when a resonant standing wave with many maxima and a nonuniform distribution of electric field parameters at the boundary of the waveguide and free half-space  $z \geq 0$  is excited in the waveguide (Fig. 13).

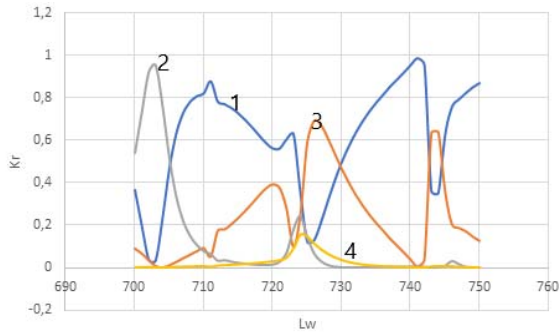


Figure 13 – Distribution of reflection coefficients (1-mirror beam, 2,3,4-nonmirror beams) by wavelength for parameter  $\alpha = 750$  nm,  $\alpha_1 = 300$  nm,  $h_1 = 375$  nm,  $\theta = 40^\circ$ ,  $\varphi = 45^\circ$

In the wave range (Fig. 13)  $\lambda \in [700,750]$ nm of the incident field, there are zones where the nature of the scattered electromagnetic field and the composition of the diffraction orders that create it change. At  $\lambda^* \approx 703$  nm we have a practically single-beam scattered field (curve 2), and at  $\lambda^* \approx 724$  nm the field is created by four beams, which changes to a single-beam field (curve 1) reflected at  $\lambda^* \approx 742$  nm. Thus, the realization of single-beam scattering is possible for a grille with not square-cell not only at angles  $\varphi = 0^\circ$  (Fig. 12), but also at other angles, for example,  $\varphi = 45^\circ$ .

We also investigated the case of a periodic grille with hexagonal elements in the period (Fig. 14). Fig. 15 shows the reflection intensity of different modes over a hexagonal grating.

The analysis of diffraction orders for a grille of regular hexagons and a grille of associated rhombuses provides different information about the composition of the set of propagation orders. Thus, applying condition (5) and condition (3), we obtain a different composition of the set of diffraction scattering orders.

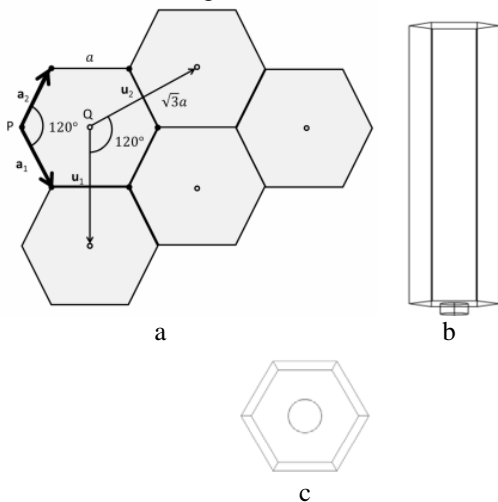


Figure 14 – Elements of periodicity of the geometry of the computational domain of the hexagonal lattice: a – general scheme, b – spatial image, c – projection on xoy

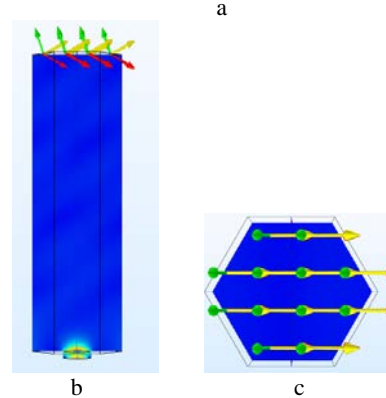
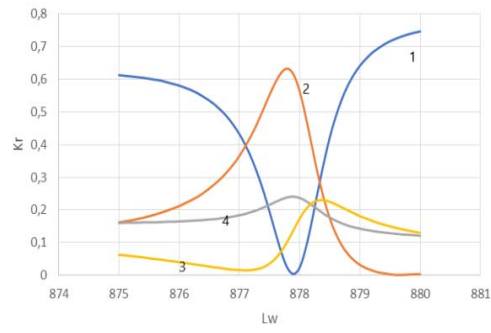


Figure 15 – Full field characteristics over a hexagonal lattice: a – distribution of reflection coefficients along the incident wavelength for parameters  $\alpha = 500$  nm,  $\alpha_1 = 155$  nm,  $h_1 = 75$  nm,

$$\theta = \frac{\pi}{3}, \varphi = 60^\circ; \text{ b – isolines of the modulus of the electric field}$$

vector above the grating; c – wave vectors of modes at the input boundary of the computational domain (plane parallel to xoy),  $\lambda = 877.8$  nm

It can be seen from Fig. 15 that the scattered field of a periodic grille made of hexagonal elements with cylindrical scatterers, the size of which is similar to a square grille, almost does not have geometric reflection at a wavelength of  $\lambda = 877.8$  nm. The energy from the incident mode is transformed into several scattered modes.

In the case  $\alpha = 500$  nm,  $\alpha_1 = 155$  nm,  $h_1 = 75$  nm,  $\theta = \frac{\pi}{3}$ ,  $\varphi = 0^\circ$ , we have a two-beam case of the scattered field above the grille in a certain range of incident wavelengths (Fig. 16).

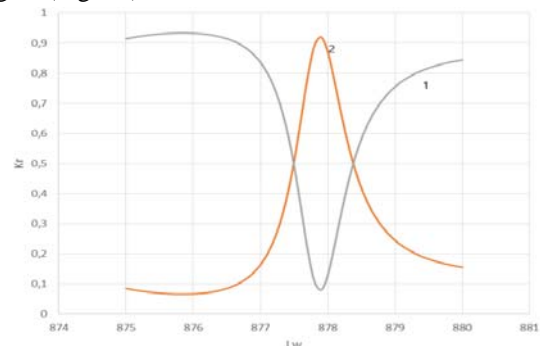


Figure 16 – Distribution of reflection coefficients (1-mirrored beam, 2-non-mirrored beam) along the incident wavelength for the parameters  $\alpha = 500$  nm,  $\alpha_1 = 155$  nm,  $h_1 = 75$  nm,  $\theta = \frac{\pi}{3}$ ,  $\varphi = 0^\circ$

We found (Fig. 16) a regime for a grille of regular hexagons where two-beam scattering with a minimum intensity of the reflected beam is realized in the main field.

It is further found that the distribution of the scattering coefficient at  $\varphi = -60^\circ$  coincides with the distribution at  $\varphi = 0$ .

## 5 RESULTS

A mathematical model of the set of diffraction orders propagating from a square and hexagonal lattice into half-space is proposed  $z \geq 0$ .

It is shown that flat periodic lattices with square or hexagonal periodicity elements and resonant scatterers in the form of cylindrical recesses filled with silicon in a metal can create a non-mirrored scattered field.

The response of gratings to a change in the wavelength of the incident field by the structure of the diffraction orders of the scattered field and a high sensitivity to the rotation of the plane of incidence have been revealed.

## 6 DISCUSSION

The behavior of the electromagnetic field in photonic crystals and near biperiodic lattices is explained by the possibility of influencing the Braggian scattering by periodic inhomogeneity of the medium.

The existence of metamaterials for which there are continuous intervals of wavelengths of the incident field with a nonreciprocal scattered field is important.

Some researchers consider metamaterials formed by hexagonal, square cells with symmetry breaking out of plane or in plane. Such designs have a free space in the middle of the cell where you can place some controls. Then a strong electric field concentration in the near field can be achieved. This field behavior can be useful in laser or sensor devices.

## CONCLUSIONS

**The scientific novelty** is the analysis of the diffraction orders of electromagnetic field rays over a biperiodic lattice, which allows us to determine the ray composition of the scattered field.

The amplitude characteristics of the rays are determined from the solution of the boundary value problem for the Helmholtz equation in the frequency domain. Numerical methods for Maxwell's equations in time-space coordinates are promising [11].

The proposed analysis of the orders of diffraction of electromagnetic field rays on a biperiodic lattice on a perfectly conducting substrate allows us to determine the ray composition of the scattered field.

The amplitude characteristics of the beams are determined from the solution of the boundary value problem for the Helmholtz equation in the frequency domain. We show the existence of wavelengths of the incident field at which only non-mirrored rays with nonzero amplitude exist. This makes it possible to use such lattices in a variety of electronic devices.

In the case of arbitrary time-dependence of the parameters of the passive field, numerical methods for Maxwell's equations in time-space coordinates are promising [11].

**The practical significance** of this work is detection of features of the behavior of the scattered field over a biperiodic lattice can be used to create non-reflective surfaces, creating anti-reflective coatings in various devices.

The revealed features of the scattered field behavior over a hyperperiodic grating can be used to create non-reflective surfaces, creating anti-reflective coatings in various devices, broadband mobile antennas, and sensor devices

**Prospects for further research** are studies on the influence of boundary conditions in the mathematical model on the composition of scattered diffraction orders and the relationship between diffraction orders of the scattered field and characteristic directions (eigenvalues and eigenvectors of Jacobi matrices).

Two-periodic gratings have prospects for creating anti-reflective surfaces for various devices.

## REFERENCES

1. Joannopoulos J. D., Johnson S. G., Winn J. N., Meade R. D. Photonic Cristal. Molding the Flow of Light. United Kingdom, Princeton University Press, 2008, 286 p.
2. Vetluzhsky A. Yu. Method of self-consistent equations in solving problems of wave scattering on systems of cylindrical bodies, *Computer research and modeling*, 2021. Vol. 13, No. 4, pp. 725–733. DOI: 10.20537/2076-7633-2021-13-4-725-733
3. Vetluzhskii A. Yu. Waveguides based on linear defects in metal electromagnetic crystals, *Technical Physics*, 2017, Vol. 62, №1, pp. 178–182. DOI:10.1134/S106378421701025X
4. Papanikolaou N., Fedotov V. A., Zheludev N. I. et al. Metamaterial analog of electromagnetically induced transparency, *Physical Review Letters*, 2008, Vol. 101, № 25, pp. 253–263. DOI:10.1103/physrevlett.101.253903
5. Dmitriev V. Symmetry properties of electromagnetic planar arrays in transfer matrix description, *IEEE Transactions on Antennas and Propagation*, 2013, Vol. 61, № 1, pp. 185–194. DOI: 10.1109/TAP.2012.2220316
6. Kawakatsu M. N., Dmitriev V. A. and Prosvirnin S. L. Microwave frequency selective surfaces with high Q-factor resonance and polarization insensitivity, *Journal of Electromagnetic Waves and Applications*, 2010, Vol. 24, pp. 261–270. DOI: 10.1163/156939310790735741
7. Carrasco E., Tamagnone M., Mosig J. R. et al. Gate-controlled mid-infrared light bending with aperiodic graphene nanoribbons array, *Nanotechnology*, 2015, Vol. 26, № 3, pp. 134–142. DOI 10.1088/0957-4484/26/13/134002
8. Lin X., Wan N., Weng L., Zhu H. FDTD Method and Models in Optical Education, *14th Conference on Education and Training in Optics and Photonics, Hangzhou, 29–31 May 2017: proceedings*. Hangzhou, Zhejiang Univ, 2017, pp. 104–124. DOI 10.1117/12.2268324
9. Gao Y. J., Yang H. W., Wang G. B. A research on the electromagnetic properties of Plasma Photonic Crystal based on the Symplectic Finite-Difference Time-Domain method, *Optik*, 2016, Vol. 127, Iss. 4, pp. 1838–1841. DOI: 10.1016/j.ijleo.2015.11.089
10. Cardoso J. R. Electromagnetics through the Finite Element Method: A Simplified Approach Using Maxwell's equations. Boca Raton, Taylor & Francis, 2016, 212 p. DOI: 10.1201/9781315366777
11. Prosvirnin S. L., Vanin V. A. Monotonous differences schemes for the Maxwell equations in the problem of non-stationary

УДК 519+537.874.6

## РОЗСІЮВАННЯ ЕЛЕКТРОМАГНІТНИХ ХВИЛЬ НА ПЛОСКИХ РЕШІТЧАТИХ ДВОХПЕРІОДИЧНИХ СТРУКТУРАХ

**Ванін В. А.** – д-р техн. наук, професор, професор кафедри вищої математики Національного технічного університету «Харківський політехнічний інститут», Харків, Україна.

**Першина Ю. І.** – д-р фіз.-мат. наук, професор, завідувач кафедри вищої математики Національного технічного університету «Харківський політехнічний інститут», Харків, Україна.

### АНОТАЦІЯ

**Актуальність.** Одна з наукових гіпотез створення невзаємних контрольованих оптичних метаповерхонь є використання хвильового каналу, який базується на променях прямого та зворотного сценаріїв дифракції на двоперіодичних плоских структурах з нелінійними елементами. Такі процеси в нанометровому діапазоні хвиль електронних пристроїв вимагають точних розрахунків процесів взаємодії хвиль і мікροструктур приладів. Важливо також описати поведінку антенних пристроїв в засобах мобільного зв'язку. Розширення діапазону довжин хвиль стабільного зв'язку досягається на дофрактальних структурах в антенних пристроях у поєднанні із періодичним структуруванням. Схожі проблеми моделювання виникають і при проникненні електромагнітних хвиль через матеріали із кристалічною структурою (радіопрозорість).

**Мета.** Для перевірки цієї гіпотези необхідно провести математичне моделювання процесу розсіяння електромагнітних хвиль метаповерхнями в умовах збудження декількох дифракційних порядків. Як відомо, серед двоперіодичних плоских решіток різних структур є п'ять типів, які покривають площину. Це є решітки Браве. Розглядалась задача розсіювання падаючої монохроматичної ТЕ поляризованої хвилі на металевий екран із заглибленнями в двоперіодичних структурах, заповнених кремнієм.

**Метод.** В роботі побудовані математичні моделі для вивчення просторових амплітудних спектрів метаповерхонь на решітках Браве та наведені деякі результати їх чисельного дослідження. Запропонована умова визначення дифракційних порядків які розповсюджуються над решіткою. Амплітуди розсіяного поля знаходяться із розв'язання крайової задачі для рівняння Гельмгольца в пакеті COMSOL Multiphysics 5.4. Аналогічні постановки задач можливі і при дослідженні проникнення електромагнітного поля в кристалічну речовину.

**Результати.** Отримані співвідношення для дифракційних порядків розсіяних електромагнітних хвиль дифракційною решіткою. Показано існування довжин падаючих хвиль на двоперіодичну решітку для яких відсутня віддзеркалена хвиля при різних формах (прямокутна, квадратна, шестикутна) періодичних елементів в центрі яких було виконане заглиблення, наповнене кремнієм. Приведені розподіли коефіцієнту віддзеркалення при різних геометричних розмірах періодичних елементів і заглиблення. Характеристики електричного поля на резонансних режимах у вигляді ізоляції його модуля показують характер взаємодії поля над періодичною решіткою і розсіювачами-заглибленнями. На резонансних довжинах падаючих хвиль виникають стоячі хвилі в розсіювачах.

**Висновки.** Запропонована математична модель множини дифракційних порядків які розповсюджуються від квадратної та шестикутної решітки в півпростір. Показано, що плоскі періодичні решітки із квадратними або шестикутними елементами періодичності та резонансними розсіювачами у вигляді циліндричних заглиблень, заповнених кремнієм, у металі можуть створювати недзеркальне розсіяне поле. Виявлена реакція решіток на зміну довжини хвилі падаючого поля структурою дифракційних порядків розсіяного поля та висока чутливість до повороту площини падіння. Двоперіодичні решітки мають перспективу при створенні антиблікових поверхонь різних пристроїв. The two-periodic lattices have prospects for creating anti-reflective surfaces of various devices. Двоперіодичні решітки мають перспективу при створенні антиблікових поверхонь різних пристроїв, лазерних чи сенсорних радіоелектронних пристроїв, антен в елементах мобільного зв'язку, радіопрозорих елементів. Вони мають більш розвинені технології виготовлення по відношенню до просторових кристалічних структур.

**КЛЮЧОВІ СЛОВА:** рівняння Максвела, періодичні елементи решітки, дифракція, дифракційні порядки, невзаємність дифракційних явищ, чисельні методи досліджень, резонансна метаповерхня, невзаємне віддзеркалення.

### ЛІТЕРАТУРА

1. Photonic Cristal. Molding the Flow of Light / [J. D. Joannopoulos, S. G. Johnson, J. N. Winn, R. D. Meade]. – United Kingdom: Princeton University Press, 2008. – 286 p.
2. Vetluzhsky A. Yu. Method of self-consistent equations in solving problems of wave scattering on systems of cylindrical bodies/ A. Yu. Vetluzhsky // Computer research and modeling. – 2021. – Vol. 13, No. 4 – P. 725–733. DOI: 10.20537/2076-7633-2021-13-4-725-733
3. Vetluzhskii A. Yu. Waveguides based on linear defects in metal electromagnetic crystals / A. Yu. Vetluzhsky // Technical Physics. – 2017. – Vol. 62, №1. – P. 178–182. DOI:10.1134/S106378421701025X
4. Metamaterial analog of electromagnetically induced transparency / [N. Papasimakis, V. A. Fedotov, N. I. Zheludev et al.] // Physical Review Letters. – 2008. – Vol. 101, № 25. – P. 253–263. DOI:10.1103/physrevlett.101.253903
5. Dmitriev V. Symmetry properties of electromagnetic planar arrays in transfer matrix description / V. Dmitriev // IEEE Transactions on Antennas and Propagation. – 2013. – Vol. 61, № 1. – P. 185–194. DOI: 10.1109/TAP.2012.2220316
6. Kawakatsu M. N. Microwave frequency selective surfaces with high Q-factor resonance and polarization insensitivi / M. N. Kawakatsu, V. A. Dmitriev, and S. L. Prosvirnin // Journal of Electromagnetic Waves and Applications. – 2010. – Vol. 24. – P. 261–270. DOI: 10.1163/156939310790735741
7. Gate-controlled mid-infrared light bending with aperiodic graphene nanoribbons array [E. Carrasco, M. Tamagnone, J. R. Mosig et al.] // Nanotechnology. – 2015. – Vol. 26, № 3. – P. 134–142. DOI 10.1088/0957-4484/26/13/134002
8. FDTD Method and Models in Optical Education [X. Lin, N. Wan, L. Weng, H. Zhu] // 14th Conference on Education and Training in Optics and Photonics, Hangzhou, 29–31 May 2017: proceedings.– Hangzhou, Zhejiang Univ, 2017. – P. 104–124. DOI 10.1117/12.2268324
9. Gao Y. J. A research on the electromagnetic properties of Plasma Photonic Crystal based on the Symplectic Finite-Difference Time-Domain method / Y. J. Gao, H. W. Yang, G. B. Wang // Optik. – 2016. – Vol. 127, Iss. 4. – P. 1838–1841. DOI: 10.1016/j.ijleo.2015.11.089
10. Cardoso J. R. Electromagnetics through the Finite Element Method: A Simplified Approach Using Maxwell's equations / J. R. Cardoso. – Boca Raton: Taylor & Francis, 2016. – 212 p. DOI: 10.1201/9781315366777
11. Prosvirnin S. L. Monotonous differences schemes for the Maxwell equations in the problem of non-stationary wave diffraction by double periodic arrays/ S. L. Prosvirnin, V. A. Vanin // Ultrawide band and Ultrashort Impulse Signals: VI International conference, Sevastopol, 19–22 September 2004 : proceedings. – Sevastopol, 2004. – P. 115–117.

# МАТЕМАТИЧНЕ ТА КОМП'ЮТЕРНЕ МОДЕЛЮВАННЯ

## MATHEMATICAL AND COMPUTER MODELING

UDC 656.073.28

### DECISION-MAKING MODELS AND THEIR APPLICATION IN TRANSPORT DELIVERY OF BUILDING MATERIALS

**Bashkatov A. M.** – PhD, Associate Professor at the Department of Computer Software and Automated Systems, Transnistrian State University named T. G. Shevchenko, Tiraspol, Moldova.

**Yuldashova O. A.** – Student of the Institute of Business, Economics and Information Technology, State University “Odessa Polytechnic”, Odessa, Ukraine.

#### ABSTRACT

**Context.** The task of determining a generalized parameter characterizing a comprehensive assessment of the action of criteria affecting the sequence of execution of orders for the manufacture and delivery of products to the customer.

**Objective.** The purpose of the work is to develop an algorithm for calculating priorities when solving the problem of transport services in conditions of uncertainty of choice.

**Method.** When considering the problem of the efficiency of order fulfillment, the reasons are given that affect the efficiency of the tasks being solved for the delivery of paving slabs to the customer in the shortest possible time. In order to select a scheme that reflects the main stages of decision-making, a justification was carried out and a comparative analysis of existing models was carried out. The criteria for the requirements for describing such models have been determined. It is indicated that the objective function depends on a group of reasons, i.e. represents a composite indicator. The stochastic nature of such factors led to the use of statistical analysis methods for their assessment. The limits of variation of the parameters used in the calculations are established. The solution to the multicriteria problem consists in bringing the role of the acting factors to one unconditional indicator, grouping and subsequent ranking of their values. The decision-making and the choice of the indicator will depend on the set threshold and the priority level of the factor. The indices that form the priority of the factor are determined analytically or expertly. The sequence of actions performed is presented in the form of an algorithm, which allows automating the selection of a model and the calculation of indicators. To assess the adequacy of the proposed solutions, tables of comparative results for the selection of the priority of the executed orders are given.

**Results.** The method allows a comprehensive approach to taking into account the heterogeneous factors that determine the order in which the order is selected when making managerial decisions, ensuring the achievement of a useful effect (streamlining the schedule for the delivery of paving slabs to the customer) by ranking the values of priority indices.

**Conclusions.** The proposed scheme for the transition to a complex unconditional indicator (priority index) makes it possible to quantitatively substantiate the procedure for choosing the next order when performing work. A special feature is that the list of operating factors can be changed (reduced or supplemented with new criteria). The values of these parameters will improve and have a higher reliability with the expansion of the experimental design, depending on the retrospective of their receipt, the accuracy of the data. As a prospect of the proposed method, the optimization of the process of selecting applications using queuing methods (for the type of the corresponding flow – homogeneous, without consequences, stationary, gamma flow, etc.) can be considered.

**KEYWORDS:** decision making model, factor, priority, ranking, order sequence, algorithm.

#### ABBREVIATIONS

MM – mathematical model;  
MED – multidimensional experimental data.

#### NOMENCLATURE

$\$$  – cost of the order;  
 $t$  – time of delivery of a tile to the consumer;  
 $t_{day}$  – delivery within a day;  
 $t_{2week}$  – order delivery within 2 weeks;  
 $L$  – the distance of the location of the object from the supplier;  
 $L_0$  – minimum delivery distance (self-pickup);  
 $L_{del}$  – distance traveled by transport when delivering the goods;  
 $p$  – type of work;  
 $s$  – terms of performance of work (order);  
 $w$  – weight of the delivered tile;  
 $w_{carry}$  – carrying capacity of the transport unit;

$g$  – work schedule;  
 $m$  – weather conditions at the time of the order;  
 $e$  – availability of products in stock;  
 $I_{general}$  – priority factor;  
 $Z$  – number of calls / orders for the accounting period of time;  
 $f$  – frequency of customer appeals;  
 $I_{\$}$  – order value index;  
 $I_t$  – product delivery time index;  
 $I_l$  – index of remoteness of the customer's location;  
 $I_p$  – index of the type of work, which may include only delivery, or delivery and installation of tiles;  
 $I_w$  – order volume index;  
 $I_s$  – index, taking into account the urgency of the order (delivery);  
 $I_g$  – index, which provides for coordination with other works;  
 $D$  – priority coefficient;

$I_m$  – index determined by the action of meteorological conditions;

$I_e$  – index, taking into account the availability of goods (tiles) in stock;

$j$  – number of customers for the reporting period (for example, a year);

$r$  – correlation coefficient;

$\sigma_r$  – error rate;

$\chi^2$  – Pearson distribution with  $f$  degrees of freedom;

$N$  – sample size;

$V$  – number of sample elements where the sign matches;

$W$  – number of sample elements where the sign does not matches;

$v$  – number of sample rows;

$n$  – number of parameters;

$C_{\text{conting}}$  – contingency coefficient.

## INTRODUCTION

The efficiency of the production and related processes depends on many factors. Among them are the availability of a financial backlog, and the provision of the necessary means of production, technological and raw material base, the solution of personnel problems, and supply issues.

However, this kind of data is presented in a different format, does not reflect the presence of connections, the specifics of the work performed, and can vary widely. This makes it difficult not only to control potential costs, but also the very process of planning work. Therefore, modeling of possible situations is of particular importance [16].

The development of such models is a difficult task due to the multi-criteria conditions and the uncertainty of the boundaries of their action. The main thing, probably, will be what models form the basis of such an analysis, how effective they are and how close they are to the working conditions of a real enterprise. If they are logical, thought out from different angles (financial, technical, organizational, etc.), then their implementation will give the desired effect.

All this fully applies to such an area as the production of building materials. In particular, the manufacture of paving slabs and the provision of related services (delivery to the customer and installation work). However, the demand for such materials (as well as services) is unstable and subject to seasonal and temporal fluctuations and changes.

**The object of study** is the process of a comprehensive assessment of the criteria that affect the manufacture and sale of construction products (paving slabs) by an enterprise.

**The subject of study** is the task of determining the priority of orders to form the order of their execution. It is planned to implement it based on modeling the change of factors that affect the timing and quality of work performed based on the results of a passive experiment.

**The purpose of the work** is the development of an algorithm for the complex accounting of parameters based on the analysis of thematically related statistical data.

## 1 PROBLEM STATEMENT

Operational provision of the customer with building materials has always been distinguished by the complexity of its implementation, which is due to a number of reasons and conditions for the performance of work. This is confirmed, for example, in one of the areas that have been actively developing in recent years – the delivery and laying of paving slabs. Consider what complicates the execution of such orders.

Firstly, this is a variety of operating schemes for the delivery of tiles and bulk materials. Differences depend on the number and type of tiles, the distance of the buyer, the timing of the order.

The heterogeneity of the existing conditions before the fulfillment of orders causes the use of different supply schemes, the choice of different-tonnage freight transport and the variation in schedules for the delivery of raw materials.

Secondly, there are problems in planning shipments that arise due to the limited transport fleet, the presence / absence of a stock of products in the warehouse and the effect of force majeure situations (equipment breakdown, traffic jams, worsening road conditions). This should also be taken into account in delivery planning. In addition, they require the adoption of adequate organizational measures.

Thirdly, seasonality and volumes of work performed. There is no permanent component here. Although initially, especially for large contracts or subcontractors, special conditions are negotiated in advance.

The actions of other manufacturers also affect the planning of work, as they in turn increase competition in the market. Applying sometimes unpopular measures (dumping, anti-advertising) to worsen the reputation of a competitor.

All these factors are important in the choice of management decisions. In addition, no one has canceled the effect of market, sometimes market conditions.

Therefore, at the input we have a number of variable parameters –  $\$, t, L, p, w, m, e, Z$ . Depending on the production possibilities, certain limitations apply. For instance:  $t_{\text{day}} \leq t \leq t_{\text{2week}}$ ;  $L \in [L_0, L_{\text{del}}]$ ;  $p$  accepts one of 3 outcomes: pickup, delivery, delivery + laying tiles;  $w \in [50, w_{\text{carry}}]$ ;  $e \in [1, 2, \dots, 10]$  shows the presence of a warehouse stock of products;  $Z$  varies widely  $Z \in [0, 15]$ .

It is necessary to find a solution to the objective function, at which the maximum reduction in the order lead-time is achieved, with the achievement of maximum profit and ensuring the schedule.

At the initial stage of solving problems of this kind, it is necessary to single out a number of factors under study. Then the MM of the adopted decision  $D$  will have a complex form, and will be determined by the dependence of the form:

$$D = f(\$, t, L, n, s, w, g, m, e) . \quad (1)$$

Let us add some to the factors given in (1).

Therefore, the cost of an order, although it is the dominant factor, may lose its original priority if this order is difficult to implement. For example, unrealistic deadlines are set, or the object is far enough from the supplier.

Its implementation can become problematic if a number of conditions are met.

There are time limit, lack of free heavy vehicles to deliver a large batch, violation of the schedule of planned work or lack of the required number of tiles of a given type in the warehouse. No one has canceled the influence of weather conditions, the deterioration of which can violate the terms of the contract.

Thus, the created model should take into account the impact of heterogeneous factors, according to the following conditions:

$$\left\{ \begin{array}{l} \$ \rightarrow \max \\ T \rightarrow \min \\ S \rightarrow \min \\ w_{\min} < w \leq w_{\max} \\ g \rightarrow \text{optimum} \\ e \neq 0 \\ m \rightarrow \min. \end{array} \right. \quad (2)$$

## 2 REVIEW OF THE LITERATURE

In connection with the action of a number of factors, a comprehensive analysis of their influence is necessary, which will make it possible to establish the order of execution of a particular order. The search for a solution requires taking into account DER and involves a model experiment with the choice of appropriate models. Therefore, we consider which models have been used in practice.

As follows from [1], each of the models has its own purpose. The classification is shown in table 1 and is determined by the area of application where they give the greatest effect.

Table 1 – Models in the decision-making

Based on the approach used to obtain data	
descriptive	normative
By the way of data processing	
inductive	deductive
By purpose	
problem-oriented	formal
By way of action	
static	dynamic

Specialists [16] note that the use of descriptor models is justified by the presence of experimental data, i.e. field of observation. Such models [17] are local, selective in nature, since they are formulated because of numerical indications of particular object/objects and are based on identifying patterns in existing data. Possessing high reliability, accuracy, they, however, are not universal. This limits their application in practice.

Normative [18] models, which include those given in [19], are built on the observance of predetermined boundaries, certain rules. Their actions may not be so precise, but they are universal, easily transferable from one object to another. Within the framework of use, they

are better prone to automating the control of parameters and their further comparison with the standards.

Now regarding the way data is processed when looking for patterns. There are two approaches here. The first is inductive, which involves obtaining selective readings (they will become key for making generalizing managerial decisions).

Deductive, on the contrary, is built on the collection of the maximum possible information about the object of study. Further, it is analyzed, and certain conclusions are drawn. Then they make the required decisions based on them. Examples of such models are the situations described in [17, 20].

An important aspect at the stage of choosing a model is the determination of its effectiveness (adequacy) taking into accounts the given restrictions. Based on the fact that in some cases it is required to comply with formal conditions, the so-called formal models, examples of which are presented in [6,18].

In another situation (in the presence of specific conditions), the construction of models with high reliability and accuracy is required. They are aimed at solving well-defined, pre-set problems. That is why they are called problem-oriented. Examples of such models used in transport problems are given in [7, 19].

The effectiveness of the constructed model, in addition to its adequacy to the given conditions, also depends on the duration and frequency of practical application.

Therefore, models of this type are those that provide for changes in conditions (therefore, they are not constant). This is the so-called dynamic models.

Others, on the contrary, are based on the processing of a pre-known numerical data array. The construction of such models is based on the statistical processing of indicators that are pre-selected, ordered, normalized.

Regression analysis methods are applied to them, and the models themselves are called static (most of which require the processing of statistical data, i.e. collected and constant for a given period of time data) [5].

## 3 MATERIALS AND METHODS

Based on the properties listed above, let us consider which models can be used for the tasks set. In addition, given that there are many criteria that affect the fulfillment of orders, and the conditions themselves are subject to change, the goal will be to find the best option when they are taken into account together.

The solution of such a multicriteria problem is seen in the reduction of individual characteristics to unconditional numerical indicators and the grouping of these values in the form of a single parameter [7].

Then they can be ranked, ordered by the degree of decreasing priority. The choice taking into account the rating will serve as the basis for the order of execution of this or that order when working with an array of such applications [8].

Conventionally, the entire process of operations performed can be represented as the following diagram on Figure 1.

In the practical implementation of the attached model, the question arises of quantifying the factors influencing decision-making under conditions of demand uncertainty [9, 10]. The priority coefficient D can serve as such a criterion. To calculate it, it is proposed to use a dependence that takes into account significance indices and has the form:

$$D = I_{\text{general}} = \frac{1}{2} \sum_{i=1}^k I_s I_t I_l I_p I_s I_w I_g I_m I_e \quad (3)$$

1. There are a number of restrictions on:
2. Order cost index ( $0.1 \leq I_s < 1$ );
3. Product delivery time index ( $0.2 < I_t < 1$ );
4. remote location of the customer ( $0 < I_l < 1$ );
5. Index of the type of work, which may include only delivery, or delivery and laying tiles ( $0 < I_p < 1$ );
6. Order volume index, and  $I_w = f(I_s)$ , therefore ( $0.1 \leq I_w < 1$ );
7. Index that takes into account the urgency of the order  $0 < I_s < 1$ ;
8. An index that provides for coordination with other works (for example, preparatory ones)  $I_g = f(I_s)$ . Thus:  $0.1 < I_g < 1$ ;
9. Index from the influence of meteorological conditions on the day of delivery of the order  $0 < I_m < 0.5$ ;
10. An index that takes into account the availability of goods (tiles) in stock. It mostly depends on the size of the order.

So,  $I_e = f(I_w)$  and is in the range  $0.1 < I_p < 1$ .

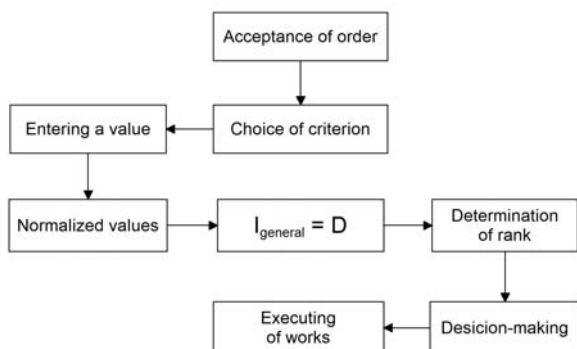


Figure 1 – Order prioritization scheme

The existing database of orders for the delivery of tiles, bulk materials and the performance of related work form a sample.

In the course of it, records are divided into groups, converted into a numerical format, and, having established significance indices, they are included in the calculation of D (3).

The obtained values of D form a series of data, which are normalized according to the ranges (ranks) of Table 2, as well as the correlation ratios in [25].

Table 2 – The rank of factor significance

№	Criterion ( $I_{\text{general}}$ )	Rank
1	Dominant	$0.75 \leq I_{\text{general}} < 1$
2	Important	$0.5 \leq I_{\text{general}} < 0.75$
3	Having a value	$0.2 \leq I_{\text{general}} < 0.5$
4	Less significant	$0 < I_{\text{general}} < 0.2$

The quantitative determination of indices (3) can be done in two ways:

1. Analytically, according to the formula:

$$I_{\text{general}} = \frac{\sum_{j=0}^k I_j f}{k} \quad (4)$$

2. Expertly [10].

With this approach, a questionnaire is developed and a survey of experts is conducted. Customers who have previously been provided with tile delivery services use them. Of course, this is done on condition of anonymity and the formation of presentable samples. These data serve as the basis for setting up and conducting a passive experiment.

Now let us look at its practical implementation.

#### 4 EXPERIMENTS

For the approbation of complex accounting, 54 records of the last period were selected from the received applications and a data table was formed in Table 3.

The original sample data were scaled down to numbers using a substitution scale in Table 4.

Table 3 – Initial data on the execution of orders

Order cost	Days from order	Km to the place	Delivery or installation	Order weight (kg)	Receipt day of the order	Product availability
29317	14	17	Del. + laying	13026.2	21.11.21	1 week
95000	52	14	Del. + laying	45163.5	19.11.21	9 days
22078	15	11	Delivery	11401	13.11.21	3 days
7560	4	19.2	Delivery	2775	10.11.21	4 days
33900	2	73.5	Delivery	14520	28.10.21	In stock
5120	1	13.7	Delivery	2563	27.10.21	In stock
11384	5	27.3	Delivery	4644	25.10.21	3 days
320	0	–	Self-delivery	200	22.10.21	In stock
2158	1	19.2	Delivery	716	21.10.21	In stock
1684	5	4.5	Delivery	468	16.10.21	In stock
23875	0	18.3	Delivery	11830	14.10.21	In stock
16082	7	21.5	Delivery	7726.5	11.10.21	In stock
5910	1	46	Delivery	1120	08.10.21	In stock
38418.5	7	–	Self-delivery	21325	08.10.21	1 week
18600	1	107	Delivery	8600	07.10.21	In stock
17271	8	84.3	Delivery	7288	02.10.21	1 week
1501.5	0	84.3	Self-delivery	803	06.10.21	In stock
19851	2	107	Del. + laying	9517	30.09.21	In stock
2014.9	2	10.6	Self-delivery	854.5	30.09.21	In stock
7019.4	0	11.2	Delivery	2446	29.09.21	In stock
1905	5	–	Self-delivery	975	29.09.21	3 days
5558	0	9.2	Delivery	2903.5	28.09.21	In stock
22331	13	16.2	Del. + laying	12088	21.09.21	8 days
23705	5	14.1	Del. + laying	17209	20.09.21	In stock

Table 4 – Scale substitutions of natural values

Price	Type of work	Weight	Receiving an order	Backlog
1=<10000	0-Self-Delivery	1=<4500	Day of week	10-stock
2=<10000 <20000	1-Delivery	2=<9000	1...7	1-9 days
	2-Del.+laying	...		
9=<80000. AND. <90000		10<10000		
10=<100000				

After substitution of values in the fields of records, the data table acquired the following form in Table 5.

Table 5 – Fragment of the initial normalized data

Count	Delay (days)	Distance (km)	Works	Weight	Date	Epsent
3	14	17	2	3	7	10
10	52	14	2	10	5	9
3	15	11	1	3	6	3
1	4	19	1	1	3	4
4	2	74	1	4	4	10
6	1	14	1	1	3	10
2	5	27	1	2	1	3
1	0	0	0	1	5	10
1	1	19	1	1	4	10
1	5	5	1	1	6	10
3	0	18	1	3	4	10
2	7	22	1	2	1	10
1	1	46	1	1	5	10
4	7	0	0	5	5	7
2	1	107	1	2	4	10
2	8	84	1	2	6	7
1	0	84	0	1	3	10
2	2	107	2	3	4	10
1	2	11	0	1	4	10
1	0	11	1	1	3	10
1	5	0	0	1	3	3
1	0	9	1	1	2	10
3	13	16	2	3	2	8
3	5	14	2	4	1	10

The number of individual fields is characterized by a large difference in values. Therefore, this sample was checked for normal distribution.

Of the available arrays, the Gaussian distribution was noted only for 6 factors (day of the week), which is reflected in Figure 2.

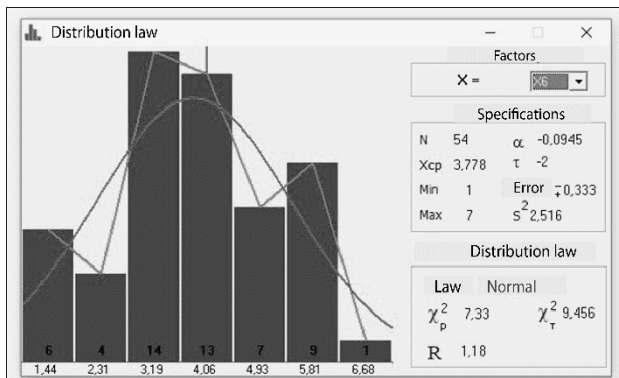


Figure 2 – Graph and parameters of the distribution of the factor “day of the week of receipt of the order”

For the assessment, the software system of statistical modeling MathModel [24] was used, which is used in a number of mathematical studies.

A comprehensive assessment involves knowing the rank of the factor being investigated. In this case, the target function is the delay in order execution, and the rest will be used as influencing factors. Their list is given in Table 3.

The investigated factors were tested for the presence of a pair wise correlation of the available data. The result of checking in MathModel is shown in Figures 3–8.

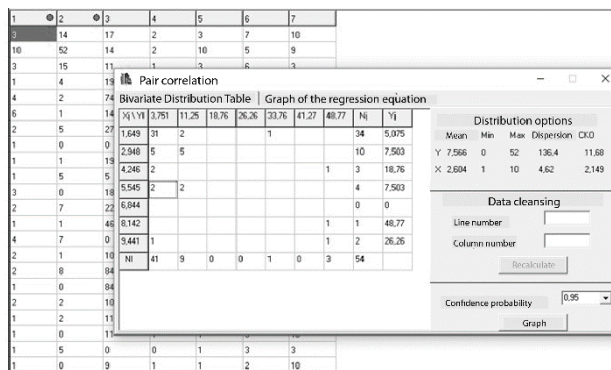


Figure 3 – Cost-time distribution table

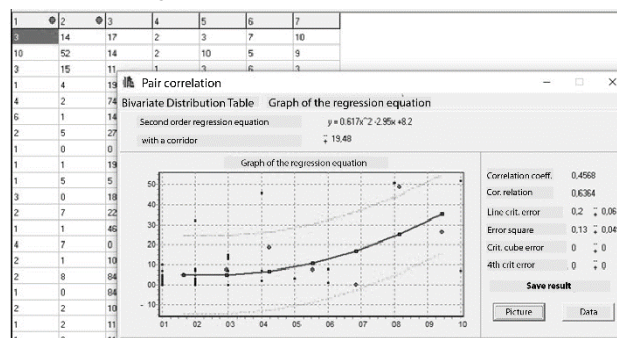


Figure 4 – Graph of the regression equation “cost-time”

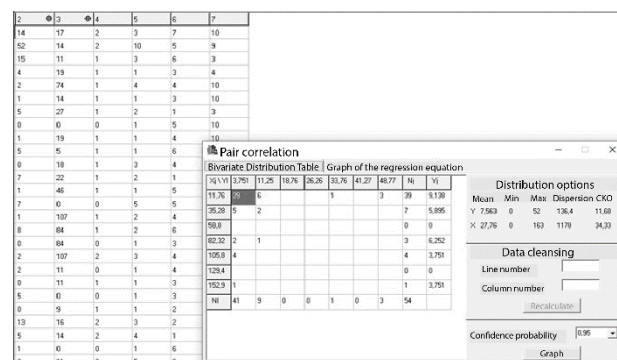


Figure 5 – Table of distribution “distance-timing”

For pairs of other factors (“Terms-type of work”, “Terms-date of order fulfillment” and “Terms-availability of backlog in stock”), it was not possible to find a stable relationship, which led to the need to use other methods of analysis.

One of them, which has shown its effectiveness in practice, was the method of calculating the contingency coefficient with the construction of pleiades and nuclei. Its detailed description is given in [23].

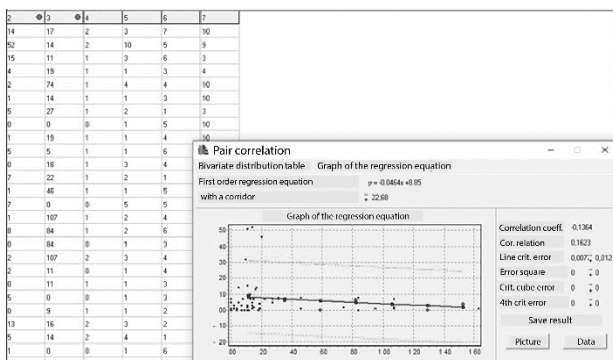


Figure 6 – Graph of the regression equation “distance-timing”

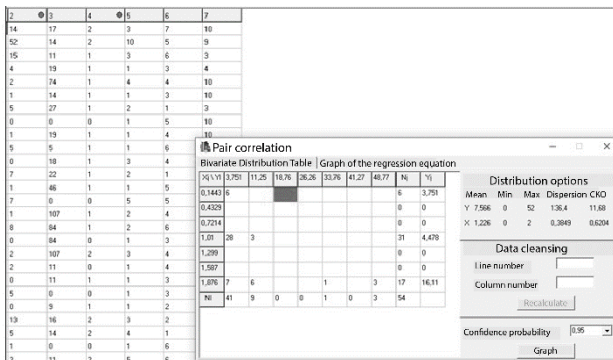


Figure 7 – Table of distribution “cargo weight-terms”

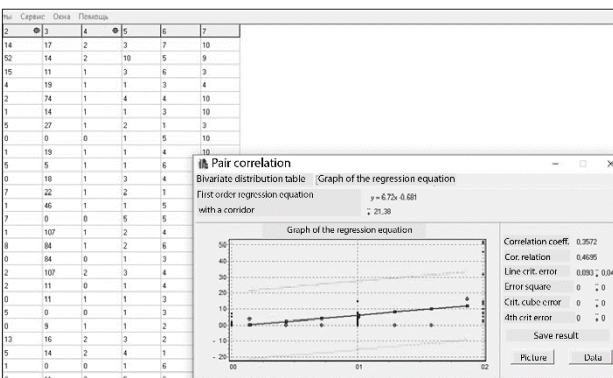


Figure 8 – Graph of the regression equation “cargo weight-terms”

Let us dwell on the key points of its application in the framework of solving the problem.

The calculation of the contingency coefficient is based on establishing the presence of an associative relationship between features.

Directly to calculate the Pearson contingency coefficient [23,25], an expression of the form:

$$C_{conting} = \sqrt{\frac{\chi^2}{\chi^2 + N}} \quad (5)$$

In this case, the parameter  $f$  is the Fechner index and determines the presence of gross blunders. Index  $f$  is determined by the formula:

$$f = \frac{v-w}{v+w} = (v-1)(w+1) \quad (6)$$

Let us see how this technology is implemented using the MathModel program.

In the menu of the Correlation Pleiades and Nuclei Method group, activate the Contingency coefficient method. This will open a table window with data in Figure 9.

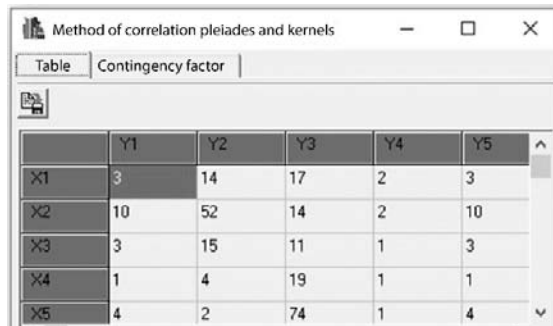


Figure 9 – Table data for calculation contingency coefficient

Opening the contingency coefficient will display the formula with the calculation of the quintile of the  $\chi^2$  distribution and the obtained value of the coefficient on Figure 10.

The bottom line shows the magnitude of the error that determines the significance of the correlation coefficient.

So, if it is significant, then according to [9], the relation.

$$r \geq 3\sigma_r, \quad (7)$$

$$\sigma_r = \frac{1-r^2}{\sqrt{N}}$$

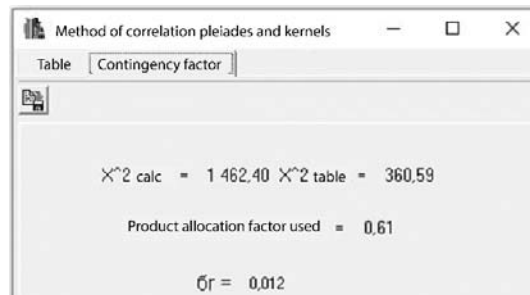


Figure 10 – Calculation of the contingency coefficient

Next, we start the process of calculating the correlation pleiades and nuclei [26] by selecting the appropriate menu line. A tabular data window will open on Figure 11.

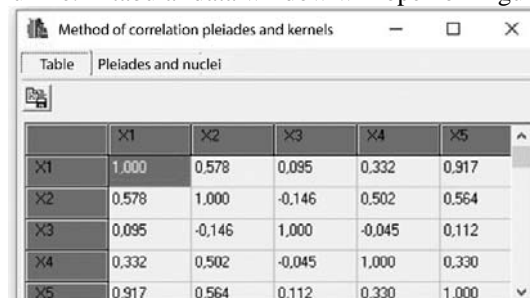


Figure 11 – Window with data for calculating correlation pleiades and nuclei

In the tab Pleiades and kernels, set the threshold value for the calculation for the separation of the pleiades 0.5 on Figure 12.

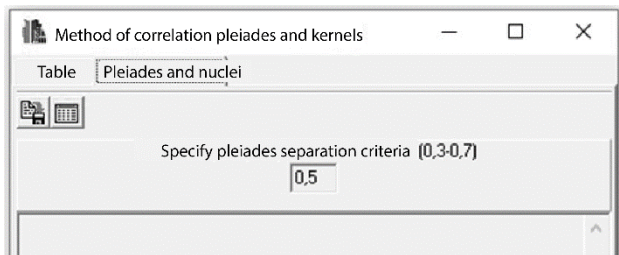


Figure 12 – Setting the threshold for constructing the pleiades

After clicking on the icon and moving along the vertical scroll bar, the window will display a table on Figure 13 with the calculated pleiades, kernels according to the correlation ratios of the factors under study and pairs with maximum connections.

The graphical interpretation of the magnitude of the connection between individual factors is the length of the edges of the pleiades graph.

The factor numbers are shown in circles. Correlation coefficient values are indicated above the edges connecting the circles. The shorter the lines, the stronger the connection. The formed constellations are highlighted with frames.

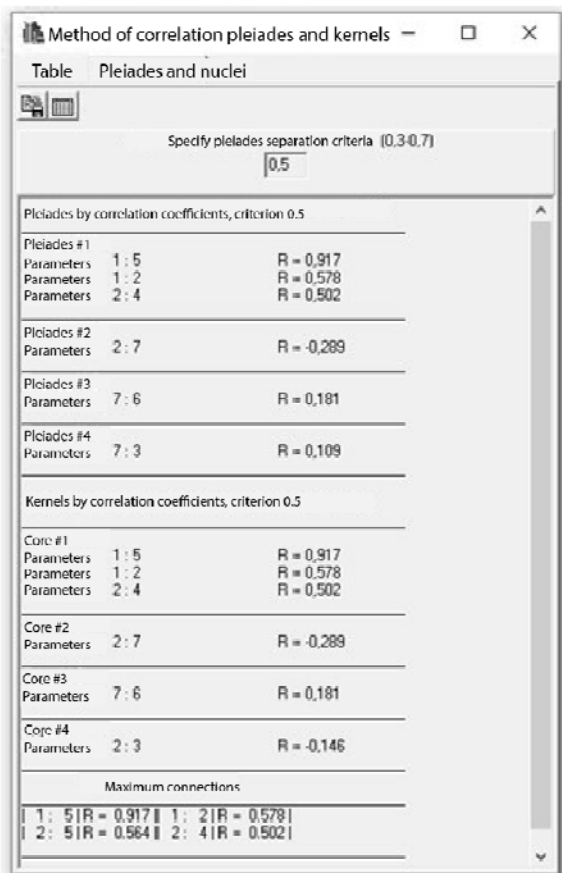


Figure 13 – The window with the results of calculation by the method of correlation and pleiades nuclei

The graph constructed according to the recommendations of [24] can be represented in the following form on Figure 14.

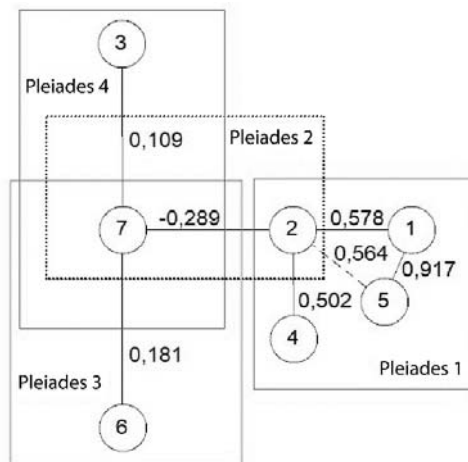


Figure 14 – Graph of pleiades and kernels of correlation of factors

## 5 RESULTS

Because of the study of the sample, the normal nature of the data distribution was revealed only for the days of the week on which the order was received.

To assess the degree of connection with other signs of performance, check for the presence of pair correlation according to the “factor-cause-factor-effect” scheme. The target function, according to the task, is set – the terms of the order. Of the six factors for which the analysis was carried out, a correlation was established with 3: costs, distance to the customer and the weight of the supplied products.

This is reflected in the graphs (Fig. 4, 6 and 8) and regression equations reflecting:

– cost-time relationship

$$y = 0.617x_{costs}^2 - 2.95x + 8.2 \quad (8)$$

with a range of  $\pm 19.48$ ;

– the relationship “distance-timing”

$$y = -0.0464x_{dist} + 8.85 \quad (9)$$

with a range of  $\pm 22.68$ ;

– dependence “weight of cargo-terms”

$$y = 6.72x_{weight} - 0.681 \quad (10)$$

with a range of  $\pm 21.38$ .

It was found that the correlation is weak [25], at which the coefficient  $r \in [0.136 \dots 0.456]$ .

In addition, if for indicators of cost and weight, the trend curve shows a growth, and then an increase in the distance of delivery of goods reflects a decrease in terms [22].

The study of pair wise correlation for other factors did not reveal the presence of a connection and made it possible to programmatically build models.

Therefore, to study the overall relationship between factors, the contingency coefficient was calculated and a graph of the pleiades and correlation kernels was formed. Because of the construction, as the size of the bonds decreases, 4 pleiades are formed. The greatest relationship is determined between 1, 2 and 5 factors (cost, lead time and cargo weight, respectively).

## 6 DISCUSSION

The use of statistical analysis of data reflecting the fulfillment of orders for the delivery of paving slabs made it possible to study the factors based on a passive experiment.

According to experts, mistakes made when planning transportation schemes can lead to significant costs (up to 50% of those declared in advance).

The difference between this approach and the solutions proposed by other authors is that the key calculation parameters are formed based on empirical data, i.e., according to the results of natural observations.

What does not cancel the existing planned activities (based on logistics [3], normative indicators), but only increases their accuracy, in accordance with the actual traffic conditions along the routes during the delivery of building materials.

Of course, the methods of expert analysis, which provide for a questionnaire and data processing, are left outside the scope of the study.

This circumstance is caused by objective reasons for the change in the staffing and reorganization measures in the work of the construction company.

Therefore, such an assessment under current conditions cannot be recognized as possible, and the results cannot be final.

Nevertheless, the main goal of such a study is to obtain grounds for assigning the weights of the significance indices, the calculation of which is carried out according to the scheme on Figure 1 and formulas (1–4).

To automate the execution of such procedures, a program can be used, the algorithm of which is given below on Figure 15.

## CONCLUSIONS

The urgent problem of developing mathematical models using small samples to make adequate management decisions on the delivery of building materials to the customer is being solved.

**The scientific novelty** of the results obtained lies in the fact that mathematical models have been developed to assess the complex action of various factors influencing the achievement of the target function – the delivery of building materials. At the same time, the samples were systematized and analyzed for normality of distribution, weights were determined, and a graph of correlation galaxies and kernels was formed to assess the relationship between factors. The calculation of the contingent coefficient determines the degree of such a connection and allows us to establish stochastic patterns in the form of mathematical models. The use of programs allows you to automate the analysis of samples and speed up the construction of such models, which makes the data processing process unified, excluding criteria that are not critical for achieving the target function.

**The practical significance** of the results obtained lies in the fact that the developed technology makes it possible to use various software that allows processing statistical data. The field of experiment can be expanded, which will increase the quality of the resulting models and the ability to use other factors that are not included in the list of those studied, but can be considered additionally. The results of the conducted research make it possible to narrow the list of factors, eliminating unimportant parameters and increase the efficiency of management actions taken to solve related problems (planning raw materials reserves, delivery dates and schedules, etc.).

**Prospects for further research** are in study the capabilities of the proposed set of parameters for assessing other economic indicators that affect the operation of an enterprise (financial, material, energy, labor).

## ACKNOWLEDGEMENTS

The authors express their gratitude to the management of the enterprises “Na Himke” and Dvor.ua for the pro-

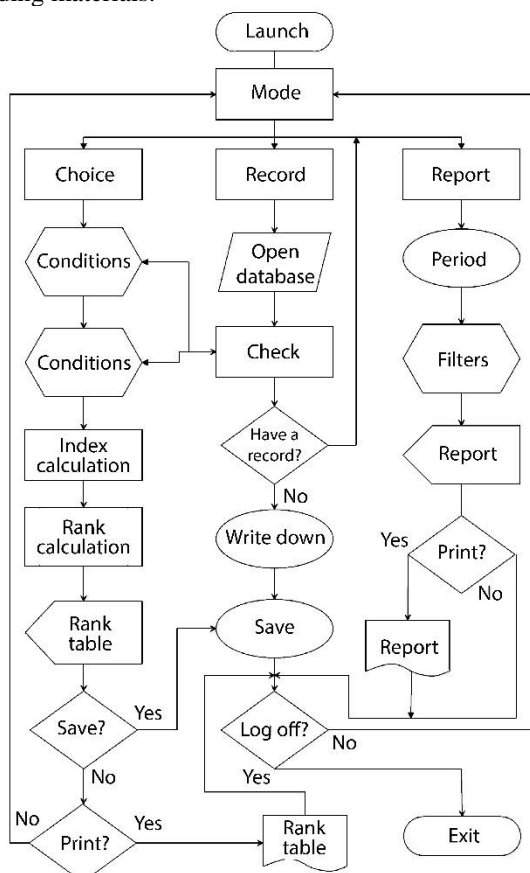


Figure 15 – Block diagram of the decision-making program

vided data, associate professor Vasyutkina for the opportunity to use the MathModel program in the calculations.

The work was carried out within the scope of research work “Mathematical Modeling” of the Transnistrian State University named after T.G. Shevchenko when conducting statistical research on the work of industrial transport and preparing materials for the final work of the master.

## REFERENCES

1. Yannis George et al. State-of-the-art review on multi-criteria decision-making in the transport sector [Electronic resource], *Journal of traffic and transportation engineering (English edition)*, 2020, Vol. 7, No. 4, pp. 413–431. – DOI: <https://doi.org/10.1016/j.jtte.2020.05.005>
2. Galić M., Kraus I. Simulation model for scenario optimization of the ready-mix concrete delivery problem [Electronic resource], *Selected scientific papers – journal of civil engineering*, 2016, Vol. 11, No. 2, pp. 7–18. DOI: <https://doi.org/10.1515/sspjce-2016-0014>.
3. Gonzalez-Feliu J., Jean-Louis R. Modeling urban goods movement: how to be oriented with so many approaches? [Electronic resource], *Procedia – social and behavioral sciences*, 2012, Vol. 39, pp. 89–100. DOI: <https://doi.org/10.1016/j.sbspro.2012.03.093>.
4. Misanova I. et al. Risk management in the organization of delivery of construction materials [Electronic resource], *MATEC web of conferences*, 2020, Vol. 329, P. 03060. DOI: <https://doi.org/10.1051/mateconf/202032903060>
5. Akter T. et al. A spatial panel regression model to measure the effect of weather events on freight truck traffic [Electronic resource], *Transportmetrica A: transport science*, 2020, Vol. 16, No. 3, pp. 910–929. DOI: <https://doi.org/10.1080/23249935.2020>.
6. Kukharchyk A. G. Transport task of optimization of costs with multimodal transportation [Electronic resource], *Economic innovations*, 2017, Vol. 19, No. 2(64), pp. 157–163. DOI: [https://doi.org/10.31520/ei.2017.19.2\(64\).157-163](https://doi.org/10.31520/ei.2017.19.2(64).157-163)
7. Gorzelanczyk Piotr et al. Optimizing the choice of means of transport using operational research [Electronic resource], *Communications – scientific letters of the university of zilina*, 2021, Vol. 23, No. 3, pp. A193–A207. DOI: <https://doi.org/10.26552/com.c.2021.3.a193-a207>
8. Mohammadnazari Z. Ghannadpour S. F. Sustainable construction supply chain management with the spotlight of inventory optimization under uncertainty [Electronic resource], *Environment, development and sustainability*, 2020. DOI: <https://doi.org/10.1007/s10668-020-01095-0>
9. Govindan K., Fattahi M., Keyvanshokoo E. Supply chain network design under uncertainty: a comprehensive review and future research directions [Electronic resource], *European journal of operational research*, 2017, Vol. 263, No. 1, pp. 108–141. DOI: <https://doi.org/10.1016/j.ejor.2017.04.009>.
10. Doustmohammadi M., Anderson M., Doustmohammadi Eh. Regression analysis to create new truck trip generation equations for medium sized communities [Electronic resource], *Current urban studies*, 2019, Vol. 07, No. 03, pp. 480–491. DOI: <https://doi.org/10.4236/cus.2019.73024>.
11. Sanchez-Diaz I. Assessing the magnitude of freight traffic generated by office deliveries [Electronic resource], *Transportation research part A: policy and practice*, 2020, Vol. 142, pp. 279–289. DOI: <https://doi.org/10.1016/j.tra.2020.11.003>
12. Lu Ch. et al. Analysis of factors affecting freight demand based on input-output model [Electronic resource], *Mathematical problems in engineering*, 2021, Vol. 2021, pp. 1–19. DOI: <https://doi.org/10.1155/2021/5581742>.
13. Oliskevych M. Optimization of periodic unitary online schedule of transport tasks of highway road trains [Electronic resource], *Transport problems*, 2018, Vol. 13, No. 1, pp. 111–122. DOI: <https://doi.org/10.21307/tp.2018.13.1.10>.
14. Machado T. et al. Multi-constrained joint transportation tasks by teams of autonomous mobile robots using a dynamical systems approach [Electronic resource], *2016 IEEE international conference on robotics and automation (ICRA)*. Stockholm, 16–21 May 2016, [S.l.], 2016. DOI: <https://doi.org/10.1109/icra.2016.7487477>.
15. Nieoczym Al. et al. Autonomous vans – the planning process of transport tasks [Electronic resource], *Open engineering*, 2020, Vol. 10, No. 1, pp. 18–25. DOI: <https://doi.org/10.1515/eng-2020-0006>.
16. Al-Mamary Y. H. et al. A critical review of models and theories in field of individual acceptance of technology [Electronic resource], *International journal of hybrid information technology*, 2016, Vol. 9, No. 6, pp. 143–158. DOI: <https://doi.org/10.14257/ijhit.2016.9.6.13>
17. Taherdoost H. A review of technology acceptance and adoption models and theories [Electronic resource], *Procedia manufacturing*, 2018, Vol. 22, pp. 960–967. DOI: <https://doi.org/10.1016/j.promfg.2018.03.137>
18. Weber E. U., Coskunoglu O. Descriptive and prescriptive models of decision-making: implications for the development of decision aids [Electronic resource], *IEEE transactions on systems, man, and cybernetics*, 1990, Vol. 20, No. 2, pp. 310–317. DOI: <https://doi.org/10.1109/21.52542>
19. Hilton R. W. Integrating normative and descriptive theories of information processing [Electronic resource], *Journal of accounting research*, 1980, Vol. 18, No. 2, pp. 477. DOI: <https://doi.org/10.2307/2490589>
20. Albers M. J. Decision making [Electronic resource], *The 14th annual international conference, Research Triangle Park, North Carolina, United States, 19–22 October 1996*. New York, New York, USA, 1996. Mode of access: <https://doi.org/10.1145/238215.238256>
21. Pan N.-H., Lee M.-L., Chen Sh.-Q. Construction material supply chain process analysis and optimization / процесу аналіз і оптимізація статыбнію медзіагү тєкїмо грандїнє [Electronic resource], *Journal of civil engineering and management*, 2011, Vol. 17, No. 3, pp. 357–370. DOI: <https://doi.org/10.3846/13923730.2011.594221>
22. Visconti E. et al. Model-driven engineering city spaces via bidirectional model transformations [Electronic resource], *Software and systems modeling*, 2021, DOI: <https://doi.org/10.1007/s10270-020-00851-0>
23. Crainic T. G. Transportation science special issue on freight transportation and logistics, part I [Electronic resource], *Transportation science*, 2016, Vol. 50, No. 2, pp. 363–365. DOI: <https://doi.org/10.1287/trsc.2016.0681>
24. Boulton T. E. Optimal algorithms: tools for mathematical modeling [Electronic resource], *Journal of complexity*, 1987. Vol. 3, No. 2, pp. 183–200. DOI: [https://doi.org/10.1016/0885-064x\(87\)90026-4](https://doi.org/10.1016/0885-064x(87)90026-4)
25. Mammen E. Statistical models [Electronic resource], *The American statistician*, 2006, Vol. 60, No. 2, pp. 204–205. DOI: <https://doi.org/10.1198/tas.2006.s45>
26. Taylor R. Interpretation of the correlation coefficient: a basic review [Electronic resource], *Journal of diagnostic medi-*

- cal sonography*, 1990, Vol. 6, No. 1, pp. 35–39.  
DOI: <https://doi.org/10.1177/87564793900600106>
27. Berg R. L. The ecological significance of correlation pleiades [Electronic resource], *Evolution*, 1960, Vol. 14, No. 2, pp. 171. DOI: <https://doi.org/10.2307/2405824>
28. Nandi P. K., Parsad R., Gupta V. K. Simultaneous optimization of incomplete multi-response experiments [Electronic resource], *Open journal of statistics*, 2015, Vol. 05, No. 05, pp. 430–444. DOI: <https://doi.org/10.4236/ojs.2015.55045>.
29. Yarovenko H. Evaluating the threat to national information security [Electronic resource], *Problems and perspectives in management*, 2020, Vol. 18, No. 3, pp. 195–210. DOI: [https://doi.org/10.21511/ppm.18\(3\).2020.17](https://doi.org/10.21511/ppm.18(3).2020.17)
30. Lee D.-H. Jeong I.-J., Kim K.-J. A desirability function method for optimizing mean and variability of multiple responses using a posterior preference articulation approach [Electronic resource], *Quality and reliability engineering international*, 2018, Vol. 34, No. 3, pp. 360–376. DOI: <https://doi.org/10.1002/qre.2258>

Received 07.12.2023.

Accepted 04.02.2024.

УДК 656.073.28

## МОДЕЛІ ПРИЙНЯТТЯ РІШЕНЬ ТА ЇХ ЗАСТОСУВАННЯ В ЗАДАЧАХ ТРАНСПОРТНОЇ ДОСТАВКИ БУДМАТЕРІАЛІВ

**Башкатов О. М.** – канд. техн. наук, доцент кафедри «Програмне забезпечення обчислювальної техніки та автоматизованих систем», Придністровський державний університет ім. Т. Г. Шевченка, Тираспіль, Молдова.

**Юлдашова О. О.** – студентка кафедри економічної кібернетики інституту бізнесу, економіки та інформаційних технологій державного університету «Одеська політехніка», Одеса, Україна.

### АНОТАЦІЯ

**Актуальність.** У статті зображено, що визначення критеріїв, що впливають на черговість виконання замовлень по доставці продукції замовнику є головною задачею. Мета такої роботи міститься у розробці алгоритму щодо вибору пріоритетів при вирішенні завдання транспортного обслуговування в умовах невизначеності.

**Мета роботи** – розробка алгоритму розрахунку пріоритетів при вирішенні задачі транспортного обслуговування в умовах невизначеності вибору.

**Метод.** В контексті проблеми оперативності виконання замовлень наведені причини, що впливають на логістику розв’язуваної задачі – поставки будівельної продукції за місцем вимоги. З метою вибору схеми, що відбиває основні етапи прийняття рішень по доставці тротуарної плитки замовнику, виконано обґрунтування і проведено порівняльний аналіз існуючих моделей. Визначено критерії, що пред’являються вимоги для опису таких моделей. Зазначено, що цільова функція залежить від різних причин, тобто є комплексним показником. Стохастичний характер таких факторів зумовив використання для їх оцінки методів статистичного аналізу. Встановлено межі зміни використовуваних в розрахунках параметрів. Рішення багатокритеріальної задачі укладено в зведенні діючих факторів до безумовним показниками, їх угруповання і подальшому ранжируванні. Ухвалення рішення та вибір показника буде залежати від встановленого порога і рівня пріоритету фактору. Індекси, що формують пріоритет фактору, визначаються аналітично або експертним шляхом. Черговість виконуваних дій представлена у вигляді алгоритму, що дозволяє автоматизувати вибір моделі і визначення пріоритетів. Для оцінки адекватності запропонованих рішень наведені таблиці порівняльних результатів за вибором пріоритетності виконуваних замовлень.

**Результати.** Метод дозволяє комплексно підійти до врахування різнорідних чинників, що впливають на пріоритети вибору при прийнятті управлінських рішень, забезпечивши досягнення корисного ефекту (упорядкування графіка виконання робіт з доставки тротуарної плитки замовнику).

**Висновки.** Пропонована схема по переходу до комплексного безумовному показником (індексом пріоритету) дозволяє кількісно обґрунтувати прийняття управлінських рішень. Особливістю є те, що список діючих факторів може бути змінений або доповнений новими параметрами. Значення цих параметрів можуть уточнювати і мати більш високу вірогідність з розширенням плану пасивного експерименту, оскільки залежать від ретроспективи отримання, а також точності наявних даних. Як перспектив, при визначенні пріоритетів, можлива оптимізація вибору заявок із застосуванням методів масового обслуговування (для типу відповідного потоку – однорідного, без наслідків, стаціонарного, гамма-потоку та ін.).

**КЛЮЧОВІ СЛОВА:** модель прийняття рішень, фактор, пріоритет, ранжування, черговість замовлення, алгоритм.

### ЛІТЕРАТУРА

1. State-of-the-art review on multi-criteria decision-making in the transport sector [Electronic resource] / [George Yannis et al.] // *Journal of traffic and transportation engineering (English edition)*. – 2020. – Vol. 7, No. 4. – P. 413–431. – DOI: <https://doi.org/10.1016/j.jtte.2020.05.005>
2. Galić M. Simulation model for scenario optimization of the ready-mix concrete delivery problem [Electronic resource] / Mario Galić, Ivan Kraus // *Selected scientific papers – journal of civil engineering*. – 2016. – Vol. 11, No. 2. – P. 7–18. – DOI: <https://doi.org/10.1515/sspjce-2016-0014>.
3. Gonzalez-Feliu J. Modeling urban goods movement: how to be oriented with so many approaches? [Electronic resource] / Jesus Gonzalez-Feliu, Jean-Louis Routhier // *Procedia – social and behavioral sciences*. – 2012. – Vol. 39. – P. 89–100. – DOI: <https://doi.org/10.1016/j.sbspro.2012.03.093>.
4. Risk management in the organization of delivery of construction materials [Electronic resource] / [Irina Misanova et al.] // *MATEC web of conferences*. – 2020. – Vol. 329. – P. 03060. – DOI: <https://doi.org/10.1051/mateconf/202032903060>
5. A spatial panel regression model to measure the effect of weather events on freight truck traffic [Electronic resource] / [Taslima Akter et al.] // *Transportmetrica A: transport science*. – 2020. – Vol. 16, No. 3. – P. 910–929. – DOI: <https://doi.org/10.1080/23249935.2020>.
6. Kukharchyk A. G. Transport task of optimization of costs with multimodal transportation [Electronic resource] / A. G. Kukharchyk // *Economic innovations*. – 2017. –

- Vol. 19, No. 2(64). – P. 157–163. – DOI: [https://doi.org/10.31520/ei.2017.19.2\(64\).157-163](https://doi.org/10.31520/ei.2017.19.2(64).157-163)
7. Optimizing the choice of means of transport using operational research [Electronic resource] / [Piotr Gorzelanczyk et al.] // Communications – scientific letters of the university of zilina. – 2021. – Vol. 23, No. 3. – P. A193–A207. – DOI: <https://doi.org/10.26552/com.c.2021.3.a193-a207>
  8. Mohammadnazari Z. Sustainable construction supply chain management with the spotlight of inventory optimization under uncertainty [Electronic resource] / Zahra Mohammadnazari, Seyed Farid Ghannadpour // Environment, development and sustainability. – 2020. – DOI: <https://doi.org/10.1007/s10668-020-01095-0>
  9. Govindan K. Supply chain network design under uncertainty: a comprehensive review and future research directions [Electronic resource] / Kannan Govindan, Mohammad Fattahi, Esmail Keyvanshokoh // European journal of operational research. – 2017. – Vol. 263, No. 1. – P. 108–141. – DOI: <https://doi.org/10.1016/j.ejor.2017.04.009>
  10. Doustmohammadi M. Regression analysis to create new truck trip generation equations for medium sized communities [Electronic resource] / Mehrnaz Doustmohammadi, Michael Anderson, Ehsan Doustmohammadi // Current urban studies. – 2019. – Vol. 07, No. 03. – P. 480–491. – DOI: <https://doi.org/10.4236/cus.2019.73024>
  11. Sanchez-Diaz I. Assessing the magnitude of freight traffic generated by office deliveries [Electronic resource] / Ivan Sanchez-Diaz // Transportation research part A: policy and practice. – 2020. – Vol. 142. – P. 279–289. – DOI: <https://doi.org/10.1016/j.tra.2020.11.003>
  12. Analysis of factors affecting freight demand based on input-output model [Electronic resource] / [Changxiang Lu et al.] // Mathematical problems in engineering. – 2021. – Vol. 2021. – P. 1–19. – DOI: <https://doi.org/10.1155/2021/5581742>
  13. Olishevych M. Optimization of periodic unitary online schedule of transport tasks of highway road trains [Electronic resource] / Myroslav Olishevych // Transport problems. – 2018. – Vol. 13, no. 1. – P. 111–122. – DOI: <https://doi.org/10.21307/tp.2018.13.1.10>
  14. Multi-constrained joint transportation tasks by teams of autonomous mobile robots using a dynamical systems approach [Electronic resource] / [Toni Machado et al.] // 2016 IEEE international conference on robotics and automation (ICRA), Stockholm, 16–21 May 2016. – [S. l.], 2016. – DOI: <https://doi.org/10.1109/icra.2016.7487477>
  15. Autonomous vans – the planning process of transport tasks [Electronic resource] / [Alexander Nieoczym et al.] // Open engineering. – 2020. – Vol. 10, No. 1. – P. 18–25. – DOI: <https://doi.org/10.1515/eng-2020-0006>
  16. A critical review of models and theories in field of individual acceptance of technology [Electronic resource] / [Yaser Hasan Al-Mamary et al.] // International journal of hybrid information technology. – 2016. – Vol. 9, No. 6. – P. 143–158. – DOI: <https://doi.org/10.14257/ijhit.2016.9.6.13>
  17. Taherdoost H. A review of technology acceptance and adoption models and theories [Electronic resource] / Hamed Taherdoost // Procedia manufacturing. – 2018. – Vol. 22. – P. 960–967. – DOI: <https://doi.org/10.1016/j.promfg.2018.03.137>
  18. Weber E. U. Descriptive and prescriptive models of decision-making: implications for the development of decision aids [Electronic resource] / E. U. Weber, O. Coskunoglu // IEEE transactions on systems, man, and cybernetics. – 1990. – Vol. 20, No. 2. – P. 310–317. – DOI: <https://doi.org/10.1109/21.52542>
  19. Hilton R. W. Integrating normative and descriptive theories of information processing [Electronic resource] / Ronald W. Hilton // Journal of accounting research. – 1980. – Vol. 18, No. 2. – P. 477. – DOI: <https://doi.org/10.2307/2490589>
  20. Albers M. J. Decision making [Electronic resource] / Michael J. Albers // The 14th annual international conference, Research Triangle Park, North Carolina, United States, 19–22 October 1996. – New York, New York, USA, 1996. – Mode of access: <https://doi.org/10.1145/238215.238256>
  21. Pan N. H. Construction material supply chain process analysis and optimization / procesų analizė ir optimizacija statybinių medžiagų tiekimo grandinėje [Electronic resource] / Nai-Hsin Pan, Ming-Li Lee, Sheng-Quan Chen // Journal of civil engineering and management. – 2011. – Vol. 17, No. 3. – P. 357–370. – DOI: <https://doi.org/10.3846/13923730.2011.594221>
  22. Model-driven engineering city spaces via bidirectional model transformations [Electronic resource] / [Ennio Visconti et al.] // Software and systems modeling. – 2021. – DOI: <https://doi.org/10.1007/s10270-020-00851-0>
  23. Crainic T. G. Transportation science special issue on freight transportation and logistics, part I [Electronic resource] / Teodor Gabriel Crainic // Transportation science. – 2016. – Vol. 50, no. 2. – P. 363–365. – DOI: <https://doi.org/10.1287/trsc.2016.0681>
  24. Boulton T. E. Optimal algorithms: tools for mathematical modeling [Electronic resource] / Terrance E. Boulton // Journal of complexity. – 1987. – Vol. 3, no. 2. – P. 183–200. – DOI: [https://doi.org/10.1016/0885-064x\(87\)90026-4](https://doi.org/10.1016/0885-064x(87)90026-4)
  25. Mammen E. Statistical models [Electronic resource] / Enno Mammen // The American statistician. – 2006. – Vol. 60, No. 2. – P. 204–205. – DOI: <https://doi.org/10.1198/tas.2006.s45>
  26. Taylor R. Interpretation of the correlation coefficient: a basic review [Electronic resource] / Richard Taylor // Journal of diagnostic medical sonography. – 1990. – Vol. 6, No. 1. – P. 35–39. – DOI: <https://doi.org/10.1177/875647939000600106>
  27. Berg R. L. The ecological significance of correlation pleiades [Electronic resource] / R. L. Berg // Evolution. – 1960. – Vol. 14, no. 2. – P. 171. – DOI: <https://doi.org/10.2307/2405824>
  28. Nandi P. K. Simultaneous optimization of incomplete multi-response experiments [Electronic resource] / Pradip Kumar Nandi, Rajender Parsad, Vinod Kumar Gupta // Open journal of statistics. – 2015. – Vol. 05, No. 05. – P. 430–444. – DOI: <https://doi.org/10.4236/ojs.2015.55045>
  29. Yarovenko H. Evaluating the threat to national information security [Electronic resource] / Hanna Yarovenko // Problems and perspectives in management. – 2020. – Vol. 18, No. 3. – P. 195–210. – DOI: [https://doi.org/10.21511/ppm.18\(3\).2020.17](https://doi.org/10.21511/ppm.18(3).2020.17)
  30. Lee D.-H. A desirability function method for optimizing mean and variability of multiple responses using a posterior preference articulation approach [Electronic resource] / Dong-Hee Lee, In-Jun Jeong, Kwang-Jae Kim // Quality and reliability engineering international. – 2018. – Vol. 34, No. 3. – P. 360–376. – DOI: <https://doi.org/10.1002/qre.2258>

## DESIGN MODELS OF BIT-STREAM ONLINE-COMPUTERS FOR SENSOR COMPONENTS

**Larchenko L. V.** – PhD, Associate Professor, Associate Professor of the Design Automation Department, Kharkiv National University of Radio Electronics, Kharkiv, Ukraine.

**Parkhomenko A. V.** – PhD, Associate Professor, Associate Professor of the Department of Software Tools, National University “Zaporizhzhia Polytechnic”, Zaporizhzhia, Ukraine.

**Larchenko B. D.** – PhD, Assistant of the Design Automation Department, Kharkiv National University of Radio Electronics, Kharkiv, Ukraine.

**Korniienko V. R.** – Postgraduate student of the Design Automation Department, Kharkiv National University of Radio Electronics, Kharkiv, Ukraine.

### ABSTRACT

**Context.** Currently, distributed real-time control systems need the creation of devices that perform online computing operations close to the sensor. The proposed online-computers of elementary mathematical functions can be used as components for the functional conversion of signals in the form of pulse streams received from measuring sensors with frequency output.

**Objective.** The objective of the study is the development of mathematical, architectural and automata models for the design of bit-stream online-computers of elementary mathematical functions in order to create a unified approach to their design, due to which the accuracy of calculating functions can be increased, functional capabilities expanded, hardware costs reduced, and design efficiency increased.

**Method.** Mathematical models of devices were developed using the method of forming increments of ascending step functions based on inverse functions with minimization of calculation error. Automata models of online-computers based on Moore’s Finite State Machine have been developed, the graph diagrams of which made it possible to ensure the clarity of function implementation algorithms, to increase visibility and invariance of implementation in formal languages of programming and hardware description.

**Results.** The paper presents the results of research, development and practical approbation of design models of bit-stream online-computers of power functions and root extraction function. A generalized architecture of an online-computer was proposed.

**Conclusions.** The considered functional online-computers are effective from the point of view of calculation accuracy, simplicity of technical implementation, and universality of the architecture.

**KEYWORDS:** functional conversion, bit-stream data, bit-stream computing, mathematical model, finite state machine, FPGA, SoC.

### ABBREVIATIONS

ASIC is an Application-Specific Integrated Circuit;  
CAD is a Computer Aided Design;  
CMOS is a Complementary Metal Oxide Semiconductor;  
CORDIC is a Coordinate Rotation Digital Computer;  
FPGA is a Field Programmable Gate Arrays;  
FSM is a Finite State Machine;  
HDL is a Hardware Description Language;  
PWM is a Pulse-Width Modulation;  
VHDL is a VHSIC Hardware Description Language;  
VHSIC is a Very High-Speed Integrated Circuits;  
VSF is a Virtually Scaling Free.

### NOMENCLATURE

$|\delta_{\max}|$  is an absolute error limit value of continuous ascending functions reproduction;  
 $l-|\delta_{\max}|$  is a level of the function approximation node;  
 $\Delta_{y-1}$  is a difference obtained when comparing the increments current values of the functions;  
 $\Psi_{(y-|\delta_{\max}|)}$  is an inverse function of  $f(x)$ ;  
 $f(x^*)$  is a continuous function;  
 $f(x)$  is an approximating function;  
 $f(x_y)$  is a value of the function at the point  $x_y$ ;  
 $f(x_y-1)$  is a value of the function at the point  $(x_y-1)$ ;  
 $m$  is a numerator of the fractional exponent of the power function, positive natural number;

$n$  is a denominator of the fractional exponent of the power function, positive natural number;  
 $x$  is an input bit data stream;  
 $x_y$  is a value of selected bit from the input bit-stream  $x$  (sample);  
 $y$  is an output bit data stream;  
 $y_k$  is a value corresponding to the node of the function approximation.

### INTRODUCTION

During the development of real-time systems focused on sensor systems, the Internet of Things and distributed control systems an important task is the alignment of sensors with digital systems for collecting and processing information.

Currently, an integral part of new basic elements development needed for the mentioned systems’ creation is the design of specialized hardware functional converters and online-computers, which utilize data in bit (pulse) stream form as an information signal, which allows simpler implementation of operations compared to other types of coding [1–4].

**The object of the study** is the process of designing bit-stream online-computers of elementary mathematical functions.

**The subjects of the study** are design models of bit-stream online-computers.

**The objective of the study** is the development of mathematical, architectural and automata design models

of bit-stream online-computers of elementary mathematical functions in order to create a unified approach to their design, due to which the accuracy of calculating functions can be increased, functional capabilities expanded, hardware costs reduced, and design efficiency increased.

To achieve the objective, it was necessary to fulfill the development of mathematical models of bit-stream online-computers based on method analysis for generating increments of increasing step functions with minimization of calculation error; the creation of generalized architecture model of online-computer; development of automata models of the device based on FSM; the experimental research of the designed hardware model of a bit-stream power function computer in the hardware description language VHDL using an automata template and implementation in a Xilinx FPGA.

The paper is organized as follows. Sections 1 and 2 provide a description of problem statement and current state of the art. Section 3 discusses the method of forming increments of ascending step functions and mathematical models of online-computers obtained on its basis. A generalized online-computer architecture is presented, which allows building of pipeline architectures of online-computers of specific functions. An approach to the design of online computers based on FSMs was considered, which made it possible to develop a state diagram of the control automaton of online computers and an algorithm flowchart of the operating automaton for the implementation of functions. Sections 4, 5 presents the results of an experimental study of hardware implementation of online-computers for power functions and root extraction function, which confirm the results of theoretical developments. Section 6 provides short discussion about main achievements of this work.

## 1 PROBLEM STATEMENT

In bit-stream coding, data is presented as streams of unit amplitude pulses. In bit-stream data the informative parameter is fixed value of pulses of arbitrary duration for a time interval. The bit-stream form of signals allows the transmission and processing of information in ways that make it possible to sequentially process single bits of the stream when they are fed to the input of the device [5].

At the same time, the bit-stream form of signals, while maintaining immunity to interference, does not suffer from information redundancy and allows for high-speed operation of devices. Data processing involves both the conversion of the form of information presentation and the linearization of the sensor signal using various elementary mathematical functions [6, 7].

Moreover, bit-stream online-computers provide for the implementation of the stream method of online calculations with simultaneous parallel-serial execution of conversions over single bits of the stream according to the required function. At the same time, sequential calculation of function values is performed for adjacent values of the argument. Stream methods of processing information signals are characterized by the possibility of implementing functional conversion through the use of methods of

forming increments, as well as the implementation of sequential processing of streams in the process of receiving single bits [7, 8].

Bit stream online-computers of power functions and root extraction functions can be used in distributed control systems as components for functional conversion of bit streams obtained from measurement sensors of physical quantities with frequency output. The frequency output signal can be a stream of pulses or a signal with PWM [9, 10].

The question of analyzing the methods and means of reproducing functions using converters and online-computers arises in connection with their wide selection and the variety of solved tasks, their specifics and technical requirements. Each selected type of means corresponds to its own calculation method, and rational means of its implementation must be chosen for any method.

In the creation of nonlinear converters and online-computers of bit-stream data which operate in real time for the reproduction of elementary functions, accurate methods of calculating approximating functions based on differential equations or algebraic equations (inverse functions) are used. Thus, the design of specialized hardware functional converters and computers performing bit-stream data conversion in real time is relevant.

## 2 REVIEW OF THE LITERATURE

In works [11, 12] the need to develop online-computers for processing data which are located close to the sensor, for use in distributed sensor systems is substantiated, stream processing algorithms are shown, which provide functional conversions of signals presented in the form of a bit stream (streams of single pulses, streams of PWM signals) and binary codes at the same time. The proposed principles of stream processing algorithm organization are considered as a continuous process of result formation.

Work [13] presents an approach to the design and hardware implementation of a converter that approximates a function for an argument that is a PWM signal. In this case, an approximating function in the form of dividing polynomials is used. In work [14], the proposed device is focused on the processing of measurement results, which is represented by a pulse stream, in which the functional conversion of information is carried out in the tracking mode.

In work [15] the structure of the converter of the time-frequency signals' parameters into a digital code based on a radial neural network is proposed. A decomposition of the converter into two components is proposed, in which the second component is a radial base network.

One of the relevant directions is the further development of specialized control devices for aerospace systems, in which the most important requirements for built-in online-computers and converters are low energy consumption, the ability to perform fast rough calculations, and low memory consumption. The CORDIC algorithm is used as a mathematical apparatus for such systems.

Works [16, 17] present a conceptual design approach, and realization of CORDIC architectures. The CORDIC is reconfigurable and can function in either of two modes: for hyperbolic or for circular trajectories in rotation and vectoring. In work [18] the principle of designing and implementing FPGA various trigonometric and logarithmic functions using CORDIC algorithm are presented.

A new efficient modified CORDIC algorithm is proposed. Work [19] explores approximation in CORDIC architectures for CMOS ASIC implementation.

A new efficient modified CORDIC algorithm is proposed in work [20], which combines the conventional CORDIC algorithm with the VSF CORDIC algorithm modelled. In work [21] divider architectures are proposed based on the Newton Raphson division using the reciprocal operation.

The design process can be carried out using tools of automated design systems based on hardware description languages for further synthesis and implementation into the FPGA platform, which ensures configuration flexibility, high speed, and technological reliability [22].

### 3 MATERIALS AND METHODS

Let's consider a method for forming increments of ascending step functions.

When designing bit-stream online-computers of elementary mathematical functions, a method of forming increments of ascending step functions during functional processing of bit streams corresponding to certain integer values of the argument is proposed.

In bit-stream functional online-computers, the reproduced function changes its value at discrete points and by a discrete value. At the same time, the process of calculating a continuous function involves calculating a lattice function that approximates a continuous one. The main criterion that determines the effectiveness of approximation for computing problems is the approximation error. The search for approximating expressions implemented in hardware is carried out taking into account additional restrictions of the expression type determined by the element base used.

The method of forming increments based on inverse functions ensures the fulfilment of requirements for functional online-computers, which include accuracy and calculation time, simplicity of technical implementation, and universality of using the architecture from the point of view of using the device to perform other mathematical operations. As a result, the method allows applying a unified approach to the design of online-computers. When synthesizing functional online-computers, the absolute error of the calculation must be rational, that is, to provide for all integer values of the argument the limiting value of the absolute error of the calculation  $\pm 0.5$  of the least significant bit of the argument.

The input  $x$  and output  $y$  information signals of the considered online-computers are two periodic bit sequences. At the same time, the periodicity of the presentation of bits of the input sequence  $x$  is determined by the method of quantization of the reproduced function, and

the periodicity of the stream of output bits of the sequence  $y$  is determined by the device's functioning algorithm. At the same time, uniform quantization of the argument with integer values is ensured.

The implementation of the approximating function in the online-computer includes certain stages.

At the first stage, an approximating function is selected for a given continuous one and absolute calculation error value at integer points of the argument is determined.

At the second stage, a mathematical model of the online-computer is developed using the considered step-wise approximation method based on inverse functions.

The model establishes a functional relationship in the form of a system of difference inequalities between the bit numbers of the output data stream  $y = 1, 2, 3, \dots, k$  and their corresponding values  $x_y = x_1, x_2, x_3, \dots, x_i$  of the input data stream  $x$ .

At the third stage, the architecture of the online-computer is created.

At the fourth stage, the hardware implementation of the online-computer is performed using CAD tools, which includes the creation of an automata model of the device based on a state machine, the implementation of the automata model in HDL code for the verification of the behavioral model and further synthesis and implementation in the FPGA.

A continuous function  $y^* = f(x^*)$ , the restrictions of which are the conditions of  $x^*, y^* \geq 0, y^* \leq x^*, dy^*/dx^* > 0$ , which has an inverse  $x^* = \psi(y^*)$ , and is reproduceable at the output of a hardware bit-stream online-computer by a function that approximates a continuous one:

$$y = [f(x) + |\delta_{\max}|]. \quad (1)$$

The value of absolute error limit value of continuous ascending functions reproduction  $\delta_{\max}$  is in the range  $0.5 \leq |\delta_{\max}| < 1$ .

Continuous and its approximating step functions are shown in Fig. 1.

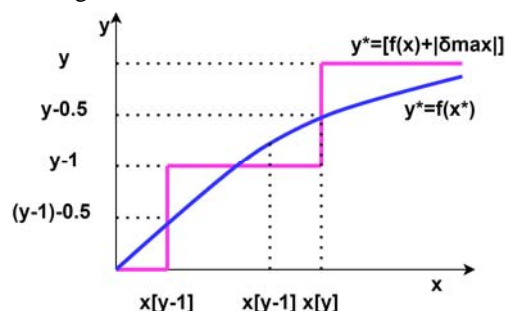


Figure 1 – Approximating step function

For any level  $1 - |\delta_{\max}|, y = 1, 2, \dots, k$  it is possible to specify a pair of integer values  $x_{y-1}$  and  $x_y$  for which a system of inequalities (2) takes place:





A bit-stream computer represented by a composition of control firmware and operating unit.

The operating unit has computational states in which pipeline calculations are performed, initiated by the signals of the control unit.

At the same time, the control unit determines the order of following the control signals and performing the sequence of microoperations based on the algorithm flowchart of the and the set of warning signals generated by the operating unit.

The graph was obtained as a result of marking the algorithm flowchart of the computer's arithmetic block (Fig. 3) and made it possible to increase the clarity and visibility of the device's computing states control.

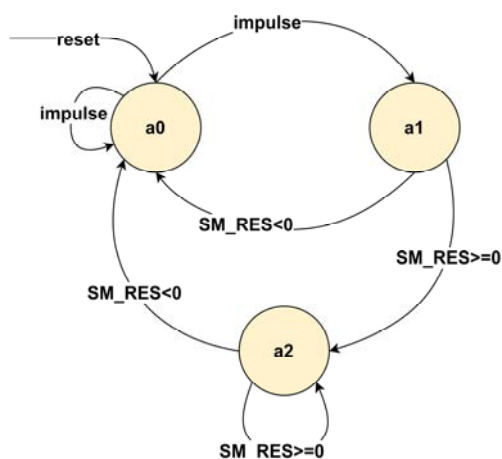


Figure 3 – State diagram of the computer control unit

An automaton template is one of the ways to describe a FSM in the hardware description language VHDL, in which the structure of the HDL model of the control unit of an online-computer is built on the basis of a state diagram.

The created HDL model of the control unit is an HDL template for the implementation of HDL models of online-computers. The control unit of the device is described by a state diagram that has three states a0, a1, a2.

At the signal reset = 1, the unit goes to state a0 and remains in it until the moment when the signal “impulse” appears.

After that, the unit goes to state a1. In state a1, pipelined computations are performed in the architecture's forward communication device components Block1.

If the content of the result adder  $SM\_RES \geq 0$  becomes non-negative, then the device output bit appears at its output and the unit goes to state a2. If  $SM\_RES < 0$  unit goes to a0 state.

In a2 pipeline calculations are performed in the feedback device components of the Block2 architecture.

If the value is  $SM\_RES < 0$ , the unit goes to state a0. Also, in a2, the unit generates a signal to form the output bit of the device. The unit is in a2 if the value is  $SM\_RES \geq 0$ .

Figures 4, 5 present algorithm flowcharts of the operating unit.

Fig. 4 shows the basic algorithm flowchart of the operating unit for the development of state diagrams of specific power and root extraction functions' implementation.

Fig. 5 shows the algorithm flowchart of the operating unit for the implementation of the power function  $y = [x^{\frac{3}{2}} + 0.5]$ .

The basic state diagram contains operator vertices a1 and a2 with computational microoperations in the device components.

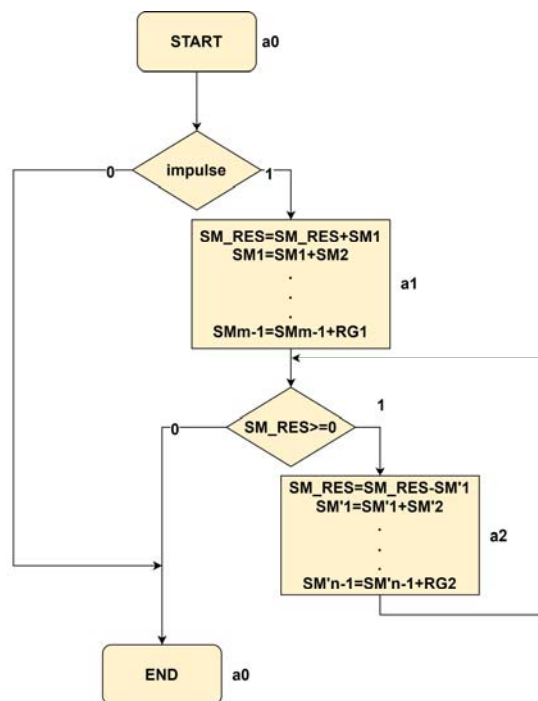


Figure 4 – Basic algorithm flowchart of the operating unit for implementation of a power function with an arbitrary fractional exponent

Figure 6 shows the algorithm flowchart of the operating unit for the implementation of the square root function.

Let's consider a block diagram of the online-computer.

As the result of the study, a block diagram of an online-computer was developed for hardware implementation, which includes two blocks: an impulse detector and a block of a bit-stream online-computer (Fig. 7).

The impulse detector unit detects the bits of the input stream  $x$  and sets the impulse = 1 signal at the output, which will be received by the arithmetic unit of the computer for further processing. The arithmetic block of the online-computer performs operations of raising the argument  $x$  to the power of a fractional-rational exponent and issues Ready signal when the block is ready to accept the next bit for processing. The result of the unit's operation is the output bit stream  $y$ , which is the result of the power function calculation.

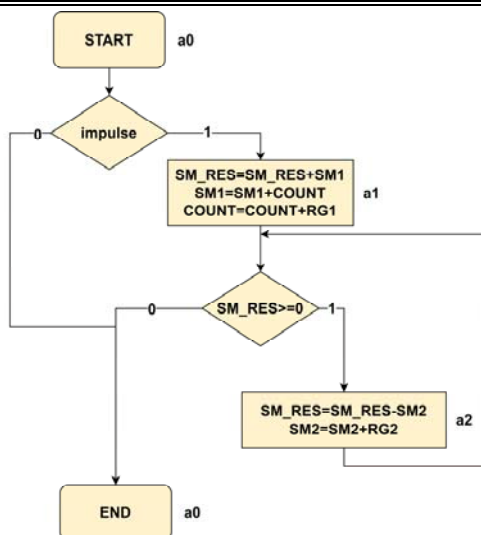


Figure 5 – Algorithm flowchart of the operating unit for implementation of power function  $y = [x^{\frac{3}{2}} + 0.5]$

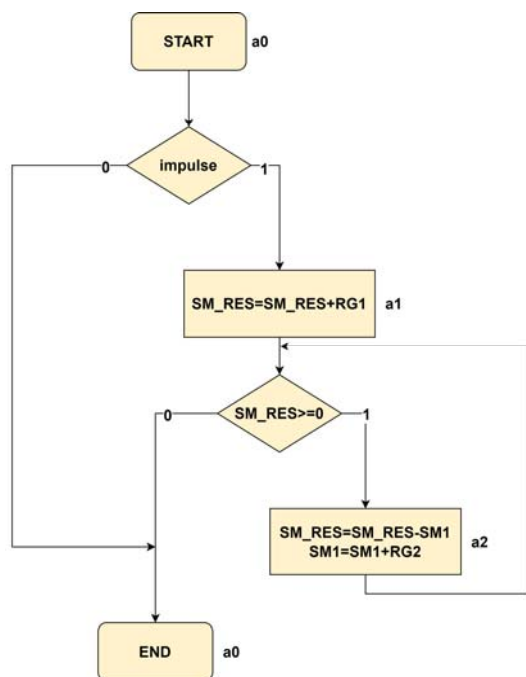


Figure 6 – Algorithm flowchart of the operating unit for square root function implementation

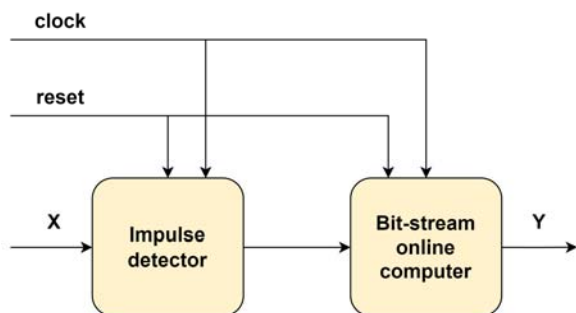


Figure 7 – Online-computer block diagram

#### 4 EXPERIMENTS

The approbation was carried out through hardware implementation and evaluation of the created design models using the example of a bit-stream real-time computers for power functions and the square root function reproduction.

Automata models of the devices were built in the hardware description language VHDL, the device was synthesized and implemented in the Xilinx FPGA, hardware costs were estimated, and modelling was carried out using Active-HDL.

Let's consider an experimental study of online-computer of power functions.

The online-computer of power functions can function in two modes.

Mode 1. Operation of the online-computer in the mode of sampling of bits from the bit stream data, i. e. number divider mode when exponents  $m < n$ .

Mode 2. Operation of the online-computer in the bit sequences series generation mode when exponents  $m > n$ .

An experimental study of the online power functions computer in the mode of sampling of bits from the bit stream data is given in [23].

For the approximating function  $y = [x^{\frac{2}{3}} + 0.5]$  sample values  $x_y$  was determined from the input bit stream using the formula  $x_y = [(y - 0.5)^{\frac{3}{2}}] + 1$ . When substituting the  $y = 1, 2, 3, 4, 5$  values, sample values are obtained  $x_y = 1, 2, 4, 7, 10$  respectively.

It is noted that the inequality  $2^3 x_y^2 \geq (2y - 1)^3$  is implemented in the online power function computer. The calculation of the left and right parts of the inequality is performed on the basis of the algorithm of pipeline calculations, which involves the calculation of arithmetic series of the second and third orders and of their arithmetic differences, respectively. At the same time, device synthesis is carried out by reducing the order of differences.

The study of online-computer of power functions in the bit sequences series generation mode was conducted.

For approximating function  $y = [x^{\frac{3}{2}} + 0.5]$ , using the formula  $x_y = [(y - 0.5)^{\frac{2}{3}}] + 1$  the number of bits in the series of bit sequences that are formed at the output of the device when each bit of  $x$  is applied to its input was determined.

If  $y = 1$ , then  $x = 1$ , that is, the first bit of the input sequence  $x$  will be selected and sent to the output of the device. If  $y = 2$  and  $y = 3$ , then  $x = 2$ , which means the formation of two series of bit sequences of 2 bits each. If  $y = 4$  and  $y = 5$ , then  $x = 3$ , that is, two series of bit sequences of three bits will be formed, and so on.

The inequality realized in device  $2^2 x_y^3 \geq (2y - 1)^2$ . In order to calculate the arithmetic series of the second and third and orders values  $x = \overline{0.8}$ ,  $x = \overline{1.7}$  should substi-

tuted to the left and right parts of the considered inequality, respectively.

For the function  $2^2 x_y^3$  the arithmetic series of the third order and the arithmetic series of differences of the first, second and third orders have the form:

$$f: 0, 4, 32, 108, 256, 500, 864, 1372, \dots;$$

$$\Delta: 4, 28, 76, 148, 244, 364, 508, \dots;$$

$$\Delta^2: 24, 48, 72, 96, 120, 144, \dots;$$

$$\Delta^3: 24, 24, 24, 24, 24, \dots$$

Considering function  $(2y-1)^2$  the arithmetic series of the second order and the arithmetic series of first and second order differences have the form:

$$f: 1, 9, 25, 49, 81, 121, 169, \dots;$$

$$\Delta: 8, 16, 24, 32, 40, 48, \dots;$$

$$\Delta^2: 8, 8, 8, 8, 8, \dots$$

The results of calculating the function values for first seven input bits are presented in Table 1.

The device architecture includes components: adders SM\_RES, SM1; counter Count; register RG1 which implement function  $2^2 x_y^3$  and adders SM\_RES, SM2; register RG2 which implement function  $(2y - 1)^2$ .

Table 1 – Calculation of power function

X	Value of function Y
X=1	$y = [1^{\frac{3}{2}} + 0.5] = [1.5] = 1$
X=2	$y = [2^{\frac{3}{2}} + 0.5] = [3.33] = 3$
X=3	$y = [3^{\frac{3}{2}} + 0.5] = [5.7] = 5$
X=4	$y = [4^{\frac{3}{2}} + 0.5] = [8.5] = 8$
X=5	$y = [5^{\frac{3}{2}} + 0.5] = [11.68] = 11$
X=6	$y = [6^{\frac{3}{2}} + 0.5] = [15.7] = 15$
X=7	$y = [7^{\frac{3}{2}} + 0.5] = [19.02] = 19$

Initialization of architecture components: Count=24, SM1=4, SM\_RES=-1, SM2=8, RG1=24, RG2 = 8.

Table 2 shows the results of computing process in components of the device.

The results of the calculation process in the components coincide with the results of the calculation of the power function for the first 7 bits of bit-stream data.

Let's consider an experimental research and approbation results by hardware implementation of online-computer of square root function.

For approximating function  $y = [\sqrt{x} + 0.5]$  sample values  $x_y$  were determined, which are selected from the input bit stream and fed to the input of the device, by the formula  $x_y = [(y - 0.5)^2] + 1$ .

Table 2 – Computing process in device components

X	SM_RES	Y	SM_1	Count	SM_2
1	-1 + 4 = 3 3 - 8 = -5	1	4 + 24 = 28	24 + 24 = 48	8 + 8 = 16
2	-5 + 28 = 23 23 - 16 = 7 7 - 24 = -17	1 1	28 + 48 = 76	48 + 24 = 72	16 + 8 = 24 24 + 8 = 32
3	-17 + 76 = 59 59 - 32 = 27 27 - 40 = -13	1 1	76 + 72 = 148	72 + 24 = 96	32 + 8 = 40 40 + 8 = 48
4	-13 + 148 = 135 135 - 48 = 87 87 - 56 = 31 31 - 64 = -33	1 1 1	148 + 96 = 244	96 + 24 = 120	48 + 8 = 56 56 + 8 = 64 64 + 8 = 72
5	-33 + 244 = 211 211 - 72 = 139 139 - 80 = 59 59 - 88 = -29	1 1 1	244 + 120 = 364	120 + 24 = 144	72 + 8 = 80 80 + 8 = 88 88 + 8 = 96
6	-29 + 364 = 335 335 - 96 = 239 239 - 104 = 135 135 - 112 = 23 23 - 120 = -97	1 1 1 1	364 + 144 = 508	144 + 24 = 168	96 + 8 = 104 104 + 8 = 112 112 + 8 = 120 120 + 8 = 128
7	-97 + 508 = 411 411 - 128 = 283 283 - 136 = 147 147 - 144 = 3 3 - 152 = -149	1 1 1 1	508 + 168 = 676	168 + 24 = 192	128 + 8 = 136 136 + 8 = 144 144 + 8 = 152 152 + 8 = 160

When substituting the values  $y = 1, 2, 3, 4$  the sample values  $x_y = 1, 3, 7, 13$ , are obtained, which will be selected from the input bit stream and applied to the output of the device. In the development of the pipeline architecture of the root extraction function computer, the algorithm of pipeline calculations is used, which is based on finding arithmetic series and their differences. The inequality  $2^2 x_y \geq (2y_k - 1)^2$  is realized in the device.

When substituting  $y = 1, 2, 3, \dots$  into the right-hand side of the inequality, the value of the function is obtained, which is an arithmetic series of the second order and the corresponding values of the difference series of the first and second orders:

- f: 1, 9, 25, 49, 81, 121, 169, 225, 289, 361, ...;
- $\Delta$ : 8, 16, 24, 32, 40, 48, 56, 64, 72, ...;
- $\Delta^2$ : 8, 8, 8, 8, 8, 8, 8, ...

The results of calculating the function values for first 13 input bits are presented in Table 3.

Table 3 – Calculation of square root function

X	Value of function Y
X=1	$y = [\sqrt{1} + 0.5] = [1.5] = 1$
X=2	$y = [\sqrt{2} + 0.5] = [1.91] = 1$
X=3	$y = [\sqrt{3} + 0.5] = [2.23] = 2$
X=4	$y = [\sqrt{4} + 0.5] = [2.5] = 2$
X=5	$y = [\sqrt{5} + 0.5] = [2.74] = 2$
X=6	$y = [\sqrt{6} + 0.5] = [2.95] = 2$
X=7	$y = [\sqrt{7} + 0.5] = [3.15] = 3$
X=8	$y = [\sqrt{8} + 0.5] = [3.33] = 3$
X=9	$y = [\sqrt{9} + 0.5] = [3.5] = 3$
X=10	$y = [\sqrt{10} + 0.5] = [3.66] = 3$
X=11	$y = [\sqrt{11} + 0.5] = [3.82] = 3$
X=12	$y = [\sqrt{12} + 0.5] = [3.96] = 3$
X=13	$y = [\sqrt{13} + 0.5] = [4.1] = 4$

Table 4 shows the results of computing process in online-computer components.

Table 4 – Computing process in the device components

X	SM_RES	Y	SM_I
1	$-1 + 4 = 3$ $3 - 8 = -5$	1	$8 + 8 = 16$
2	$-5 + 4 = -1$		
3	$-1 + 4 = 3$ $3 - 16 = -13$	1	$16 + 8 = 24$
4	$-13 + 4 = -9$		
5	$-9 + 4 = -5$		
6	$-5 + 4 = -1$		
7	$-1 + 4 = 3$ $3 - 24 = -21$	1	$24 + 8 = 32$
8	$-21 + 4 = -17$		
9	$-17 + 4 = -13$		
10	$-13 + 4 = -9$		
11	$-9 + 4 = -5$		
12	$-5 + 4 = -1$		
13	$-1 + 4 = 3$ $3 - 32 = -29$	1	$32 + 8 = 40$

## 5 RESULTS

Verification of the models of the studied online-computers was performed using the Active-HDL modelling system. Behavioral models of online computers were obtained based on the results of theoretical calculations in Section 4.

Fig. 8 shows the results of modelling the behavioural model of the device in the mode of sampling of bits from the bit stream data, i. e. number divider mode. Presented waveform shows, that when 7 bits of the input stream  $x$  are supplied to the input of the computer, 4 bits of the output bit stream  $y$  are generated at the output of the device, and therefore 1, 2, 4 and 7 bits corresponding to the sample numbers  $x_y$ .

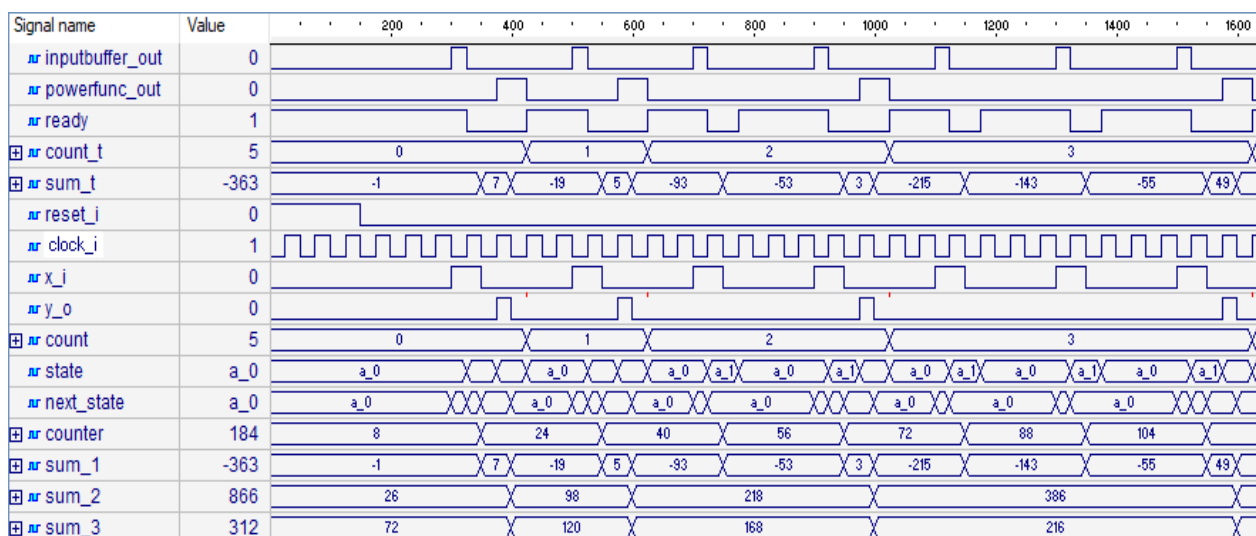


Figure 8 – The behavioral model of a power function online-computer in the mode of sampling of bits from the bit stream data

Fig. 9 shows the results of modelling the behavioural model of the bit-stream online-computer of the power function in the mode of generating bit sequences series, which coincided with the results of theoretical calculations.

The detailed waveform of the behavioural model of the online-computer contains information signals and register values of the device components that coincide with the results of the computational process.

At the output of the computer, a series of pulse sequences are generated for each input bit  $x$  starting from the second bit, which coincides with Table 2. When the second and third bits are applied to the input of the device, two series of two bits each are generated at the output. When the fourth and fifth bits are applied to the input, two series of bits of three bits each are generated at the output of the device, and so on.

Waveform confirms the correct operation of the online-computer in the mode of generating series of bit sequences.

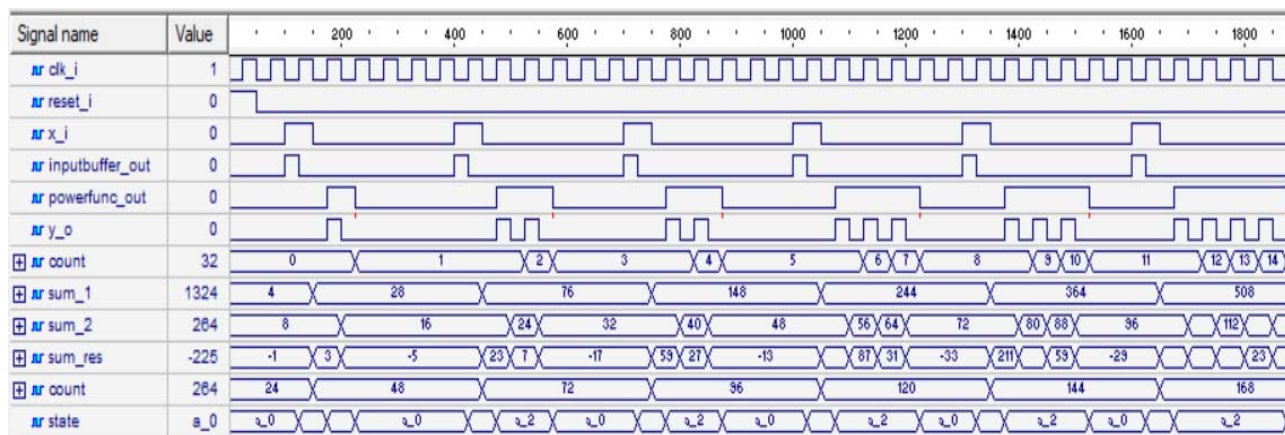


Figure 9 – The behavioural model of the bit-stream online-computer of the power function in the mode of generating bit sequences series

Fig. 10 shows the detailed waveform of the behavioural model of the square root function online-computer.

The waveform demonstrates the process of supplying 13 bits of the input stream  $x$  to the input of the computer, from which 1, 3, 7, 13 bits were selected and sent to the output of the device in the form of the output stream  $y$  ( $y=4$ ), which is the result of playing the square root function. The values of the registers coincide with the results of the computing process in the device components in accordance with Table 4.

The synthesis of the devices was carried out using CAD XILINX ISE. The schematic implementation of the computer is carried out on the XC3S100E series Xilinx SPARTAN 3E FPGA, which utilized approximately 6% of platform's resources. RTL-scheme of the synthesized power function computer is shown in Fig. 11. The maximum frequency of the devices is 125 MHz.

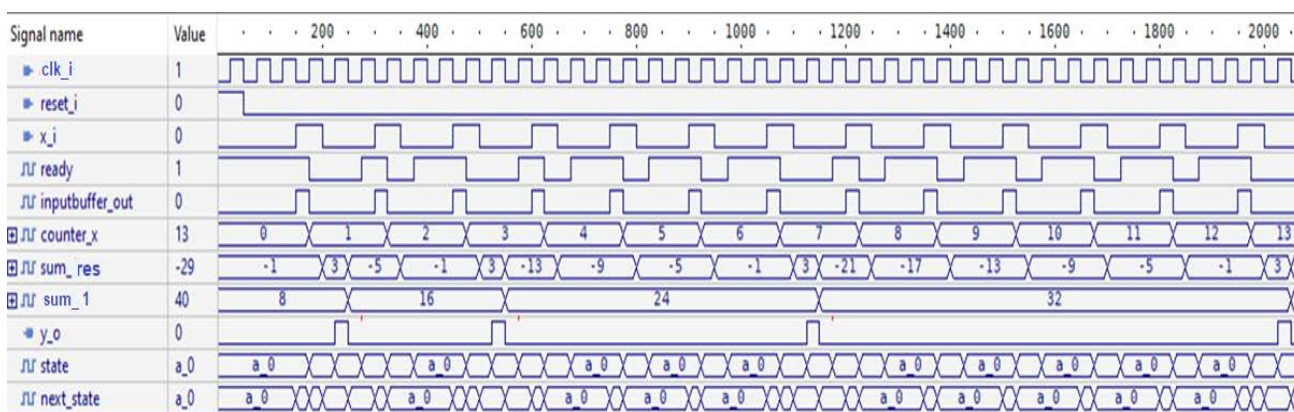


Figure 10 – The behavioural model of the bit-stream online-computer of root extraction function in the mode of sampling of bits from the bit stream data

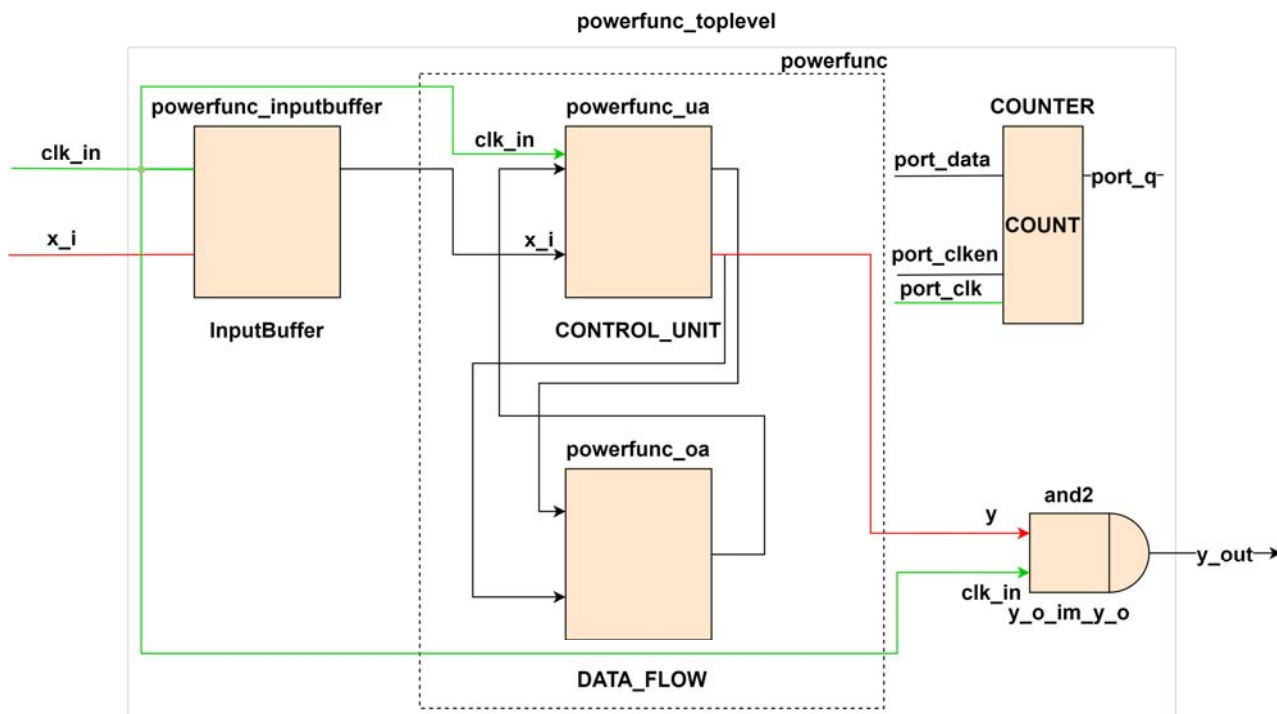


Figure 11 – RTL-scheme of the synthesized power function computer

## 6 DISCUSSION

The conducted research solves the actual scientific and practical problem of developing methods and models of designing hardware computers of mathematical functions of a specific class with bit streams data which perform calculations in real-time. In online-computers, a streaming method of calculations is organized with parallel-sequential execution of conversions over single bits of the input stream in accordance with a given function.

Increasing the accuracy of calculations and the speed of obtaining results in bit-stream online-computers of power functions and root extraction function is due to the development of improved mathematical models of computers based on the method of forming increments of ascending step functions with the minimization of absolute errors.

Expanding the functionality of online-computers is achieved by the construction of reconfigurable pipeline architectures based on the proposed generalized architecture of the computer, which allowed to develop a unified approach to their automated synthesis using hardware description languages.

Increasing the clarity and invariance of the implementation in formal languages of programming and hardware description is achieved due to the clarity and correctness of the algorithms for the implementation of functions by the proposed graph models of online-computers based on FSM.

## CONCLUSIONS

As a result of the work, the generalized architecture of an online-computer was proposed, algorithm flowchart implementations of specific functions and the state dia-

gram of Moore model control automaton of the computer's arithmetic unit were created.

Automata HDL models in the form of automata patterns were developed. The performance of the developed models of online-computers was confirmed by checking the results using the verification of behavioural models using Active-HDL CAD, automated synthesis and implementation in the Xilinx FPGA platform.

The considered functional online-computers are effective from the point of view of calculation accuracy, simplicity of technical implementation, and universality of the architecture.

**The scientific novelty** of the obtained results lies in the fact that the improved mathematical models of bit-stream online-computers of power functions and root extraction function were developed using the analysis method of forming increments of ascending step functions based on inverse functions with minimization of calculation errors. Automata models of bit-stream online-computers of elementary mathematical functions, characterized by graph models, were proposed, which made it possible to ensure the clarity and consistency of function implementation algorithms.

**The practical significance** of the obtained results lies in the fact that the use of the developed mathematical, architectural and automata design models of bit-stream online-computers of elementary mathematical functions ensures an increase in the accuracy of the calculation of mathematical functions, reduces equipment costs and development time, which ultimately increases the efficiency of the design process. It also consists in the development of automata models of bit-stream functional computers, which are formed on the basis of the finite state machine of the Moore model, which made it possible to create the

same type of graph models and HDL models in the form of an automata pattern for the implementation of algorithms of reproducible functions of online-computers with CAD tools.

**The prospects for the further research** involve the application of the developed design models to other signal encoding methods. Also, the mentioned approaches might perfectly suit to be deployed on the SoCs such as Xilinx ZYNQ which contains Programming System (ARM) part and Programmable Logic (PL) component with the optimal computation distribution between them. This includes the further research directions of using partial reconfiguration for deploying various bit-stream specific hardware accelerators with the capabilities of resource management on ARM side.

### ACKNOWLEDGEMENTS

The work was carried out within the framework of the state budget research topic of the Kharkiv National University of Radio Electronics “Smart cyber university – Cloud-Mobile services for managing scientific and educational processes 1” (state registration 0017U002524, order of the Ministry of Education of Ukraine) on the basis of the Design automation department, KNURE.

And out within the framework of the department research topic of the National University Zaporizhzhia Polytechnic “Methods, models and software tools of intelligent computing” (state registration number 0121U112837, order of the Ministry of Education of Ukraine) on the basis of the of Software Tools department, NUZP.

### REFERENCES

1. Korniienko V., Larchenko L., Parkhomenko A., Larchenko B. Design Models of Bit-Stream Online-Computers of Elementary Mathematical Functions, *12th International Conference on Intelligent Data Acquisition and Advanced Computing Systems: Technology and Applications (IDAACS)*, Sep 2023. Dortmund, Germany, pp. 585–589. DOI : 10.1109/IDAACS58523.2023.10348885.
2. Al-Makhles D., Patel N., Swain A. Bitstream Control System: Stability and Experimental Application, *2013 International Conference on Applied Electronics, Sep 2013*. Pilsen, Czech Republic, pp. 19–24. ISSN: 1803-7232.
3. Al-Makhles D., Patel N., Swain A. Conventional and Hybrid Bit-Stream in Real-Time System, *11th Workshop on Intelligent Solutions in Embedded Systems (WISES)*, Sep 2013. Pilsen, Czech Republic, pp. 1–6. ISBN:978-3-00-042899-9.
4. Li P., Lilja D. J., Qian W., Riedel M. D. Bazargan. K. Logical Computation on Stochastic Bit Streams with Linear Finite-State Machines, *IEEE Transactions on Computers*, 2014, Volume 63(6), pp. 1474–1486. DOI : 10.1109/TC.2012.231.
5. Yan M., Nan X., Liru H., Jinghua T., Weimin C. Development on Intelligent Small-Flow Target Flow Meter, *2009 International Forum on Computer Science-Technology and Applications, Dec 2009*. Chongqing, China, pp. 315–317. DOI : 10.1109/IFCSTA.2009.317.
6. Stanley M., Gervais-Ducouret S., Adams J. T. Intelligent Sensor Hub Benefits for Wireless Sensor Networks, *2012 IEEE Sensors Applications Symposium, Feb 2012*. Brescia, Italy, pp. 1–6. DOI : 10.1109/SAS.2012.6166299.
7. Gulin A. I., Safyannikov N. M., Bureneva O. I., Kaydanovich A. Yu. Assurance of Fault-Tolerance in Bit-Stream Computing Converters, *16th IEEE East-West Design & Test Symposium, Sep 2018*. Kazan, Russia, pp. 418–421. DOI : 10.1109/EWDTS.2018.8524812.
8. Ueno K., Asai T., Amemiya Y. Temperature-to-Frequency Converter Consisting of Subthreshold Mosfet Circuits for Smart Temperature-Sensor LSIs, *2009 TRANSDUCERS International Solid-State Sensors, Jun 2009, Actuators and Microsystems Conference*. Denver, CO, USA, pp. 2433–2436. DOI : 10.1109/SENSOR.2009.5285436.
9. Arbet D., Kováč M., Stopjaková V., Potočný M. Voltage-to-Frequency Converter for Ultra-Low-Voltage Applications, *42nd International Convention on Information and Communication Technology, Electronics and Micro-electronics (MIPRO), May 2019*. Opatija, Croatia, pp. 53–58. DOI : 10.23919/MIPRO.2019.8756910.
10. Areekath L., George B., Reverter F. An Auto-Balancing Capacitance-to-Pulse-Width Converter for Capacitive Sensors, *IEEE Sensors Journal*, 2021, Volume 21(1), pp. 765–775. DOI : 10.1109/JSEN.2020.3014206.
11. Safyannikov N., Bureneva O., Bit-Stream Functional Converters for Decentralized Sensor Systems, *9th Mediterranean Conference on Embedded Computing (MECO), Jun 2020*. Budva, Montenegro, pp. 1–4. DOI : 10.1109/MECO49872.2020.9134176.
12. Bureneva O., Kupriyanov M., Safyannikov N. Bit Streaming Processing Algorithms for Intelligent Hardware Converters, *Applied Sciences*, 2021, Volume 186, pp. 194–201. DOI : 10.1016/j.procs.2021.04.138.
13. Bureneva O., Mironov S., Safyannikov N. Bit-Stream Approximating Devices Based on Counters with Weight Inputs, *11th Mediterranean Conference on Embedded Computing (MECO), Jun 2022*. Budva, Montenegro, pp. 1–4. DOI : 10.1109/MECO55406.2022.9797145.
14. Bureneva O. I. Stream Tracking Devices for Soft Measurements Implementation, *XX IEEE International Conference on Soft Computing and Measurements (SCM), May 2017*. St. Petersburg, Russia, pp. 614–616. DOI : 10.1109/SCM.2017.7970666.
15. Chelebaev S. V., Chelebaeva Y. A. Converters Structures Synthesis of Time-and-Frequency Signals Parameters in the Code of Two Variables on the Radial Basis Network, *5th Mediterranean Conference on Embedded Computing (MECO), Jun 2016*. Budva, Montenegro, pp. 339–342. DOI : 10.1109/MECO.2016.7525776.
16. Aggarwal S, Meher P. K., Khare K. Concept, Design, and Implementation of Reconfigurable CORDIC, *IEEE Transactions on Very Large-Scale Integration (VLSI) Systems*, 2016, Volume 24(4), pp. 1588–1592. DOI : 10.1109/TVLSI.2015.2445855.
17. Meher P. K., Valls J., Juang T. B., Sridharan K., Maharatna K. 50 Years of CORDIC: Algorithms, Architectures, and Applications, *IEEE Transactions on Circuits and Systems I: Regular Papers*, 2009, Volume 56(9), pp. 1893–1907. DOI : 10.1109/TCSI.2009.2025803.
18. Kumar P. A. FPGA Implementation of the Trigonometric Functions Using the CORDIC Algorithm, *5th International Conference on Advanced Computing & Communication Systems (ICACCS), Mar 2019*. Coimbatore, India, pp. 894–900. DOI : 10.1109/ICACCS.2019.8728315.
19. Sapper A. N., Soares L., Costa E., Bampi S. Exploring the Combination of Number of Bits and Number of Iterations for a Power-Efficient Fixed-Point CORDIC Implementation, *24th IEEE International Conference on Electronics, Circuits*

- and Systems (ICECS), Dec 2017. Batumi, Georgia, pp. 302–305. DOI : 10.1109/ICECS.2017.8292079.
20. Xue Y., Ma Z. Design and Implementation of an Efficient Modified CORDIC Algorithm, *4th International Conference on Signal and Image Processing (ICSIP), Jul 2019*. Wuxi, China, pp. 480–484. DOI : 10.1109/SIPROCESS.2019.8868732.
21. Rodriguez-Garcia A., Pizano-Escalante L., Parra-Michel R., Longoria-Gandara O., Cortez J. Fast Fixed-Point Divider Based on Newton-Raphson Method and Piecewise Polynomial Approximation, *2013 International Conference on Reconfigurable Computing and FPGAs (ReConFig), Dec 2013*. Cancun, Mexico, pp. 1–6. DOI : 10.1109/ReConFig.2013.6732291.
22. Dang Pham K., Horta E., Koch D. BITMAN: A Tool and API for FPGA Bitstream Manipulations, *2017 Design, Automation & Test in Europe Conference & Exhibition (DATE), Mar 2017*. Lausanne, Switzerland, pp. 894–897. DOI : 10.23919/DATE.2017.7927114.
23. Shkil A. S., Larchenko L. V., Larchenko B. D. Bit-Stream Power Function Online Computer, *2020 East-West Design & Test Symposium (EWDTS), Sep 2020*. Varna, Bulgaria, pp. 1–6. DOI : 10.1109/EWDTS50664.2020.9224764.
- Received 04.01.2024.  
Accepted 28.02.2024.

УДК 004.31

## МОДЕЛІ ПРОЄКТУВАННЯ БІТ-ПОТОКОВИХ ОНЛАЙН-ОБЧИСЛЮВАЧІВ ДЛЯ СЕНСОРНИХ КОМПОНЕНТІВ

**Ларченко Л. В.** – канд. техн. наук, доцент, доцент кафедри автоматизації проєктування обчислювальної техніки Харківського національного університету радіоелектроніки, Харків, Україна.

**Пархоменко А. В.** – канд. техн. наук, доцент, доцент кафедри програмних засобів Національного університету «Запорізька політехніка», Запоріжжя, Україна.

**Ларченко Б. Д.** – канд. техн. наук, асистент кафедри автоматизації проєктування обчислювальної техніки Харківського національного університету радіоелектроніки, Харків, Україна.

**Корнієнко В. Р.** – аспірант кафедри автоматизації проєктування обчислювальної техніки Харківського національного університету радіоелектроніки, Харків, Україна.

### АНОТАЦІЯ

**Актуальність.** В даний час розподілені системи управління реального часу потребують створення пристроїв, які виконують онлайн-обчислювальні операції в оточенні датчика. Запропоновані online-обчислювачі елементарних математичних функцій можуть бути використані як компоненти для функціонального перетворення сигналів у вигляді імпульсних потоків, що надходять від вимірювальних датчиків з частотним виходом.

**Мета роботи.** Розробка математичних, архітектурних та автоматних моделей проєктування біт-потоків онлайн-обчислювачів елементарних математичних функцій з метою створення єдиного підходу до їх проєктування, завдяки якому можливо підвищити точність обчислення функцій, розширити функціональні можливості, зменшити апаратні витрати та підвищити ефективність проєктування.

**Метод.** Розроблено математичні моделі пристроїв з використанням методу формування приростів ступінчастих функцій на основі обернених функцій з мінімізацією похибки обчислень. Розроблено автоматні моделі онлайн-обчислювачів на основі кінцевого автомата Мура, графові моделі яких дозволили забезпечити чіткість алгоритмів реалізації функцій, підвищити наочність та інваріантність реалізації на формальних мовах програмування та опису апаратури.

**Результати.** У статті наведено результати дослідження, розробки та практичної апробації моделей проєктування біт-потоків онлайн-обчислювачів степеневі функції та функції вилучення кореня. Запропоновано узагальнену архітектуру онлайн-обчислювача.

**Висновки.** Розглянуті функціональні онлайн-обчислювачі ефективні з точки зору точності обчислень, простоти технічної реалізації та універсальності архітектури.

**КЛЮЧОВІ СЛОВА:** функціональне перетворення, бітові дані, бітові обчислення, математична модель, кінцевий автомат, FPGA, SoC.

### ЛІТЕРАТУРА

- Design Models of Bit-Stream Online-Computers of Elementary Mathematical Functions / [V. Korniienko, L. Larchenko, A. Parkhomenko et al.] // *12th International Conference on Intelligent Data Acquisition and Advanced Computing Systems, Technology and Applications (IDAACS), Sep 2023, Dortmund, Germany. – Germany. – P. 585–589. DOI : 10.1109/IDAACS58523.2023.10348885.*
- Al-Makhles D. Bitstream Control System: Stability and Experimental Application / D. Al-Makhles, N. Patel, A Swain // *2013 International Conference on Applied Electronics, Sep 2013, Pilsen, Czech Republic. – Czech Republic. – P. 19–24. ISSN: 1803-7232.*
- Al-Makhles, D. Conventional and Hybrid Bit-Stream in Real-Time System / D. Al-Makhles, N. Patel, A. Swain // *11th Workshop on Intelligent Solutions in Embedded Systems (WISES), Sep 2013, Pilsen, Czech Republic. – Czech Republic. – P. 1–6. ISBN:978-3-00-042899-9.*
- Logical Computation on Stochastic Bit Streams with Linear Finite-State Machines / [P. Li, D. J. Lilja, W. Qian et al.] // *IEEE Transactions on Computers. – 2014. – Volume 63(6). – P. 1474–1486. DOI: 10.1109/TC.2012.231.*
- Development on Intelligent Small-Flow Target Flow Meter / [M. Yan, X. Nan, H. Liru et al.] // *2009 International Forum on Computer Science-Technology and Applications, Dec 2009, Chongqing, China. – China. – P. 315–317. DOI : 10.1109/IFCSTA.2009.317.*
- Stanley M. Intelligent Sensor Hub Benefits for Wireless Sensor Networks / M. Stanley, S. Gervais-Ducouret, J. T Adams // *2012 IEEE Sensors Applications Symposium, Feb 2012, Brescia, Italy. – Italy. – P. 1–6. DOI: 10.1109/SAS.2012.6166299.*

7. Assurance of Fault-Tolerance in Bit-Stream Computing Converters / [A. I. Gulin, N. M. Safyannikov, O.I. Bureneva et al.] // 16th IEEE East-West Design & Test Symposium, Sep 2018, Kazan, Russia. – Russia. – P. 418–421. DOI: 10.1109/EWDTS.2018.8524812.
8. Ueno K. Temperature-to-Frequency Converter Consisting of Subthreshold Mosfet Circuits for Smart Temperature-Sensor LSIs / K. Ueno, T. Asai, Y. Amemiya // 2009 TRANSDUCERS International Solid-State Sensors, Actuators and Microsystems Conference, Jun 2009, Denver, CO, USA. – USA. – P. 2433–2436. DOI: 10.1109/SENSOR.2009.5285436.
9. Voltage-to-Frequency Converter for Ultra-Low-Voltage Applications / [D. Arbet, M. Kováč; V. Stopjaková et al.] // 42nd International Convention on Information and Communication Technology, Electronics and Micro-electronics (MIPRO), May 2019, Opatija, Croatia. – Croatia. – P. 53–58. DOI : 10.23919/MIPRO.2019.8756910.
10. Areekath L. An Auto-Balancing Capacitance-to-Pulse-Width Converter for Capacitive Sensors / L. Areekath, B. George, F. Reverter // IEEE Sensors Journal. – 2021. – Volume 21(1). – P. 765–775. DOI: 10.1109/JSEN.2020.3014206.
11. Safyannikov, N. Bit-Stream Functional Converters for Decentralized Sensor Systems / N. Safyannikov, O. Bureneva // 9th Mediterranean Conference on Embedded Computing (MECO), Jun 2020, Budva, Montenegro. – Montenegro. – P. 1–4. DOI: 10.1109/MECO49872.2020.9134176.
12. Bureneva O. Bit Streaming Processing Algorithms for Intelligent Hardware Converters / [O. Bureneva, M. Kupriyanov, N. Safyannikov] // Applied Sciences. – 2021. – Volume 186. – P. 194–201. DOI: 10.1016/j.procs.2021.04.138.
13. Bureneva O. Bit-Stream Approximating Devices Based on Counters with Weight Inputs / O. Bureneva, S. Mironov, N. Safyannikov // 11th Mediterranean Conference on Embedded Computing (MECO), Jun 2022, Budva, Montenegro. – Montenegro. – P. 1–4. DOI: 10.1109/MECO55406.2022.9797145.
14. Bureneva O. I. Stream Tracking Devices for Soft Measurements Implementation / O. I. Bureneva // XX IEEE International Conference on Soft Computing and Measurements (SCM), May 2017, St. Petersburg, Russia. – Russia. – P. 614–616. DOI : 10.1109/SCM.2017.7970666.
15. Chelebaev S. V. Converters Structures Synthesis of Time-and-Frequency Signals Parameters in the Code of Two Variables on the Radial Basis Network / S. V. Chelebaev, Y. A. Chelebaeva // 5th Mediterranean Conference on Embedded Computing (MECO), Jun 2016, Budva, Montenegro. – Montenegro. – P. 339–342. DOI: 10.1109/MECO.2016.7525776.
16. Aggarwal, S. Concept, Design, and Implementation of Reconfigurable CORDIC / S. Aggarwal, P. K. Meher, K. Khare // IEEE Transactions on Very Large-Scale Integration (VLSI) Systems. – 2016. – Volume 24(4). – P. 1588–1592. DOI: 10.1109/TVLSI.2015.2445855.
17. 50 Years of CORDIC: Algorithms, Architectures, and Applications / [P. K. Meher, J. Valls, T. B. Juang et al.] // IEEE Transactions on Circuits and Systems I: Regular Papers. – 2009. – Volume 56(9). – P. 1893–1907. DOI: 10.1109/TCSI.2009.2025803.
18. Kumar, P. A. FPGA Implementation of the Trigonometric Functions Using the CORDIC Algorithm / P. A. Kumar // 5th International Conference on Advanced Computing & Communication Systems (ICACCS), Mar 2019, Coimbatore, India. – India. – P. 894–900. DOI: 10.1109/ICACCS.2019.8728315.
19. Exploring the Combination of Number of Bits and Number of Iterations for a Power-Efficient Fixed-Point CORDIC Implementation / [A. N. Sapper, L. Soares, E. Costa et al.] // 24th IEEE International Conference on Electronics, Circuits and Systems (ICECS), Dec 2017, Batumi, Georgia. – Georgia. – P. 302–305. DOI: 10.1109/ICECS.2017.8292079.
20. Xue Y. Design and Implementation of an Efficient Modified CORDIC Algorithm / Y. Xue, Z. Ma // 4th International Conference on Signal and Image Processing (ICSIP), Jul 2019, Wuxi, China. – China. – P. 480–484. DOI: 10.1109/SIPROCESS.2019.8868732.
21. Fast Fixed-Point Divider Based on Newton-Raphson Method and Piecewise Polynomial Approximation / [A. Rodriguez-Garcia, L. Pizano-Escalante, R. Parra-Michel et al.] // 2019 International Conference on Reconfigurable Computing and FPGAs (ReConFig), Dec 2013, Cancun, Mexico. – Mexico. – P. 1–6. DOI: 10.1109/ReConFig.2013.6732291.
22. Dang Pham, K. BITMAN: A Tool and API for FPGA Bit-stream Manipulations / K. Dang Pham, E. Horta, D. Koch // 2017 Design, Automation & Test in Europe Conference & Exhibition (DATE), Mar 2017, Lausanne, Switzerland. – Switzerland. – P. 894–897. DOI: 10.23919/DATE.2017.7927114.
23. Shkil, A. S. Bit-Stream Power Function Online Computer / A. S. Shkil, L. V. Larchenko, B. D. Larchenko // 2020 IEEE East-West Design & Test Symposium (EWDTS), Sep 2020, Varna, Bulgaria. – Bulgaria. – P. 1–6. DOI : 10.1109/EWDTS50664.2020.9224764.

## EVALUATION OF THE INFLUENCE OF ENVIRONMENTAL FACTORS AND COGNITIVE PARAMETERS ON THE DECISION-MAKING PROCESS IN HUMAN-MACHINE SYSTEMS OF CRITICAL APPLICATION

**Perederyi V. I.** – Dr. Sc., Professor of the Department of Information Technologies, V.O.Sukhomlynsky Mykolaiv National University, Mykolaiv, Ukraine.

**Borchik E. Y.** – PhD, Associate Professor of the Department of Information Technologies, Mykolaiv National Agrarian University, Mykolaiv, Ukraine.

**Zosimov V. V.** – Dr. Sc., Professor of the Department of Applied Information Systems, Taras Shevchenko National University of Kyiv, Kyiv, Ukraine.

**Bulgakova O. S.** – PhD, Associate Professor of the Department of Applied Information Systems, Taras Shevchenko National University of Kyiv, Kyiv, Ukraine.

### ABSTRACT

**Context.** A feature of human-machine systems of critical application operating in real time is that they include as elements both technical systems and people interacting with these systems. At the same time, the main difficulties are associated not only with the improvement of hardware and software, but also with the insufficient development of methods for reliably predicting the impact of the production environment on the human factor and, as a result, on the relevance of decisions made by decision makers. As a result, the task of developing methods for determining the mutual influence of environmental factors and cognitive parameters of decision makers on the decision-making process becomes very relevant.

**Objective.** The aim of the work is to propose methodological foundations for the development and study of fuzzy hierarchical relational cognitive models to determine the influence of environmental factors and cognitive parameters of decision makers on the DMP.

**Method.** When building FHRM methods of “soft computing”, methodologies of cognitive and fuzzy cognitive modeling were used, providing an acceptable formalization uncertainty of mutual influence of factors on the DMP.

**Results.** A fuzzy cognitive model based on a fuzzy Bayesian belief network has been developed, which makes it possible to draw a connection between qualitative and quantitative assessments of mutually influencing factors on the DMP. The proposed model makes it possible to probabilistically predict the influence of factors and choose rational ways of their interaction in the DMP.

**Conclusions.** The results of the experiments make it possible to recommend using the developed model, which takes into account the mutual influence of factors of various nature, including cognitive ones, in the DMP in order to improve the efficiency of HMSCA management as a whole.

**KEYWORDS:** man-machine systems of critical application, decision making, decision making person, fuzzy cognitive models, environmental factors, working environment factors, relational cognitive models.

### ABBREVIATIONS

HMSCA is a human-machine systems of critical application;

DM is a decision maker;

FHRM is a fuzzy hierarchical relational cognitive model;

BBN is a Bayesian trust networks;

DS is a decision support;

DMP is a decision making process;

MRD is a making relevant decision;

OTSCA is an organizational and technical system of critical application;

HMS is a human-machine system.

### NOMENCLATURE

$I_n$  is an indicator of noise level;

$E_N$  is an indicator of electromagnetic field level;

$L$  is an indicator of workplace lighting;

$T_e$  is an indicator of room temperature;

$H$  is an indicator of room humidity;

$S$  is an astate of the technological process;

$T$  is an indicator of fatigue degree;

$F$  is an indicator of psychological tension;

$I$  is an indicator of informational stress;

$E$  is a possibility of error;

$D$  is a decision time;

$R()$  is a relevance of decision making;

$A_i$  is a value of  $i$ -th fuzzy numbers;

$n_i$  is a modal value;

$\tilde{N}()$  is a fuzzy interval;

$N$  is a result of defuzzification;

$b_j$  is a value of  $j$ -th number on a BBN;

$B$  is a vertex on a BBN;

$P()$  is a probability of joint distribution of a Bayesian belief network;

$S_e()$  is a function that characterizes the influence of external and production factors;

$S_p()$  is a function that characterizes the influence of psychological and cognitive factors on the state of decision makers;

$\mu()$  is a membership function;

$\tilde{P}()$  is a fuzzy probability;

$\tilde{H}()$  is a fuzzy interval;

$e_i$  is a value of the  $i$ -th BBN  $E$ -vertice;

$r_i$  is a value of the  $i$ -th BBN  $R$ -vertice;

$d_i$  is a value of the  $i$ -th BBN  $D$ -vertice;  
 $f_i$  is a value of the  $i$ -th BBN  $F$ -vertice;  
 $t_i$  is a value of the  $i$ -th BBN  $T$ -vertice.

## INTRODUCTION

Today, when creating HMSCA, the solution of the problems of managing and monitoring processes and phenomena of an anthropogenic and natural nature comes to the fore, followed by the adoption of appropriate decisions at each hierarchical level of the system.

Modern HMSCAs are built, as a rule, on the basis of computer networks, which, together with software and users, are designed to increase management efficiency. Currently, the issues of assessing the performance of HMSCA enough attention are paid, but there is no single conceptual approach to the study of such systems.

It is noted that, in general, research in this area is reduced to the study of the perception of information in verbal and visual form, its analysis, and comparison of DS alternatives. However, there are practically no studies of the mutual influence of external factors of various natures, including cognitive ones, on the DMP.

Also, issues related to management decisions at each hierarchical level of the system have not been sufficiently developed, due to the imperfection of the mathematical, statistical and intellectual tools used.

**The objects of study** are fuzzy hierarchical relational cognitive decision-making models in multi-level OTSCA.

**The subjects of study** are models and methods of decision-making in multi-level HMSCA.

**The purpose of the work** is to introduce methodological fundamentals of development and research of fuzzy hierarchical relational cognitive models to determine the mutual influence of environmental factors and cognitive parameters of DMs on the DMP.

## 1 PROBLEM STATEMENT

In the process of work, the decision maker is under the influence of external factors of the environment and the production environment and factors that characterize his psychological and cognitive state.

It is required to assess the degree of relevance of decisions made by the decision maker, under the influence of the above factors, in multi-level OTSCA in a limited time.

Suppose that the values of external and production, as well as psychological and cognitive factors  $H, S, Te, EN, In, L, F, D, T, E$  are known.

It is necessary, based on an expert assessment of the degree of relationship between these factors, to estimate the value of the function  $R=f(H,S,Te,EN,In,L,F,D,T,E)$ , which characterizes the degree of relevance of the decision maker's decision in real time and draw a conclusion about the relevance of the decision made by the decision-maker, provided: the decision is relevant if  $R \geq R^*$  and irrelevant if  $R < R^*$ .

## 2 REVIEW OF THE LITERATURE

In the scientific works of a number of authors, it has been noted that one of the most important methodological problems in the theory of decision making and multi-criteria choice is the problem of overcoming the factor of subjectivity, which is due to the presence of psychological characteristics of the behavior of individuals participating in the DMP. In works authors [2-5] noted that the decision-making function "crystallizes" in specific formations – structures of individual qualities that affect individual stylistic differences in the selection processes. Therefore, the management of the mental processes of the decision maker impossible without an assessment of these individual qualities.

Research in ergonomics and engineering psychology conducted over the past decades has made it possible to identify a number of factors that affect the DMP of a human operator. Among these factors, it is necessary to single out those that can dynamically, chaotically change in the process of HMSCA. But such changes cannot be predicted in advance, at the design stage.

Literature analysis [6, 7] allows you to establish the relationship between factors from the group of environmental impact on the psycho-functional state of the decision maker, which in turn affects the adequacy of its actions. However, the adequacy of actions is determined not only by external conditions, but also by the ability of the decision maker's organism to prevent the negative impact of external conditions. These factors include the level of the cognitive component and the tension of the nervous system. The variety of relationships between the characteristics of the psycho-functional state of the decision maker, external factors and the quality of his activity complicates the task of constructing mathematical models for assessing the mutual influence of these factors on the process of making appropriate decisions.

In works [8, 9] an algorithm for increasing the efficiency of interaction between an operator and technical devices in "man-machine" systems is proposed, which allows solving the problem of ensuring the efficiency of managing complex technical and production systems under conditions of fuzzy risk. The results of studies of the influence of the functional state of operators on efficiency and quality in the "man-machine" systems are presented. Based on the above analysis, it was concluded that it is necessary to develop modern methods for improving efficiency, taking into account the dependence of the functional state of operators on the influence of external and internal factors on the process of making adequate decisions.

In literature [10, 11] issues considered determination of a comfortable working environment for the decision maker during the operation of the system. Developments on the creation of mathematical models and algorithms for assessing the relevance of decisions taken are considered in detail, taking into account the influence of external and personal factors on the safety of HMS. Algorithms for formalizing the relationship between external factors and psycho-functional characteristics of decision makers are

proposed to optimize decision making. But all this does not make it possible to describe with maximum accuracy the factors for which there are no known exact patterns and for which it is necessary to make an association between qualitative and quantitative assessments of factors affecting the effectiveness of HMSCA.

Common questions analyzed building fuzzy cognitive models of information technology to determine and evaluate the influence of factors on the DMP in multilevel HMSCA using [12].

Determination of the functional dependence of the effectiveness of multi-level systems of critical purpose on the influence of external factors and the fuzzy risk of making inadequate decisions by the decision maker, as well as the construction of fuzzy cognitive models of DMP under conditions of fuzzy risk is considered in [13–17]

In [18–20] the development of mathematical models and algorithms for determining and evaluating the optimal influence of external factors of the working environments on the cognitive state of decision makers.

Based on the analysis of literary sources, it is noted that in order to overcome the difficulties caused by uncertain factors (inaccuracy, fuzziness) for solving assessment problems their influence on DMP, in a multilevel HMSCA is a need to improve and develop new modern methods of work efficiency HMSCA. It is advisable to apply DS methods using “soft computing”, the methodology of cognitive and fuzzy cognitive modeling, which provides an acceptable formalization of uncertainty due to the presence of subjective judgments of experts.

### 3 MATERIALS AND METHODS

Because acceptance decisions defined by many influence factors external and production environment and factors characterizing the current psychological and cognitive state of the decision maker, then one of stages of assessing its relevance is to identify cause-and-effect relationships and dependencies between these factors.

The information model of the above factors of influence on the DMP is shown in Figure 1.

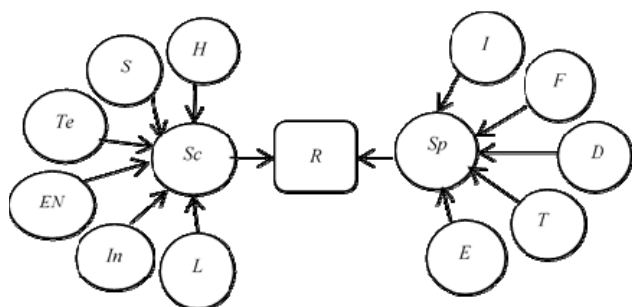


Figure 1 – Information model of the influence of factors on the DMP

Here  $S_c=f(H,S,Te,EN,In,L)$  is a function that characterizes the influence of external and production factors;  $S_p=f(I,F,D,T,E)$  is a function that characterizes the influence of psychological and cognitive factors on the state of

decision makers, and  $R=f(H,S,Te,EN,In,L,F,D,T,E)$  is a function that characterizes the degree of relevance of decisions made by decision makers.

Exploring and revealing causal relationships and dependencies between the factors of the information model allows building the following relational model, Fig. 2.

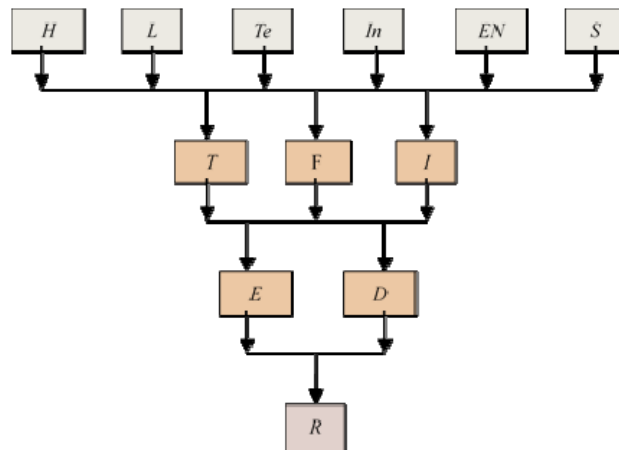


Figure 2 – Relational model of mutual influence of factors on the MRD

In [21] Bayesian Belief Networks are used as a mathematical tool, which have shown themselves well in modeling complex systems with uncertainties.

BBN is a probabilistic graphical model, which is a set of random variables and their conditional probabilities using an acyclic directed graph.

For any set of random variables (vertices)  $A_1, A_2, \dots, A_n$  of a Bayesian belief network, the probability of joint distribution is calculated from conditional probabilities according to the chain rule as follows:

$$P(A_1, \dots, A_n) = \prod_{i=1}^n P(A_i | Parents(A_i)) \quad (1)$$

To calculate the probability that a variable  $B$  takes on the value  $b_j$  on a BBN consisting of vertices  $B, A_1, \dots, A_n$  the formula is used:

$$P(B = b_j) = \sum_{A_1, \dots, A_n} P(B = b_j, A_1, A_2, \dots, A_n). \quad (2)$$

Here the summation is over all values of the variables  $A_1, A_2, \dots, A_n$ . Taking into account (1), formula (2) for calculating the probability at the vertex  $B$  takes the form:

$$P(B = b_j) = \sum_{A_1, \dots, A_n} P(B = b_j | Parents(B)) \times \prod_{i=1}^n P(A_i | Parents(A_i)) \quad (3)$$

These formulas are enough to perform direct inference on a Bayesian network, i.e. determining the probability of the values of the vertex-leaf by the known probabilities of the values of the input (root) vertices and the conditional probabilities of the values of the remaining vertices of the BBN.

Based on the relational model of the mutual influence of factors on the adoption of appropriate decisions, a Bayesian trust network is built (Fig. 3) to assess the MRD.

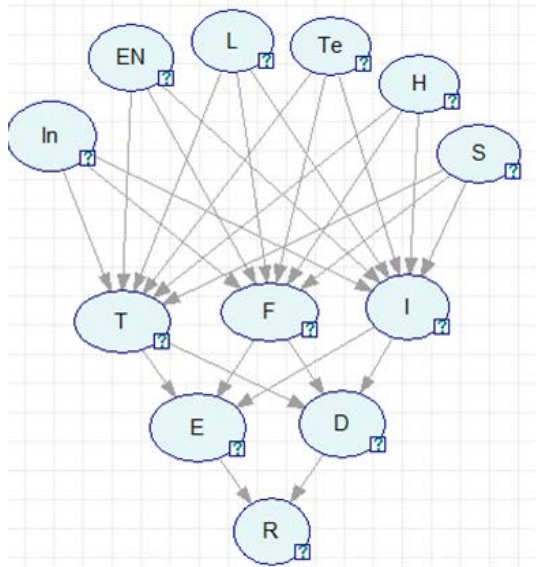


Figure 3 – BBN for a MRD Evaluation

The vertices of the BBN (Fig. 3) have the same names as the vertices of the relational model (Fig. 2). All vertices of the proposed BBN, with the exception of vertex R, take on two values:  $\langle \text{vertex name} \rangle_1$  = “within normal limits”.  $\langle \text{vertex name} \rangle_2$  = “out of normal limits”. For example, if the vertex *In* takes the value  $in_1$ , then it means, that the intensity and level of noise are within the normal range. If the vertex *In* takes the value  $in_2$ , then it means, that the intensity and level of noise are outside the norm. Vertex *R* takes values  $r_1$  = “irrelevant”.  $r_2$  = “relevant”.

Since the values of the unconditional probabilities of the root vertices *In*, *EN*, *L*, *Te*, *H*, *S* and conditional probabilities of vertices *T*, *F*, *I*, *E*, *D*, *R* established on the basis of the results of an expert survey, they are defined vaguely. Therefore, fuzziness is introduced into the Bayesian network (Fig. 3) by replacing the probabilities of states with fuzzy numbers, and ordinary arithmetic operations on real numbers with extended operations on fuzzy numbers [22].

All unconditional and conditional probabilities of the considered Bayesian network are estimated by fuzzy intervals  $\tilde{N}(n_1, n_2, n_3, n_4)$  defined on the universal set  $\{x | 0 \leq x \leq 1\}$ , where  $x$  is a probability of a vertex states. In this case, the membership function of these intervals is given by the formula (4):

$$\mu_L(x) = \begin{cases} 0, & x < 0, \\ \frac{x - n_1}{n_2 - n_1}, & n_1 \leq x \leq n_2, \\ 1, & n_2 \leq x \leq n_3, \\ \frac{n_4 - x}{n_4 - n_3}, & n_3 < x \leq n_4, \\ 0, & x > 1, \end{cases} \quad (4)$$

where  $n_1 \leq n_2 \leq n_3 \leq n_4$  are some real numbers, and  $0 \leq n_2 \leq n_3 \leq 1$ ;  $n_2, n_3$  are lower and upper modal values, respectively;  $n_2 - n_1, n_4 - n_3$  are left and right fuzziness coefficients of a fuzzy interval  $\tilde{N}(n_1, n_2, n_3, n_4)$ . In particular, if  $0 \leq n_1 \leq n_2 \leq n_3 \leq n_4 \leq 1$ , then the membership function (4) defines a trapezoidal fuzzy number.

Rules for addition and multiplication of fuzzy intervals  $\tilde{N}(n_1, n_2, n_3, n_4)$  and  $\tilde{P}(p_1, p_2, p_3, p_4)$ , determined by the membership functions (4), when using the principle of generalization to arithmetic operations take the form (5).

$$\begin{aligned} \tilde{N}(n_1, n_2, n_3, n_4) \oplus \tilde{P}(p_1, p_2, p_3, p_4) &= \\ = \tilde{S}(n_1 + p_1, n_2 + p_2, n_3 + p_3, n_4 + p_4), \\ \tilde{N}(n_1, n_2, n_3, n_4) \otimes \tilde{P}(p_1, p_2, p_3, p_4) &= \\ = \tilde{H}(n_2 p_2 - \alpha, n_2 p_2, n_3 p_3, n_3 p_3 + \beta), \\ \alpha &= n_2(p_2 - p_1) + p_2(n_2 - n_1), \\ \beta &= n_3(p_4 - p_3) + p_3(n_4 - n_3). \end{aligned} \quad (5)$$

If it is necessary to compare fuzzy probabilities, it is considered that of the two fuzzy probabilities, the one whose defuzzified value of the membership function is greater is greater. As a defuzzification method, the center of maxima method is used, which consists in finding the arithmetic mean of the elements of the universal set that have the maximum degrees of membership. This method is for fuzzy numbers  $\tilde{N}(n_1, n_2, n_3, n_4)$  with membership function (4) gives:

$$N = \frac{\int_{n_2}^{n_3} x dx}{\int_{n_2}^{n_3} dx} = \frac{n_2 + n_3}{2}. \quad (6)$$

In (6)  $N$  is the result of defuzzification, the “exact” value of the fuzzy number.

When calculating fuzzy probability  $\tilde{P}_f$  at the vertices of the Bayesian network, formulas (1), (3) are transformed by replacing the probabilities of states with fuzzy numbers, and ordinary arithmetic operations on real numbers with extended operations on fuzzy numbers, into formulas for calculating the fuzzy joint probability distribution and fuzzy probability, respectively:

$$\tilde{P}_f(A_1, \dots, A_n) \cong \bigoplus_{i=1}^n \tilde{P}_f(A_i | Parents(A_i)). \quad (7)$$

$\bigotimes_{i=1}^n A_i$  denotes the product of fuzzy numbers

$$A_1, \dots, A_n, \text{ i.e. } \bigotimes_{i=1}^n A_i = A_1 \otimes A_2 \otimes \dots \otimes A_n.$$

$$\tilde{P}_f(B = b_j) \cong \bigoplus_{A_1, \dots, A_n} \tilde{P}_f(B = b_j | Parents(B)) \otimes \left[ \bigoplus_{i=1}^n \tilde{P}_f(A_i | Parents(A_i)) \right]. \quad (8)$$

Expression (7) is called the chain rule for the fuzzy joint probability distribution. Formula (8) makes it possible to calculate the fuzzy probability at the vertex  $B$ , which takes the value  $b_j$ , on the BBN, which consists of vertices  $B, A_1, \dots, A_n$ .

It should be noted that for ease of determining conditional probabilities by experts, it is considered that the conditional probability at any vertex depends on the values of the parent vertices individually, and not on the joint distribution of the values of these vertices. Then, if among the vertices  $A_1, \dots, A_n$  only the vertex  $A_1$  has parent peaks and these peaks are peaks  $A_2, A_3, \dots, A_n$ , then the last assumption allows rewrite formula (7) as:

$$\tilde{P}_f(A_1, \dots, A_n) \cong \bigotimes_{i=2}^n \tilde{P}_f(A_i) \bigotimes_{j=2}^n \tilde{P}_f(A_1 | A_j) \quad (9)$$

In the following, a simplified Bayesian network will be considered as an example (Fig. 4).

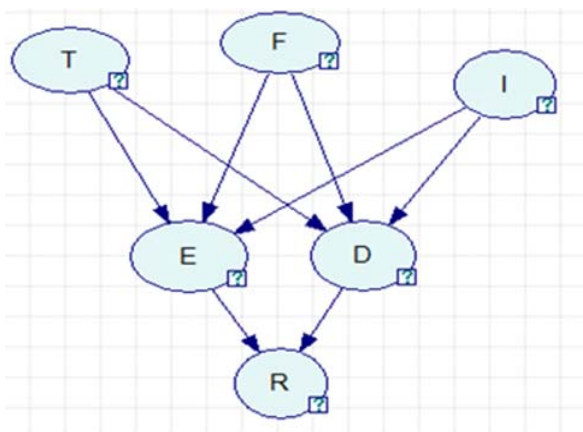


Figure 4 – Fragment of fuzzy BBN

The procedure for calculating the probability values for this Bayesian network includes the following steps. At the first stage, using (7)–(9), the fuzzy total probabilities

of the vertices  $E, D$ , which have 3 parent vertices  $T, F, I$  are calculated:

$$\begin{aligned} \tilde{P}_f(E = e_2) &\cong \bigoplus_{T, F, I} \tilde{P}_f(e_2 | T, F, I) = \\ &= \bigoplus_{T, F, I} \tilde{P}_f(T) \otimes \tilde{P}_f(F) \otimes \tilde{P}_f(I) \otimes \tilde{P}_f(e_2 | T, F, I) = \\ &= \bigoplus_{T, F, I} \tilde{P}_f(T) \otimes \tilde{P}_f(F) \otimes \tilde{P}_f(I) \otimes \tilde{P}_f(e_2 | T) \otimes \\ &\otimes \tilde{P}_f(e_2 | F) \otimes \tilde{P}_f(e_2 | I). \end{aligned} \quad (10)$$

$$\begin{aligned} \tilde{P}_f(D = d_2) &\cong \bigoplus_{T, F, I} \tilde{P}_f(d_2 | T, F, I) = \\ &= \bigoplus_{T, F, I} \tilde{P}_f(T) \otimes \tilde{P}_f(F) \otimes \tilde{P}_f(I) \otimes \tilde{P}_f(d_2 | T, F, I) = \\ &= \bigoplus_{T, F, I} \tilde{P}_f(T) \otimes \tilde{P}_f(F) \otimes \tilde{P}_f(I) \otimes \tilde{P}_f(d_2 | T) \otimes \\ &\otimes \tilde{P}_f(d_2 | F) \otimes \tilde{P}_f(d_2 | I). \end{aligned} \quad (11)$$

According to formulas (10–12) in the MATLAB environment, the values of the fuzzy probability of the nodes of the network under consideration were calculated. Then, using formula (7), the defuzzification values of these probabilities were calculated. Based on the defuzzification value of the probability  $P(R = r_2)$ , a conclusion was made about the degree of relevance of the decision made by the decision maker.

At the second stage, with (7)–(9) the fuzzy total probabilities of the leaf-vertex are calculated:

$$\begin{aligned} \tilde{P}_f(R = r_2) &\cong \bigoplus_{T, F, I, E, D} \tilde{P}_f(r_2 | T, F, I, E, D) = \\ &= \bigoplus_{T, F, I, F, D} \tilde{P}_f(T) \otimes \tilde{P}_f(F) \otimes \tilde{P}_f(I) \otimes \tilde{P}_f(E | T, F, I) \otimes \\ &\tilde{P}_f(D | T, F, I) \otimes \tilde{P}_f(r_2 | E, D) = \\ &= \bigoplus_{T, F, I, E, D} \tilde{P}_f(T) \otimes \tilde{P}_f(F) \otimes \tilde{P}_f(I) \otimes \tilde{P}_f(E | T) \otimes \\ &\otimes \tilde{P}_f(E | F) \otimes \tilde{P}_f(E | I) \otimes \tilde{P}_f(D | T) \otimes \tilde{P}_f(D | F) \otimes \\ &\otimes \tilde{P}_f(D | I) \otimes \tilde{P}_f(r_2 | E) \otimes \tilde{P}_f(r_2 | D). \end{aligned} \quad (12)$$

#### 4 EXPERIMENTS

To test the proposed model, numerical experiments were carried out, the essence of which was as follows.

Specialist experts were asked to evaluate the unconditional and conditional probabilities of the possible states of the factors influencing the decision maker for the process of making relevant decisions. The results are presented as fuzzy values of unconditional  $\tilde{P}_f(T), \tilde{P}_f(F), \tilde{P}_f(I)$  and conditional probabilities in Tables 1–3.

### 5 RESULTS

Numerical experiments were carried out for two characteristic cases. In the first case, the probability values that the decision maker is in a state of significant fatigue (factor  $T$ ) or significant psychological tension (factor  $F$ ) were taken low, and the susceptibility of the decision maker to informational stress was considered unlikely. In the second case, the probability value that the decision maker is in a state of significant fatigue (factor  $T$ ) was considered high. The results of numerical calculations are given in Table 2 and Table 3.

Table 2 shows that in the first case, the probability of implementing the relevant decision of the DM is equal to  $P(R = r_2) = 0.78$ .

In accordance with the results of research in the literature and normative sources, for many human-machine systems of critical application, at a probability value  $P(R = r_2) \geq 0.7$ , the decision taken is considered relevant.

In the second case, as can be seen from Table 3, the probability of making a relevant decision is  $P(R = r_2) = 0.56$ , which is less than 0.7. Therefore, in this case, it cannot be considered that the decision made by the decision maker is relevant.

Table 1 – The result of evaluating fuzzy conditional probabilities at nodes  $E, D, R$

	Fuzzy probability value		Fuzzy probability value	
	Vertex $E$		Vertex $D$	
$T$	$\tilde{P}_f(E = e_1   T)$	$\tilde{P}_f(E = e_2   T)$	$\tilde{P}_f(D = d_1   T)$	$\tilde{P}_f(D = d_2   T)$
$t_1$	(0.7; 0.8; 0.9; 1.0)	(0.0; 0.1; 0.2; 0.3)	(0.3; 0.4; 0.4; 0.5)	(0.5; 0.6; 0.6; 0.7)
$t_2$	(0.0; 0.0; 0.0; 0.0)	(1.0; 1.0; 1.0; 1.0)	(0.0; 0.0; 0.0; 0.0)	(1.0; 1.0; 1.0; 1.0)
$F$	$\tilde{P}_f(E = e_1   F)$	$\tilde{P}_f(E = e_2   F)$	$\tilde{P}_f(D = d_1   F)$	$\tilde{P}_f(D = d_2   F)$
$f_1$	(0.4; 0.5; 0.6; 0.7)	(0.3; 0.4; 0.5; 0.6)	(0.1; 0.2; 0.3; 0.4)	(0.6; 0.7; 0.8; 0.9)
$f_2$	(0.0; 0.0; 0.0; 0.0)	(1.0; 1.0; 1.0; 1.0)	(0.0; 0.0; 0.0; 0.0)	(1.0; 1.0; 1.0; 1.0)
$I$	$\tilde{P}_f(E = e_1   I)$	$\tilde{P}_f(E = e_2   I)$	$\tilde{P}_f(D = d_1   I)$	$\tilde{P}_f(D = d_2   I)$
$i_1$	(0.1; 0.2; 0.3; 0.4)	(0.6; 0.7; 0.8; 0.9)	(0.0; 0.1; 0.2; 0.3)	(0.7; 0.8; 0.9; 1.0)
$i_2$	(0.0; 0.0; 0.0; 0.0)	(1.0; 1.0; 1.0; 1.0)	(0.0; 0.0; 0.0; 0.0)	(1.0; 1.0; 1.0; 1.0)
	Vertex $R$			
$E$	$\tilde{P}_f(R = r_1   E)$		$\tilde{P}_f(R = r_2   E)$	
$e_1$	(0.4; 0.5; 0.6; 0.7)		(0.3; 0.4; 0.5; 0.6)	
$e_2$	(0.0; 0.0; 0.0; 0.0)		(1.0; 1.0; 1.0; 1.0)	
$D$	$\tilde{P}_f(R = r_1   D)$		$\tilde{P}_f(R = r_2   D)$	
$d_1$	(0.2; 0.3; 0.4; 0.5)		(0.5; 0.6; 0.7; 0.8)	
$d_2$	(0.0; 0.0; 0.0; 0.0)		(1.0; 1.0; 1.0; 1.0)	

Table 2 – The results of calculating the probabilities in the nodes of the fuzzy BBN in the first case

Values of the BBN vertices	Fuzzy probability value	Defuzzification result	Values of the BBN vertices	Fuzzy probability value	Defuzzification result
$T$			$F$		
	$\tilde{P}_f(T)$	$P(T)$		$\tilde{P}_f(F)$	$P(F)$
$t_1$	(0.1; 0.2; 0.2; 0.3)	0.2	$f_1$	(0.2; 0.3; 0.3; 0.5)	0.3
$t_2$	(0.7; 0.8; 0.8; 0.9)	0.8	$f_2$	(0.5; 0.7; 0.7; 0.8)	0.7
$I$			$E$		
	$\tilde{P}_f(I)$	$P(I)$		$\tilde{P}_f(E)$	$P(E)$
$i_1$	(0.0; 0.1; 0.1; 0.3)	0.1	$e_1$	(-0.2; 0.3; 0.35; 0.85)	0.32
$i_2$	(0.7; 0.9; 0.9; 1.0)	0.9	$e_2$	(0.15; 0.65; 0.7; 1.2)	0.68
$D$			$R$		
	$\tilde{P}_f(D)$	$P(D)$		$\tilde{P}_f(R)$	$P(R)$
$d_1$	(-0.54; 0.14; 0.18; 0.85)	0.16	$r_1$	(-1.65; 0.14; 0.3; 1.81)	0.22
$d_2$	(0.15; 0.82; 0.86; 1.54)	0.84	$r_2$	(-0.81; 0.7; 0.86; 2.65)	0.78

Table 3 – The results of calculating the probabilities in the nodes of the fuzzy BS in the second case

Values of the BBN vertices	Fuzzy probability value	Defuzzification result	Values of the BBN vertices	Fuzzy probability value	Defuzzification result
<i>T</i>			<i>F</i>		
	$\tilde{P}_f(T)$	$P(T)$		$\tilde{P}_f(F)$	$P(F)$
$t_1$	(0.5; 0.7; 0.7; 0.8)	0.7	$f_1$	(0.2; 0.3; 0.3; 0.5)	0.3
$t_2$	(0.2; 0.3; 0.3; 0.5)	0.3	$f_2$	(0.5; 0.7; 0.7; 0.8)	0.7
<i>I</i>			<i>E</i>		
	$\tilde{P}_f(I)$	$P(I)$		$\tilde{P}_f(E)$	$P(E)$
$i_1$	(0.0; 0.1; 0.1; 0.3)	0.1	$e_1$	(0.19; 0.63; 0.71; 1.04)	0.67
$i_2$	(0.7; 0.9; 0.9; 1.0)	0.9	$e_2$	(-0.04; 0.29; 0.37; 0.81)	0.33
<i>D</i>			<i>R</i>		
	$\tilde{P}_f(D)$	$P(D)$		$\tilde{P}_f(R)$	$P(R)$
$d_1$	(-0.38; 0.33; 0.36; 1.02)	0.34	$r_1$	(-1.16; 0.34; 0.54; 1.63)	0.44
$d_2$	(-0.02; 0.64; 0.67; 1.38)	0.66	$r_2$	(-0.63; 0.46; 0.66; 2.16)	0.56

## 6 DISCUSSION

The obtained results of numerical experiments are in good agreement with practical decision-making situations in critical systems. In the first case, the negative impact of cognitive factors on decision makers was low. Therefore, the decision maker made the relevant decision with sufficient probability. At the same time, it was not required to adjust the degree of negative impact of factors affecting the decision maker. In the second case, the negative impact of one of the cognitive factors became high. This led to the fact that the decision taken by the decision maker cannot be considered relevant. In this case, it is necessary to correct the degree of negative impact on the decision maker of the corresponding factor in accordance with engineering and psychological recommendations and requirements.

Thus, the results of the experiments make it possible to recommend the use of the developed model, which takes into account the mutual influence of factors of various nature on the decision-making process of the decision maker, to improve the efficiency of the management of the HMSCA as a whole.

## CONCLUSIONS

The actual scientific and applied problem of assessing the influence of factors of various nature, including cognitive ones, on the decision-making process of the decision maker to improve the efficiency of the management of the HMSCA as a whole has been solved.

**The scientific novelty** of the results obtained lies in the fact that for the first time:

- fuzzy hierarchical relational cognitive models are proposed that allow assessing the impact of qualitative and quantitative factors of various nature, including cognitive ones, on the decision-making process of decision makers;

- to assess the influence of fuzzy factors on the relevance of decision-making, a fuzzy BBN is proposed and an algorithm for calculating the fuzzy probabilities of its nodes is developed.

**The practical significance** of the results obtained lies in the fact that the proposed fuzzy hierarchical relational cognitive models can be recommended for assessing the influence of environmental factors and cognitive parameters of decision makers on the decision-making process in human-machine systems of critical application.

**Prospects for further research** are to develop of tools and methods for modeling and regulating the process of making relevant decisions in real time and uncertainty to improve the efficiency of functioning of human-machine systems of critical application.

## ACKNOWLEDGEMENTS

The work was carried out with the collaborative assistance of the Department of Applied Information Systems, Taras Shevchenko National University of Kyiv, Department of Information Technologies, Mykolaiv National Agrarian University, Department of Information Technologies, V. O. Sukhomlynsky Mykolaiv National University of the research topic “Intelligent search and Internet data processing” (registration number 0121U109370).

## REFERENCES

- Alvarenga M., Frutuoso P. A review of the cognitive basis for human reliability analysis, *Progress in Nuclear Energy*, 2019, Vol. 117(103050). DOI: 10.1016/j.pnucene.2019.103050
- Deo N. Graph theory with applications to engineering and computer science. Courier Dover Publications, 2017, 496 p.
- Gigerenzer G. Simply rational: Decision making in the real world. Evolution and Cognition. New York, Oxford University, 2015, 328 p. DOI:10.1093/acprof:oso/9780199390076.001.0001
- Berdnik P. G., Kuchuk G. A., Kuchuk N. G., Obidin D. N., Pavlenko M. A., Petrov A. V., Rudenko V. N., Timochko O. I. Matematicheskie osnovy jergonomicheskikh issledovanij: monografija. Kropivnickij, KLA NAU, 2016, 248 p.
- Havlikova M., Jirgl M., Bradac Z. Human Reliability in Man-Machine Systems, *Procedia Engineering*, 2015, Vol. 100, pp. 1207–1214. DOI: 10.1016/j.proeng.2015.01.485
- Castillo E., Gutierrez J., Hadi A. Expert systems and probabilistic network models: project report (final): Castillo E. Springer Science & Business Media. New York, 2012, 597 p. DOI: 10.1007/978-1-4612-2270-5
- Perederyi V., Borchik Eu., Lytvynenko V., Ohnieva O. Information Technology for Performance Assessment of Complex

- Multilevel Systems in Managing Technogenic Objects problem, *CEUR Workshop Proceedings*, 2020, Vol. 2805, pp. 175–188.
8. Alvarenga M., Frutuoso A., Melo P. A Review of the Cognitive Basis for Human Reliability Analysis, *Progress in Nuclear Energy*, 2019, Vol. 117, 103050. DOI: 10.1016/j.pnucene.2019.103050
  9. Perederyi V., Borchik E., Ohnieva O. Information Technology for Decision Making Support and Monitoring in Man-Machine Systems for Managing Complex Technical Objects of Critical Application, *Advances in Intelligent Systems and Computing*, 2021, Vol. 1246, pp. 448–466. DOI: 10.1007/978-3-030-1246-3
  10. Romanjuk A. O., Tymochko O. I., Marchenko Ju. M. Development of indicators to assess the quality of activity models automated command points operators, *Military technical issues*, 2020, № 1(61), pp. 60–66. DOI: 10.30748/soivt.2020.61.07
  11. Perederyi V., Borchik E. Information technology for determination, assessment and correction of functional sustainability of the human-operator for the relevant decision-making in human-machine critical application systems, *Theoretical and practical aspects of the development of modern science: the experience of countries of Europe and prospects for Ukraine*. Riga, Latvia, "Baltija Publishing", 2019, pp. 490–509. DOI: 10.30525/978-9934-571-78-7\_57
  12. De Maio C., Fenza G., Loia V., Orciuoli F. Linguistic fuzzy consensus model for collaborative development of fuzzy cognitive maps: a case study in software development risks, *Fuzzy Optimization and Decision Making*, 2017, Vol. 16, Iss. 4, pp. 463–479. DOI: 10.1007/s10700-016-9259-3
  13. Chen Z., Lan Y., Zhao R. Impacts of risk attitude and outside option on compensation contracts under different information structures, *Fuzzy Optimization and Decision Making*, 2018, Vol. 17, Iss. 1, pp. 13–47. DOI: 10.1007/s10700-016-9263-7
  14. Lahno V. Information security of critical application data processing systems, *Commission of motorization and energetics in agriculture*, 2014, Vol. 14, № 1, pp. 134–143. DOI: 10.15587/1729-4061.2016.71769
  15. Sharko O., Marasanov V., Stepanchikov D. Technique of System Operator Determination Based on Acoustic Emission Method, *Lecture Notes in Computational Intelligence and Decision Making. Advances in Intelligent System of Computing*, 2020, Vol. 1246, pp. 3–22. DOI: 10.1007/978-3-030-54215-3
  16. Perederyi V., Voronenko M., Borchik E., Krejci J. Information technology of operative formation and evaluation of relevant alternatives of decision-making in human-machine systems of critical application, *CSIT-2018 Computer Science and Information Technology, XIII international scientific and technical conference, Lviv, 11–14 September 2018: proceedings*. Los Alamitos, IEEE, 2018, pp. 33–36. DOI: 10.1109/STC-CSIT.2018.8526750
  17. Zosimov V., Bulgakova O. Calculation the Measure of Expert Opinions Consistency Based on Social Profile Using Inductive Algorithms, *Advances in Intelligent Systems and Computing*, 2020, Vol. 1020, pp. 622–636. DOI: 10.1007/978-3-030-26474-1\_43
  18. Mygal G., Mygal V. Interdisciplinary approach to the human factor problem, *Municipal economy of cities*, 2020, Vol. 3, pp. 149–157. DOI: 10.33042/2522-1809-2020-3-156-149-157
  19. Castillo E., Gutierrez J. M., Hadi A. S. Expert systems and probabilistic network models, *Springer Science & Business Media*. New York, 2012. DOI: 10.1007/978-1-4612-2270-5
  20. Zosimov V., Bulgakova O. Web Data Displaying Approach Based on User's Semantic Profile Templates, *CSIT-2020 Computer Science and Information Technology, XX international scientific and technical conference, Lviv, proceedings*. Los Alamitos, IEEE, 2020, pp. 428–431. DOI: 10.1109/CSIT49958.2020.9321839
  21. Parasyuk I. N., Verevka O. V. Mathematical Foundations of Probabilistic Estimation in Fuzzy Bayesian Belief Networks, *Cybernetics and System Analysis*, 2016, Vol. 52, № 2, pp. 62–67. DOI: 10.1007/s10559-016-9816-3
  22. Halliwell J., Keppens J., Shen Q. Linguistic Bayesian networks for reasoning with subjective probabilities in forensic statistics, *AI and Law : 9th International Conference, Scotland United Kingdom, 24–28 June*. NY, 2003, pp. 42–50. DOI: 10.1145/1047788.1047795

Received 03.01.2024.  
Accepted 24.02.2024.

УДК 004.8:62–83

## ОЦІНКА ВПЛИВУ НЕЧІТКИХ ФАКТОРІВ НАВКОЛИШНЬОГО СЕРЕДОВИЩА НА ПРОЦЕС ПРИЙНЯТТЯ РІШЕНЬ В ЛЮДИНО-МАШИНИХ СИСТЕМАХ КРИТИЧНИХ ЗАСТОСУВАНЬ

**Передерій В. І.** – д-р техн. наук, професор кафедри інформаційних технологій, Миколаївського національного університету імені В.О. Сухомлинського, Миколаїв, Україна.

**Борчик С. Ю.** – канд. техн. наук, доцент кафедри інформаційних технологій Миколаївського національного аграрного університету, Миколаїв, Україна.

**Зосімов В. В.** – д-р техн. наук, професор кафедри прикладних інформаційних технологій Київського національного університету імені Тараса Шевченка, Київ, Україна.

**Булгакова О. С.** – канд. техн. наук, доцент кафедри прикладних інформаційних технологій Київського національного університету імені Тараса Шевченка, Київ, Україна.

### АНОТАЦІЯ

**Актуальність.** Особливість людино-машинних систем критичного застосування, що працюють в режимі реального часу, полягає в тому, що в якості елементів вони включають як технічні системи, так і людей, що взаємодіють з цими системами. При цьому основні труднощі пов'язані не тільки з удосконаленням апаратного і програмного забезпечення, але і з недостатньою розробленістю методів достовірного прогнозування впливу виробничого середовища на людський фактор і, як наслідок, на релевантність рішень, прийнятих особами, що приймають рішення. В результаті задача розробки способів визначення взаємного впливу факторів зовнішнього середовища і когнітивних параметрів ОІП, на процес прийняття рішень стає актуальною.

**Мета роботи** – методологічна основа розробки та дослідження нечітких ієрархічних реляційних когнітивних моделей для визначення впливу факторів навколишнього середовища та когнітивних параметрів осіб, що приймають рішення, на процес прийняття рішень.

**Метод.** При побудові нечітких ієрархічних реляційних когнітивних моделей використані методи «м'яких обчислень», методологія когнітивного і нечіткого когнітивного моделювання, які забезпечують прийнятну формалізацію невизначеності взаємного впливу факторів на процес прийняття рішень.

**Результати.** Розроблені нечіткі когнітивні моделі на основі нечітких байєсівських мереж довіри, які дозволяють провести зв'язок між якісними та кількісними оцінками факторів взаємного впливу на процес прийняття рішень особами, що приймають рішення. Запропоновані моделі мають можливість імовірнісного прогнозування впливу факторів і вибору раціональних способів їх взаємодії в процесі прийняття рішень.

**Висновки.** Результати експериментів дозволяють рекомендувати розроблені моделі, що враховують взаємний вплив факторів різної природи, в тому числі когнітивних, на процес прийняття рішень особами, що приймають рішення, та підвищують ефективність управління в людино-машинних системах критичного застосування в цілому.

**КЛЮЧОВІ СЛОВА:** людино-машинні системи критичного застосування, прийняття рішень, релевантні рішення, нечіткі когнітивні моделі, фактори навколишнього середовища, фактори робочого середовища, реляційні когнітивні моделі, особа що приймає рішення.

#### ЛІТЕРАТУРА

- Alvarenga M. A review of the cognitive basis for human reliability analysis/ M. Alvarenga, P. Frutuoso // *Progress in Nuclear Energy*. – 2019. – Vol. 117(103050). DOI: 10.1016/j.pnucene.2019.103050
- Deo N. Graph theory with applications to engineering and computer science / N. Deo. – Courier Dover Publications, 2017. – 496 p.
- Gigerenzer G. Simply rational: Decision making in the real world. Evolution and Cognition / G. Gigerenzer. – New York : Oxford University, 2015. – 328 p. DOI:10.1093/acprof:oso/9780199390076.001.0001
- Matematische osnovy jergonomicheskikh issledovanij: monografija / [P. G. Berdnik, G. A. Kuchuk, N. G. Kuchuk et al.]. – Kropivnickij : KLA NAU, 2016. – 248 p.
- Havlikova M. Human Reliability in Man-Machine Systems / M. Havlikova, M. Jirgl, Z. Bradac // *Procedia Engineering*. – 2015. – Vol. 100. – P. 1207–1214. DOI: 10.1016/j.proeng.2015.01.485
- Expert systems and probabilistic network models: project report (final): Castillo E. / E. Castillo, J. Gutierrez, A. Hadi / Springer Science & Business Media, New York. – 2012. – 597 p. DOI: 10.1007/978-1-4612-2270-5
- Information Technology for Performance Assessment of Complex Multilevel Systems in Managing Technogenic Objects problem / [V. Perederyi, Eu. Borchik, V. Lytvynenko, O. Ohnieva] // *CEUR Workshop Proceedings*. – 2020. – Vol. 2805, – P. 175–188.
- Alvarenga M. A Review of the Cognitive Basis for Human Reliability Analysis / M. Alvarenga, A. Frutuoso, P. Melo // *Progress in Nuclear Energy*. – 2019. – Vol. 117: 103050. DOI: 10.1016/j.pnucene.2019.103050
- Perederyi V. Information Technology for Decision Making Support and Monitoring in Man-Machine Systems for Managing Complex Technical Objects of Critical Application / V. Perederyi, Eu. Borchik, O. Ohnieva // *Advances in Intelligent Systems and Computing*. – 2021. – Vol. 1246. – P. 448–466. DOI: 10.1007/978-3/
- Romanjuk A. O. Development of indicators to assess the quality of activity models automated command points operators/ A. O. Romanjuk, O. I. Tymochko, Ju. M. Marchenko // *Military technical issues*. – 2020. – № 1(61). – P. 60–66. DOI: 10.30748/soivt.2020.61.07
- Perederyi V. Information technology for determination, assessment and correction of functional sustainability of the human-operator for the relevant decision-making in human-machine critical application systems / V. Perederyi, E. Borchik // *Theoretical and practical aspects of the development of modern science: the experience of countries of Europe and prospects for Ukraine*. – Riga, Latvia: "Baltija Publishing". – 2019. – P. 490–509. DOI: 10.30525/978-9934-571-78-7\_57
- Linguistic fuzzy consensus model for collaborative development of fuzzy cognitive maps: a case study in software development risks / [C. De Maio, G. Fenza, V. Loia, F. Orciuoli] // *Fuzzy Optimization and Decision Making*. – 2017. – Vol. 16, Iss. 4. – P. 463–479. DOI:10.1007/s10700-016-9259-3
- Chen Z. Impacts of risk attitude and outside option on compensation contracts under different information structures / Z. Chen, Y. Lan, R. Zhao // *Fuzzy Optimization and Decision Making*. – 2018. – Vol. 17, Iss. 1. – P. 13–47. DOI: 10.1007/s10700-016-9263-7
- Lahno V. Information security of critical application data processing systems /V. Lahno// *Commission of motorization and energetics in agriculture*. – 2014. – Vol. 14, № 1. – P. 134–143. DOI: 10.15587/1729-4061.2016.71769
- Sharko O. Technique of System Operator Determination Based on Acoustic Emission Method / O. Sharko, V. Marasanov, D. Stepanchikov // *Lecture Notes in Computational Intelligence and Decision Making, Advances in Intelligent System of Computing*. – 2020. – Vol. 1246. – P. 3–22. DOI: 10.1007/978-3-030-54215-3
- Information technology of operative formation and evaluation of relevant alternatives of decision-making in human-machine systems of critical application / [V. Perederyi, M. Voronenko, E. Borchik, J. Krejci] // *CSIT-2018 Computer Science and Information Technology : XIII international scientific and technical conference, Lviv, 11–14 September 2018: proceedings*. – Los Alamitos: IEEE, 2018. – P. 33–36. DOI: 10.1109/STC-CSIT.2018.8526750
- Zosimov V. Calculation the Measure of Expert Opinions Consistency Based on Social Profile Using Inductive Algorithms / V. Zosimov, O. Bulgakova // *Advances in Intelligent Systems and Computing*. – 2020. – Vol. 1020. – P. 622–636. DOI: 10.1007/978-3-030-26474-1\_43
- Mygal G. Interdisciplinary approach to the human factor problem / G. Mygal, V. Mygal // *Municipal economy of cities*. – 2020. – Vol. 3. – P. 149–157. DOI: 10.33042/2522-1809-2020-3-156-149-157
- Castillo E. Expert systems and probabilistic network models / E. Castillo, J. M. Gutierrez, A. S. Hadi // *Springer Science & Business Media, New York*. – 2012. DOI: 10.1007/978-1-4612-2270-5
- Zosimov V. Web Data Displaying Approach Based on User's Semantic Profile Templates / V. Zosimov, O. Bulgakova // *CSIT-2020 Computer Science and Information Technology: XX international scientific and technical conference, Lviv: proceedings*. – Los Alamitos : IEEE, 2020. – P. 428–431. DOI: 10.1109/CSIT49958.2020.9321839
- Parasyuk I.N. Mathematical Foundations of Probabilistic Estimation in Fuzzy Bayesian Belief Networks / I. N. Parasyuk, O. V. Verevka // *Cybernetics and System Analysis*. – 2016. – Vol. 52, № 2. – P. 62–67. DOI: 10.1007/s10559-016-9816-3
- Halliwel J. Linguistic Bayesian networks for reasoning with subjective probabilities in forensic statistics / J. Halliwel, J. Keppens, Q. Shen // *AI and Law : 9th International Conference, Scotland United Kingdom, 24–28 June*. – NY. – 2003. – P. 42–50. DOI: 10.1145/1047788.1047795

## A NONLINEAR REGRESSION MODEL FOR EARLY LOC ESTIMATION OF OPEN-SOURCE KOTLIN-BASED APPLICATIONS

**Prykhodko S. B.** – Dr. Sc., Professor, Head of the Department of Software for Automated Systems, Admiral Makarov National University of Shipbuilding, Mykolaiv, Ukraine.

**Prykhodko N. V.** – PhD, Associate Professor, Associate Professor of the Finance Department, Admiral Makarov National University of Shipbuilding, Mykolaiv, Ukraine.

**Koltsov A. V.** – Post-graduate student of the Department of Software for Automated Systems, Admiral Makarov National University of Shipbuilding, Mykolaiv, Ukraine.

### ABSTRACT

**Context.** The early lines of code (LOC) estimation in software projects holds significant importance, as it directly influences the prediction of development effort, covering a spectrum of different programming languages, and open-source Kotlin-based applications in particular. The object of the study is the process of early LOC estimation of open-source Kotlin-based apps. The subject of the study is the nonlinear regression models for early LOC estimation of open-source Kotlin-based apps.

**Objective.** The goal of the work is to build the nonlinear regression model with three predictors for early LOC estimation of open-source Kotlin-based apps based on the Box-Cox four-variate normalizing transformation to increase the confidence in early LOC estimation of these apps.

**Method.** For early LOC estimation in open-source Kotlin-based apps, the model, confidence, and prediction intervals of nonlinear regression were constructed using the Box-Cox four-variate normalizing transformation and specialized techniques. These techniques, relying on multiple nonlinear regression analyses incorporating multivariate normalizing transformations, account for the dependencies between variables in non-Gaussian data scenarios. As a result, this method tends to reduce the mean magnitude of relative error (MMRE) and narrow confidence and prediction intervals compared to models utilizing univariate normalizing transformations.

**Results.** An analysis has been carried out to compare the constructed model with nonlinear regression models employing decimal logarithm and Box-Cox univariate transformation.

**Conclusions.** The nonlinear regression model with three predictors for early LOC estimation of open-source Kotlin-based apps is constructed using the Box-Cox four-variate transformation. Compared to the other nonlinear regression models, this model demonstrates a larger multiple coefficient of determination, a smaller value of the MMRE, and narrower confidence and prediction intervals. The prospects for further research may include the application of other data sets to construct the nonlinear regression model for early LOC estimation of open-source Kotlin-based apps for other restrictions on predictors.

**KEYWORDS:** estimation, lines of code, open-source app, Kotlin, nonlinear regression model, Box-Cox transformation, class, weighted methods per class, depth of inheritance tree.

### ABBREVIATIONS

DIT is a depth of inheritance tree;  
KLOC is a thousand lines of code;  
LB is a lower bound;  
LCOM is a lack of cohesion of methods;  
LOC are lines of code;  
MMRE is a mean magnitude of relative error;  
MRE is a magnitude of relative error;  
PRED is a percentage of prediction;  
RFC is a response for class;  
SMD is a squared Mahalanobis distance;  
UB is an upper bound;  
WMC are weighted methods per class.

### NOMENCLATURE

$\hat{\mathbf{b}}$  is an estimator for a vector of linear regression equation parameters;  
 $\hat{b}_i$  is an estimator for the  $i$ -th parameter of linear regression equation;  
 $k$  is a number of predictors (independent variables);  
 $N$  is a number of data points;  
 $\mathbf{P}$  is a non-Gaussian random vector;  
 $R^2$  is a multiple coefficient of determination;

$\mathbf{S}_Z$  is a sample covariance matrix for normalized data;  
 $\text{SMD}_Z$  is a squared Mahalanobis distance for normalized data;  
 $\mathbf{T}$  is a Gaussian random vector;  
 $t_{\alpha/2, \nu}$  is a quantile of the student's  $t$ -distribution with  $\nu$  degrees of freedom and  $\alpha/2$  significance level;  
 $X_1$  is a number of classes;  
 $X_2$  is a WMC metric at the app level (a WMC mean value per class);  
 $X_3$  is a DIT metric at the app level (a DIT mean value per class);  
 $Y$  is an actual software size in KLOC;  
 $Z_j$  is a  $j$ -th Gaussian variable that is obtained by transforming the variable  $X_j$ ;  
 $Z_Y$  is a Gaussian variable that is obtained by transforming variable  $Y$ ;  
 $\bar{Z}_Y$  is a sample mean of the  $Z_Y$  values;  
 $\hat{Z}_Y$  is a prediction result by linear regression equation for normalized data;  
 $\alpha$  is a significance level;

$\beta_1$  is a multivariate skewness;  
 $\beta_2$  is a multivariate kurtosis;  
 $\varepsilon$  is a Gaussian random variable that defines residuals;  
 $\nu$  is a number of degrees of freedom;  
 $\sigma_\varepsilon$  is a standard deviation of  $\varepsilon$ ;  
 $\Psi$  is a vector of multivariate normalizing transformation.

## INTRODUCTION

As we know [1], Lines of Code (LOC) is the number of lines of code excluding comments. Early software size estimation, including LOC, is one of the project managers' significant problems in evaluating software development efforts using mathematical models like COCOMO II [2].

The multi-platform nature of Kotlin language simplifies the development of cross-platform apps, primarily mobile ones. That is why, Kotlin Multiplatform Mobile (KMM) already has a handful of successful apps on the market [3].

Despite a large number of currently existing methods and models for estimating the software size [4–9], research in this direction does not stop [10–15]. This is primarily due to the low accuracy of estimating the size of the software in the early stages of its development. One way to solve this problem is to develop appropriate models for estimating the size of the software developed in a specific programming language. Today some LOC estimation models based on the software metrics that can be measured from the class diagram are known [4, 6, 8, 10–12]. The above models are constructed for such languages as Java [4, 6, 10, 11], C++ [8], PHP [4, 6, 12], and Visual Basic [4, 6]. However, there are no models, both linear and nonlinear ones, for early LOC estimation of open-source Kotlin-based apps. This demands the construction of the models for early LOC estimation of open-source Kotlin-based apps.

**The object of study** is the process of early LOC estimation of open-source Kotlin-based apps.

**The subject of study** is the regression models for early LOC estimation of open-source Kotlin-based apps.

**The purpose of the work** is to increase confidence in early LOC estimation of open-source Kotlin-based apps.

## 1 PROBLEM STATEMENT

Suppose given the original sample as the four-dimensional non-Gaussian data set: actual software size in the thousand lines of code (KLOC)  $Y$ , the total number of classes  $X_1$ , the WMC metric at the app level  $X_2$ , the DIT metric at the app level  $X_3$  from  $N$  open-source Kotlin-based apps. Suppose that there are four-variate normalizing transformation of non-Gaussian random vector  $\mathbf{P} = \{Y, X_1, X_2, X_3\}^T$  to Gaussian random vector  $\mathbf{T} = \{Z_Y, Z_1, Z_2, Z_3\}^T$  is given by

$$\mathbf{T} = \Psi(\mathbf{P}) \quad (1)$$

and the inverse transformation for (1)

$$\mathbf{P} = \Psi^{-1}(\mathbf{T}). \quad (2)$$

It is required to build the nonlinear regression model in the form  $Y = Y(X_1, X_2, X_3, \varepsilon)$  based on the transformations (1) and (2).

## 2 REVIEW OF THE LITERATURE

In paper [6] the linear regression equations were proposed for LOC estimation of software of open-source PHP- and Java-based information systems. These equations are developed based on three metrics that can be gained from a conceptual data model derived from a class diagram: the total number of classes, the total number of relationships, and the average number of attributes per class. However, the application of linear regression models is grounded on four primary assumptions, one of which relates to the normality of the error distribution. Nevertheless, this assumption is applicable only in specific scenarios. Therefore, in paper [10], the nonlinear regression model was constructed using the same above metrics for LOC estimation of software of Java-based information systems. However, the size of software apps may depend on other metrics. That is why in [11] the nonlinear regression model was constructed for early LOC estimation of Java-based apps. This model depends on four factors (predictors), namely the total number of classes, the number of static methods, the LCOM metric, and the RFC metric. However, the size of open-source Kotlin-based apps may depend on other metrics too. This leads to the need to build the nonlinear regression model for early LOC estimation of open-source Kotlin-based apps.

Although machine learning methods are becoming increasingly popular for the estimation of various software metrics [13, 15–22], including software size [13, 15], methods and models based on regression analysis have not yet reached their full potential [12, 23–28]. We suggest using the nonlinear regression models for early LOC estimation of open-source Kotlin-based apps because, firstly, there are two random variables, both a dependent variable (response) and an error term (residuals), in a regression model, and, secondly, the error distribution is not Gaussian.

One should note, that employing a normalizing transformation is frequently an effective approach to construct nonlinear regression models for early LOC estimation of various software apps [10–12]. As commonly understood, transformations serve essentially four purposes, with two main aims: firstly, to attain an approximate normal distribution for the error term in linear regression with normalized data, and secondly, to modify the response and/or predictor variables to enhance the linear relationship strength between new variables (normalized variables) compared to the original relationship between dependent and independent variables.

Commonly utilized methods for constructing nonlinear regression models typically rely on univariate normalizing transformations, such as the decimal logarithm and the Box-Cox transformation. However, these techniques fail to consider the correlation between dependent and independent variables. As a result, using such univariate normalizing transformations in the construction of nonlinear regression models does not consistently ensure optimal normality and linear relationships between normalized variables [12]. This emphasizes the necessity of employing multivariate normalizing transformations. Thus, following the methodology outlined in [12], we employ the technique for constructing nonlinear regression models based on multivariate normalizing transformations and prediction intervals to develop a model with three predictors for early estimation of lines of code (LOC) in open-source Kotlin-based applications. In this approach, prediction intervals from nonlinear regression models are applied to identify outliers during model construction. We detect the outliers due to residuals according to [29]. Typically, this procedure is iterative as we rebuild the model for new data after outlier removal. If there are no outliers, the process of constructing the model ends.

### 3 MATERIALS AND METHODS

The technique to build nonlinear regression models based on multivariate normalizing transformations and prediction intervals is comprised of six steps. The first step involves normalizing multivariate non-Gaussian data through a dedicated transformation (1). To do this, as in [12], we use the four-variate Box-Cox transformation with components

$$Z_j = x(\lambda_j) = \begin{cases} (X_j^{\lambda_j} - 1) / \lambda_j, & \text{if } \lambda_j \neq 0; \\ \ln(X_j), & \text{if } \lambda_j = 0. \end{cases} \quad (3)$$

Here  $Z_j$  is a Gaussian variable;  $\lambda_j$  is a parameter of the Box-Cox transformation,  $j = 1, 2, 3$ . The variable  $Z_Y$  is defined analogously (3) with the only difference that instead of  $Z_j$ ,  $X_j$ , and  $\lambda_j$  should be put respectively  $Z_Y$ ,  $Y$ , and  $\lambda_Y$ .

In the second step, we determine whether one multidimensional data point of a multivariate non-Gaussian data set is a multidimensional outlier. If there is a multidimensional outlier in a multivariate non-Gaussian data set then we discard the one and go to step 1, else continue.

To determine whether one data point of a multivariate non-Gaussian data set is a multidimensional outlier, we apply the statistical technique based on the normalizing transformations and the squared Mahalanobis distance (SMD) as in [12].

In the third step, we build the linear regression model for normalized data in the form

$$Z_Y = \hat{Z}_Y + \varepsilon = \hat{b}_0 + \hat{b}_1 Z_1 + \hat{b}_2 Z_2 + \hat{b}_3 Z_3 + \varepsilon, \quad (4)$$

$\varepsilon$  is a Gaussian random variable that defines residuals,  $\varepsilon \sim N(0, \sigma_\varepsilon^2)$ .

In the fourth step, we test the normality of the distribution of residuals in the linear regression model for normalized data. If the distribution of the residuals in the linear regression model for the normalized data is not Gaussian, then we discard the multivariate data point for which the modulus of the residual in the model is the maximum and go to step 1 otherwise continue.

The nonlinear regression model using the transformation (1) and (2) for the linear regression model for normalized data as in [12] is constructed in the fifth step

$$Y = \Psi_Y^{-1}(\hat{Z}_Y + \varepsilon). \quad (5)$$

For the four-variate Box-Cox transformation with components (3), the model has the form [12]

$$Y = [\hat{\lambda}_Y (\hat{Z}_Y + \varepsilon) + 1]^{1/\hat{\lambda}_Y}, \quad (6)$$

where  $\varepsilon$  is a Gaussian random variable,  $\varepsilon \sim N(0, \sigma_\varepsilon^2)$ , with the estimate  $\hat{\sigma}_\varepsilon$ ;  $\hat{Z}_Y$  is a prediction result by the linear regression equation  $\hat{Z}_Y = \hat{b}_0 + \hat{b}_1 Z_1 + \hat{b}_2 Z_2 + \hat{b}_3 Z_3$  for normalized data, which are transformed by the four-variate Box-Cox transformation with components (3).

Finally, in the sixth step, we build the prediction interval of nonlinear regression and determine whether one or more values of the response (dependent random variable) are outliers (its values are outside the prediction interval). If there are outliers in the data for the nonlinear regression model then we discard these and go to step 1, otherwise we complete constructing the nonlinear regression model.

We define the prediction interval of nonlinear regression as in [12]

$$\Psi_Y^{-1} \left( \hat{Z}_Y \pm t_{\alpha/2, v} S_{Z_Y} \left\{ 1 + \frac{1}{N} + (\mathbf{z}_X^+)^T \mathbf{S}_Z^{-1} (\mathbf{z}_X^+) \right\}^{1/2} \right), \quad (7)$$

where  $t_{\alpha/2, v}$  is a student's  $t$ -distribution quantile with  $\alpha/2$  significance level and  $v$  degrees of freedom;  $v = N - k - 1$ ;  $k$  is the number of independent variables (in our case,  $k$  is 3);  $\mathbf{z}_X^+$  is a vector with components  $Z_{1_i} - \bar{Z}_1, Z_{2_i} - \bar{Z}_2, \dots, Z_{k_i} - \bar{Z}_k$  for  $i$ -row;  $\bar{Z}_j = \frac{1}{N} \sum_{i=1}^N Z_{j_i}$ ,  $j = 1, 2, \dots, k$ ;  $S_{Z_Y}^2 = \frac{1}{v} \sum_{i=1}^N (Z_{Y_i} - \hat{Z}_{Y_i})^2$ ,  $v = N - k - 1$ ;  $\mathbf{S}_Z$  is a  $k \times k$  matrix

$$S_Z = \begin{pmatrix} S_{Z_1Z_1} & S_{Z_1Z_2} & \dots & S_{Z_1Z_k} \\ S_{Z_1Z_2} & S_{Z_2Z_2} & \dots & S_{Z_2Z_k} \\ \dots & \dots & \dots & \dots \\ S_{Z_1Z_k} & S_{Z_2Z_k} & \dots & S_{Z_kZ_k} \end{pmatrix}. \quad (8)$$

In (8)  $S_{Z_qZ_r} = \sum_{i=1}^N [Z_{q_i} - \bar{Z}_q][Z_{r_i} - \bar{Z}_r]$ ,  $q, r = 1, 2, \dots, k$ .

We constructed a nonlinear regression model for early LOC estimation of open-source Kotlin-based apps by the above technique from 54 apps hosted on GitHub (<https://github.com>). We acquired the dataset utilizing the CodeMR tool [30], focusing on the following variables: the actual software size measured in thousand lines of code (KLOC)  $Y$ , the total number of classes  $X_1$ , the WMC metric at the application level  $X_2$ , and the DIT metric at the same level  $X_3$ . Table 1 contains that data set. We chose the above predictors  $X_1$ ,  $X_2$ , and  $X_3$  for two reasons. Firstly, these predictors can be obtained from the class diagram, and, secondly, there is no multicollinearity between these predictors since variance inflation factors for predictors  $X_1$ ,  $X_2$ , and  $X_3$  are equal to 1.06, 1.46, and 1.40, respectively.

We checked the four-dimensional data from Table 1 for multivariate outliers. Before analyzing the four-dimensional data from Table 1 for multivariate outliers, we assessed the normality of the multivariate data in Table 1. This preliminary check was essential, as common statistical methods, including multivariate outlier detection based on the squared Mahalanobis distance (SMD), are designed to identify outliers assuming a Gaussian distribution. We applied a multivariate normality test proposed by Mardia and based on measures of the multivariate skewness  $\beta_1$  and kurtosis  $\beta_2$  [31]. According to this test, the distribution of four-dimensional data from Table 1 is not Gaussian since the test statistic for multivariate skewness  $N\beta_1/6$  of this data exceeds 40.00, that is the quantile of the Chi-Square distribution, applicable for 20 degrees of freedom and a for significance level of 0.005.

Similarly, the test statistic for multivariate kurtosis  $\beta_2$ , which equals 66.74, is greater than the value of the Gaussian distribution quantile, which is 28.86 for 24 mean, 3.56 variance, and 0.005 significance level. Because, as in [17], to detect multivariate outliers in the four-dimensional non-Gaussian data from Table I, we used the statistical technique based on the multivariate normalizing transformations and the SMD for normalized data. To normalize the data from Table 1, the four-variate Box-Cox transformation with components (3) was applied. The parameter estimates of the four-variate Box-Cox transformation for the data from Table 1 are calculated by the maximum likelihood method and are

$$\hat{\lambda}_Y = -0.137228, \quad \hat{\lambda}_1 = -0.138740, \quad \hat{\lambda}_2 = -0.220743, \quad \hat{\lambda}_3 = -1.067093.$$

There are two multivariate outliers in four-dimensional non-Gaussian data in Table 1 since the  $SMD_Z$  values for rows 35 and 47 exceed 14.86, which is the quantile of the Chi-Square distribution, applicable for a significance level of 0.005. In Table 1, rows that should be considered outliers are highlighted in bold. There are two iterations in step 1, Next, we go to step 1 of the third iteration.

In step 1 of the third iteration, we discard the outliers (rows 35 and 47) and normalize 52 rows of data from Table 1 (without rows 35 and 47). In this case, the parameter estimates of the four-variate Box-Cox transformation for the data from Table 1 (without rows 35 and 47) are calculated by the maximum likelihood method and are  $\hat{\lambda}_Y = -0.136019$ ,  $\hat{\lambda}_1 = -0.156183$ ,  $\hat{\lambda}_2 = -0.210099$ ,  $\hat{\lambda}_3 = -1.294445$ .

Table 1 – The data set

No	Y	X <sub>1</sub>	X <sub>2</sub>	X <sub>3</sub>	No	Y	X <sub>1</sub>	X <sub>2</sub>	X <sub>3</sub>
1	1.682	73	5.37	0.959	28	4.111	157	5.82	1.408
2	1.256	55	3.56	1.473	29	12.248	331	6.12	0.894
3	14.867	546	5.40	0.987	30	0.829	31	5.71	0.871
4	23.149	1033	4.60	3.206	31	22.069	623	7.76	0.681
5	28.699	1090	5.33	1.156	32	2.179	92	5.78	1.424
6	8.303	266	7.25	1.711	33	11.800	199	11.82	1.472
7	5.508	122	9.66	1.648	34	1.425	77	4.10	1.429
8	22.078	1292	4.71	0.971	<b>35</b>	<b>2.220</b>	<b>221</b>	<b>3.67</b>	<b>0.561</b>
9	2.010	47	7.68	0.851	36	1.872	101	4.25	1.198
10	11.629	425	4.95	1.416	37	2.097	91	3.64	0.934
11	1.728	69	6.22	1.116	38	5.639	313	3.82	1.125
12	1.538	102	2.17	0.873	39	1.933	80	6.25	1.125
13	38.101	1151	6.85	0.929	40	17.575	776	4.30	0.932
14	7.655	290	5.90	1.062	41	5.437	167	7.59	1.192
15	4.975	354	3.91	0.833	42	2.357	83	3.59	1.145
16	24.324	701	4.48	1.126	43	0.762	24	6.71	1.000
17	1.031	19	26.53	1.053	44	1.201	37	8.00	0.865
18	9.971	150	13.02	0.773	45	1.591	42	14.36	1.095
19	12.001	346	6.17	1.121	46	4.682	212	4.46	1.236
20	1.804	41	11.98	1.049	<b>47</b>	<b>6.341</b>	<b>55</b>	<b>30.80</b>	<b>6.073</b>
21	0.614	23	6.48	0.826	48	5.865	207	9.44	1.048
22	1.704	59	7.51	1.000	49	5.443	179	5.44	0.849
23	16.979	927	3.59	1.027	50	2.441	136	3.71	0.794
24	25.845	405	8.92	1.254	51	4.672	66	13.58	0.879
25	3.116	123	4.42	1.016	52	1.727	74	3.41	1.838
26	9.494	254	12.48	1.496	53	28.267	595	13.54	1.183
27	8.599	237	7.32	2.325	54	0.861	44	4.75	0.773

There are no multivariate outliers among 52 rows of data from Table 1 (without rows 35 and 47) since their  $SMD_Z$  values do not exceed 14.86, which is the quantile of the Chi-Square distribution, applicable for a significance level of 0.005. That is why we go to the third step.

In the third step, we build the linear regression model (4) for 52 rows of normalized data from Table 1 (without rows 35 and 47). The estimates  $\hat{b}_0$ ,  $\hat{b}_1$ ,  $\hat{b}_2$ , and  $\hat{b}_3$  equal  $-6.2999$ ,  $1.8251$ ,  $0.86530$ , and  $0.003968$ , respectively. The estimate  $\hat{\sigma}_\varepsilon$  of a standard deviation of  $\varepsilon$  is 0.1548.

In the fourth step, we test the normality of the distribution of residuals in the linear regression model (4) for 52 rows of normalized data from Table 1 (without rows 35 and 47). To achieve this, we employ the Pearson Chi-Squared test. We accepted the null hypothesis  $H_0$ , affirming that the observed frequency distribution of the  $\varepsilon$  values in (4) closely resembles the normal distribution (indicating no significant difference between the distributions). This decision was reached because the test  $\chi^2$  statistic, measuring 6.98 does not exceed 9.49, that is the quantile of the Chi-Square distribution, applicable for 4 degrees of freedom and a significance level of 0.05. Therefore, we go to step 5.

In the fifth step, the nonlinear regression model (6) was constructed. Then, in the sixth step, the prediction interval of nonlinear regression by (7) was built and it was determined whether one or more values of the response (dependent random variable) were outliers.

In this case, the inverse matrix of (8) is

$$\mathbf{S}_Z^{-1} = \begin{pmatrix} 0.0807 & 0.0278 & -0.0316 \\ 0.0278 & 0.2101 & -0.0138 \\ -0.0316 & -0.0138 & 0.4056 \end{pmatrix}.$$

The values of averages (sample means)  $\bar{Z}_1$ ,  $\bar{Z}_2$ , and  $\bar{Z}_3$  are 3.459, 1.502, and 0.060, respectively. The  $S_{Z_Y}$  value equals 0.1596. The  $t_{\alpha/2, \nu}$  value equals 2,0106 for a 0.05 significance level and 48 degrees of freedom.

There is one outlier in the data for the nonlinear regression model (6) since the  $Y$  value for row 51 is outside the prediction interval. Therefore, we discard row 51 and go to step 1 of the fourth iteration.

In step 1 of the fourth iteration, we normalize the data of 51 rows from Table 1 (without rows 35, 47, and 51). In this case, the parameter estimates of the four-variate Box-Cox transformation for the data from Table 1 (without rows 35, 47, and 51) are calculated by the maximum likelihood method and are  $\hat{\lambda}_Y = -0.161328$ ,  $\hat{\lambda}_1 = -0.159392$ ,  $\hat{\lambda}_2 = -0.239815$ ,  $\hat{\lambda}_3 = -1.253682$ .

There are no multivariate outliers among data of 51 rows from Table 1 (without rows 35, 47, and 51) since their  $SMD_Z$  values do not exceed 14.86, which is the quantile of the Chi-Square distribution, applicable for a significance level of 0.005. That is why we go to the third step.

In the third step, we build the linear regression model (4) for 51 rows of normalized data from Table 1 (without rows 35, 47, and 51). The estimates  $\hat{b}_0$ ,  $\hat{b}_1$ ,  $\hat{b}_2$ , and  $\hat{b}_3$  equal  $-6.1084$ ,  $1.7898$ ,  $0.84037$ , and  $0.04182$ , respectively. The estimate  $\hat{\sigma}_\varepsilon$  is 0.1421.

In the fourth step, we test the normality of the distribution of residuals in the linear regression model (4) for 51 rows of normalized data from Table 1 (without rows

35, 47, and 51). To achieve this, we employ the Pearson Chi-Squared test. We accepted the null hypothesis  $H_0$ , affirming that the observed frequency distribution of the  $\varepsilon$  values in (4) closely resembles the normal distribution (indicating no significant difference between the distributions). This decision was reached because the test  $\chi^2$  statistic, measuring 5.57 does not exceed 9.49, that is the quantile of the Chi-Square distribution, applicable for 4 degrees of freedom and a significance level of 0.05. Therefore, we go to step 5.

In the fifth step, we construct the nonlinear regression model (6). Then, in the sixth step, we build the prediction interval of nonlinear regression by (7) and determine whether one or more values of the response are outliers.

In our case the inverse matrix of (8) is

$$\mathbf{S}_Z^{-1} = \begin{pmatrix} 0.0834 & 0.0284 & -0.0313 \\ 0.0284 & 0.2468 & -0.0232 \\ -0.0313 & -0.0232 & 0.4084 \end{pmatrix}. \quad (9)$$

The values of averages  $\bar{Z}_1$ ,  $\bar{Z}_2$ , and  $\bar{Z}_3$  are 3.441, 1.454, and 0.065, respectively. The  $S_{Z_Y}$  value equals 0.1466. The  $t_{\alpha/2, \nu}$  value equals 2,0117 for a 0.05 significance level and 47 degrees of freedom.

No outliers are present in the data for the nonlinear regression model (6) since all  $Y$  values for 51 rows of the data from Table 1 (without rows 35, 47, and 51) are inside the prediction interval. Therefore, we complete constructing the nonlinear regression model (6).

The nonlinear regression model (6) has the parameter estimates  $\hat{\lambda}_Y$ ,  $\hat{\lambda}_1$ ,  $\hat{\lambda}_2$ ,  $\hat{\lambda}_3$ ,  $\hat{b}_0$ ,  $\hat{b}_1$ ,  $\hat{b}_2$ , and  $\hat{b}_3$ , which equal  $-0.161328$ ,  $-0.159392$ ,  $-0.239815$ ,  $-1.253682$ ,  $-6.1084$ ,  $1.7898$ ,  $0.84037$ , and  $0.04182$ , respectively. The estimate  $\hat{\sigma}_\varepsilon$  of a standard deviation  $\varepsilon$  is 0.1421. The nonlinear regression model (6) is limited to estimating LOC of open-source Kotlin-based apps with the following restrictions on predictors: the interval for  $X_1$  is from 19 to 1292, the interval for  $X_2$  is from 2.167 to 26.526, and the interval for  $X_3$  is from 0.681 to 3.206.

To assess the predictive accuracy of the nonlinear regression model (6), we utilized standard metrics namely  $R^2$ , MMRE, and PRED(0.25). The acceptable values of MMRE and PRED(0.25) are not more than 0.25 and not less than 0.75 respectively. For model (6) with the above parameter estimates, predicated upon the four-variate Box-Cox transformation applied to the dataset of the 51 apps from Table 1 (excluding entries from rows 35, 47, and 51), the computed values for  $R^2$ , MMRE, and PRED(0.25) are 0.9235, 0.1458, and 0.8235, respectively.

These values indicate good model quality. However, the data from the table 1 is the training set. To avoid the problem of overfitting the model [32], the predictive accuracy of the model (6) should be checked on the test set, the data of which were not used to build the model. That

we do next. In addition, we compare the built model (6) with two other models that are obtained based on the univariate transformations.

#### 4 EXPERIMENTS

The test dataset was obtained using the CodeMR tool [30] around the variables and for the training set from Table 1. Table 2 contains the test dataset.

For comparison of the model (6) with other nonlinear regression models with three predictors, two nonlinear regression models are built based on normalizing the data of 51 rows from Table 1 (without rows 35, 47, and 51) using the univariate transformation.

The nonlinear regression model based on the linear regression model (4) for the normalized data and the decimal logarithm univariate transformation has the form

$$Y = 10^{\varepsilon + \hat{b}_0} X_1^{\hat{b}_1} X_2^{\hat{b}_2} X_3^{\hat{b}_3}, \quad (10)$$

where the estimators for parameters are:  $\hat{b}_0 = -2.11196$ ,  $\hat{b}_1 = 1.02339$ ,  $\hat{b}_2 = 0.652935$ ,  $\hat{b}_3 = 0.047833$ . The estimate  $\hat{\sigma}_\varepsilon$  is 0.08605.

Table 2 – The test dataset

No	App name	Y	X <sub>1</sub>	X <sub>2</sub>	X <sub>3</sub>
1	moko-resources	3.996	173	3.908	1.145
2	Loritta	79.295	2815	5.304	1.497
3	kable	1.818	56	4.393	1.054
4	binary-compatibility-validator	1.149	46	5.37	1.022
5	contacts-android	27.109	1149	5.148	1.55
6	strikt	2.418	74	8.676	1.203
7	kotlin-power-assert	1.017	29	6.172	1.172
8	kroto-plus	10.909	153	17.353	1.007
9	Hexagon	6.65	212	7.943	1
10	beagle	11.132	636	5.634	1.06
11	MoshiX	8.35	154	8.26	0.721
12	BleGattCoroutines	1.834	46	5.261	1.457
13	kotlin-spark-api	13.344	216	23.685	1.167
14	data2viz	1.573	51	6.137	1.078
15	Confetti	14.425	313	6.042	1.201
16	locus-android	0.842	25	5.8	1.64
17	actions-on-google-java	4.542	149	4.604	0.872
18	aws-sdk-kotlin	6.556	300	3.467	1.107
19	moko-kswift	1.023	41	5.366	1.195
20	EzXHelper	1.557	49	9.939	1.082
21	ktgbotapi	0.539	24	3.292	1.042
22	detekt-intellij-plugin	0.934	42	4.81	1.595
23	swiftpoet	2.883	84	9.881	0.893
24	Fuck-Storage-Access-Framework	2.821	56	12.411	1.036
25	kowasm	4.629	389	2.956	0.817

The nonlinear regression model based on the Box-Cox univariate transformation is analogously (6) with the only difference being that the data for variables are normalized by the Box-Cox univariate transformation using the maximum likelihood method. The estimators for parameters of the Box-Cox univariate transformation for each from variables  $Y$ ,  $X_1$ ,  $X_2$ , and  $X_3$  are  $\hat{\lambda}_Y = -0.067289$ ,  $\hat{\lambda}_1 = -0.034850$ ,  $\hat{\lambda}_2 = -0.459658$ ,  $\hat{\lambda}_3 = -1.289541$ . The

parameter estimators of the linear regression model for normalized data by the Box-Cox univariate transformation are  $\hat{b}_0 = -5.33943$ ,  $\hat{b}_1 = 1.09177$ ,  $\hat{b}_2 = 1.38983$ ,  $\hat{b}_3 = 0.069187$ . The estimate  $\hat{\sigma}_\varepsilon$  is 0.17507.

To carry out experiments, a computer program was developed to implement the constructed models (6) and (10). The program was coded using sci-language compatible with the Scilab system. Scilab, accessible at <http://www.scilab.org>, stands as a cost-free, open-source software option.

#### 5 RESULTS

The values of  $R^2$ , MMRE and PRED(0.25) equal respectively 0.9138, 0.1538, and 0.8431 for the model (6) based on the Box-Cox univariate transformation, and equal respectively 0.9166, 0.1548, and 0.8039 for the model (10) for the decimal logarithm univariate transformation for the training dataset. In this case, the MMRE and  $R^2$  values are better for the model (6) based on the Box-Cox four-variate transformation. The PRED(0.25) value is better for model (6) based on the Box-Cox univariate transformation (0.8431 against 0.8235).

For model (6) with the parameter estimates, calculated upon the four-variate Box-Cox transformation for the training dataset of the 51 apps from Table 1 (excluding entries from rows 35, 47, and 51) applied to the test dataset of the 25 apps from Table 2, the computed values for  $R^2$ , MMRE, and PRED(0.25) are 0.9818, 0.1871, and 0.7600, respectively. For model (10) applied to the test dataset of the 25 apps from Table 2, the computed values for  $R^2$ , MMRE, and PRED(0.25) are 0.9811, 0.1925, and 0.7600, respectively. For model (6) with the parameter estimates, calculated upon the univariate Box-Cox transformation for the dataset of the 51 apps from Table 1 (excluding entries from rows 35, 47, and 51) applied to the test dataset of the 25 apps from Table 2, the computed values for  $R^2$ , MMRE, and PRED(0.25) are 0.9619, 0.1943, and 0.7200, respectively. In the case of the test dataset, the MMRE and  $R^2$  values are better for the model (6) based on the Box-Cox four-variate transformation too.

The prediction results  $\hat{Y}$  of models (6) and (10) for values of predictors from Table 2 and values of MRE are presented in Table 3. Prediction results obtained from model (6) and the corresponding MRE values are presented in Table 3, showcasing two cases: utilizing univariate and four-variate Box-Cox transformations. The MRE values for model (6) based on the Box-Cox four-variate transformation exhibit a reduction compared to those of model (6) based on the Box-Cox univariate transformation for 15 from 25 rows of data (rows 1–6, 8, 10, 11, 17, 19–22, 25). Also, the MRE values for model (6) based on the Box-Cox four-variate transformation are less than for model (10) based on the decimal logarithm univariate transformation for 16 from 25 rows of data (rows 3, 5–8, 10–12, 14–17, 20, 21, 23, 25).

Table 3 – The prediction results and confidence intervals of nonlinear regressions

No	Y	The four-variate Box-Cox transformation				The univariate transformations							
						the decimal logarithm				the Box-Cox			
		$\hat{y}$	MRE	LB	UB	$\hat{y}$	MRE	LB	UB	$\hat{y}$	MRE	LB	UB
1	3.996	3.631	0.0914	3.373	3.912	3.696	0.0750	3.407	4.009	3.598	0.0996	3.317	3.905
2	79.295	77.070	0.0281	62.905	95.076	79.378	0.0010	67.528	93.307	89.295	0.1261	73.915	108.140
3	1.818	1.302	0.2839	1.213	1.399	1.253	0.3109	1.139	1.378	1.296	0.2873	1.191	1.411
4	1.149	1.206	0.0493	1.127	1.291	1.166	0.0149	1.064	1.278	1.226	0.0671	1.132	1.329
5	27.109	30.183	0.1134	25.990	35.183	31.167	0.1497	27.473	35.358	32.565	0.2013	28.256	37.583
6	2.418	2.613	0.0808	2.435	2.807	2.615	0.0815	2.409	2.838	2.638	0.0911	2.431	2.864
7	1.017	0.822	0.1918	0.757	0.893	0.802	0.2117	0.718	0.895	0.864	0.1504	0.783	0.954
8	10.909	8.639	0.2081	7.505	9.976	8.574	0.2140	7.396	9.940	7.706	0.2936	6.752	8.805
9	6.65	7.412	0.1146	6.877	7.997	7.185	0.0804	6.668	7.741	7.233	0.0876	6.704	7.807
10	11.132	17.686	0.5887	15.972	19.617	17.722	0.5920	16.131	19.470	18.146	0.6301	16.450	20.030
11	8.35	5.318	0.3631	4.646	6.105	5.232	0.3734	4.664	5.869	5.163	0.3817	4.475	5.964
12	1.834	1.206	0.3425	1.105	1.317	1.170	0.3619	1.044	1.312	1.234	0.3274	1.112	1.369
13	13.344	15.695	0.1762	13.006	19.052	15.057	0.1284	12.498	18.141	12.753	0.0443	10.858	15.005
14	1.573	1.448	0.0792	1.359	1.545	1.418	0.0987	1.304	1.541	1.481	0.0586	1.373	1.598
15	14.425	9.154	0.3654	8.509	9.855	9.033	0.3738	8.443	9.663	9.164	0.3647	8.523	9.857
16	0.842	0.691	0.1794	0.622	0.769	0.672	0.2018	0.578	0.781	0.733	0.1295	0.644	0.835
17	4.542	3.486	0.2324	3.233	3.763	3.485	0.2327	3.204	3.791	3.451	0.2402	3.179	3.749
18	6.556	5.601	0.1457	5.109	6.148	5.995	0.0856	5.458	6.584	5.626	0.1419	5.096	6.215
19	1.023	1.080	0.0560	1.001	1.166	1.044	0.0204	0.944	1.154	1.107	0.0822	1.012	1.212
20	1.557	1.816	0.1666	1.680	1.966	1.865	0.1976	1.690	2.057	1.865	0.1981	1.701	2.047
21	0.539	0.483	0.1046	0.435	0.536	0.436	0.1915	0.375	0.507	0.469	0.1301	0.411	0.535
22	0.934	1.048	0.1217	0.950	1.157	1.010	0.0814	0.884	1.154	1.068	0.1435	0.950	1.202
23	2.883	3.179	0.1027	2.920	3.466	3.195	0.1083	2.901	3.520	3.147	0.0914	2.860	3.463
24	2.821	2.353	0.1658	2.148	2.581	2.466	0.1258	2.202	2.762	2.367	0.1611	2.134	2.626
25	4.629	6.135	0.3253	5.359	7.044	6.946	0.5004	6.093	7.918	6.150	0.3285	5.315	7.126

Note, that a more significant advantage of the model (6) constructed by the four-variate Box-Cox transformation compared with the two above models relying on univariate transformations, is the reduced widths of the confidence and prediction intervals. These intervals are defined by data from Table 2. Table 3 contains the lower (LB) and upper (UB) bounds of the confidence intervals of nonlinear regressions utilizing both univariate and four-variate transformations, with a significance level of 0.05. We defined the confidence intervals for  $\hat{Y}$  using (7) with the sole distinction being the absence of 1 in the summation within curly brackets. Also, we used the inverse matrix (9) in this case. The widths of the confidence interval of nonlinear regression based on the Box-Cox four-variate transformation are less than for nonlinear regression based on the Box-Cox univariate transformation for 20 from 25 rows of data (except rows 8–10, 13, and 15).

Additionally, for 18 of the 25 data rows (excluding rows 2, 5, 9–11, 13, and 15), the confidence intervals' widths for nonlinear regression, based on the Box-Cox four-variate transformation, are less than those based on the decimal logarithm univariate transformation. Similar results are observed in the prediction intervals of nonlinear regressions using the test dataset from Table 2.

The lower (LB) and upper (UB) bounds of prediction intervals for nonlinear regressions, based on univariate and four-variate transformations respectively, are presented in Table 4 at a significance level of 0.05. It's worth

noting that the width of the confidence interval for nonlinear regression for the four-variate Box-Cox transformation is less than after the univariate Box-Cox transformation for 20 (with the difference up to 23%) from 25 data rows (except rows 8, 9, 10, 13, and 15 with the difference of 20.3, 1.5, 1.8, 45.8, and 0.9%, respectively) and less than after decimal logarithm univariate transformation for 18 from (with the difference up to 27%) from 25 data rows (except rows 2, 5, 9, 10, 11, 13, and 15 with the difference of 24.8, 16.6, 1.8, 4.4, 9.1, 21.1, and 7.1%, respectively). It's also worth noting that the width of the confidence interval for nonlinear regression for four-variate Box-Cox transformation is less than after the univariate Box-Cox transformation for 18 (with the difference up to 26.4%) from 25 data rows (except rows 2, 5, 8, 9, 10, 13, and 15 with the difference of 7.8, 5.4, 14.3, 1.4, 5.2, 35.8, and 0.8%, respectively) and less than after decimal logarithm univariate transformation for 18 from (with the difference up to 30.7%) from 25 data rows (except rows 2, 5, 8, 9, 10, 13, and 15 with the difference of 48.1, 25.1, 3.6, 3.8, 16.9, 18.9, and 5.9%, respectively).

The largest deviation between the widths of the intervals we obtained for the data of app 2 is from Table 2. That result can be explained by the fact that the value 2815 of the predictor  $X_1$  exceeds the upper bound of the corresponding restriction ( $X_1$  is from 19 to 1292 according to the training dataset from Table 1), for which model (6) was built, by more than two times.

Table 4 – The bounds of the prediction interval

No	Y	univariate				four-variate	
		decimal logarithm		Box-Cox		Box-Cox	
		LB	UB	LB	UB	LB	UB
1	3.996	2.431	5.620	2.415	5.421	2.533	5.320
2	<b>79.295</b>	<b>51.031</b>	<b>123.471</b>	<b>53.201</b>	<b>152.706</b>	<b>42.332</b>	<b>149.615</b>
3	1.818	0.821	1.911	0.891	1.903	0.957	1.800
4	1.149	0.765	1.777	0.845	1.796	0.890	1.659
5	27.109	20.273	47.915	20.288	53.093	18.104	52.688
6	2.418	1.720	3.977	1.784	3.943	1.857	3.753
7	1.017	0.524	1.227	0.598	1.261	0.615	1.115
8	10.909	5.539	13.272	5.007	12.012	5.642	13.651
9	6.65	4.731	10.912	4.771	11.097	4.964	11.380
10	11.132	11.624	27.020	11.622	28.727	11.141	29.140
11	8.35	3.414	8.018	3.378	7.990	3.577	8.123
12	1.834	0.764	1.793	0.845	1.818	0.886	1.668
13	13.344	9.588	23.647	8.104	20.359	9.724	26.369
14	1.573	0.932	2.157	1.017	2.178	1.061	2.011
15	14.425	5.955	13.701	6.010	14.147	6.053	14.259
16	0.842	0.434	1.041	0.504	1.075	0.517	0.937
17	4.542	2.291	5.302	2.318	5.195	2.437	5.098
18	6.556	3.932	9.139	3.718	8.614	3.801	8.470
19	1.023	0.684	1.594	0.763	1.621	0.800	1.482
20	1.557	1.222	2.846	1.269	2.770	1.312	2.561
21	0.539	0.281	0.675	0.325	0.682	0.366	0.644
22	0.934	0.656	1.556	0.732	1.575	0.772	1.444
23	2.883	2.095	4.875	2.112	4.739	2.229	4.633
24	2.821	1.610	3.778	1.597	3.545	1.673	3.376
25	4.629	4.511	10.693	4.002	9.572	4.094	9.457

## 6 DISCUSSION

Utilizing appropriate techniques, we employ four-variate normalizing transformations to construct the nonlinear regression model for early estimation of LOC in open-source Kotlin-based applications, as in [13]. This approach is chosen due to the non-Gaussian distribution of errors in the linear regression model, as the chi-squared test result indicated. Moreover, the four-variate distribution of the data from Table 1 is not Gaussian what the Mardia multivariate normality test based on measures of the multivariate skewness and kurtosis indicates. We utilize the statistical technique based on the multivariate normalizing transformations and the SMD for normalized data to detect four-variate outliers in the non-Gaussian data from Table 1. Note, that we have more four-variate outliers for the data from Table 1 without applying normalization.

For a larger number of data rows, the widths of both confidence and prediction intervals in multiple nonlinear regression, utilizing the Box-Cox four-variate transformation, are smaller compared to nonlinear regressions models employing univariate transformations, including both the decimal logarithm and the Box-Cox. Moreover, model (6) utilizing the Box-Cox four-variate transformation demonstrates a smaller MMRE value compared with all other nonlinear models employing univariate transformations. This may prove the Box-Cox four-variate transformation to be the best four-variate normalization transformation for non-Gaussian data from Table 1.

The advantages of the proposed model (6) include the possibility of early LOC estimation of open-source Kotlin-based apps using the values of three metrics at the app level (the total number of classes, WMC, and DIT), that

can be measured from the class diagram. The disadvantages of the proposed model (6) include, first of all, the fact that the early LOC estimation can be performed only for a part of the open-source Kotlin-based apps. The proposed model (6) is limited to the early LOC estimation of open-source Kotlin-based apps for which there are the following restrictions on predictors: the interval for  $X_1$  is from 19 to 1292, the interval for  $X_2$  is from 2.167 to 26.526, and the interval for  $X_3$  is from 0.681 to 3.206.

The obtained results indicate that a constructed model with three predictors for early LOC estimation of open-source Kotlin-based apps improves confidence in estimating the LOC metric of the above apps.

## CONCLUSIONS

The task of improving confidence in early LOC estimation for open-source Kotlin-based applications has been accomplished.

**The scientific novelty** of the obtained results is that the three-factor nonlinear regression model for early LOC estimation of open-source Kotlin-based apps is firstly constructed based on the Box-Cox four-variate transformation. Compared to the other nonlinear regression models, this model demonstrates a smaller mean magnitude of relative error and narrower confidence and prediction intervals with three predictors for more cases.

**The practical significance** of the obtained results is that the computer program to implement the constructed model using sci-language for Scilab was developed. With the experimental results at hand, we are confident in recommending the developed model for practical use.

**Prospects for further research** may include the application of other multivariate normalizing transformations and data sets to construct multiple nonlinear regression models for early LOC estimation of open-source Kotlin-based apps for other restrictions on predictors.

## ACKNOWLEDGEMENTS

This work is proactive. The research was performed within the scope of the scientific activity of the authors' working hours according to the main positions.

## REFERENCES

1. Ponnala R., Reddy C. R. K. Object Oriented Dynamic Metrics in Software Development: A Literature Review, *International Journal of Applied Engineering Research*, 2019, Vol. 14, No. 22, pp. 4161–4172.
2. Boehm B. W., Abts C., Brown A. W. et al. Software cost estimation with COCOMO II. Upper Saddle River, NJ: Prentice Hall PTR, 2000, 506 p.
3. Rumiński B. Top Apps Built with Kotlin Multiplatform [2023 Update] [Electronic resource]. Access mode: <https://www.netguru.com/blog/top-apps-built-with-kotlin-multiplatform>
4. Kaczmarek J., Kucharski M. Size and effort estimation for applications written in Java, *Information and Software Technology*, 2004, Vol. 46, Issue 9, pp. 589–601. DOI: 10.1016/j.infsof.2003.11.001
5. Laird L. M., Brennan M. C. Software measurement and estimation. A practical approach. quantitative software engineering series. Wiley-IEEE Computer Society Press, 2006, 379 p.

6. Tan H. B. K., Zhao Y., Zhang H. Conceptual data model-based software size estimation for information systems, *Transactions on Software Engineering and Methodology*, 2009, Vol. 19, Issue 2, pp. 1–37. DOI: 10.1145/1571629.1571630
7. Zifen Y. An improved software size estimation method based on object-oriented approach, *Electrical & Electronics Engineering : IEEE Symposium EEESYM'12*, Kuala Lumpur, Malaysia, 24–27 June 2012, proceedings. Los Alamitos: IEEE, 2012, pp. 615–617. DOI: 10.1109/EEESym.2012.6258733.
8. Kiewkanya M., Surak S. Constructing C++ software size estimation model from class diagram, *Computer Science and Software Engineering : 13th International Joint Conference, Khon Kaen, Thailand, 13–15 July 2016 : proceedings.* – Los Alamitos: IEEE, 2016, pp. 1–6. DOI: 10.1109/JCSSE.2016.7748880
9. Sholiq S., Dewi R. S., Subriadi A. P. A comparative study of software development size estimation method: UCPabc vs Function Points, *Procedia Computer Science*, 2017, Vol. 124, pp. 470–477. DOI: 10.1016/j.procs.2017.12.179
10. Prykhodko N. V., Prykhodko S. B. The non-linear regression model to estimate the software size of open source Java-based systems, *Radio Electronics, Computer Science, Control*, 2018, No. 3 (46), pp. 158–166. DOI: 10.15588/1607-3274-2018-3-17
11. Prykhodko S. B., Prykhodko N. V., Smykodub T. G. Chytrykhfaktorna neliniynna regresiyina model dlia otsiniuvannya rozmiru Java-zastosunkiv z vidkrytym kodom, *Vcheni zapysky TNU imeni V.I. Vernads'kogo. Serija: tehnicni nauky*, 2020, Vol. 31 (70), Issue 2, pp. 157–162. DOI: <https://doi.org/10.32838/2663-5941/2020.2-1/25>
12. Prykhodko S. B., Shutko I. S., Prykhodko A. S. A nonlinear regression model to estimate the size of web apps created using the CakePHP framework, *Radio Electronics, Computer Science, Control*, 2021, No. 4 (59), pp. 129–139. DOI: 10.15588/1607-3274-2021-4-12
13. Manisha, Rishi, R. Early size estimation using machine learning, *Proceedings of the 2021 8th International Conference on Computing for Sustainable Global Development (INDIACom)*, New Delhi, India, 17–19 March 2021 : proceedings. Los Alamitos, IEEE, 2021, pp. 757–762. DOI: 10.1109/INDIACom51348.2021.00135
14. Daud M., Malik A. A. Improving the accuracy of early software size estimation using analysis-to-design adjustment factors (ADAFs), *IEEE Access*, 2021, Vol. 9, pp. 81986–81999. DOI: 10.1109/ACCESS.2021.3085752
15. Zhang K., Wang X., Ren J. et al. Efficiency improvement of function point-based software size estimation with deep learning model. Los Alamitos, IEEE, 2021, Vol. 9, pp. 107124–107136. DOI: 10.1109/ACCESS.2020.2998581
16. Ritu, Garg Y. Comparative Analysis of Machine Learning Techniques in Effort Estimation, *Proceedings of the 2022 International Conference on Machine Learning, Big Data, Cloud and Parallel Computing (COM-IT-CON)*, Faridabad, India, 2022 : proceedings. Los Alamitos, IEEE, 2022. pp. 401–405. DOI: 10.1109/COM-IT-CON54601.2022.9850592
17. Brar P., Nandal D. A Systematic Literature Review of Machine Learning Techniques for Software Effort Estimation Models, *Proceeding of the 2022 Fifth International Conference on Computational Intelligence and Communication Technologies (CCICT)*. Sonapat, India, 08–09 July 2022 – Los Alamitos, IEEE, 2022, pp. 494–499, DOI: 10.1109/CCICT56684.2022.00093.
18. Assefa Y., Berhanu F., Tilahun A. et al. Software Effort Estimation using Machine learning Algorithm, *Proceeding of the 2022 International Conference on Information and Communication Technology for Development for Africa (ICT4DA)*, Bahir Dar, Ethiopia, 28–30 November 2022 : proceedings. Los Alamitos, IEEE, 2022, pp. 163–168, DOI: 10.1109/ICT4DA56482.2022.9971209
19. Jadhav A., Shandilya S. K., Izonin I. et al. Effective Software Effort Estimation Leveraging Machine Learning for Digital Transformation, *IEEE Access*, 2023, Vol. 11, pp. 83523–83536. DOI: 10.1109/ACCESS.2023.3293432
20. Kumar S., Arora M., Sakshi et al. A Review of Effort Estimation in Agile Software Development using Machine Learning Techniques, *Proceedings of the 2022 4th International Conference on Inventive Research in Computing Applications (ICIRCA)*, Coimbatore, India, 21–23 September 2022 : proceedings. Los Alamitos, IEEE, pp. 416–422. DOI: 10.1109/ICIRCA54612.2022.9985542
21. R. K. B. N. Software Effort Estimation using ANN (Back Propagation), *Proceedings of the 2023 7th International Conference on Computing Methodologies and Communication (ICCMC)*, Erode, India, 23–25 February 2023 : proceedings. Los Alamitos, IEEE, pp. 1–2. DOI: 10.1109/ICCMC56507.2023.10084264.
22. Sousa A. O., Veloso D. T., Gonçalves H. M. et al. Applying Machine Learning to Estimate the Effort and Duration of Individual Tasks in Software Projects, *IEEE Access*, 2023, Vol. 11, pp. 89933–89946. DOI: 10.1109/ACCESS.2023.3307310
23. Nassif A. B., AbuTalib M., Capretz L. F. Software effort estimation from use case diagrams using nonlinear regression analysis, *Electrical and Computer Engineering : IEEE Canadian Conference CCECE'20*. London, ON, Canada, 30 Aug.–2 Sept., 2020 : proceedings. IEEE, 2020, pp. 1–4. DOI: 10.1109/CCECE47787.2020.9255712.
24. Prykhodko S., Prykhodko N., Knyrik K. Estimating the efforts of mobile application development in the planning phase using nonlinear regression analysis, *Applied Computer Systems*, 2020, Vol. 25, No. 2, pp. 172–179. DOI: 10.2478/acss-2020-0019
25. [Nhung H. L. T. K., Hai V. V., Silhavy R. et al. Parametric Software Effort Estimation Based on Optimizing Correction Factors and Multiple Linear Regression, *IEEE Access*, 2022. Vol. 10, pp. 2963–2986. DOI: 10.1109/ACCESS.2021.3139183
26. Sahoo P., Behera D. K., Mohanty J. R. et al. Effort Estimation of Software products by using UML Sequence models with Regression Analysis, *Proceedings of the 2022 OITS International Conference on Information Technology (OCIT)*, Bhubaneswar, India, 14–16 December 2022 : proceedings. Los Alamitos, IEEE, pp. 97–101, DOI: 10.1109/OCIT56763.2022.00028.
27. Cibir E., Ayyildiz T. E. An Empirical Study on Software Test Effort Estimation for Defense Projects, *IEEE Access*, 2022, Vol. 10, pp. 48082–48087. DOI: 10.1109/ACCESS.2022.3172326
28. Yuan X., Su J., Yu C. and Ye S. Power Grid Software Cost Estimation Based on Improved COCOMO Model, *Proceeding of the 2023 IEEE 3rd International Conference on Electronic Technology, Communication and Information (ICETCI)*, Changchun, China, 26–28 May 2023 : proceedings. Los Alamitos, IEEE, pp. 1265–1269. DOI: 10.1109/ICETCI57876.2023.10176686
29. Prykhodko S., Prykhodko N., Makarova L. et al. Outlier Detection in Non-Linear Regression Analysis Based on the

- Normalizing Transformations, *Proceedings of the 15th International Conference on Advanced Trends in Radioelectronics, Telecommunications and Computer Engineering (TCSET), IEEE, Lviv-Slavske, 25–29 February 2020* : proceeding. Los Alamitos, IEEE, pp. 407–410. DOI: 10.1109/TCSET49122.2020.235464
30. CodeMR [Electronic resource]. Access mode: <https://plugins.jetbrains.com/plugin/10811-codemr>
31. Mardia K. V. Measures of multivariate skewness and kurtosis with applications, *Biometrika*, 1970, Vol. 57, pp. 519–530. DOI: 10.1093/biomet/57.3.519
32. Frost J. Overfitting Regression Models: Problems, Detection, and Avoidance [Electronic resource]. Access mode: <https://statisticsbyjim.com/regression/overfitting-regression-models/>

Received 05.01.2024.  
Accepted 16.02.2024.

УДК 004.412:519.237.5

## НЕЛІНІЙНА РЕГРЕСІЙНА МОДЕЛЬ ДЛЯ РАНЬОГО ОЦІНЮВАННЯ МЕТРИКИ LOC ЗАСТОСУНКІВ З ВІДКРИТИМ КОДОМ НА KOTLIN

**Приходько С. Б.** – д-р техн. наук, професор, завідувач кафедри програмного забезпечення автоматизованих систем Національного університету кораблебудування імені адмірала Макарова, Миколаїв, Україна.

**Приходько Н. В.** – канд. екон. наук, доцент, доцент кафедри фінансів Національного університету кораблебудування імені адмірала Макарова, Миколаїв, Україна.

**Кольцов А. В.** – аспірант кафедри програмного забезпечення автоматизованих систем Національного університету кораблебудування імені адмірала Макарова, Миколаїв, Україна.

### АНОТАЦІЯ

**Актуальність.** Раннє оцінювання рядків коду (LOC) у проектах програмного забезпечення має важливе значення, оскільки це безпосередньо впливає на прогнозування зусиль з розробки програмного забезпечення для цілого спектру мов програмування, включаючи застосунки з відкритим кодом на Kotlin. Об'єктом дослідження є процес раннього оцінювання метрики LOC застосунків з відкритим кодом на Kotlin. Предметом дослідження є нелінійні регресійні моделі для раннього оцінювання метрики LOC застосунків з відкритим кодом на Kotlin.

**Мета.** Метою роботи є побудова нелінійної регресійної моделі з трьома предикторами для раннього оцінювання метрики LOC застосунків з відкритим кодом на Kotlin на основі чотирьохвимірною нормалізуючого перетворення Бокса-Кокса для підвищення достовірності раннього оцінювання LOC цих застосунків.

**Метод.** Для раннього оцінювання LOC у застосунках із відкритим кодом на Kotlin модель, довірчі та прогнозні інтервали нелінійної регресії були побудовані за допомогою нормалізуючого перетворення Бокса-Кокса з чотирма змінними та за допомогою відповідних методів. Ці методи базуються на множинному нелінійному регресійному аналізі з використанням багатовимірних нормалізуючих перетворень та враховують кореляцію між залежними та незалежними змінними у випадку негаусових даних. Як наслідок, такий підхід має тенденцію до зменшення середньої величини відносної похибки, зменшення ширини довірчих інтервалів та інтервалів прогнозування порівняно з моделями, що використовують однофакторні нормалізуючі перетворення.

**Результати.** Проведено порівняння побудованої моделі з моделями нелінійної регресії з використанням десяткового логарифму та одновимірною перетворення Бокса-Кокса.

**Висновки.** Модель нелінійної регресії з трьома предикторами для ранньої оцінки метрики LOC застосунків із відкритим вихідним кодом на Kotlin побудовано на основі перетворення чотирьох змінних Бокса-Кокса. Порівняно з іншими моделями нелінійної регресії, ця модель демонструє більший множинний коефіцієнт детермінації, менше значення середньої величини відносної похибки та менші ширини довірчих інтервалів та інтервалів прогнозування. Перспективи подальших досліджень можуть включати застосування інших багатовимірних нормалізуючих перетворень і наборів даних для побудови моделі нелінійної регресії для ранньої оцінки метрики LOC застосунків із відкритим вихідним кодом на Kotlin для інших обмежень на предиктори.

**КЛЮЧОВІ СЛОВА:** оцінка, рядки коду, застосунок з відкритим вихідним кодом, Kotlin, нелінійна регресійна модель, перетворення Бокса-Кокса, клас, зважені методи на клас, глибина дерева успадування.

### ЛІТЕРАТУРА

1. Ponnala R. Object Oriented Dynamic Metrics in Software Development: A Literature Review / R. Ponnala, C. R. K. Reddy // *International Journal of Applied Engineering Research*. – 2019. – Vol. 14, No. 22. – P. 4161–4172.
2. Software cost estimation with COCOMO II / [B. W. Boehm, C. Abts, A. W. Brown et al.]. – Upper Saddle River, NJ: Prentice Hall PTR, 2000. – 506 p.
3. Rumiński B. Top Apps Built with Kotlin Multiplatform [2023 Update] [Electronic resource] / B. Rumiński. – Access mode: <https://www.netguru.com/blog/top-apps-built-with-kotlin-multiplatform>
4. Kaczmarek J. Size and effort estimation for applications written in Java / J. Kaczmarek, M. Kucharski // *Information and Software Technology*. – 2004. – Vol. 46, Issue 9. – P. 589–601. DOI: 10.1016/j.infsof.2003.11.001
5. Laird L. M. Software measurement and estimation. A practical approach. quantitative software engineering series / L. M. Laird, M. C. Brennan. – Wiley-IEEE Computer Society Press, 2006. – 379 p.
6. Tan H. B. K. Conceptual data model-based software size estimation for information systems / H. B. K. Tan, Y. Zhao, H. Zhang // *Transactions on Software Engineering and Methodology*. – 2009. – Vol. 19, Issue 2. – P. 1–37. DOI: 10.1145/1571629.1571630
7. Zifen Y. An improved software size estimation method based on object-oriented approach / Y. Zifen // *Electrical & Electronics Engineering : IEEE Symposium EESYM'12, Kuala Lumpur, Malaysia, 24–27 June 2012* : proceedings. – Los Alamitos:

- IEEE, 2012. – P. 615–617. DOI: 10.1109/EEESym.2012.6258733.
8. Kiewkanya M. Constructing C++ software size estimation model from class diagram / M. Kiewkanya, S. Surak // Computer Science and Software Engineering : 13th International Joint Conference, Khon Kaen, Thailand, 13–15 July 2016 : proceedings. – Los Alamitos: IEEE, 2016. – P. 1–6. DOI: 10.1109/JCSSE.2016.7748880
  9. Sholiq S. A comparative study of software development size estimation method: UCPabc vs Function Points / S. Sholiq, R. S. Dewi, A. P. Subriadi // Procedia Computer Science, – 2017. – Vol. 124, – P. 470–477. DOI: 10.1016/j.procs.2017.12.179
  10. Prykhodko N. V. The non-linear regression model to estimate the software size of open source Java-based systems / N. V. Prykhodko, S. B. Prykhodko // Radio Electronics, Computer Science, Control. – 2018. – No. 3 (46). – P. 158–166. DOI: 10.15588/1607-3274-2018-3-17
  11. Приходько С.Б. Чотирихфакторна нелінійна регресійна модель для оцінювання розміру Java-застосунків з відкритим кодом / С. Б. Приходько, Н. В. Приходько, Т. Г. Смикодуб // Науковий журнал «Вчені записки Таврійського національного університету імені В. І. Вернадського. Серія: Технічні науки». 2020 – Том 31 (70) № 2. – С. 157–162. DOI: <https://doi.org/10.32838/2663-5941/2020.2-1/25>
  12. Prykhodko S.B. A nonlinear regression model to estimate the size of web apps created using the CakePHP framework / S. B. Prykhodko, I. S. Shutko, A. S. Prykhodko // Radio Electronics, Computer Science, Control. – 2021. – No. 4 (59). – P. 129–139. DOI: 10.15588/1607-3274-2021-4-12
  13. Manisha Early size estimation using machine learning / Manisha, R. Rishi // Proceedings of the 2021 8th International Conference on Computing for Sustainable Global Development (INDIACom), New Delhi, India, 17–19 March 2021 : proceedings. – Los Alamitos: IEEE, 2021. – P. 757–762. DOI: 10.1109/INDIACom51348.2021.00135
  14. Daud, M. Improving the accuracy of early software size estimation using analysis-to-design adjustment factors (ADAFs) / M. Daud, A. A. Malik // IEEE Access. – 2021. – Vol. 9. – P. 81986–81999. DOI: 10.1109/ACCESS.2021.3085752
  15. Efficiency improvement of function point-based software size estimation with deep learning model / [K. Zhang, X. Wang, J. Ren et al.] // Los Alamitos: IEEE. – 2021. – Vol. 9. – P. 107124–107136. DOI: 10.1109/ACCESS.2020.2998581
  16. Ritu. Comparative Analysis of Machine Learning Techniques in Effort Estimation / Ritu, Y. Garg // Proceedings of the 2022 International Conference on Machine Learning, Big Data, Cloud and Parallel Computing (COM-IT-CON), Faridabad, India, 2022 : proceedings. – Los Alamitos: IEEE, 2022. – P. 401–405, DOI: 10.1109/COM-IT-CON54601.2022.9850592
  17. Brar P. A Systematic Literature Review of Machine Learning Techniques for Software Effort Estimation Models / P. Brar, D. Nandal // Proceeding of the 2022 Fifth International Conference on Computational Intelligence and Communication Technologies (CCICT), Sonapat, India, 08–09 July 2022 – Los Alamitos: IEEE, 2022. – P. 494–499, DOI: 10.1109/CCICT56684.2022.00093
  18. Software Effort Estimation using Machine learning Algorithm / [Y. Assefa, F. Berhanu, A. Tilahun et al.] // Proceeding of the 2022 International Conference on Information and Communication Technology for Development for Africa (ICT4DA), Bahir Dar, Ethiopia, 28–30 November 2022 : proceedings. – Los Alamitos : IEEE, 2022. – P. 163–168, DOI: 10.1109/ICT4DA56482.2022.9971209
  19. Effective Software Effort Estimation Leveraging Machine Learning for Digital Transformation / [A. Jadhav, S. K. Shandilya, I. Izonin et al.] // IEEE Access. – 2023. – Vol. 11. – P. 83523–83536. DOI: 10.1109/ACCESS.2023.3293432
  20. A Review of Effort Estimation in Agile Software Development using Machine Learning Techniques / [S. Kumar, M. Arora, Sakshi et al.] // Proceedings of the 2022 4th International Conference on Inventive Research in Computing Applications (ICIRCA), Coimbatore, India, 21–23 September 2022 : proceedings. – Los Alamitos: IEEE. – P. 416–422. DOI: 10.1109/ICIRCA54612.2022.9985542
  21. R. K. B. N. Software Effort Estimation using ANN (Back Propagation) / R. K. B. N., Y. Suresh // Proceedings of the 2023 7th International Conference on Computing Methodologies and Communication (ICCMC), Erode, India, 23–25 February 2023 : proceedings. – Los Alamitos : IEEE. – P. 1–2, DOI: 10.1109/ICCMC56507.2023.10084264.
  22. Applying Machine Learning to Estimate the Effort and Duration of Individual Tasks in Software Projects / [A. O. Sousa, D. T. Veloso, H. M. Gonçalves et al.] // IEEE Access. – 2023. – Vol. 11. – P. 89933–89946. DOI: 10.1109/ACCESS.2023.3307310
  23. Nassif A.B. Software effort estimation from use case diagrams using nonlinear regression analysis / A. B. Nassif, M. AbuTalib, L. F. Capretz // Electrical and Computer Engineering : IEEE Canadian Conference CCECE'20, London, ON, Canada, 30 Aug.–2 Sept., 2020 : proceedings. – IEEE, 2020. – P. 1–4. DOI: 10.1109/CCECE47787.2020.9255712.
  24. Prykhodko S. Estimating the efforts of mobile application development in the planning phase using nonlinear regression analysis / S. Prykhodko, N. Prykhodko, K. Knyrik // Applied Computer Systems. – 2020. – Vol. 25, No. 2. – P. 172–179. DOI: 10.2478/acss-2020-0019
  25. Parametric Software Effort Estimation Based on Optimizing Correction Factors and Multiple Linear Regression / [H. L. T. K. Nhung, V. V. Hai, R. Silhavy et al.] // IEEE Access. – 2022. – Vol. 10. – P. 2963–2986. DOI: 10.1109/ACCESS.2021.3139183
  26. Effort Estimation of Software products by using UML Sequence models with Regression Analysis / [P. Sahoo, D. K. Behera, J. R. Mohanty et al.] // Proceedings of the 2022 OITS International Conference on Information Technology (OCIT), Bhubaneswar, India, 14–16 December 2022 : proceedings. – Los Alamitos : IEEE. – P. 97–101. DOI: 10.1109/OCIT56763.2022.00028.
  27. Cibir E. An Empirical Study on Software Test Effort Estimation for Defense Projects / E. Cibir, T. E. Ayyildiz // IEEE Access. – 2022. – Vol. 10. – P. 48082–48087. DOI: 10.1109/ACCESS.2022.3172326
  28. Power Grid Software Cost Estimation Based on Improved COCOMO Model / [X. Yuan, J. Su, C. Yu and S. Ye] // Proceeding of the 2023 IEEE 3rd International Conference on Electronic Technology, Communication and Information (ICETCI), Changchun, China, 26–28 May 2023 : proceedings. – Los Alamitos : IEEE. – P. 1265–1269, DOI: 10.1109/ICETCI57876.2023.10176686
  29. Outlier Detection in Non-Linear Regression Analysis Based on the Normalizing Transformations / [S. Prykhodko, N. Prykhodko, L. Makarova et al.] // Proceedings of the 15th International Conference on Advanced Trends in Radioelectronics, Telecommunications and Computer Engineering (TCSET), IEEE, Lviv-Slavske, 25–29 February 2020 : proceeding. – Los Alamitos : IEEE. – P. 407–410. DOI: 10.1109/TCSET49122.2020.235464
  30. CodeMR [Electronic resource]. – Access mode: <https://plugins.jetbrains.com/plugin/10811-codemr>
  31. Mardia K. V. Measures of multivariate skewness and kurtosis with applications / K. V. Mardia // Biometrika. – 1970. – Vol. 57. – P. 519–530. DOI: 10.1093/biomet/57.3.519
  32. Frost J. Overfitting Regression Models: Problems, Detection, and Avoidance [Electronic resource]. – Access mode: <https://statisticsbyjim.com/regression/overfitting-regression-models/>

# НЕЙРОІНФОРМАТИКА ТА ІНТЕЛЕКТУАЛЬНІ СИСТЕМИ

## NEUROINFORMATICS AND INTELLIGENT SYSTEMS

UDC 004.94

### REFINEMENT AND ACCURACY CONTROL OF THE SOLUTION METHOD FOR THE DURABILITY PROBLEM OF A CORRODING STRUCTURE USING NEURAL NETWORK

**Brychkovskiy O. D.** – Post-graduate student of the Department of Information Systems, Ukrainian State University of Chemical Technology, Dnipro, Ukraine.

#### ABSTRACT

**Context.** The prediction of the time until failure of corroding hinge-rod structures is a crucial component in risk management across various industrial sectors. An accurate solution to the durability problem of corroding structures allows for the prevention of undesired consequences that may arise in the event of an emergency situation. Alongside this, the question of the effectiveness of existing methods for solving this problem and ways to enhance them arises.

**Objective.** The objective is to refine the method of solving the durability problem of a corroding structure using an artificial neural network and establish accuracy control.

**Method.** To refine the original method, alternative sets of input data for the artificial neural network which increase information about the change in axial forces over time are considered. For each set of input data a set of models is trained. Based on target metric values distribution among the obtained sets, a set is selected where the minimum value of the mathematical expectation of the target metric is achieved. For the set of models corresponding to the identified best set, accuracy control of the method is determined by establishing the relationship between the mathematical expectation of the target metric and the parameters of the numerical solution.

**Results.** The conditions under which a lower value of the mathematical expectation of the target metric is obtained compared to the original method are determined. The results of numerical experiments, depending on the considered case, show, in average, an improvement on 43.54% and 9.67% in the refined method compared to the original. Additionally, the proposed refinement reduces the computational costs required to find a solution by omitting certain steps of the original method. An accuracy control rule of the method is established, which allows to obtain on average a given error value without performing extra computations.

**Conclusions.** The obtained results indicate the feasibility of applying the proposed refinement. A higher accuracy in predicting the time until failure of corroding hinge-rod structures allows to reduce the risks of an emergency situation. Additionally, accuracy control enables finding a balance between computational costs and the accuracy of solving the problem.

**KEYWORDS:** artificial neural networks, accuracy control, distribution, mathematical expectation, approximation, numerical methods, durability corroding structure.

#### ABBREVIATIONS

AE is an aggressive environment;  
ANN is an artificial neural network;  
CPU is a central process unit;  
DE is a differential equation;  
FEM is a finite elements method;  
GPU is a graphical process unit;  
MSE is a mean square error;  
HRS is a hinge-rod structure;  
PDCS is the problem of durability of a corroding structure;  
RMSE is a root mean square error;  
RPROP is a resilient propagation;  
SDE is a system of differential equations.

#### NOMENCLATURE

$A_0$  is an initial area of the section;  
 $A^i$  is a cross-sectional area of the  $i$ -th structural element;  
 $a$  is a coefficient of a polynomial of degree 3 approximating the dependence of axial forces  $Q_j$  in structural elements on time  $t$ ;  
 $B$  is a bias unit;  
 $b$  is a coefficient of a polynomial of degree 3 approximating the dependence of axial forces  $Q_j$  in structural elements on time  $t$ ;  
 $c$  is a coefficient of a polynomial of degree 3 approximating the dependence of axial forces  $Q_j$  in structural elements on time  $t$ ;  
 $D$  is a differentiation matrix;  
 $d$  is a number of neurons in the ANN input layer;  
 $E$  is an elasticity matrix;

$i$  is an index of HRS element;  
 $i_0$  is an index of HRS element that first fails;  
 $j$  is a number of nodes of the finite-difference grid;  
 $K$  is a stiffness matrix;  
 $k$  is a coefficient of influence of stress on the rate of the corrosion process;  
 $N$  is a number of structural elements;  
 $n$  is both training and test dataset size;  
 $n_{\text{test}}$  is a number of samples in the test dataset;  
 $P_0$  is an initial perimeter of the section;  
 $Q^i$  is a value of the axial force in the  $i$ -th structural element;  
 $Q_j$  is values of axial forces at nodal points of the approximate solution  $\tilde{t}$  ;  
 $\bar{R}$  is a vector of nodal loads;  
 $s$  is a number of neurons in the ANN hidden layer;  
 $T_j$  is a time values at  $j$  nodal points of the approximate solution  $\tilde{t}$  ;  
 $t$  is a time;  
 $t^*$  is a reference numerical solution of the PDCS, obtained at a large number of nodal points;  
 $\tilde{t}$  is a approximate numerical solution of the PDCS, obtained with lower computational costs than for the reference;  
 $t_i^*$  is a reference solution of the PDCS for the  $i$ -th sample;  
 $t_i^*(u)$  is an approximate solutions of the PDCS for the  $i$ -th sample;  
 $\bar{u}$  is vector of displacements;  
 $v_0$  is a corrosion rate in the absence of stress;  
 $Z$  is a number of weight coefficients;  
 $\alpha$  is a shape parameter of the two-parameter inverse gamma distribution;  
 $\beta$  is a scale parameter of the two-parameter inverse gamma distribution;  
 $\Gamma(\cdot)$  is a gamma function.  
 $\bar{\delta}$  is a vector of values of the depth of corrosion damage of each structural element;  
 $\delta^i(t)$  is a value of the depth of corrosion damage in the  $i$ -th structural element (damage parameter);  
 $\bar{\varepsilon}$  is a vector of deformations;  
 $\varepsilon_i$  is a value of the target function for the  $i$ -th sample;  
 $\varepsilon_i(u)$  is an output value of the model from  $M_u$  for the  $i$ -th sample;  
 $\sigma^i$  is a current stress in the  $i$ -th structural element;  
 $\sigma_0$  is an initial stress;  
 $\bar{\sigma}$  is a vector of stresses;  
 $[\sigma]$  is an yield stress.

## INTRODUCTION

In many strategic industrial sectors including nuclear and thermal energy, chemical and petrochemical industries, the use of metal structures in aggressive environments leading to corrosion is involved. Corrosion is a primary factor contributing to the catastrophic failure of

© Brychkovskyi O. D., 2024

DOI 10.15588/1607-3274-2024-1-9

equipment, which can be accompanied by significant financial losses and severe environmental consequences [1]. Ensuring the ability to respond promptly to the mentioned risks raises the relevant issue of determining the duration during which a structure will perform its functions – the durability of the structure. This matter is typically addressed through computer modeling. Moreover, the latter is complicated by the fact that the rate of the corrosion process is influenced by mechanical stresses in the structural elements. Existing models of corrosion-induced deformation consist of systems of differential equations and systems of mechanics equations, the solution of which requires significant computational costs. To solve the problem of reducing computing costs in 2021, Zelenstov D.G., Korotka L.I. and Denysiuk O.R. proposed (see [2]) a method for solving the PDCS using ANN (hereinafter Method). However, the authors do not consider the problem of establishing accuracy control of Method. Also, in [2] and related approaches (see, for example, [3, 4]), the dependence of the output of the neural network model on the set of initial values of the weight coefficients of the neural network is not taken into account. These coefficients represent the realization of a certain random variable, meaning that depending on a particular realization, the output of the neural network, in general, will be different. Therefore, it is appropriate to consider not just the individual result in the form of the output of the neural network, but rather certain characteristics of the distribution of the results, such as mathematical expectation.

The paper investigates the refinement of the method proposed in [2] and establishes accuracy control. At the same time, the presence of the aforementioned dependence of the ANN's output on a set of random initial values of weight coefficients is taken into account.

The **object of the study** is the problem of accuracy-controlled numerical analysis of the problem of solving PDCS.

The **subject of the study** is artificial neural networks as a means of enhancing the efficiency of numerical methods while simultaneously ensuring a specified level of result accuracy.

The **purpose of the study** is to refine the method of solving PDCS using ANN and establish accuracy control rule.

## 1 PROBLEM STATEMENT

Let's consider the model of corrosive deformation of HRS operating in aggressive environments based on the FEM (for more details, see [2, 5]):

$$\frac{d\delta^i(t)}{dt} = v_0 \cdot \left(1 + k \cdot \sigma_i \left(A^i(\delta^i(t)), Q^i(\bar{\delta})\right)\right), \quad (1)$$

$$\delta^i(t)\Big|_{t=0} = 0; \quad i = \overline{1, N}.$$

Assuming  $Q = \text{const}$ , by knowing the solutions  $\delta_i(t)$  of the differential equations (1) and the limit values of the corrosion damage depths  $\delta_i^*$  one can find the time values  $t_i = t_i^*$ , at which the  $\delta_i^*$  values are reached. The value  $t_{i0}^* = \min t_i^*, i = (1, N)$  is referred to as the durability of the structure. To calculate  $\sigma_i$  in the right-hand side of (1) deformable solid mechanics equation are utilized, which in the form of the FEM system of equations are represented as:

$$\begin{cases} \bar{R} = K^{-1} \cdot \bar{u}, \\ \bar{\varepsilon} = D \cdot \bar{u}, \\ \bar{\sigma} = E \cdot \bar{\varepsilon}. \end{cases} \quad (2)$$

As the cross-sectional areas of elements change during the process of corrosive wear, the elements of the structural stiffness matrix  $K$ , as well as the stresses  $\sigma_i$  in the elements, vary over time. Thus, in the numerical solution of (1), it is necessary to compute (2) at each node of the finite difference grid. This significantly increases computational costs.

Methods that address the issue of reducing computational costs may require both the absence of accuracy loss and the ability to control this accuracy. Therefore, following the Method in [2], we will explore the problem of its refinement and accuracy control. By accuracy of the method, will mean the value of the mathematical expectation of the target metric – E(RMSE); by refinement of the method – identification of conditions that allow reducing the value of E(RMSE) compared to the corresponding value of the inherited method without, at least, increasing computational costs; and by accuracy control – determination of the dependence between the values of E(RMSE) and the parameters of the approximate solution.

## 2 REVIEW OF THE LITERATURE

The use of Artificial Neural Networks (ANNs) in the algorithm for controlling the accuracy of numerical solution of the differential equation of the form (1) was proposed in [3]. The authors considered a trained ANN, which determined the parameter of numerical integration to achieve the specified solution error. This method was further developed in [4], where instead of training separate ANNs for different error values, a unified ANN with the error value as an input parameter was suggested. A common feature of these algorithms is the ignoring of changes in axial forces in elements of corroding structures during the formation of training samples for ANNs. As a result, the predicted error value did not always meet the specified level.

In [2], a method of correction functions was proposed, in which the solution of the PDCS was approximated with minimal computational costs and refined using a correction function. The corrective function included an ANN that approximated the dependency between the error of

the approximate solution and certain input parameters of the PDCS, including the coefficients of a polynomial used to describe the variation in time of axial forces in the HRS elements. The coefficients of this polynomial were determined at the stage of finding the approximate solution of the PDCS. This approach reduced computational costs and solved the problem of taking into account changes in axial forces over time, but the problem of accuracy control of the algorithm remained open.

## 3 MATERIALS AND METHODS

First, let's outline the general scheme of refining the Method, after which we will proceed to a more detailed exposition. The general refinement scheme of the Method consists of the following steps:

1) by varying the input parameters sets of the ANN, the Method will be using to solve the PDCS. In other words, models will be training according to the Method on different input parameters sets, including the proposed Method set;

2) let's create a set  $V$ , which includes  $L$  different sets of initial values of weight coefficients  $\{w_p\}_{p=1}^P, w_p \in [0, 1]$ , where  $P$  – the number of weight coefficients. The procedure from the previous step for each input parameters set and for each element of set  $V$  will be performed. As a result, for each input parameters set, we will have a distribution of target metric values; the distribution parameters will be estimated using the maximum likelihood method [6];

3) for each distribution calculate the mathematical expectation and compare the obtained values;

4) the input parameters set on which the smallest value of the mathematical expectation is achieved is the sought-after condition that refines the Method, if at least it does not increase computational costs at the stage of applying the obtained refinement. Remark: we ignore changes in computational costs arising from a certain increase in the number of input parameters of the ANN, because the application stage of the Method requires the existence of a previously trained ANN.

Let's now consider in more detail the outlined scheme, using also [2].

Dataset forming. A sample of volume  $n$  with training samples is generated, containing construction parameters  $A_0, P_0, [\sigma]$ , environmental parameters  $(v_0, k)$ , value  $t^*$  of the reference solution of the PDCS, time values and axial forces  $(T_j, Q_j)$  at  $j = 4$  nodal points  $T_j = \{t_1, t_2, \dots, t_j\}$  and  $Q_j = \{q_1, q_2, \dots, q_j\}$ , where  $t_j = \tilde{t}$ , coefficients  $(a, b, c)$  of a polynomial of degree 3 that approximates the dependence  $Q(t)$  at points  $(T_j, Q_j)$ . The target function is defined

as the error  $\varepsilon = \frac{t^*}{\tilde{t}}$  between the reference and approximate solutions of the PDCS.

Models training. To refine the Method, we will consider sets of input parameters that enhance the information about the variation of axial forces over time compared to those proposed in the Method. Let's define the set  $V$  and on the next sets of input parameters for the

ANN:  $u_{a,b,c} = (A_0, P_0, \sigma_0, a, b, c)$ ,  
 $u_{a,b,c,T_j} = (A_0, P_0, \sigma_0, a, b, c, T_j)$ ,  $u_{Q_j} = (A_0, P_0, \sigma_0, Q_j)$ ,  
 $u_{Q_j,T_j} = (A_0, P_0, \sigma_0, Q_j, T_j)$  will be trained  $L$  models accordingly. These sets of  $L$  models will be denoted as  $M_{(a,b,c)}$ ,  $M_{((a,b,c),T)}$ ,  $M_{(Q)}$ ,  $M_{(Q,T)}$ , or simply  $M_u$ , when referring to the set of models corresponding to a specific  $u$  as defined above. Note that  $u_{a,b,c}$  is the set which is used in the Method itself; hence, this set will be referred to as the base set, and the set of models  $M_{(a,b,c)}$  – will be called the set of base models. As the metric to be minimized during the training of the ANN, we will consider

$$\text{MSE} = \frac{1}{n_{\text{test}}} \sum_{i=1}^{n_{\text{test}}} (\varepsilon_i - \varepsilon_i(u))^2$$

PDCS will have the form  $t^*(u) = \tilde{t} \cdot \varepsilon(u)$ , which means  $t^* \approx \tilde{t} \cdot \varepsilon(u)$ .

Distributions constructing. To each model from  $M_u$  will assign the value of the target metric

$$\text{RMSE} = \sqrt{\frac{1}{n_{\text{test}}} \sum_{i=1}^{n_{\text{test}}} (t_i^* - t_i^*(u))^2}$$

the value of the MSE metric depends, among other things, on the set of initial weight coefficients of the ANN  $\{w_z\}_{z=1}^Z, w_z \in [0,1]$ , which is an realization of a random variable  $W$ , (in practice, it can be, for example,  $W \sim U([0,1])$ ). Thus, under the defined conditions, MSE, and consequently RMSE, are functions of the random variable  $W$ . Having obtained the set  $M_u$  comprising  $L$  models, where the latter differ only in the initial sets  $\{w_z^l\}$ ,  $z = \overline{1, Z}$ ,  $l = \overline{1, L}$ , can be constructed the distribution of the target metric RMSE for each set  $M_u$  find estimates of its parameters, and calculate the mathematical expectation  $E(\text{RMSE})$ .

Refinement of the Method. The set  $u_0$ , which corresponds to the smallest value of mathematical expectation (or the best set), is the sought-after condition that refines the Method.

Accuracy control rule. Let  $J = \{2, 3, \dots, j'\}$ . For the identified best set, will be constructed several sets  $M_{u_0}(j)$  each of size  $L'$ , where  $j \in J$ . For each of these sets, values of  $E(\text{RMSE}(j))$  will be calculated. By approximating the points  $(j, E(\text{RMSE}(j)))$ ,  $j \in J$ , will be built the dependency  $y = g(x)$ ,  $x \in [2, \infty)$ ,  $y \in (0, \infty)$ . The function  $h(y) = [g^{-1}(y)]^-$ ,  $h(y) \in \{2, 3, \dots, j', \dots\}$ , where  $[\cdot]^-$  denotes rounding to the nearest integer value, represents the sought dependence between the values of  $E(\text{RMSE})$  and the number of required nodes  $j$ , which are parameters of the approximate solution.

#### 4 EXPERIMENTS

For further research, two cases were considered based on the nature of the variation of axial forces  $Q$  over time  $t$  in the elements of the corroding structure, differing in the

number of monotonicity intervals. The number of monotonicity intervals in this case affects the quality of approximation of these dependencies by a polynomial of degree 3. In case A there is one monotonicity interval, while in case B there are two monotonicity intervals. The graphs illustrating the variation of axial forces over time and their approximation by a polynomial of degree 3 at 4 nodes are presented in Fig. 1 and Fig. 2 for case A and case B, respectively.

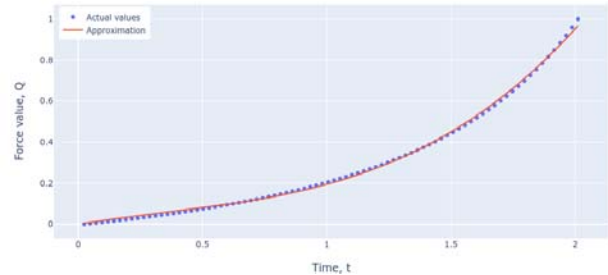


Figure 1 – Case A. One interval of monotonicity

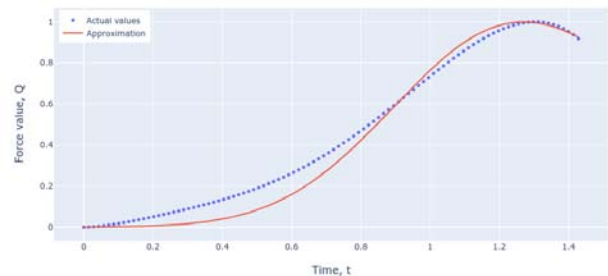


Figure 2 – Case B. Two interval of monotonicity

For numerical experiments, two datasets were generated for case A and case B, each containing  $n = 20,000$  samples. An I-beam profile was chosen as the type of the leading element of the HRS. Initial geometric parameters of the I-beam profile for each sample were randomly selected from the set of standard sizes defined for this type of profile. The datasets were divided into training and testing sets in a ratio of 70% to 30%, meaning the training set consisted of 14,000 samples and the testing set of 6,000 samples.

The architecture of the ANN takes the form of a multi-layer perceptron (see Fig. 3) with dimensions  $d \times s \times 1$ , where  $d$  equal to the number of features in the input set,  $s = 2 \cdot d + 1$  calculating according to the Hecht-Nielsen theorem [7]. The activation function for the hidden and output layers is Sigmoid [8]. Each model was trained for 1000 epochs using the RPROP learning algorithm [9] in batch mode.

The number of models  $L$  for refining the method is equal to 100. The number of models  $L$  for determining the accuracy control is equal to 500. According to the values of  $L$  and  $L'$ , sets  $V$  and  $V'$  of random seed values are generated from a discrete uniform distribution, which is equivalent to creating sets of initial weight coefficient values.

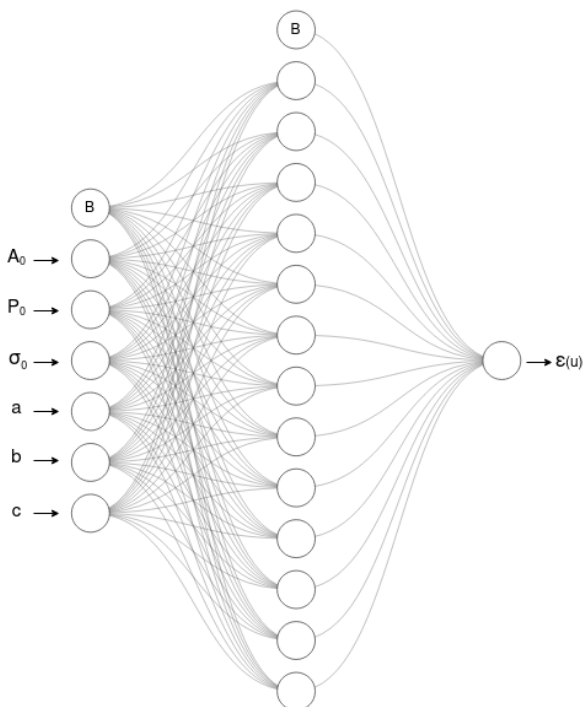


Figure 3 – ANN architecture for the base model

To obtain distributions of RMSE values for models from the sets  $M_u, M_{u_0}(j), j \in J = \{2, 3, 4, 6, 8, 12, 16\}$ , a two-parameter inverse gamma distribution [10] is considered as a hypothetical distribution, and its probability

density function is given by

$$f(x, \alpha, \beta) = \frac{\beta^\alpha}{\Gamma(\alpha)} \cdot \left(\frac{1}{x}\right)^{\alpha+1} \cdot \exp\left(\frac{-\beta}{x}\right), x > 0.$$

The distribution parameters  $\alpha$  and  $\beta$  are estimated using the maximum likelihood method, and the mathematical expectation of the distribution is calculated as  $\frac{\beta}{\alpha - 1}$  for  $\alpha > 1$ .

The implementation of this approach was carried out in the PyCharm and Jupyter Notebook environments using the Python programming language and the following modules and libraries: Numpy, Pandas, scikit-learn for data preprocessing and manipulation; module stats from SciPy for working with probability distributions; Plotly for data visualization. The PyTorch machine learning framework [11] was chosen for working with ANNs. Computations were performed on a CPU 3.7 GHz AMD Ryzen 9 5900X, a GeForce RTX 3060 GPU, and 32GB of RAM.

### 5 RESULTS

For each set  $M_u, L$  models were trained with different initial values of weight coefficients. Based on the results of these models, distributions for RMSE values were constructed. Table 1 presents the mean RMSE values and mathematical expectations  $E(RMSE)$  for the sets of obtained models.

Table 1 – Results of models training

	$M_{(Q,T)}$	$M_{(Q)}$	$M_{(a,b,c,T)}$	$M_{(a,b,c)}$
Case A, mean(RMSE)	$1.20626 \cdot 10^{-3}$	$1.47549 \cdot 10^{-3}$	$1.91016 \cdot 10^{-3}$	$2.13634 \cdot 10^{-3}$
Case A, E(RMSE)	$1.20624 \cdot 10^{-3}$	$1.47031 \cdot 10^{-3}$	$1.91096 \cdot 10^{-3}$	$2.13673 \cdot 10^{-3}$
Case B, mean(RMSE)	$4.311255 \cdot 10^{-2}$	$4.376519 \cdot 10^{-2}$	$4.730537 \cdot 10^{-2}$	$4.762757 \cdot 10^{-2}$
Case B, E(RMSE)	$4.311258 \cdot 10^{-2}$	$4.376514 \cdot 10^{-2}$	$4.730537 \cdot 10^{-2}$	$4.772759 \cdot 10^{-2}$

Thus, in comparison with the baseline set, for case A, the mathematical expectation value corresponding to the best set is less by

$$\left(0.0021364 \cdot 10^{-3} - 0.00120626 \cdot 10^{-3}\right) \cdot 100\% \approx 43.54\% ;$$

and for case B, it is less by

$$\left(0.04772759 \cdot 10^{-2} - 0.04311258 \cdot 10^{-2}\right) \cdot 100\% \approx 9.67\% .$$

The constructed distributions for case A and case B are shown in Fig. 4 and Fig. 5, respectively.

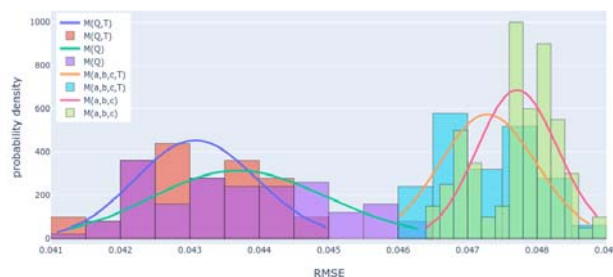


Figure 5 – RMSE distributions of trained models for case B

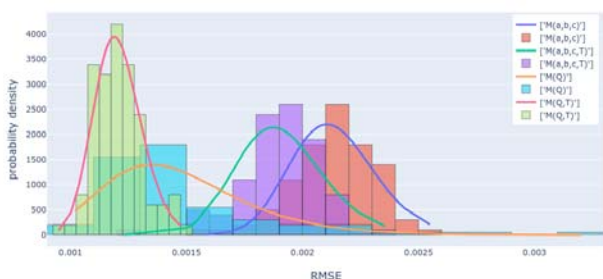


Figure 4 – RMSE distributions of trained models for case A

For the best set  $u_{Q_j, T_j}$   $L$  models were built for each number of nodes  $j$  from  $J$ . For each set of obtained models, distributions were constructed, and the mathematical expectations  $E(RMSE)$  were calculated. Fig. 6 shows the correspondence between  $E(RMSE)$  values and number of nodes  $j$ , their approximation by the function  $y = g(x) = a \cdot (x+c)^b$ , which obtained based on points  $j \in \{2, 3, 4, 6\}$ , and the mean values of RMSE before refining the solution using artificial neural network (the mean value of RMSE at the point  $j = 2$  is equal to 0.10217255).

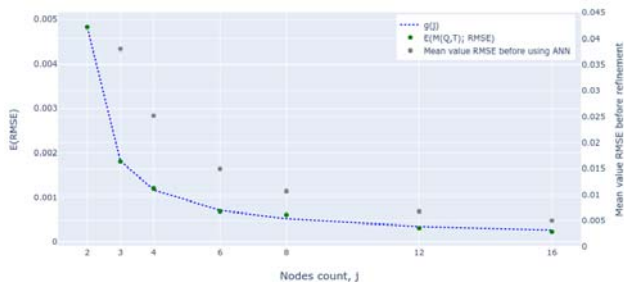


Figure 6 – Graph of the approximate dependence of E(RMSE) on the number of nodes

Table 2 provides consolidated information about dependence between E(RMSE) and number of nodes  $j$  based on approximation by points  $j \in \{2, 3, 4, 6\}$ . Accordingly, at points  $j < 6$ , the behavior of the obtained approximation is demonstrated on the data to which the approximating function was fitted, and at  $j > 6$  on new data.

Table 2 – Dependence of E(RMSE) on the number of nodes  $j$  based on approximation

$j$	E(RMSE)	$g(j)$
2	0.0048214	0.0048209
3	0.0018037	0.0018175
4	0.0012030	0.0011706
6	0.0006873	0.0007089
8	0.0006061	0.0005188
12	0.0003082	0.0003457
16	0.0002238	0.0002631

Using the function  $g^{-1}(y)$  a function was constructed:

$$h(y) = \left[ g^{-1}(y) \right]^{\sim} = \left[ \left( \frac{y}{a} \right)^{\frac{1}{b}} - c \right]^{\sim}, \quad (3)$$

where  $a = 0.00249686$ ,  $b = -0.84226492$ ,  $c = -1.54206767$ , which is the sought accuracy control rule for the Method. The graph of the obtained accuracy control rule is shown in Fig. 7.

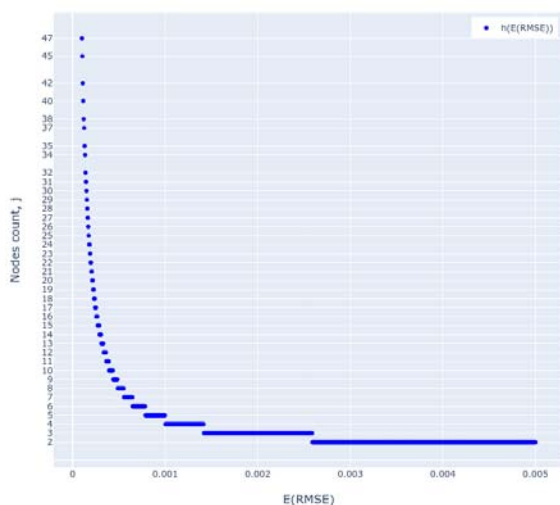


Figure 7 – Graph  $h(y)$

## 6 DISCUSSION

The smallest value of the mathematical expectation of the target metric E(RMSE) for both case A and case B corresponds to the set  $u_{Q,T}$ . At the same time, the E(RMSE) value of the base set  $u_{a,b,c}$  is the largest for both cases. This allows us to conclude that all proposed sets refine the results of the Method. Note that the set  $u_{a,b,c}$  contains the least information about the variation of axial forces over time compared to other sets. Additionally, the models from the set  $M_{(Q,T)}$  do not require a separate approximation of the dependence of axial forces when obtaining input data for ANN. This reduces computational costs in solving PDCS.

The obtained accuracy control rule for the method (3) takes the form of a piecewise-linear function. It allows for determining the necessary number of nodes in a finite-difference grid immediately for a desired value of the mathematical expectation of RMSE. Subsequently, using the obtained value of the number of nodes  $j$  as a parameter in the search for an approximate solution  $\tilde{t}$ , it is possible to construct a set  $M_{u_0}(j)$  to which the model corresponding to the desired RMSE value belongs.

Analyzing the graph in Figure 6, it can be observed that with an increase in the number of nodes  $j$  the distance between the mean value of RMSE before refining the solution  $\tilde{t}$  and the corresponding value of E(RMSE) after refinement decreases. This can be interpreted as follows: the more nodal points we use to find the approximate solution, the closer it becomes to the reference solution. Consequently, there is a reduction in the error value remaining for the refinement of the ANN.

Depending on the accuracy requirements of the method, instead of the mathematical expectation, other distribution characteristics, such as quintile values, etc., may be considered. Additionally, it may be relevant to introduce a penalty for errors leading to an overestimation of the structure's durability in the metric being optimized.

## CONCLUSIONS

**The scientific novelty:** Developed an approach for solving PDCS using ANN. The existing method was refined by revising the input parameters to the ANN and, as a result, abandoned the approach of preliminary approximation of the dependence of axial forces on time. The dependency of the target metric mathematical expectation on the numerical solution parameters was identified, making the method accuracy-controllable. The evaluation of the models took into account the dependence of the ANN output on random initial values of weight coefficients.

**The practical significance:** According to the results of numerical studies, it was established that, depending on the case under consideration, the refinement allows a reduction in the error by an average on 9.54% and 43.54% compared to the original method. The potential impact of implementing the proposed model lies in more accurately predict the durability of corroding hinge-rod structures in terms of mathematical expectation, thereby reducing the risk of emergency situations and associated finan-

cial and environmental consequences. The accuracy control of the method allows solving PDCS with the required accuracy while reducing unnecessary computations.

**Prospects for further research** are the consideration of the possibility to introduce a penalty for errors that lead to an overestimation of the HRS predicted failure time for the metric being optimized, and the study of the application of the proposed approach in other related problems, for example, for the calculation of the constraint function in the problem of the HRS optimization.

#### ACKNOWLEDGEMENTS

The author expresses gratitude to Dmytro Zelentsov, Doctor of technical science, professor and Head of Department of Information Systems of Ukrainian State University of Chemical Technology for his valuable advice and constructive discussion during the planning and development of this study.

#### REFERENCES

1. Khoma M. C. State and Prospects of Research Development in the Field of Corrosion and Corrosion Protection of Construction Materials in Ukraine: According to the Materials of Report at the Meeting of the Presidium of NAS of Ukraine, October 27, 2021, *Visn. Nac. Akad. Nauk Ukr.*, 2021, pp. 99–106. DOI: <https://doi.org/10.15407/visn2021.12.099>
2. Zelentsov D. G., Korotka L. I., Denysiuk O. R. The Method of Correction Functions in Problems of Optimization of Corroding Structures, *Advances in Computer Science for Engineering and Education III. ICCSEE 2020. Advances in Intelligent Systems and Computing*, 2020, Vol. 1247, pp. 132–142. DOI: [https://doi.org/10.1007/978-3-030-55506-1\\_12](https://doi.org/10.1007/978-3-030-55506-1_12)
3. Zelentsov D. G., Korotkaya L. I. Use of neural networks at the decision of problems durability of designs subject to corrosion, *Transactions of Kremenchuk Mykhailo Ostrohradskiy National University*, 2011, № 3 (68), Part 1, pp. 24–27.
4. Denysiuk O. R. Determination of rational parameters for the numerical solution of systems of differential equations, *Visnyk of Kherson National Technical University*, 2016, № 3(58), pp. 208–212.
5. Zelentsov D. G., Korotkaya L. I. Technologies of computational intelligence in problems of modeling dynamic systems, *Monograph. Balans-Klub*, 2018, P. 179. DOI: 10.32434/mono-1-ZDG-KLI
6. Rudenko V. M. *Matematychna statystyka. Navch. Posib.* Kyiv, Tsentru uchbovoi literatury, 2012, 304 p.
7. Hecht-Nielsen R. Kolmogorov's mapping neural network existence theorem, *IEEE First Annual Int. Conf. on Neural Networks*, 1987, Vol. 3, pp. 11–13.
8. Goyal M., Goyal R., Venkatappa Reddy P., Lall B. In: Pedrycz W., Chen S.-M. (eds) *Activation Functions, Deep Learning: Algorithms and Applications. Studies in Computational Intelligence*, 2020, Vol. 865, pp. 1–28. DOI: [https://doi.org/10.1007/978-3-030-31760-7\\_1](https://doi.org/10.1007/978-3-030-31760-7_1)
9. Riedmiller M., Braun H. A direct adaptive method for faster backpropagation learning: The RPROP algorithm, *Proc. IEEE Int. Conf. Neural Netw.*, 1993, pp. 586–591. DOI: 10.1109/ICNN.1993.298623
10. Cook J. D. Inverse gamma distribution. Online: [http://www.johndcook.com/inverse\\_gamma.pdf](http://www.johndcook.com/inverse_gamma.pdf), Technical. Report, 2008.
11. Ketkar N., Moolayil J. Introduction to PyTorch. In: *Deep Learning with Python*. Apress, Berkeley, CA, 2021, pp. 27–91. DOI: [https://doi.org/10.1007/978-1-4842-5364-9\\_2](https://doi.org/10.1007/978-1-4842-5364-9_2)

Received 25.12.2023.  
Accepted 31.01.2024.

УДК 004.94

### УТОЧНЕННЯ І КЕРОВАНІСТЬ ЗА ТОЧНІСТЮ МЕТОДУ РОЗВ'ЯЗАННЯ ЗАДАЧІ ДОВГОВІЧНОСТІ КОРДУЮЧОЇ КОНСТРУКЦІЇ ІЗ ВИКОРИСТАННЯМ НЕЙРОННОЇ МЕРЕЖІ

**Бричковський О. Д.** – аспірант кафедри інформаційних систем Українського державного хіміко-технологічного університету, Дніпро, Україна.

#### АНОТАЦІЯ

**Актуальність.** Прогнозування часу виходу з ладу кордуючих шарнірно-стрижневих конструкцій є важливою складовою управління ризиками багатьох сфер промисловості. Точний розв'язок задачі довговічності кордуючої конструкції дозволяє попередити ряд небажаних наслідків, що виникають у разі настання аварійної ситуації. Разом з цим постає питання ефективності існуючих методів розв'язання даної задачі та способів їх покращення.

**Мета роботи** полягає в уточненні методу розв'язання задачі довговічності кордуючої конструкції із використанням штучної нейронної мережі і встановлення керованості за точністю.

**Метод.** Для уточнення оригінального методу розглядаються альтернативні набори вхідних даних для штучної нейронної мережі, що дозволяють збільшити інформацію про зміну осьових зусиль у часі. Для кожного набору вхідних даних навчається множина моделей. На основі розподілів значень цільової метрики моделей із отриманих множин обирається набір, на якому досягається найменше значення математичного сподівання цільової метрики. Для множини моделей, що відповідає знайденому найкращому набору, визначається керованість за точністю методу шляхом встановлення залежності між математичним сподіванням цільової метрики і параметрами чисельного розв'язання.

**Результати.** Визначено умови, за яких отримано менше значення математичного сподівання цільової метрики порівняно з оригінальним методом. Результати чисельних експериментів, в залежності від розглядуваного випадку, показують в середньому на 43.54% і 9.67% кращі результати уточненого методу порівняно з оригінальним. Окрім цього, запропоноване уточнення зменшує необхідні для знаходження розв'язку обчислювальні витрати за рахунок відмови від деяких кроків оригінального методу. Отримано закон керованості методу за точністю, який дозволяє в середньому отримувати задане значення похибки без виконання зайвих обчислень.

**Висновки.** Отримані результати свідчать про доцільність застосування запропонованого уточнення. Більш висока точність прогнозування часу виходу з ладу кордуючих шарнірно-стрижневих конструкцій дозволяє зменшити ризики настан-

ня аварійних ситуацій, а керованість за точністю – знаходити баланс між обчислювальними витратами і точністю розв'язання задачі.

**КЛЮЧОВІ СЛОВА:** нейронна мережа, керованість за точністю, розподіл, математичне сподівання, апроксимація, чисельні методи, довговічність кородуючої конструкції.

#### ЛІТЕРАТУРА

1. Хома М. С. Стан і перспективи розвитку досліджень у галузі корозії та протикорозійного захисту конструкційних матеріалів в Україні / М. С. Хома // За матеріалами доповіді на засіданні Президії НАН України 27 жовтня 2021 року. Вісник НАН України. – 2021. – № 12. – С. 99–106. DOI: <https://doi.org/10.15407/vsn2021.12.099>
2. Zelentsov D. G. The Method of Correction Functions in Problems of Optimization of Corroding Structures / D. G. Zelentsov, L. I. Korotka, O. R. Denysiuk // Advances in Computer Science for Engineering and Education III. ICCSEEA 2020. Advances in Intelligent Systems and Computing. – 2020. – Vol. 1247. – P. 132–142. DOI: [https://doi.org/10.1007/978-3-030-55506-1\\_12](https://doi.org/10.1007/978-3-030-55506-1_12)
3. Zelentsov D. G. Use of neural networks at the decision of problems durability of designs subject to corrosion / D. G. Zelentsov, L. I. Korotkaya // Transactions of Kremenchuk Mykhailo Ostrohradskyi National University. – 2011. – № 3 (68), Part 1. – P. 24–27.
4. Denysiuk O. R. Determination of rational parameters for the numerical solution of systems of differential equations / O. R. Denysiuk // Visnyk of Kherson National Technical University. – 2016. – № 3(58). – P. 208–212.
5. Zelentsov D. G. Technologies of computational intelligence in problems of modeling dynamic systems / D. G. Zelentsov L. I. Korotkaya // Monograph. Balans-Klub. – 2018. – P. 179. DOI: [10.32434/mono-1-ZDG-KLI](https://doi.org/10.32434/mono-1-ZDG-KLI)
6. Руденко В. М. Математична статистика : навч. посіб. / В. М. Руденко. – К. : Центр учбової літератури, 2012. – С. 304.
7. Hecht-Nielsen R. Kolmogorov's mapping neural network existence theorem / R. Hecht-Nielsen // IEEE First Annual Int. Conf. on Neural Networks. – 1987. – Vol. 3. – P. 11–13.
8. Activation Functions / [M. Goyal, R. Goyal, Reddy P. Venkatappa, B. Lall] In: Pedrycz W., Chen S.-M. (eds) // Deep Learning: Algorithms and Applications. Studies in Computational Intelligence. – 2020. – Vol. 865. – P. 1–28. DOI: [https://doi.org/10.1007/978-3-030-31760-7\\_1](https://doi.org/10.1007/978-3-030-31760-7_1)
9. Riedmiller M. A direct adaptive method for faster back-propagation learning: The RPROP algorithm / M. Riedmiller, H. Braun // Proc. IEEE Int. Conf. Neural Netw. – 1993. – P. 586–591
10. Cook J. D. Inverse gamma distribution / J. D. Cook. // Online: [http://www.johndcook.com/inverse\\_gamma.pdf](http://www.johndcook.com/inverse_gamma.pdf), Technical. Report, 2008.
11. Ketkar N. Introduction to PyTorch / N. Ketkar, J. Moolayil // In: Deep Learning with Python. Apress, Berkeley, CA. – 2021. – P. 27–91. DOI: [https://doi.org/10.1007/978-1-4842-5364-9\\_2](https://doi.org/10.1007/978-1-4842-5364-9_2)

## METHOD OF GENERATIVE-ADVERSARIAL NETWORKS SEARCHING ARCHITECTURES FOR BIOMEDICAL IMAGES SYNTHESIS

**Berezsky O. M.** – Dr. Sc., Professor, Professor of the Department of Automated Control Systems, Lviv Polytechnic National University, Lviv, Ukraine.

**Liashchynskiy P. B.** – Post-graduate student of the Department of Automated Control Systems, Lviv Polytechnic National University, Lviv, Ukraine.

### ABSTRACT

**Context.** The article examines the problem of automatic design of architectures of generative-adversarial networks. Generative-adversarial networks are used for image synthesis. This is especially true for the synthesis of biomedical images – cytological and histological, which are used to make a diagnosis in oncology. The synthesized images are used to train convolutional neural networks. Convolutional neural networks are currently among the most accurate classifiers of biomedical images.

**Objective.** The aim of the work is to develop an automatic method for searching for architectures of generative-adversarial networks based on a genetic algorithm.

**Method.** The developed method consists of the stage of searching for the architecture of the generator with a fixed discriminator and the stage of searching for the architecture of the discriminator with the best generator.

At the first stage, a fixed discriminator architecture is defined and a generator is searched for. Accordingly, after the first step, the architecture of the best generator is obtained, i.e. the model with the lowest FID value.

At the second stage, the best generator architecture was used and a search for the discriminator architecture was carried out. At each cycle of the optimization algorithm, a population of discriminators is created. After the second step, the architecture of the generative-adversarial network is obtained.

**Results.** Cytological images of breast cancer on the Zenodo platform were used to conduct the experiments. As a result of the study, an automatic method for searching for architectures of generatively adversarial networks has been developed. On the basis of computer experiments, the architecture of a generative adversarial network for the synthesis of cytological images was obtained. The total time of the experiment was ~39.5 GPU hours. As a result, 16,000 images were synthesized (4000 for each class). To assess the quality of synthesized images, the FID metric was used. The results of the experiments showed that the developed architecture is the best. The network's FID value is 3.39. This result is the best compared to well-known generative adversarial networks.

**Conclusions.** The article develops a method for searching for architectures of generative-adversarial networks for the problems of synthesis of biomedical images. In addition, a software module for the synthesis of biomedical images has been developed, which can be used to train CNN.

**KEYWORDS:** generative adversarial network, biomedical images, cytological images, search for neural network architectures, genetic algorithms, FID metrics, computer systems for automatic diagnostics.

### ABBREVIATIONS

ATTN is a shorthand for Self-Attention;  
GAN is a generative adversarial network;  
CNN is a convolutional neural network;  
CAD is a computer-aided diagnosis;  
NAS is a neural architecture search;  
AutoGAN is neural architecture search for GAN;  
CIFAR-10 dataset – Canadian Institute for Advanced Research, 10 classes is a subset of the tiny images dataset and consists of 60000 32x32 color images;  
AWS is a Amazon Web Services;  
ELU is exponential linear unit activation function;  
Zenodo is a general-purpose open repository developed under the European OpenAIRE program and operated by CERN;  
ReLU is a rectified linear unit;  
GA is a genetic algorithm;  
Aging Evolution GA (AGA) is an evolutionary algorithm for neural architecture search.  
Batch Norm is batch normalization;  
ELU (exponential linear unit) is an activation function for neural networks;  
Self-Attention operates by transforming the input sequence into three vectors: query, key, and value;

Hinge loss function is measure the distance of data points from the decision boundary;

Nvidia A6000 GPU is the videocard of the company Nvidia;

IS metric is a metric (Inception Score) based on the Google Inception V3 image classification model;

FID is Fréchet inception distance;

PyTorch is an open source machine learning framework Python Torch;

AWS S3 is a Amazon Web Services Simple Storage Service;

RAM is a Random Access Memory;

vCPU is a virtual Central processing unit;

GPU is a graphical processing unit;

TFLOPS is a Tera Floating-point Operations per Second;

Adam optimizer is an adaptive moment stochastic gradient descent method;

H, W, and C are image height, width, and number of channels respectively.

### NOMENCLATURE

$I_t$  is a training set of images;

$I_G$  is a set of generated images;

$G$  is a generator;  
 $D$  is a discriminator;  
 $L$  is a set of discriminator layers;  
 $Q$  is a set of generator layers;  
 $n$  is a number of discriminator layers;  
 $m$  is a number of generator layers;  
 $i$  is an index of discriminator layers;  
 $j$  is an index of generator layers;  
 $CELL_D$  is a cell of discriminator;  
 $CELL_G$  is a cell of generator;  
 $o$  is a number of nodes in the generator cell;  
 $p$  is a number of nodes in the discriminator cell;  
 $A_G$  is a generator architecture;  
 $A_D$  is a discriminator architecture;  
 $O_G$  is a set of generator operations;  
 $O_D$  is a set of discriminator operations;  
 $P_G$  is a the set of parameters of generator operations;  
 $P_D$  is a set of parameters of discriminator operations;  
 $V(G, D)$  is the loss function for the generator and discriminator;  
 $q$  is the power of the training sample set;  
 $r$  is the power of the set of the generated sample;  
 $P_i(x)$  is the density of the distribution function of the training sample;  
 $P(z)$  is the density of the generator's noise distribution function;  
 $E(x)$  is the expected value of a random variable  $x$ .  
 $M_F$  is a FID metric;  
 $\langle C \rangle$  is a set of convolution functions;  
 $\langle K \rangle$  is a set of activation functions;  
 $\langle U \rangle$  is a set of operations of the Upsample block;  
 $\langle W \rangle$  is a set of operations of the generator cell  
 $CELL_G$ ;  
 $\langle Z \rangle$  is a set of operations of the discriminator  $CELL_D$ ;  
 $\langle T \rangle$  is a set of operations of the Downsample block;  
 $S$  is a Self Attention operation.

## INTRODUCTION

Image synthesis is a popular trend in artificial intelligence. A separate class of images are biomedical images. A biomedical image is a structural and functional image of human and animal organs, designed to diagnose diseases and study the anatomical and physiological picture of the body.

A subclass of biomedical images are cytological, histological and immunohistochemical images. These images are used to make a diagnosis in oncology. The widespread use of deep neural networks for image classification has led to the problem of datasets. To achieve the required accuracy of biomedical image classification, it is necessary to provide powerful datasets.

Hence, there is a contradiction between achieving high accuracy in biomedical image classification and providing powerful datasets to train convolutional neural networks. To resolve this contradiction, it is necessary to develop a

method and means of generating biomedical images. One of the modern approaches to solve this problem is the use of generative adversarial networks. Since their inception in 2014, generative adversarial networks have become the primary tool for synthesizing high-quality and diverse images [1–5]

Synthesized images help improve the training of machine learning models (in particular, classifiers) by extending existing training datasets, which are often low-power [6].

The complex process of synthesizing GAN architectures manually makes them difficult to use. Manual design of GAN architecture requires a deep understanding of machine learning principles and knowledge of the specifics of the subject area. This process is time-consuming and often requires developers to make a number of complex decisions. For example, developers have to choose between different types of layers, activation functions, and optimization techniques that have a big impact on the performance of the neural network.

One of the main challenges of manual architecture design is scalability. The more complex biomedical imaging becomes, the more complex GAN architectures become. Manual architecture design depends on the experience and intuition of the developer.

Thus, the creation of an automatic method for searching for GAN network architectures is an urgent task. The automatic method of searching for GAN architectures will allow you to quickly and thoroughly explore a large search space (types of layers, activation functions, etc.), finding the best network configurations. This method will reduce the synthesis time of GAN architectures and increase the efficiency of the process.

**The object of research is the process of biomedical images synthesis.**

**The subject of the research is the synthesis of generative-adversarial network architectures.**

**The aim of the work is to develop an automatic method for searching the architectures of generative-adversarial networks based on a genetic algorithm. This will make it possible to synthesize GAN network architectures in automatic mode for the synthesis of biomedical images.**

## 1 PROBLEM STATEMENT

Let be given a training sample of images  $I_t$  with a cardinality of  $q$ . Generating a set of images  $I_G$  with a cardinality of  $r$ , and  $r \gg q$ . To generate  $I_G$  we use GAN. The GAN consists of a generator and a discriminator. In addition, the architecture of the generator and discriminator  $A_G$  and  $A_D$ , respectively, is given.

The discriminator architecture is described as follows:

$$A_D = \{L_i, i = \overline{1, n}\},$$

and the architecture of the generator as follows:

$$A_G = \{Q_j, j = \overline{1, m}\}.$$

The set of discriminator operations is represented as follows:

$$O_D = \{\langle C \rangle; \langle K \rangle; \langle Z \rangle; \langle T \rangle\},$$

and the set of generator operations is as follows:

$$O_G = \{\langle C \rangle; \langle K \rangle; \langle U \rangle; S\}.$$

Then it is necessary to carry out a two-level optimization of the discriminator and generator architectures, i.e.:

$$A_D = \arg \min_{O_D, P_D} M_F(P_D, O_D, I_t, I_G),$$

$$A_G = \arg \min_{O_G, P_G} M_F(P_G, O_G, I_t, I_G).$$

In this case, the loss function of the discriminator and the generator will be defined as follows:

$$V(G, D) = \min_G \max_D F(G, D) = \\ = E_{x \sim P_q(x)} (\log D(x)) + E_{z \sim p(z)} (\log(1 - D(G(z))))).$$

## 2 REVIEW OF THE LITERATURE

In deep learning, the development of generative adversarial networks has been a big step for image synthesis. Generative adversarial networks have a great potential for the synthesis of realistic images.

In the early days of GAN research, the main goal was to synthesize realistic images from random noise. The work of Radford, et al. gave a push to the improvement of the quality of synthesized images and the stability of GAN learning [7]. This work laid the groundwork for future research, as it proved GAN's ability to handle complex image distributions.

In biomedicine, GANs are used to augment training data, which is essential to address the scarcity of annotated medical images. The authors [8] presented an innovative approach to the synthesis of retinal images using the generative model method. Based on generative models, realistic retinal images were synthesized and used to train diagnostic algorithms. Likewise, the authors Frid-Adar et al. used generative adversarial networks to expand the liver lesion image datasets that were used by the classifier [9]. Thus, the authors demonstrated the practical utility of GAN for expanding datasets and improving the accuracy of neural networks in biomedical image classification tasks.

The complexity of designing neural network architectures has led to the development of automatic search for NAS neural network architectures. Zof and Le were among the first to introduce the concept of

automatic architecture search for CNN. This concept has been adapted by researchers to automate the design of GAN architectures [10]. In their work, the authors applied the reinforcement learning method to explore the search space for architectures. This work shows the potential of NAS to reduce the human factor in the design of new neural network architectures. Since the field of NAS was primarily focused only on convolutional neural networks, NAS for generative networks is a relatively new area of research. Early work in NAS for GAN focused on finding efficient architectures that could generate high-quality images with reduced computing resources.

A fundamental paper in this area is [11], which develops a method for automatically searching for GAN architectures. The authors applied the reinforcement learning method to optimize the GAN architecture [12]. The AutoGAN framework has demonstrated that automated architecture design can compete with human-made models. To evaluate the method, the authors used the FID metric, the final value of which is 12.42. The architecture search time is 48 GPU hours. The main disadvantages of the work are: limited search space, fixed discriminator, unconditional image generation.

The development of the preliminary research is the work [13]. In the paper, the authors applied a genetic algorithm to optimize the neural network architecture and expanded the search space with operations such as skip connection, a convolution with different kernel sizes (1, 3, and 5, respectively) [14]. The advantage of this work is the search for the architecture of the generator and discriminator. The search for architecture is divided into two stages – the first stage is the search for the architecture of the generator (the discriminator is fixed), and the second stage is the search for the discriminator. According to the authors, this approach has significantly stabilized the training of the GAN network. The experiments took 1.2 GPU days and showed a FID of 9.91 on the CIFAR-10 dataset. The disadvantage of the work is the unconditional generation of images.

In terms of optimizing GAN architectures, researchers have identified several key factors that affect the performance of networks. Brock et al. introduced the concept of scaling GANs, showing that larger models and batch sizes can lead to improved image quality [15]. This concept is essential for automatically searching for GAN architectures. Search algorithms must take into account the trade-off between model complexity and computational capability.

In addition, the evaluation of biomedical images generated by GAN networks presents particular challenges. When evaluating synthesized images, it is necessary to take into account not only visual accuracy, but also the preservation of diagnostic features. Automatic search for GAN architectures should result in models that are statistically powerful and clinically relevant.

Despite the progress made, significant gaps remain in the literature. The analyzed articles in the field of NAS for GAN do not focus on the synthesis of biomedical images and use an open dataset – CIFAR. This can be

explained by the difficulty of obtaining the datasets of biomedical images themselves, which in turn further emphasizes the relevance of their synthesis. Also, the considered methods have a limited search space, do not use the most modern operations (ELU, Self-Attention) in the search space, do not synthesize images by tags (use unconditional generation).

The article [16] developed a method for the synthesis and classification of breast cancer histological images. At the same time, well-known GAN structures are used.

In this paper, we propose an automatic method for searching for architectures of generatively adversarial networks for the synthesis of biomedical images.

### 3 MATERIALS AND METHODS

Defining the search space is the first important step in the development of generative adversarial network architectures. In this step, you define the range of possible types of layers and their combinations that will be used in the process of building the model.

The search space in the developed method is cell-based. A cell consists of a certain number of nodes and operations between them. An example of a cell is shown in Figure 1.

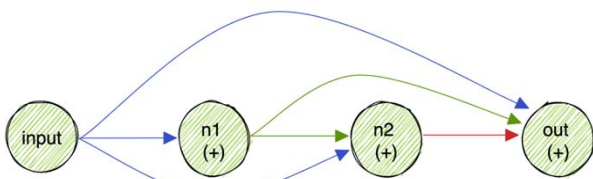


Figure 1 – Cell Structure

Figure 1 shows a cell with four nodes. The arrows represent the type of operation between the two nodes. Nodes  $n1$ ,  $n2$ ,  $n3$  signify the addition operation.

One of the disadvantages of classical neural network architectures is that all layers follow each other sequentially. This option of connection gives rise to the problem of gradient attenuation, which significantly impairs the training of the neural network [17]. In this method, each successive node in the cell can receive input from all the previous nodes, depending on the selected operation between them.

We analyzed modern architectures of GAN networks and identified a set of layers that are most often used in research. These include the following operations: kernel convolution operation  $1 \times 1$ ,  $3 \times 3$  and  $5 \times 5$ , max- and average-pooling operations, self-attention mechanism. Also, the generator and discriminator architectures in most GANs consist of repeating convolutional blocks, and the input noise vector is transformed into a matrix of size  $4 \times 4$ . The number of such blocks varies depending on the resolution of the generated image. Accordingly, if the generator synthesizes an image with a resolution of

$64 \times 64$ , then it consists of 4 convolutional blocks. The full set of possible operations we have chosen for the cell is listed below.

*Zero.* This operation replaces the node's output with a matrix of zeros. It can be used to remove a node from a cell architecture to simplify it.

*Skip connection.* This operation can be thought of as a function that receives and returns data. Using such an operation allows you to directly connect the output of one node in a cell to the input of another.

*Convolutional block.* batch normalization is often used along with convolution operations. Therefore, this layer uses three sequential operations: convolutions, activation functions, and batch normalization. We used convolution kernels  $1 \times 1$ ,  $3 \times 3$ , and  $5 \times 5$ . As an activation function, ELU is used – an improved modification of ReLU.

*Pooling.* We use pooling only in the discriminator model. The two types of pooling are max pooling with a  $3 \times 3$  kernel and step  $1 \times 1$  and average pooling with a  $3 \times 3$  kernel and step 1.

The Self-Attention operation is placed outside the cells. The integration of the Self-Attention mechanism into CNN allows to focus on the most informative features, which can be useful for object detection, segmentation and image recognition [18].

The search space for the generator and discriminator is shown in Figure 2.

In the developed method, we applied the Conditional GAN strategy, which allows to synthesize images of classes. Accordingly, in the generator model, we use the Conditional Batch Normalization operation in each UpSample block. In the discriminator model, we use an Embedding layer in combination with a fully connected layer. The sum of the outputs of these two layers is the output of the discriminator model.

The generator consists of one deconvolution layer to convert the input noise vector to dimension  $4 \times 4 \times 1024$ , four cells, four blocks to double the resolution, and two convolutional layers at the network output. The final resolution of the synthesized image is  $64 \times 64 \times 3$ .

The main element in the generator's search space is the cell, which consists of  $o$  nodes. The available operations in a cell are defined as follows: convolution by the kernel  $1 \times 1$ ,  $3 \times 3$ ,  $5 \times 5$ ; separable convolution by kernel  $3 \times 3$ ; zero; skip connection. The cell architecture remains the same for the entire generator model. Accordingly, the search space of the generator is reduced to determining the number of nodes in the cell, selecting operations between nodes, as well as selecting layers after which you need to apply the Self-Attention operation through the residual connection (shown in the figure by *ATTN* (*represents Self-Attention*) arrows).

The generator's search space is encoded as  $\{N, C, [ATTN]\}$ . Let's review in details these parameters.

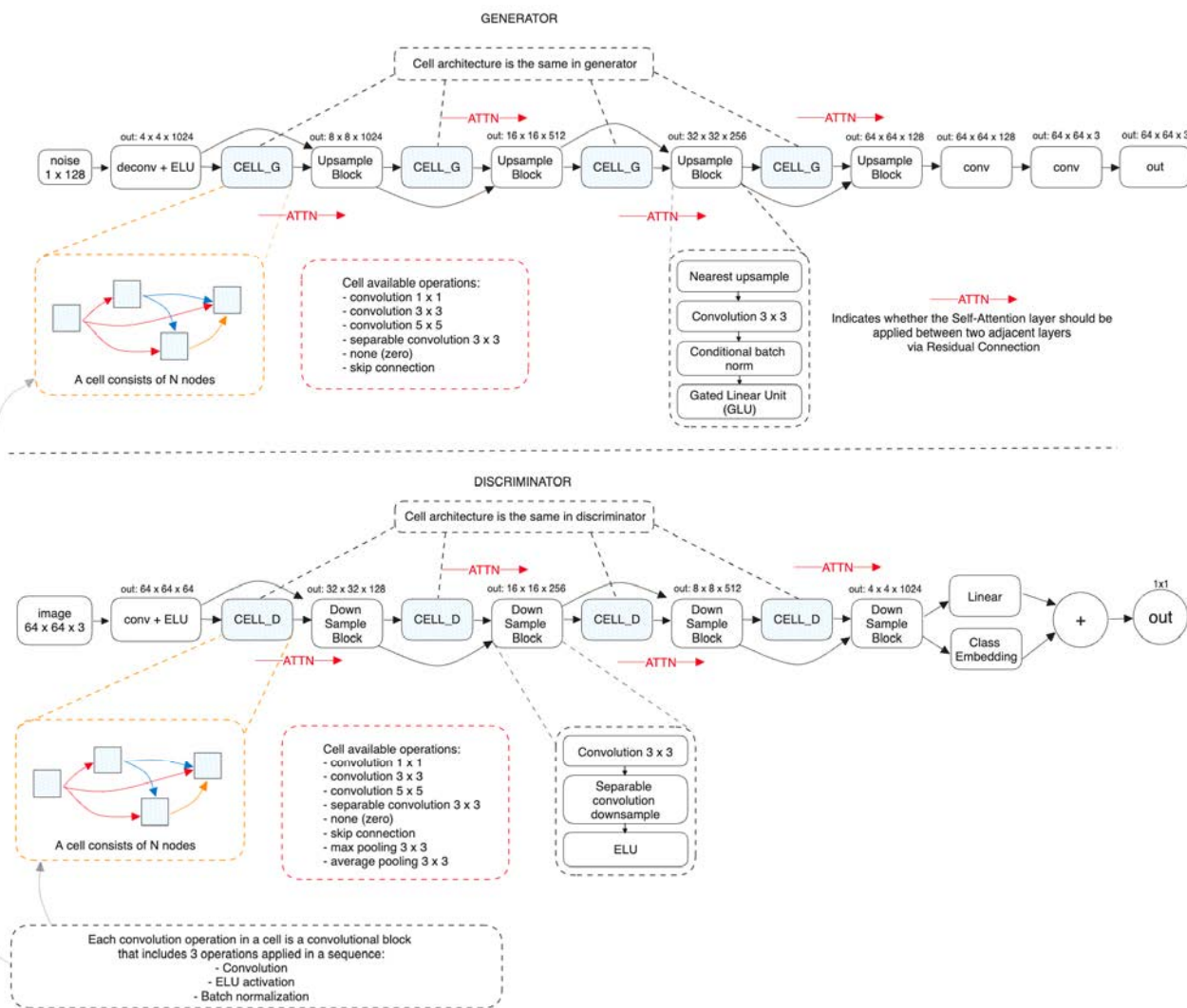


Figure 2 – Generator and Discriminator Search Spaces

The  $N$  parameter is the number of nodes in the cell. The minimum value is 3, the maximum value is 5. This decision was made due to limited computing resources. In addition, our study uses mostly small images, specifically 64×64 pixel in size. This aspect has a significant impact on network architectures, as such images usually require fewer layers. Therefore, the decision to limit the number of layers in the model is also due to the nature of the data.

Parameter  $C$  is the architecture of the cell in which the operations between nodes are encoded. It is represented by a tape  $xxx-xx-x$ , the length of which varies depending on the number of nodes in the cell. For example, for a cell with a number of nodes of 3, the encoded tape might look like 12-6. The first fraction separated by a hyphen represents the operations between the first node and all subsequent ones, the second – between the second node and all subsequent ones. Respectively 1 means kernel convolution operation 1×1 between the first and second nodes (see Fig. 2), 2 is the kernel convolution operation 3×3 between the first and second nodes. The number 6 means the skip connection operation between the second and third nodes.

The  $ATTN$  parameter represents the cell numbers after which you want to apply Self-Attention operations.

According to the described encoding and the above example, the encoding of the generator architecture is {3, 12-6, [1, 2]}. As you can see from the example, the Self-Attention operation is applied after the first and second cells.

The discriminator consists of one convolution layer, four cells, four blocks for halving the resolution, and one linear and embedding layer.

The main element in the discriminator search space is the cell, which consists of  $p$  nodes. Unlike the generator, the available set of operations in the discriminator cell is extended by two operations: the maximum pooling by the kernel 3×3 and the average pooling by the kernel 3×3.

For the dimensionality reduction operation, the Separable Downsample Convolution operation is used. The authors of the paper state that this is the most optimal method of reducing dimensionality in convolutional networks at present [19].

The cell architecture also remains the same for the entire discriminator model. The discriminator search

space boils down to the same steps as for the generator. These steps are as follows: determining the number of nodes in a cell, selecting operations between nodes, selecting layers. After these steps, you need to apply the Self-Attention operation through the residual connection (shown by the ATTN arrows in the figure).

The discriminator's search space is encoded in the same way as the generator's:  $\{N, C, [ATTN]\}$ .

The developed method consists of the following stages:

1. Search for a generator architecture with a fixed discriminator.
2. Search for a discriminator architecture with the best generator.

The general framework of the method is shown in Figure 3.

At the first stage, we define a fixed discriminator architecture and search for only the generator. The discriminator architecture is manually defined as follows: four nodes in a cell, the cell architecture is encoded as 235-66-7 (convolution by kernel 3×3 and 5×5, zero, skip connection, skip connection, max pooling by kernel 3×3), Self-Attention mechanism is applied only after the last cell.

At each cycle of the optimization algorithm, we initialize the population with random generator architectures. Next, we create a generator and discriminator pair for each generator in the population. The resulting pairs of GAN networks are trained and evaluated at the end of each cycle using FID metrics [20, 21]. At the end of the cycle, we select the generator with the lowest FID value and copy its weights. Further in the next cycle, we initialize all generators with copied weights. Accordingly, after the first step, we get the architecture of the best generator, i.e. the model with the lowest FID value.

In the second step, we use the best generator architecture and search for the discriminator architecture. At each cycle of the optimization algorithm, we create a population of discriminators and initialize it with random architectures. Then, by analogy with the first step, we create pairs of generators and discriminators. The resulting pairs of GAN networks are trained independently of each other and evaluated using the FID metric. At the end of each cycle, we copy the weights of the best discriminator and initialize all the discriminators in the next cycle with them. After the second step, we get the architecture of the best discriminator, and, accordingly, the best architecture of the GAN network.

At both stages, the input images of the discriminator model are subjected to the technique of Differentiable Augmentations with the application of a random color and translation policy. This technique helps

to further expand the training dataset directly during the learning process and is especially effective on small datasets [22].

We used a modified Aging Evolution GA (AGA) algorithm to optimize the generative adversarial network architecture [23]. The AGA maintains a population of potential solutions, where each solution represents a unique GAN architecture.

A variation in the genetic algorithm known as Aging Evolution GA adds an aging component to increase population diversity and prevent early convergence.

The main steps of this algorithm are:

1. Train and evaluate each architecture in the population by calculating the FID metric.
2. Selection of a subset of architectures from the population. The selection process is based on a random strategy.
3. Selection of the parent architecture and application of the genetic operator (mutation) to it to create a new architecture.
4. Evaluate the new architecture by training it and computing the FID metric and adding the architecture to the population.
5. Remove the oldest architecture from the population.

At the first step of the algorithm, the population is initialized by random architectures to achieve a given population size – *population\_size*. Simultaneously with initialization, architectures are trained with the calculation of the FID metric value.

Further, evolution occurs cyclically. The number of cycles is also set by the user (*cycles* parameter). On each of the cycles, a given number of architectures is randomly selected – *sample\_size*. Then, among these architectures, the one with the lowest FID value is selected. This architecture is called the parent architecture.

Based on the parent architecture, a new child architecture is created by applying a mutation. In this algorithm, the mutation changes the architecture randomly. Next, the mutated architecture learns.

The mutation is applied to each element in the encoded architecture with a probability of *mutation\_prob*. For example, the network architecture is set to tape 107590. In order to mutate, you need to go through each element of the tape in a loop and change it randomly with a given probability of *mutation\_prob*.

Accordingly, after applying a mutation, we get a new child architecture that is added to the population. At the same time, the oldest architecture is being removed from the population. The algorithm then returns the architecture with the lowest FID value.

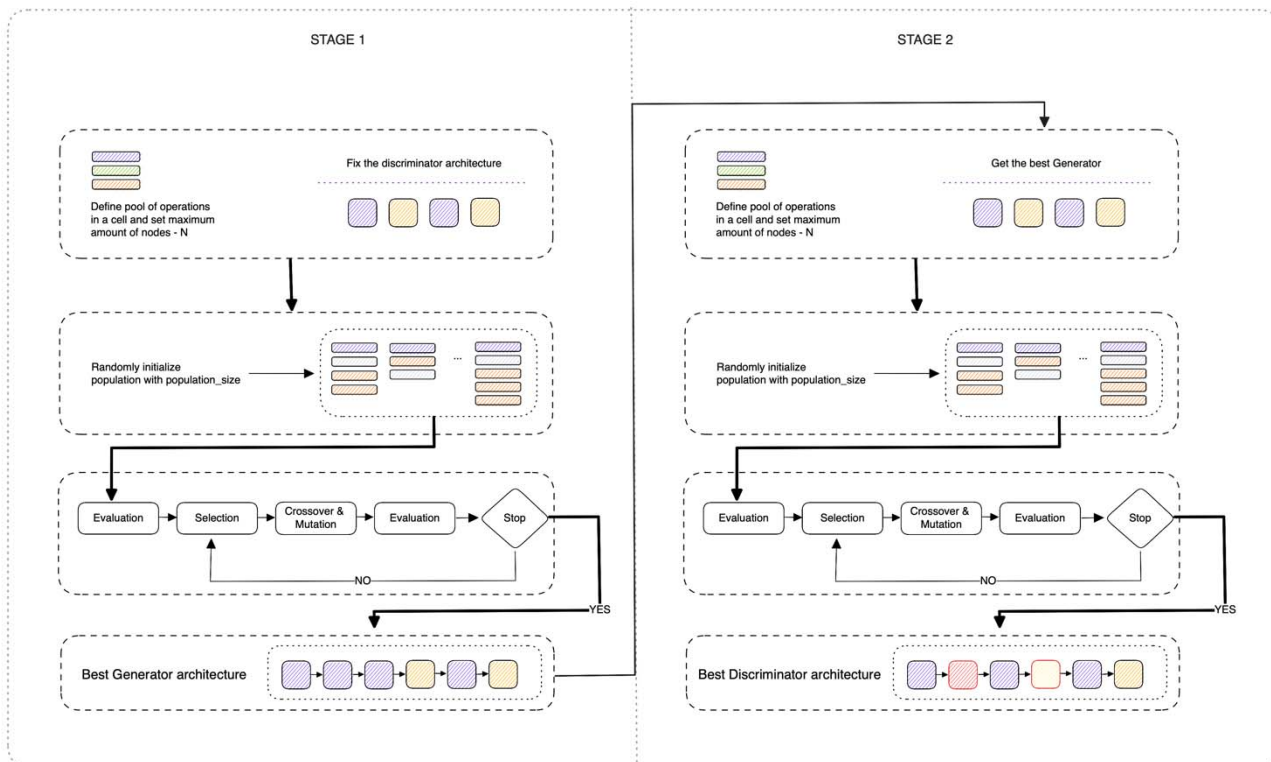


Figure 3 – General GAN Synthesis Method Framework

#### 4 EXPERIMENTS

The experiments were based on the Python 3.10 programming language, the PyTorch 2.0 framework, and a virtual machine with the following configuration: 32 GB RAM, 7 vCPU, Nvidia A6000 GPU, 48 GB RAM.

The software module consists of two main Python scripts: `train.py` and `generate.py`. The `train.py` script is designed to build and train generative adversarial network (GAN) architectures. It allows users to define basic parameters for GAN search, including noise vector dimension, activation functions, and optimization parameters. After training, the architecture that gives the best results is chosen. The trained model is stored in Amazon S3 storage, ensuring that the model is saved and can be accessed or downloaded as needed.

The second script, `generate.py`, runs after the GAN model has been trained and configured. This script is responsible for generating new images using the best architecture found during the learning phase. It can be run as a command-line tool where the user specifies the path to the model and the preferred directory to output the generated images. The script loads the trained GAN model and uses it to synthesize new images that are expected to demonstrate the learned distribution of the training data. The results can be used for further analysis or as input for other stages of research.

In this study, we used cytological images to test the method. A cytological image is a microscopic image of individual cells or cell formations obtained by cytological examination.

Cytological images of breast cancer on the Zenodo platform were used for the experiments [24]. This dataset is designed to test and configure automatic biomedical image processing systems. The structure of the dataset is as follows:

- 1) files of cytological images and the indicated diagnosis (size 3264×2448).
- 2) files of histological and immunohistochemical images of sections of breast tissue (size 2048×1536) and the indicated diagnosis.

Examples of cytological images are shown in Figure 4 (one image per class).

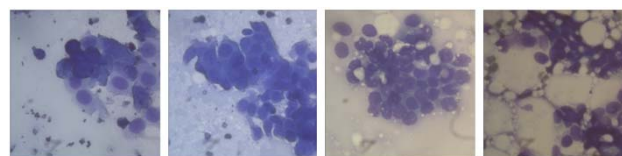


Figure 4 – Example of images from the dataset

For the experiments, the image was converted to a resolution of 64×64 pixels. Since the initial number of images in the sample is quite small (about 100 images per class), it was expanded to 700 images per class by applying affine distortions (random rotation, displacement, twisting, etc.) [25].

For both stages of the search, we used the Hinge loss function [26] and the Adam optimizer (betas = 0.5, 0.999) [27]. We also applied the Two Time-scale Update Rule [28]. Accordingly, the learning rate of the generator is 0.0001, and the discriminator is 0.0004.

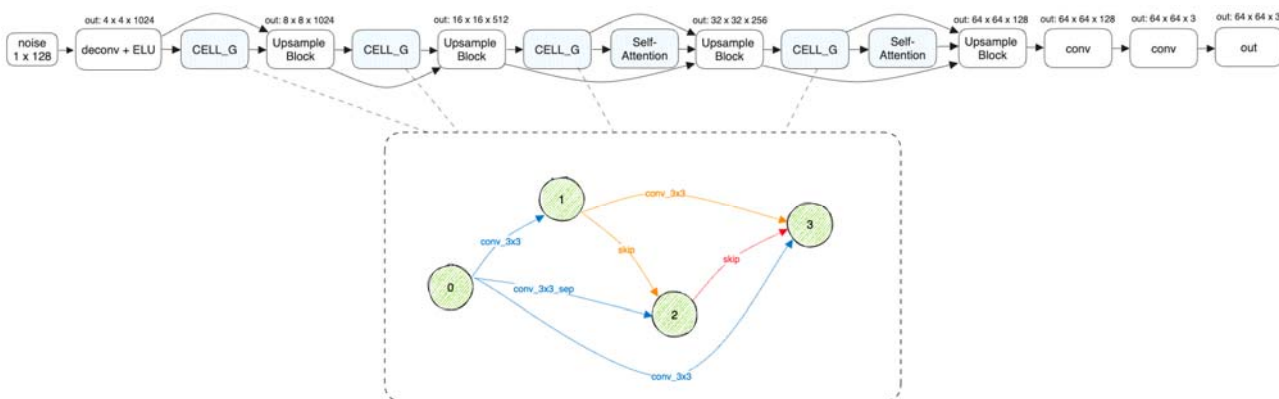


Figure 5 – Synthesized Generator Architecture

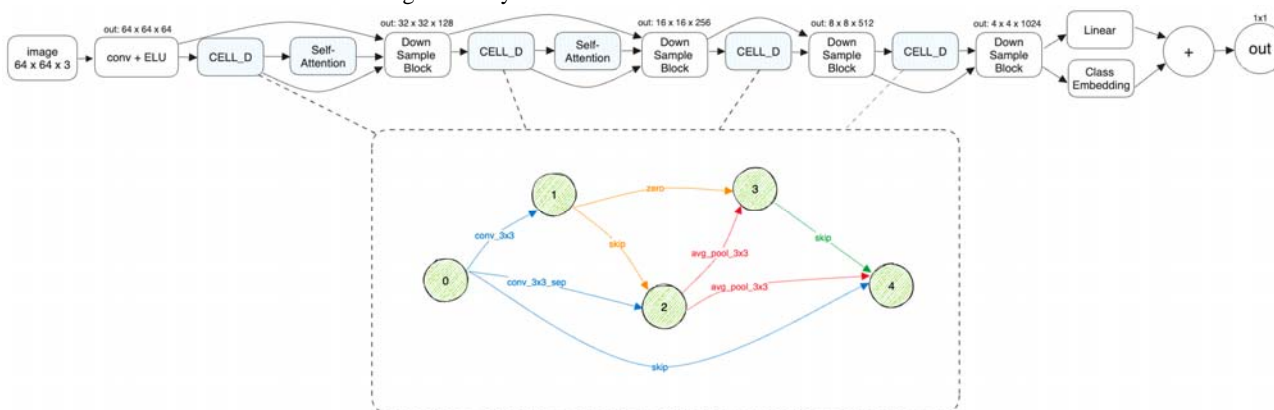


Figure 6 – Synthesized Discriminator Architecture

For all convolutional, deconvolutional, and linear layers in both models, we applied the spectral normalization technique, which allows us to stabilize the learning of the GAN network [29].

The total number of cycles of the optimization algorithm at each stage is 25, and the number of epochs of training for each model in the population is 30. The population size (population\_size) is 100. The number of randomly selected candidates for further selection of the parent architecture for mutation (sample\_size) is 25. The probability of mutation (mutation\_prob) is 0.05. Batch size (batch\_size) for the generator and discriminator is the same and is 128 images.

To evaluate architectures, the FID metric was used, which is calculated after each architecture is trained.

In total, the first and second stages took 15.6 and 10.3 GPU hours, respectively.

Upon completion of both phases, the resulting GAN network was trained from scratch for 100,000 iterations. It took another ~13.6 GPU hours. That is, the total time spent on finding architectures to obtaining a fully trained GAN network is 39.5 GPU hours.

As a result of the experiments, 4000 images with a resolution of 64x64 for each class from the educational

dataset were synthesized. Accordingly, the total number of synthesized images is 16,000.

## 5 RESULTS

The architecture of the found generator and discriminator is shown in Figures 5 and 6 and in Tables 1–4.

As you can see from the figures, the number of nodes in the generator and discriminator cells is 4 and 5, respectively. There are two skip connection operations in the generator cell, and there are 3 in the discriminator cell. There is also a zero operation in the discriminator cell, which is not present in the generator. The Self-Attention operation is applied 2 times in both the generator and the discriminator. However, in the generator, this operation is placed towards the end of the network, and in the discriminator, on the contrary, it is closer to the beginning.

The FID metric value for the found GAN network architecture is 3.39, and the IS metric value is 3.95.

Examples of comparison of synthesized images with the original ones for each class are shown in Figures 7–10. The images are selected randomly.

Table 1 – Generator Structure

Layer name	Params	Output shape
L1: Input	Gaussian noise	1×128
L2: Transposed Conv + ELU activation	Kernel = 4, stride = 1, padding = 0	4×4×1024
L3: CELL <sub>G</sub>	Nodes = 4	4×4×1024
L4: L2 + L3		4×4×1024
L5: Upsample	Scale = 2	8×8×1024
L6: CELL <sub>G</sub>	Nodes = 4	8×8×1024
L7: L5 + L6		8×8×1024
L8: Upsample	Scale = 2	16×16×512
L9: CELL <sub>G</sub>	Nodes = 4	16×16×512
L10: Self Attention	Input channels = 512	16×16×512
L11: L8 + L10 + L9		16×16×512
L11: Upsample	Scale = 2	32×32×256
L12: CELL <sub>G</sub>	Nodes = 4	32×32×256
L13: Self Attention	Input channels = 256	32×32×256
L14: L11 + L13 + L12		32×32×256
L15: Upsample	Scale = 2	64×64×128
L16: Convolution	Kernel = 3, stride = 1, padding = 1	64×64×128
L17: Convolution	Kernel = 3, stride = 1, padding = 1	64×64×3
L18: Output		64×64×3

Table 2 – Generator CELL<sub>G</sub> Structure

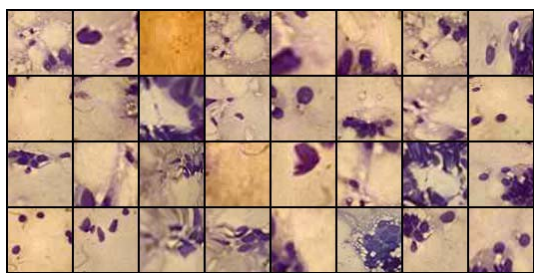
Layer name	Params	
L0: Input		
L1: Conv → ELU → Batch Norm	Kernel = 3, stride = 1, padding = 1	
L2: L1 + Conv 3×3 → Conv 1×1 → ELU → Batch Norm	Conv 3×3 = (Kernel = 3, stride = 1, padding = 1), Conv 1×1 = (Kernel = 1, stride = 1, padding = 0)	
L3: L2 + Conv (L1) + Conv (L0)	Kernel = 3, stride = 1, padding = 1	
L0: Input		
L1: Conv → ELU → Batch Norm	Kernel = 3, stride = 1, padding = 1	
Upsample block structure		
Layer name	Params	Output shape
L0: Input		H × W × C
L1: Upsample	Scale = 2, mode = nearest	(H × 2) × (W × 2) × C
L2: Convolution	Kernel = 3, stride = 1, padding = 1	(H × 2) × (W × 2) × C
L3: Conditional Batch Norm	Number of classes = 4	(H × 2) × (W × 2) × C
L4: Gated Linear Unit (GLU)	Dimension = 1	(H × 2) × (W × 2) × (C / 2)

Table 3 – Discriminator Structure

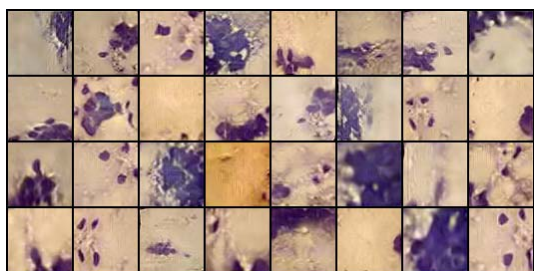
Layer name	Params	Output shape
L1: Input	Image	64×64×3
L2: Conv + ELU activation	Kernel = 3, stride = 1, padding = 1	64×64×64
L3: CELL <sub>D</sub>	Nodes = 5	64×64×64
L4: Self Attention	Input channels = 64	64×64×64
L5: L2 + L4 + L3		64×64×64
L6: Downsample	Scale = 2	32×32×128
L7: CELL <sub>D</sub>	Nodes = 5	32×32×128
L8: Self Attention	Input channels = 64	32×32×128
L9: L6 + L8 + L7		32×32×128
L10: Downsample	Scale = 2	16×16×256
L11: CELL <sub>D</sub>	Nodes = 5	16×16×256
L12: L10 + L11		16×16×256
L13: Downsample	Scale = 2	8×8×512
L14: CELL <sub>D</sub>	Nodes = 5	8×8×512
L15: L13 + L14		8×8×512
L16: Downsample	Scale = 2	4×4×1024
L17: Linear(Sum(L16))		1×1
L18: Sum(Multiply(Sum(L16), Embedding))	Number of classes = 4	1×1
L19: L17 + L18		1×1
L20: Output		1×1

Table 4 – Discriminator  $CELL_D$  Structure

Layer name		Params
L0: Input		
L1: Conv → ELU → Batch Norm		Kernel = 3, stride = 1, padding = 1
L2: L1 + Conv 3×3 → Conv 1×1 → ELU → Batch Norm		(Kernel = 3, stride = 1, padding = 1), (Kernel = 1, stride = 1, padding = 0)
L3: AvgPool 3×3 (L2)		Kernel = 3, stride = 1
L4: L0 + L3 + AvgPool 3×3 (L2)		Kernel = 3, stride = 1
Downsample block structure		
Layer name	Params	Output shape
L0: Input		H × W × C
L2: Convolution	Kernel = 3, stride = 1, padding = 1	H × W × (C × 2)
L3: Pixel Rearrange → Convolution	Kernel = 1, stride = 1, padding = 0	(H / 2) × (W / 2) × (C × 2)
L4: Exponential Linear Unit (ELU)		(H / 2) × (W / 2) × (C × 2)

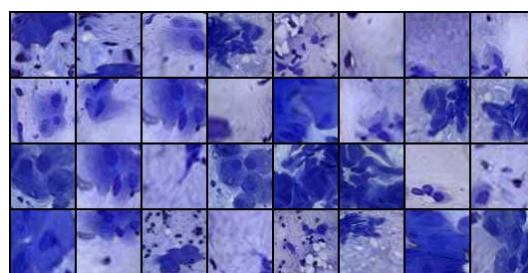


a

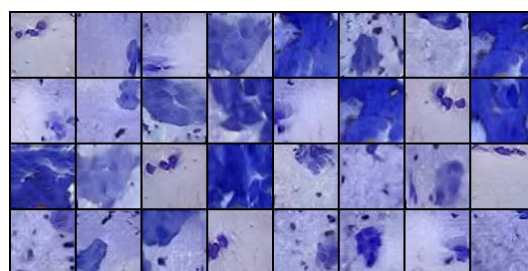


b

Figure 7 – Original (a) and Synthesized (b) Images, Class 1

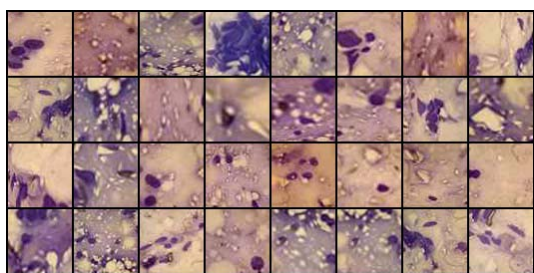


a

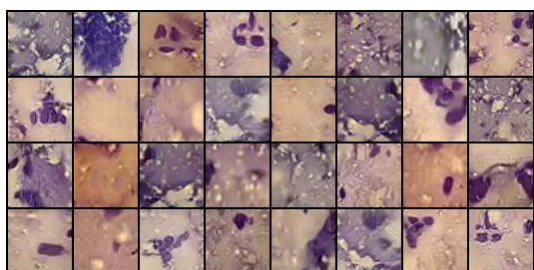


b

Figure 9 – Original (a) and Synthesized (b) Images, Class 3

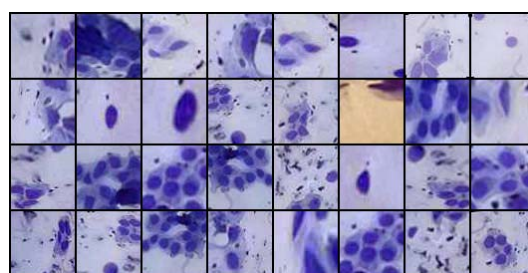


a

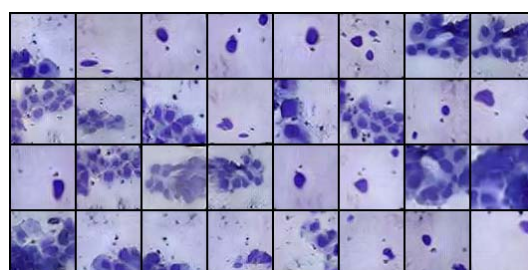


b

Figure 8 – Original (a) and Synthesized (b) Images, Class 2



a



b

Figure 10 – Original (a) and Synthesized (b) Images, Class 4

We also compared different GAN architectures for the synthesis of cytological images. The results of the comparison are shown in Table 5.

Table 3 – Comparison of GANs by FID metric using same images

Method	FID
DCGAN	12.67
WGAN	12.72
WGAN-GP	19.09
BGAN	10.03
BEGAN	15.32
Our method GA-GAN	3.39

## 6 DISCUSSION

As a result of the study, the architecture of the generative-adversarial network for the synthesis of cytological images was obtained (Fig. 5, Fig. 6). To assess the quality of synthesized images, the FID metric was used.

Table 3 shows that the network architecture designed by our method showed the best results compared to other GAN network architectures for the same images.

Unlike the above architectures, our method uses the Self-Attention mechanism in the generator and discriminator, which allowed us to improve the quality of synthesized images. Also, our method supports the mechanism of image synthesis by labels (conditional generation), which is not relevant for the above architectures and approaches.

Figures 7–10 show a comparison of original pairs and synthesized images for each class from the original and synthesized dataset. The synthesized images are difficult to visually distinguish from the original ones, which further indicates the power of the resulting network.

We did not test the method on higher-resolution images, as this would have led to an increase in search time. Therefore, the limitation of our research is the relatively low resolution of the synthesized images – 64×64 pixels. In order to synthesize images of higher resolution, you need to increase the number of cells in the generator and discriminator.

We also conducted experiments on only one subclass of biomedical images – cytological images. Accordingly, a further direction of research may be testing and adaptation of the developed method to other classes and resolutions of biomedical images.

## CONCLUSIONS

As a result of the study, the automatic method for searching for architectures of generatively adversarial networks for the tasks of synthesis of cytological images was developed.

Architectural search space is defined in terms of cells, which consist of a set of nodes and operations between

them. The architectural features of the cell allow you to expand the search space and reduce the likelihood of a gradient attenuation problem.

The developed method consists of two stages: the search for the architecture of the generator with a fixed discriminator and the search for the architecture of the discriminator paired with the fixed best generator.

As a result of computer experiments, the architecture of a generatively competitive network for the synthesis of cytological images was obtained. The total time of the experiment was ~39.5 GPU hours. As a result, 16,000 images were synthesized (4000 for each class).

Comparison of the synthesized architecture with other architectures of generative-adversarial networks, using the same training dataset, is carried out on the basis of the FID metric. The results showed that the designed architecture is the best. The FID value of the developed network (3.39) is two and a half times better than the FID metric of the above architectures.

**The scientific novelty** is the development of a method for finding generative-adversarial network architectures for the synthesis of biomedical images.

**The practical significance** is the development of a software module for the synthesis of biomedical images that can be used to train CNN.

The authors of the article have many years of experience in the development of biomedical image analysis systems [30–34].

A software module for the synthesis of biomedical images will be integrated into image analysis systems.

**Prospects for further research** is the development of a CAD system for the classification and synthesis of biomedical images.

## REFERENCES

1. Goodfellow I., Pouget-Abadie J., Mirza M. et al. Generative Adversarial Nets, *Advances in Neural Information Processing Systems*, 2014, №27.
2. Salimans T., Goodfellow I., Zaremba W. et al. Improved Techniques for Training GANs [Electronic resource], *arXiv.org*, 2016. Access mode: <https://arxiv.org/abs/1606.03498>.
3. Karras T., Aila T., Laine S. et al. Progressive Growing of GANs for Improved Quality, Stability, and Variation [Electronic resource], *arXiv.org*, 2017. Access mode: <https://arxiv.org/abs/1710.10196>.
4. Analyzing and Improving the Image Quality of StyleGAN [Electronic resource], *Conference on Computer Vision and Pattern Recognition (CVPR): proceedings, Seattle, 2020*, P. 8107–8116. Access mode: <https://doi.org/10.1109/CVPR42600.2020.00813>.
5. Arjovsky M., Chintala S. Wasserstein Generative Adversarial Networks [Electronic resource], *International Conference on Machine Learning: proceedings, 2017*. Access mode: <https://leon.bottou.org/publications/pdf/icml-2017.pdf>.
6. Düzyel O., Kuntalp M. Data Augmentation with GAN increases the Performance of Arrhythmia Classification for an Unbalanced Dataset [Electronic resource], *arXiv.org*. – 2023. Access mode: <https://doi.org/10.48550/arXiv.2302.13855>.

7. Radford A., Metz L. Unsupervised Representation Learning with Deep Convolutional Generative Adversarial Networks [Electronic resource], arXiv.org, 2016. Access mode: <https://doi.org/10.48550/arXiv.2302.13855>.
8. Costa Pedro et al. End-to-End Adversarial Retinal Image Synthesis [Electronic resource], *IEEE Transactions on Medical Imaging*, 2018, Vol. 37, № 3, pp. 781–791. Access mode: <https://doi.org/10.1109/tmi.2017.2759102>.
9. Frid-Adar Maayan et al. GAN-based synthetic medical image augmentation for increased CNN performance in liver lesion classification [Electronic resource], *Neurocomputing*, 2018, Vol. 321, pp. 321–331. Access mode: <https://doi.org/10.1016/j.neucom.2018.09.013>.
10. Zoph B., Le Q. Neural Architecture Search with Reinforcement Learning [Electronic resource], arXiv.org, 2017. Access mode: <https://doi.org/10.48550/arXiv.1611.01578>.
11. Gong Xinyu et al. AutoGAN: Neural Architecture Search for Generative Adversarial Networks [Electronic resource], *2019 IEEE/CVF International Conference on Computer Vision (ICCV)*. Seoul, Korea (South), 2019. Access mode: <https://doi.org/10.1109/iccv.2019.00332>.
12. Baker B., Gupta O. Designing Neural Network Architectures using Reinforcement Learning [Electronic resource], arXiv.org, 2017. Access mode: <https://doi.org/10.48550/arXiv.1611.02167>.
13. Ying G., He X., Gao B. et al. Efficient Two-stage Evolutionary Architecture Search for GANs [Electronic resource], arXiv.org, 2020. Access mode: <https://doi.org/10.48550/arXiv.2111.15097>.
14. Gao Chen et al. AdversarialNAS: Adversarial Neural Architecture Search for GANs [Electronic resource], *2020 IEEE/CVF Conference on Computer Vision and Pattern Recognition (CVPR)*. Seattle, WA, USA, 2020. Access mode: <https://doi.org/10.1109/cvpr42600.2020.00572>.
15. Brock A., Donahue J., Simonyan K. Large Scale GAN Training for High Fidelity Natural Image Synthesis [Electronic resource], *Semantic Scholar*, 2018. Access mode: <https://www.semanticscholar.org/paper/Large-Scale-GAN-Training-for-High-Fidelity-Natural-Brock-Donahue/22aab110058ebbd198edb1f1e7b4f69fb13c0613>.
16. Berezsky O. M., Liashchynskiy P. B., Pitsun O. Y. et al. Deep network-based method and software for small sample biomedical image generation and classification, *Radio Electronics, Computer Science, Control*, 2024, № 4, P. 76.
17. He Kaiming et al. Deep Residual Learning for Image Recognition [Electronic resource], *2016 IEEE Conference on Computer Vision and Pattern Recognition (CVPR)*. Las Vegas, NV, USA, 2016. Access mode: <https://doi.org/10.1109/cvpr.2016.90>.
18. Vaswani A., Shazeer N., Parmar N. et al. Attention is All you Need [Electronic resource], *Semantic Scholar*, 2017. Access mode: <https://www.semanticscholar.org/paper/Attention-is-All-you-Need-Vaswani-Shazeer/204e3073870fae3d05bcbc2f6a8e263d9b72e776>.
19. Sunkara R., Luo T. No More Strided Convolutions or Pooling: A New CNN Building Block for Low-Resolution Images and Small Objects [Electronic resource], *Machine Learning and Knowledge Discovery in Databases*. Cham, 2023, pp. 443–459. Access mode: [https://doi.org/10.1007/978-3-031-26409-2\\_27](https://doi.org/10.1007/978-3-031-26409-2_27).
20. Barratt S., Sharma R. A Note on the Inception Score. [Electronic resource], arXiv.org, 2018. Access mode: <https://arxiv.org/abs/1801.01973>.
21. Borji A. Pros and cons of GAN evaluation measures [Electronic resource], *Computer Vision and Image Understanding*, 2019, Vol. 179, pp. 41–65. Access mode: <https://doi.org/10.1016/j.cviu.2018.10.009>.
22. Zhao S., Liu Z., Lin J. et al. Differentiable Augmentation for Data-Efficient GAN Training [Electronic resource], arXiv.org, 2020. Access mode: <https://arxiv.org/abs/2006.10738>.
23. Real Esteban et al. Regularized Evolution for Image Classifier Architecture Search [Electronic resource], *Proceedings of the AAAI Conference on Artificial Intelligence*, 2019, Vol. 33, pp. 4780–4789. Access mode: <https://doi.org/10.1609/aaai.v33i01.33014780>.
24. Cytological and histological images of breast cancer. (n.d.) [Electronic resource] // Zenodo. – 2023. – Access mode: <https://doi.org/10.5281/zenodo.7890874>.
25. Liashchynskiy P. Rudi – Python library [Electronic resource], GitHub, 2018. Access mode: <https://github.com/liashchynskiy/rudi>.
26. Ye J., Lim J. Geometric GAN [Electronic resource], arXiv.org, 2017. – Access mode: <https://arxiv.org/abs/1705.02894>.
27. Kingma D., Ba J. Adam: A Method for Stochastic Optimization [Electronic resource], arXiv.org, 2017. Access mode: <https://arxiv.org/abs/1412.6980>.
28. Bynagari N. B. GANs Trained by a Two Time-Scale Update Rule Converge to a Local Nash Equilibrium [Electronic resource], *Asian Journal of Applied Science and Engineering*. 2019, Vol. 8, № 1, pp. 25–34. Access mode: <https://doi.org/10.18034/ajase.v8i1.9>.
29. Miyato T., Kataoka T., Koyama M. Spectral Normalization for Generative Adversarial Networks [Electronic resource], arXiv.org, 2018. Access mode: <https://arxiv.org/abs/1802.05957>.
30. Berezsky O. M. Liashchynskiy P. B. Comparison of generative adversarial networks architectures for biomedical images synthesis [Electronic resource], *Applied Aspects of Information Technology*, 2021, Vol. 4, № 3, pp. 250–260. Access mode: <https://doi.org/10.15276/aait.03.2021.4>.
31. Berezsky O. M., Berezska K. M., Melnyk G. M. et al. Design of computer systems for biomedical image analysis, *Proceedings of the Xth International Conference «The Experience of Designing and Application of CAD Systems in Microelectronics» CADSM 2009*. Lviv, Publishing House Vezha&CoC, pp. 186–191.
32. Berezsky O. Verbovy S., Datsko T. The intelligent system for diagnosing breast cancers based on image analysis [Electronic resource], *2015 Information Technologies in Innovation Business Conference (ITIB)*. Kharkiv, Ukraine, 7–9 October 2015, 2015. Access mode: <https://doi.org/10.1109/itib.2015.7355067>.
33. Berezsky Oleh et al. Fuzzy system diagnosing of precancerous and cancerous conditions of the breast [Electronic resource], *2016 XIth International Scientific and Technical Conference “Computer Sciences and Information Technologies (CSIT)*. Lviv, Ukraine, 6–10 September 2016. 2016. Access mode: <https://doi.org/10.1109/stc-csit.2016.7589906>.
34. Berezsky O., Verbovy S., Pitsun O. Hybrid Intelligent Information Technology for Biomedical Image Processing [Electronic resource], *IEEE 13th International Scientific and Technical Conference on Computer Sciences and Information Technologies*, 2018. Access mode: <https://ieeexplore.ieee.org/document/8526711>.
35. Berezsky O., Dubchak L., Batryn T. et al. Fuzzy System For Breast Disease Diagnosing Based On Image Analysis [Elec-

УДК 004.93

## МЕТОД ПОШУКУ АРХІТЕКТУР ГЕНЕРАТИВНО-ЗМАГАЛЬНИХ МЕРЕЖ ДЛЯ СИНТЕЗУ БІОМЕДИЧНИХ ЗОБРАЖЕНЬ

**Березький О. М.** – д-р техн. наук, професор, професор кафедри автоматизованих систем управління НУ «Львівська політехніка», Львів, Україна.

**Ляшинський П. Б.** – аспірант кафедри автоматизованих систем управління НУ «Львівська політехніка», Львів, Україна.

### АНОТАЦІЯ

**Актуальність.** У статті досліджено проблему автоматичного проектування архітектур генеративно-змагальних мереж. Генеративно-змагальні мережі використовуються для синтезу зображень. Особливо це актуально для синтезу біомедичних зображень – цитологічних і гістологічних, які використовуються для постановки діагнозу в онкології. Синтезовані зображення використовуються для навчання згорткових нейронних мереж. Згорткові нейронні мережі є одними із найточніших класифікаторів біомедичних зображень на сьогодні..

**Мета роботи** – це розробка автоматичного методу для пошуку архітектур генеративно-змагальних мереж на основі генетичного алгоритму.

**Метод.** Розроблений метод складається з етапу пошуку архітектури генератора з фіксованим дискримінатором і етапу пошуку архітектури дискримінатора із найкращим генератором. На першому етапі визначається фіксована архітектура дискримінатора та здійснюється пошук генератора. Відповідно після першого кроку отримується архітектура найкращого генератора, тобто модель із найнижчим значенням FID.

На другому етапі використано найкращу архітектуру генератора та проведено пошук архітектури дискримінатора. На кожному циклі алгоритму оптимізації створюється популяція дискримінаторів. Після другого кроку отримується архітектура генеративно-змагальної мережі.

**Результати.** Для проведення експериментів використано цитологічні зображення раку молочної залози на платформі Zenodo. В результаті дослідження розроблено автоматичний метод пошуку архітектур генеративно-змагальних мереж. В результаті комп'ютерних експериментів отримано архітектуру генеративно-змагальної мережі для синтезу цитологічних зображень. Загальний час експерименту склав ~39.5 GPU годин. В результаті синтезовано 16 000 зображень (по 4000 на кожен клас). Для оцінки якості синтезованих зображень використано метрику FID. Результати експериментів показали, що розроблена архітектура є найкращою. Значення FID мережі становить 3.39. Цей результат є найкращим, порівняно з відомими генеративно-змагальними мережами.

**Висновки.** У статті розроблено метод пошуку архітектур генеративно-змагальних мереж для задач синтезу біомедичних зображень. Крім цього розроблено програмний модуль для синтезу біомедичних зображень, який може бути використаний для навчання CNN.

**КЛЮЧОВІ СЛОВА:** генеративно-змагальна мережа, біомедичні зображення, цитологічні зображення, пошук архітектур нейронних мереж, генетичні алгоритми, метрика FID, комп'ютерні системи автоматичної діагностики.

### ЛІТЕРАТУРА

1. Generative Adversarial Nets / [I. Goodfellow, J. Pouget-Abadie, M. Mirza et al.] // *Advances in Neural Information Processing Systems*. – 2014. – № 27.
2. Improved Techniques for Training GANs [Electronic resource] / [T. Salimans, I. Goodfellow, W. Zaremba et al.] // *arXiv.org*. – 2016. – Access mode: <https://arxiv.org/abs/1606.03498>.
3. Progressive Growing of GANs for Improved Quality, Stability, and Variation [Electronic resource] / [T. Karras, T. Aila, S. Laine et al.] // *arXiv.org*. – 2017. – Access mode: <https://arxiv.org/abs/1710.10196>.
4. Analyzing and Improving the Image Quality of StyleGAN [Electronic resource] // *Conference on Computer Vision and Pattern Recognition (CVPR) : proceedings, Seattle*. – 2020. – P. 8107–8116. – Access mode: <https://doi.org/10.1109/CVPR42600.2020.00813>.
5. Arjovsky M. Wasserstein Generative Adversarial Networks [Electronic resource] / M. Arjovsky, S. Chintala // *International Conference on Machine Learning : proceedings*. – 2017. – Access mode: <https://leon.bottou.org/publications/pdf/icml-2017.pdf>.
6. Düzyel O. Data Augmentation with GAN increases the Performance of Arrhythmia Classification for an Unbalanced Dataset [Electronic resource] / O. Düzyel, M. Kuntalp // *arXiv.org*. – 2023. – Access mode: <https://doi.org/10.48550/arXiv.2302.13855>.
7. Radford A. Unsupervised Representation Learning with Deep Convolutional Generative Adversarial Networks [Electronic resource] / A. Radford, L. Metz // *arXiv.org*. – 2016. – Access mode: <https://doi.org/10.48550/arXiv.2302.13855>.
8. End-to-End Adversarial Retinal Image Synthesis [Electronic resource] / [Pedro Costa et al.] // *IEEE Transactions on Medical Imaging*. – 2018. – Vol. 37, № 3. – P. 781–791. – Access mode: <https://doi.org/10.1109/tmi.2017.2759102>.
9. GAN-based synthetic medical image augmentation for increased CNN performance in liver lesion classification [Electronic resource] / [Maayan Frid-Adar et al.] // *Neurocomputing*. – 2018. – Vol. 321. – P. 321–331. – Access mode: <https://doi.org/10.1016/j.neucom.2018.09.013>.
10. Zoph B. Neural Architecture Search with Reinforcement Learning [Electronic resource] / B. Zoph, Q. Le // *arXiv.org*. – 2017. – Access mode: <https://doi.org/10.48550/arXiv.1611.01578>.

11. AutoGAN: Neural Architecture Search for Generative Adversarial Networks [Electronic resource] / [Xinyu Gong et al.] // 2019 IEEE/CVF International Conference on Computer Vision (ICCV), Seoul, Korea (South). – 2019. – Access mode: <https://doi.org/10.1109/iccv.2019.00332>.
12. Baker B. Designing Neural Network Architectures using Reinforcement Learning [Electronic resource] / B. Baker, O. Gupta // [arXiv.org](https://arxiv.org). – 2017. – Access mode: <https://doi.org/10.48550/arXiv.1611.02167>.
13. Efficient Two-stage Evolutionary Architecture Search for GANs [Electronic resource] / [G. Ying, X. He, B. Gao et al.] // [arXiv.org](https://arxiv.org). – 2020. – Access mode: <https://doi.org/10.48550/arXiv.2111.15097>.
14. AdversarialNAS: Adversarial Neural Architecture Search for GANs [Electronic resource] / [Chen Gao et al.] // 2020 IEEE/CVF Conference on Computer Vision and Pattern Recognition (CVPR), Seattle, WA, USA. – 2020. – Access mode: <https://doi.org/10.1109/cvpr42600.2020.00572>.
15. Brock A. Large Scale GAN Training for High Fidelity Natural Image Synthesis [Electronic resource] / A. Brock, J. Donahue, K. Simonyan // Semantic Scholar. – 2018. – Access mode: <https://www.semanticscholar.org/paper/Large-Scale-GAN-Training-for-High-Fidelity-Natural-Brock-Donahue/22aab110058ebbd198edb1f1e7b4f69fb13c0613>.
16. Deep network-based method and software for small sample biomedical image generation and classification / [O. M. Berezsky, P. B. Liashchynskiy, O. Y. Pitsun et al.] // Radio Electronics, Computer Science, Control. – 2024. – № 4. – P. 76.
17. Deep Residual Learning for Image Recognition [Electronic resource] / [Kaiming He et al.] // 2016 IEEE Conference on Computer Vision and Pattern Recognition (CVPR), Las Vegas, NV, USA. – 2016. – Access mode: <https://doi.org/10.1109/cvpr.2016.90>.
18. Attention is All you Need [Electronic resource] / [A. Vaswani, N. Shazeer, N. Parmar et al.] // Semantic Scholar. – 2017. – Access mode: <https://www.semanticscholar.org/paper/Attention-is-All-you-Need-Vaswani-Shazeer/204e3073870fae3d05bcb2f6a8e263d9b72e776>.
19. Sunkara R. No More Strided Convolutions or Pooling: A New CNN Building Block for Low-Resolution Images and Small Objects [Electronic resource] / Raja Sunkara, Tie Luo // Machine Learning and Knowledge Discovery in Databases. – Cham, 2023. – P. 443–459. – Access mode: [https://doi.org/10.1007/978-3-031-26409-2\\_27](https://doi.org/10.1007/978-3-031-26409-2_27).
20. Barratt S. A Note on the Inception Score. [Electronic resource] / S. Barratt, R. Sharma // [arXiv.org](https://arxiv.org). – 2018. – Access mode: <https://arxiv.org/abs/1801.01973>.
21. Borji A. Pros and cons of GAN evaluation measures [Electronic resource] / Ali Borji // Computer Vision and Image Understanding. – 2019. – Vol. 179. – P. 41–65. – Access mode: <https://doi.org/10.1016/j.cviu.2018.10.009>.
22. Differentiable Augmentation for Data-Efficient GAN Training [Electronic resource] / [S. Zhao, Z. Liu, J. Lin et al.] // [arXiv.org](https://arxiv.org). – 2020. – Access mode: <https://arxiv.org/abs/2006.10738>.
23. Regularized Evolution for Image Classifier Architecture Search [Electronic resource] / [Esteban Real et al.] // Proceedings of the AAAI Conference on Artificial Intelligence. – 2019. – Vol. 33. – P. 4780–4789. – Access mode: <https://doi.org/10.1609/aaai.v33i01.33014780>.
24. Cytological and histological images of breast cancer. (n.d.) [Electronic resource] // Zenodo. – 2023. – Access mode: <https://doi.org/10.5281/zenodo.7890874>.
25. Liashchynskiy P. Rudi – Python library [Electronic resource] / Petro Liashchynskiy // GitHub. – 2018. – Access mode: <https://github.com/liashchynskiy/rudi>.
26. Ye J. Geometric GAN [Electronic resource] / J. Ye, J. Lim // [arXiv.org](https://arxiv.org). – 2017. – Access mode: <https://arxiv.org/abs/1705.02894>.
27. Kingma D. Adam: A Method for Stochastic Optimization [Electronic resource] / D. Kingma, J. Ba // [arXiv.org](https://arxiv.org). – 2017. – Access mode: <https://arxiv.org/abs/1412.6980>.
28. Bynagari N. B. GANs Trained by a Two Time-Scale Update Rule Converge to a Local Nash Equilibrium [Electronic resource] / Naresh Babu Bynagari // Asian Journal of Applied Science and Engineering. – 2019. – Vol. 8, № 1. – P. 25–34. – Access mode: <https://doi.org/10.18034/ajase.v8i1.9>.
29. Miyato T. Spectral Normalization for Generative Adversarial Networks [Electronic resource] / T. Miyato, T. Kataoka, M. Koyama // [arXiv.org](https://arxiv.org). – 2018. – Access mode: <https://arxiv.org/abs/1802.05957>.
30. Berezsky O. M. Comparison of generative adversarial networks architectures for biomedical images synthesis [Electronic resource] / Oleh M. Berezsky, Petro B. Liashchynskiy // Applied Aspects of Information Technology. – 2021. – Vol. 4, № 3. – P. 250–260. – Access mode: <https://doi.org/10.15276/aait.03.2021.4>.
31. Design of computer systems for biomedical image analysis / [O. M. Berezsky, K. M. Berezska, G. M. Melnyk et al.] // Proceedings of the X<sup>th</sup> International Conference «The Experience of Designing and Application of CAD Systems in Microelectronics» CADSM 2009. – Lviv : Publishing House Vezha&CoC. – P. 186–191.
32. Berezsky O. The intelligent system for diagnosing breast cancers based on image analysis [Electronic resource] / Oleh Berezsky, Serhiy Verbovyi, Tamara Datsko // 2015 Information Technologies in Innovation Business Conference (ITIB), Kharkiv, Ukraine, 7–9 October 2015. – 2015. – Access mode: <https://doi.org/10.1109/itib.2015.7355067>.
33. Fuzzy system diagnosing of precancerous and cancerous conditions of the breast [Electronic resource] / [Oleh Berezsky et al.] // 2016 XI<sup>th</sup> International Scientific and Technical Conference “Computer Sciences and Information Technologies (CSIT), Lviv, Ukraine, 6–10 September 2016. – 2016. – Access mode: <https://doi.org/10.1109/stcsit.2016.7589906>.
34. Berezsky O. Hybrid Intelligent Information Technology for Bio-medical Image Processing [Electronic resource] / O. Berezsky, S. Verbovyi, O. Pitsun // IEEE 13<sup>th</sup> International Scientific and Technical Conference on Computer Sciences and Information Technologies. – 2018. – Access mode: <https://ieeexplore.ieee.org/document/8526711>.
35. Fuzzy System For Breast Disease Diagnosing Based On Image Analysis [Electronic resource] / [O. Berezsky, L. Dubchak, T. Batryn et al.] // Proceedings of the II International Workshop Informatics & Data-Driven Medicine (IDDM 2019). – 2019. – Access mode: <http://ceur-ws.org/Vol-2488/paper6.pdf>.

## MACHINE LEARNING FOR AUTOMATIC EXTRACTION OF WATER BODIES USING SENTINEL-2 IMAGERY

**Kashtan V. Yu.** – PhD, Associate Professor, Associate Professor of Department of Information Technology and Computer Engineering, Dnipro University of Technology, Dnipro, Ukraine.

**Hnatushenko V. V.** – Dr. Sc., Professor, Head of Department of Information Technology and Computer Engineering, Dnipro University of Technology, Dnipro, Ukraine.

### ABSTRACT

**Context.** Given the aggravation of environmental and water problems, there is a need to improve automated methods for extracting and monitoring water bodies in urban ecosystems. The problem of efficient and automated extraction of water bodies is becoming relevant given the large amount of data obtained from satellite systems. The object of study is water bodies that are automatically extracted from Sentinel-2 optical satellite images using machine learning methods.

**Objective.** The goal of the work is to improve the efficiency of the process of extracting the boundaries of water bodies on digital optical satellite images by using machine learning methods.

**Method.** The paper proposes an automated information technology for delineating the boundaries of water bodies on Sentinel-2 digital optical satellite images. The process includes eight stages, starting with data download and using topographic maps to obtain basic information about the study area. Then, the process involved data pre-processing, which included calibrating the images, removing atmospheric noise, and enhancing contrast. Next, the EfficientNet-B0 architecture is applied to identify water features, facilitating optimal network width scaling, depth, and image resolution. ResNet blocks compress and expand channels. It allows for optimal connectivity of large-scale and multi-channel links across layers. After that, the Regional Proposal Network defines regions of interest (ROI), and ROI alignment ensures data homogeneity. The Fully connected layer helps in segmenting the regions, and the Fully connected network creates binary masks for accurate identification of water bodies. The final step of the method is to analyze spatial and temporal changes in the images to identify differences, changes, and trends that may indicate specific phenomena or events. This approach allows automating and accurately identifying water features on satellite images using machine learning.

**Results.** The implementation of the proposed technology is development through Python software development. An assessment of the technology's accuracy, conducted through a comparative analysis with existing methods, such as water indices and K-means, confirms a high level of accuracy in the period from 2017 to 2023 (up to 98%). The Kappa coefficient, which considers the degree of consistency between the actual and predicted classification, confirms the stability and reliability of our approach, reaching a value of 0.96.

**Conclusions.** The experiments confirm the effectiveness of the proposed automated information technology and allow us to recommend it for use in studies of changes in coastal areas, decision-making in the field of coastal resource management, and land use. Prospects for further research may include new methods that seasonal changes and provide robustness in the selection and mapping of water surfaces.

**KEYWORDS:** extraction, water bodies, optical satellite images, water spectral indices, machine learning, Kappa coefficient, Pearson coefficient, confusion matrix.

### ABBREVIATIONS

OLI is an Operational Land Imager;  
ETM is an Enhanced Thematic Mapper Plus;  
CNNs are Convolutional Neural Networks;  
ResNet is a Residual neural network;  
ReLU is a rectified linear unit;  
ROI is a Region of Interest;  
RPN is a Regional Proposal Network;  
FCN is a fully connected network;  
TP is a True Positive;  
TN is a True Negatives;  
FP is a False Positive;  
FN is a False Negatives;  
IR is the infrared channel;  
RMSE is a Root Mean Square Error;  
PDF is a Probability Density Function;  
OA is an Overall Accuracy;  
NDSI is a Normalized Difference Snow Index;  
NDWI is a Normalized Difference Water Index;  
MNDWI is a Modified Normalized Difference Water

Index;

XGBoost is an eXtreme Gradient Boosting.

### NOMENCLATURE

$L_\lambda$  is an energy brightness for the spectral zone [W/(s<sup>2</sup> nm)];  
 $D$  is an distance from the Earth to the Sun in astronomical units for a particular period;  
 $E_{sun\lambda}$  is an average solar extraterrestrial irradiance [W/(m<sup>2</sup> nm)];  
 $\theta$  is an angle of the Sun;  
 $x'$  is an input;  $x$  is the output;  
 $y$  is an final output;  
 $L$  is an length of the coastline;  
 $W$  is an width of the coastline;  
 $\bar{x}$ ,  $\bar{y}$  are average values of two variables  $x$  and  $y$ , respectively;  
 $T$  is a total number of pixels in the Sentinel-2 image;  
 $L$  is a length of the coastline;  
 $W$  is a width of the coastline.

## INTRODUCTION

Water is an inexhaustible source of life and a critical element for urbanized ecosystems. The impacts of human exploitation, land use change, land disturbance, and climate change are hurting the hydrological cycle. These factors lead to a restructuring of the distribution of surface and groundwater on our planet [1].

The growing impact of global climate change and intense human activity is leading to significant changes like rivers: shrinking wetlands increased flooding, and other changes in the spatial and temporal distribution of water resources. Despite these transformations, the dynamics of changes in surface water bodies remain poorly understood, especially in the context of their seasonal and inter-annual characteristics. The lack of information in this context makes it difficult to fully understand the patterns that govern the dynamics of water bodies [2].

Given the importance of this issue, real-time access to information on the spatial distribution and changes over time of wetlands, estuaries, and river floods appears to be fundamental to understanding the interaction of regional hydrology and climate change, as well as to the effective management of surface water resources [3]. In this context, remote sensing is coming to the forefront as an effective means of monitoring changes in surface water bodies in real-time and providing dynamic access to information about the earth's surface [4].

**The object of study** is the water surfaces of urban ecosystems that are automatically extracted from Sentinel-2 optical satellite images using machine learning methods.

**The subject of study** is the extraction of water bodies technology on digital optical satellite images using machine learning methods.

**The purpose of the work** is to enhance the efficiency of detecting water body boundaries on digital optical satellite images using machine learning methods.

## 1 PROBLEM STATEMENT

Data obtained from space satellites such as Landsat, Advanced Spaceborne Thermal Emission and Reflection Radiometer, Satellite Pour l'Observation de la Terre, and Sentinel-1 and Sentinel-2 open up opportunities for a wide range of applications. These data allow for flood monitoring, water resource assessment [5], water quality [6], and coastal monitoring [7]. These products play a crucial role in contemporary approaches to monitoring and managing water resources and the natural environment. Nevertheless, optical satellite images may include clouds, as noted by [8], along with their shadows, posing challenges in processing such data and identifying water features. Special emphasis needs to be placed on investigating coastal ecotone zones, distinctive regions where a transitional zone emerges between land and water, frequently characterized by aquatic vegetation. These ecotones significantly influence the precision of identifying and classifying water bodies in satellite imagery.

Thus, optical satellite images can provide information for monitoring water bodies. On the other hand, given the difficulties associated with cloud shadows and low-albedo objects, it is necessary to continuously improve methods for recognizing water features on satellite images.

## 2 REVIEW OF THE LITERATURE

Currently, there are developed methods for detecting, mapping, and monitoring water bodies on satellite images. These methods can be divided into three main groups: pixel-based statistical pattern recognition analysis, which includes supervised [9] and unsupervised [10] classification approaches; image analysis, taking into account parameters such as spectral characteristics, texture, shape complexity [11] and sub-pixel analysis [12]. Water spectral indices are widely used for monitoring water bodies. The researchers compared the effectiveness of different water indices in Landsat 7 ETM+, Landsat 8 OLI, and Sentinel-2 MSI. The study [13] proposed a new water index for Landsat Thematic Mapper /Enhanced Thematic Mapper Plus (ETM+)/OLI satellites based on surface reflectance using a threshold value. This method is optimized for processing large amounts of data and provides a simple but effective approach for the automated classification of large water bodies by area. Although existing methods based on water spectral indices can provide high accuracy in determining surface water areas, they are ineffective when analyzing multispectral satellite images.

Classification methods that use feature extraction and machine learning are advanced techniques for monitoring surface water bodies, such as random forests [14], support vector machines [15], and XGBoost [16]. On the other hand, unsupervised classification methods do not require training samples and are more suitable for developing automated algorithms. CNNs are considered a popular deep learning method and are commonly used for semantic segmentation, cloud detection, water feature extraction, and other tasks [17]. A lot of new deep-learning models have been developed for surface water body extraction based on satellite data [18], for which multiscale semantic information is important.

## 3 MATERIALS AND METHODS

The extraction of water bodies technology proposed in this paper consists of eight stages, as shown in Figure 1.

The first stage consists of downloading images from 2017 to 2023 from the Sentinel-2 optical satellite in the summer. Then use the topographic maps that contain basic information about the study area. To map the contours of water bodies on topographic maps, we use geospatial analysis to determine the coordinates of the coastline on the map.

The second stage is data pre-processing, which includes calibration of satellite images, removal of atmospheric noise, and contrast enhancement. The task of radiometric calibration is to convert brightness values (Digital Number) into spectral energy brightness values at the upper atmosphere boundary.

The transmission of electromagnetic radiation and the atmosphere's glow were taken into account for atmospheric correction. At the same stage, pixel values were converted from energy brightness to reflectance coefficients from 0 to 1 [19]:

$$p_{\lambda} = \frac{\pi \times L_{\lambda} \times D^2}{E_{sun\lambda} \times \cos \theta}, \quad (1)$$

where  $L_{\lambda}$  is the energy brightness for the spectral zone [W/(s $\times$ m $\times$ nm)];  $D$  is the distance from the Earth to the Sun in astronomical units for a particular period;  $E_{sun\lambda}$  is the average solar extraterrestrial irradiance [W/(m $\times$ nm)];  $\theta$  is the angle of the Sun.

To use the EfficientNet-B0 architecture to identify water bodies. The EfficientNet architecture defines an effi-

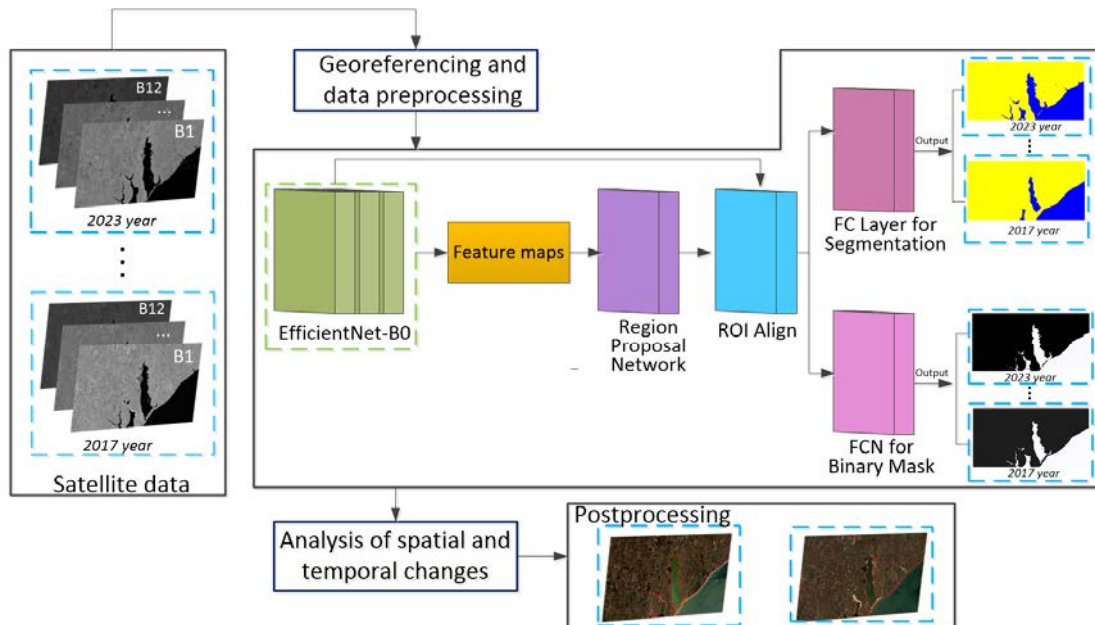
cient approach to image processing developed using the AutoML method [19]. The main idea behind this architecture is to optimally scale the network width, network depth, and image resolution.

EfficientNet consists of 8 variations, designated from B0 to B7, each with its number of parameters and accuracy. This series of architectures is designed with limited resources in mind, and B0 is the lightest version suitable for use in resource-constrained applications.

Depth convolution is performed independently for each input channel, which is a spatial convolution [20]:

$$x' = \text{DepthwiseConv}(x), \quad (2)$$

where  $x'$  is the input;  $x$  is the output; DepthwiseConv uses spatial convolution for each channel independently.



Legend: — - steps to execute the method; - - - raster data; - - - EfficientNet-B0 architecture.

Figure 1 – Algorithm of the proposed technology

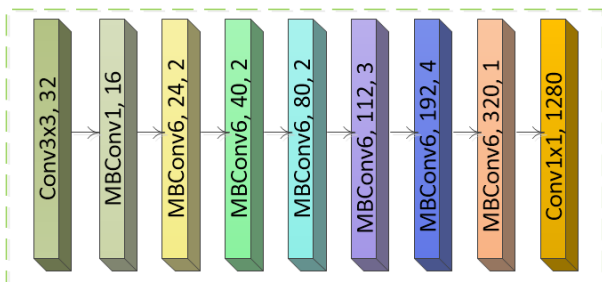


Figure 2 – EfficientNet-B0 architecture

Point convolution projects the channel output resulting from depth convolution onto a new channel space using a  $1 \times 1$  convolution [20]:

$$y = \text{PointwiseConv}(x'), \quad (3)$$

where  $y$  is the final output.

ResNet blocks consist of a layer that compresses the channels and a layer that expands the channels. This allows bandwidth-intensive connections to be linked to channel-rich connections in layers. Linear activation is used in the last layer of each block to prevent loss of information from the ReLU [21].

In the next stage, using the output data from EfficientNet-B0, feature maps are created for further use. These feature maps contain important information features of the image that will be used in the analysis and processing. The Regional Proposal Network is used to determine the ROI. The RPN is responsible for identifying potential locations where objects may be located. The ROI alignment process is performed to ensure data homogeneity. It may include resampling or other operations to bring all ROIs to the same standard size or format. A fully

connected layer is used to segment the ROIs. This layer helps to divide the image into different classes or areas that are important for further analysis. A FCN is used to create binary masks. These masks identify areas that have water features.

The final stage of the algorithm is the analysis of spatial and temporal changes in the images. It includes identifying differences, changes, and trends in the images that may indicate certain phenomena or events.

#### 4 EXPERIMENTS

This paper tested the proposed information technology on the example of the Molochnyi Lyman, located in the south of Zaporizhzhia Oblast within the Melitopol district, which is an arid region of southern Ukraine, where high temperatures are observed, especially in recent years, due to global warming. Such climatic conditions cause increased evaporation from its water surface up to 155 million m<sup>3</sup> per year, sometimes even up to 250 million m<sup>3</sup>.



Figure 3 – Study area

The Pearson's  $r$  coefficient was used to analyze the change in the area of the Molochny Lyman water mirror [22]:

$$r = \frac{\sum(x - \bar{x})(y - \bar{y})}{\sqrt{\sum(x - \bar{x})^2 \sum(y - \bar{y})^2}}, \quad (4)$$

where  $\bar{x}$ ,  $\bar{y}$  are the average values of two variables  $x$  and  $y$ , respectively.

Two metrics were calculated to assess the effectiveness of the water body monitoring technology proposed in this paper: OA and Kappa coefficient. These metrics provide an objective assessment and compare the effectiveness of the developed method with water indices and the K-means method [22]:

$$OA = \frac{TP + TN}{T}, \quad (5)$$

$$Kappa = \frac{T \times (TP + TN) - (TP + TN)^2}{T \times T - (TP + TN)^2}, \quad (6)$$

where  $T$  is the total number of pixels in the Sentinel-2 image;  $TP$ ,  $TN$  are the categorized pixels by comparing the extracted water pixels with the reference map:  $TP$  are true positives, i.e., the number of correctly extracted pixels;  $TN$  is the number of correctly identified pixels that are not water bodies and were correctly categorized into another class.

Confusion Matrix (Fig. 4) is an important tool for evaluating the effectiveness of classification models in machine learning and computer vision tasks. This tool allows you to visualize the classification results and determine the accuracy level of the model. The matrix determines the number of objects that were correctly or incorrectly classified in each category:  $TP$  is the number of correctly identified positive classes.  $TN$  is the number of correctly identified negative classes.  $FP$  is the number of false positive classes.  $FN$  is the number of false negatives identified. It is a useful tool for understanding the types of errors that can occur during classification [22].

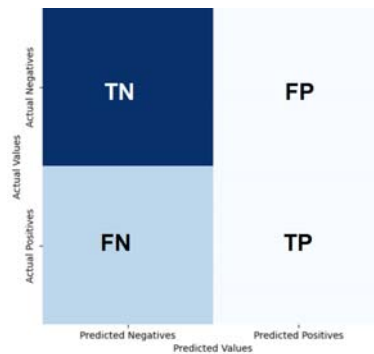


Figure 4 – Graphical presentation of Confusion Matrix

#### 5 RESULTS

The Pearson correlation coefficient was used to assess changes in water bodies and the coastline, which can have a value ranging from -1 to 1. A value close to 1 indicates a strong positive relationship between the masks, a value close to -1 indicates a strong negative relationship and a value close to 0 indicates no relationship. The results of the Pearson's coefficient values are shown in the form of a graph in Fig. 5.

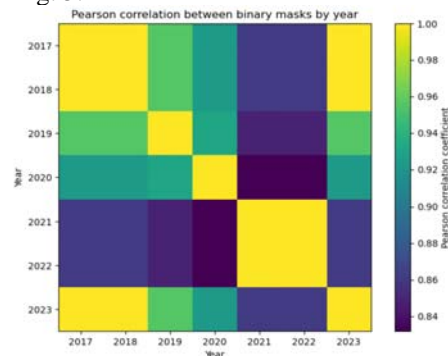


Figure 5 – Graph of Pearson's coefficient values by year

The resulting water body contours were analyzed in detail using geographic information technologies and the Python programming language (Fig. 6). The analysis of water body contours made it possible to determine the nature of changes, their intensity, and distribution along the coastal zone of the Molochny Lyman.

The next step is to analyze the average annual rate of change in the area of water bodies of the Molochny Lyman between 2017 and 2023. At this stage, the water

mirror area was calculated, as well as the nature of the changes, their intensity, and distribution along the coastal zone of the Molochny Lyman for 6 years:

$$S = L \times W, \quad (7)$$

where  $L$  is the length of the coastline;  $W$  is the width of the coastline.

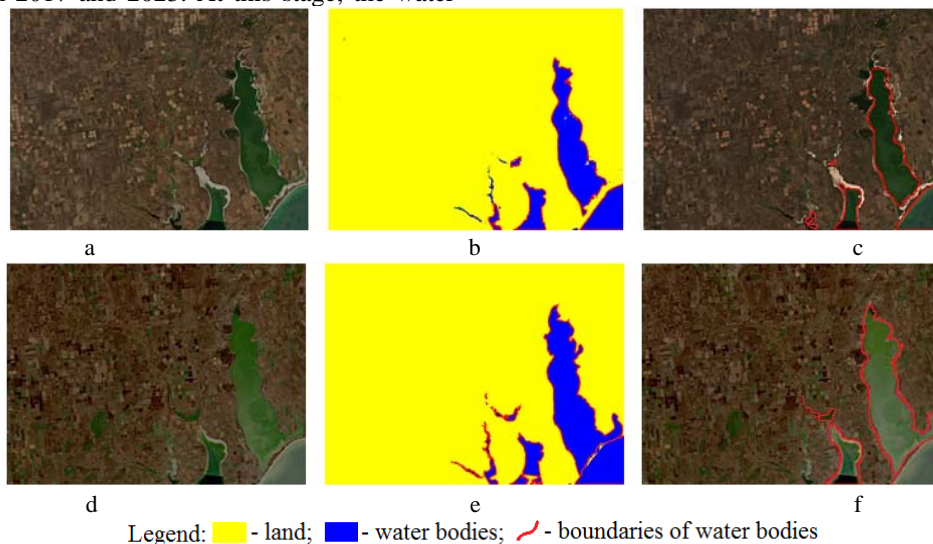


Figure 6 – The result of the proposed technology: a – Satellite image of 2017; b – selection of water bodies after segmentation in 2017; c – automated selection of water bodies on the satellite image of 2017; d – Satellite image of 2023; e – selection of water bodies after segmentation in 2023; f – automated selection of water bodies on the satellite image of 2023

Figure 7 shows a graph of changes in the water surface area of the Molochny Lyman from 2017 to 2023 years.

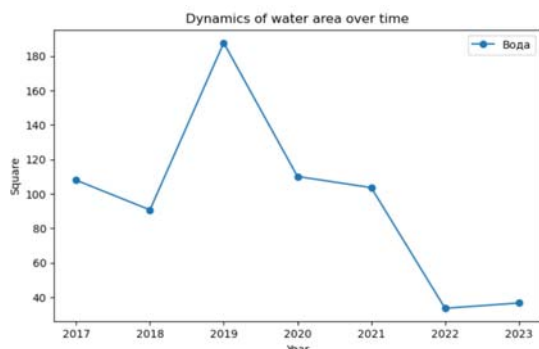


Figure 7 – Graph of changes in the area of the water mirror of the Molochny Lyman

In this study, a graph of the values of the coastal zone reflection coefficients in the IR channel for the period 2017–2023 was constructed and analyzed (Fig. 8). Changes in the values of the reflection coefficients in the IR channel indicate differences in the temperature and heat transfer of the coastal zone. It may be due to climate change, expansion or contraction of water bodies, or other natural and anthropogenic impacts.

In 2019, we took large-scale measures to restore the relationship between the Molochnyi Lyman and the Sea of Azov during the information verification. In particular,

on December 27, 2019, the estuary began to be filled with seawater, which led to a rise in water level and a decrease in water salinity in some places to 25 ppm. These actions have become a significant factor that may affect the water area in the estuary and its ecosystem in the future.

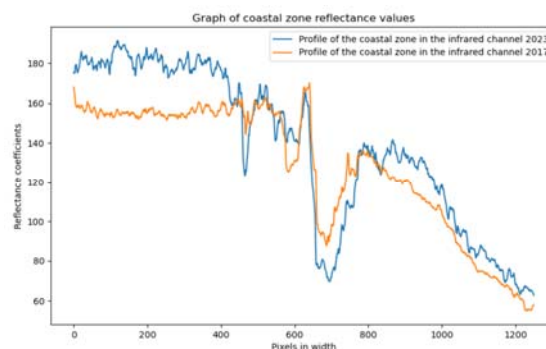


Figure 8 – Graph of coastal zone reflection coefficients in the infrared channel

Table 1 shows the results of the OA and Kappa metrics for the proposed technology and the NDWI, MNDWI [23], and K-means indices. In 2017 and 2023, the proposed technology identifies water bodies with an accuracy of 98% and a Kappa coefficient of 0.96. Compared to this, other methods, such as NDWI, MNDWI, and K-means have lower performance.

Table 1 – Results of the water body contouring accuracy assessment

Methods	2017 year		2023 year	
	OA	Kappa	OA	Kappa
NDWI	77%	0.64	77%	0.51
MNDWI	90%	0.82	93%	0.86
K-means	95%	0.88	94%	0.86
Proposed technology	98%	0.96	98%	0.96

Root Mean Square Error is used to evaluate the accuracy of a technology by comparing its predicted values to the actual values [24, 25]. A low RMSE value indicates the technology has high accuracy, while a high value may indicate low accuracy. To summarize the information according to Fig. 9, the low RMSE value for the proposed method indicates its high accuracy compared to other methods, and the high value for the NDSI method indicates a significant difference between predicted and actual values and the need for further optimization and refinement of the technology.

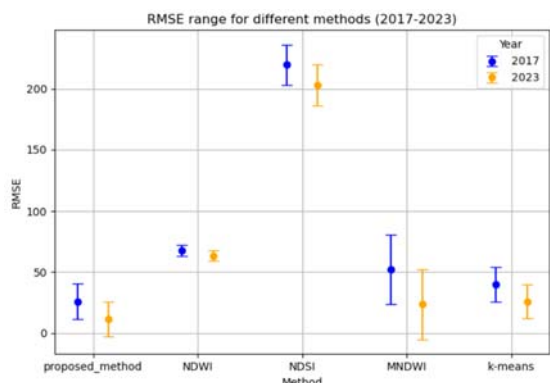


Figure 9 – RMSE value graph

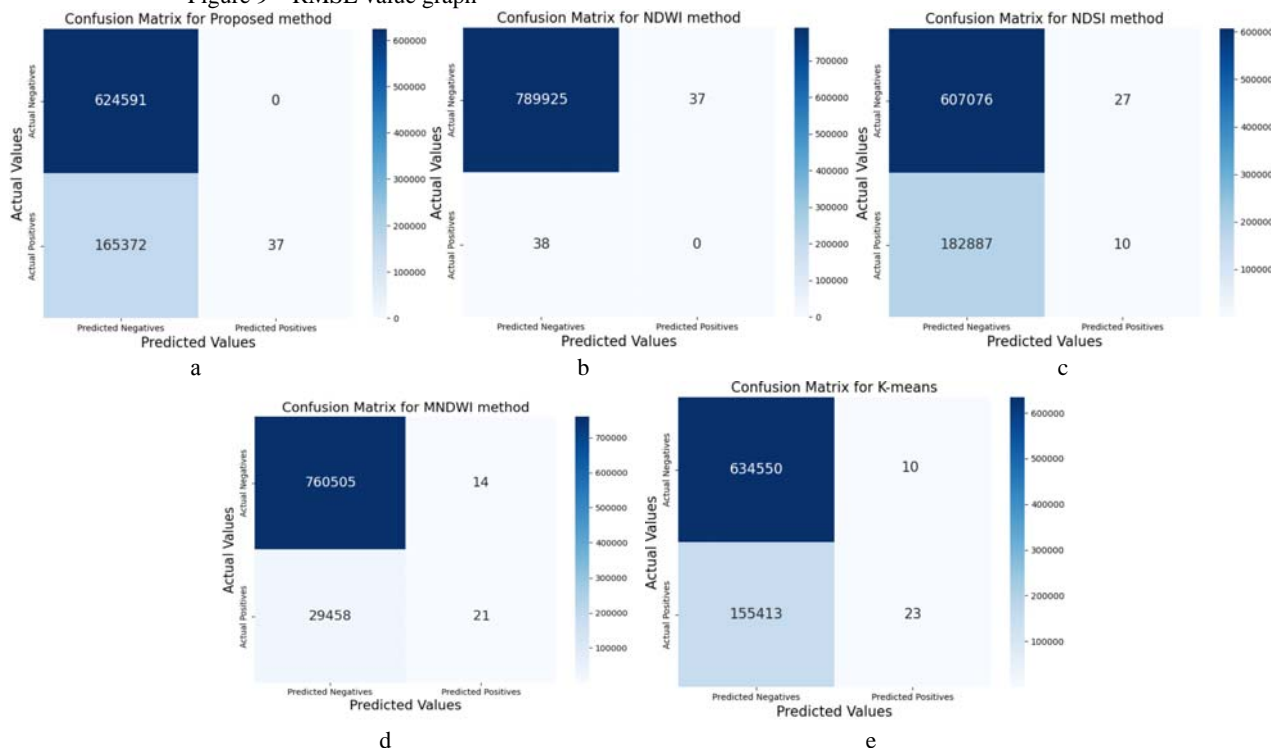


Figure 11 – Confusion matrix result for: a – proposed method; b – NDWI; c – NDSI; d – MNDWI; e – K-means

The histogram in Fig. 10 of the probability density function of the coastal zone, with the highlighting of land, water, and Otsu threshold pixels, provides information about the distribution of areas in the image.

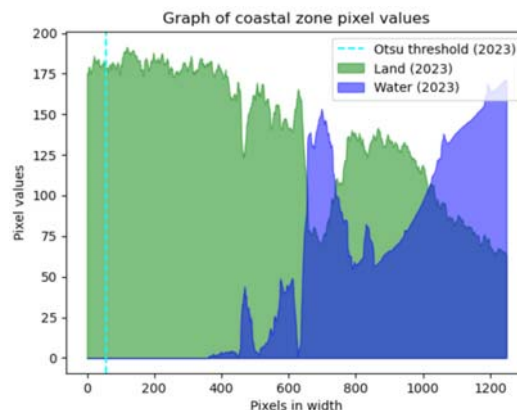


Figure 10 – Histogram of the PDF

The Confusion matrix (Fig. 11) displays the results of the classification models, showing the number of correctly and incorrectly classified objects in each category.

## 6 DISCUSSION

Analyzing the data in Fig. 7 on the area of the Molochny Lyman during the years 2017-2023, it is possible to make several conclusions. Firstly, the water area tends to increase during the analyzed years, especially from 2019 to 2020. Secondly, from 2017 to 2018, the relative change in water is positive, which may indicate an increase in water area in 2018. From 2018 to 2019, there is a decrease in the water area (negative relative change), and from 2019 to 2020 year there is a sharp increase in the water area (positive relative change); from 2020 to 2021, there is a decrease in the water area again. Various factors, including climatic conditions, anthropogenic activities, and hydrological changes, can influence changes in the area of a water body. Analyzing the dynamics of the water area of the Molochny Lyman, a significant increase was observed in 2020. This effect may be due to special climatic conditions, changes in the water supply regime, or other natural factors.

During the information verification, it was found that in 2019, large-scale measures were taken to restore the relationship between the Molochnyi Lyman and the Sea of Azov. In particular, on December 27, 2019, the estuary began to be filled with seawater, which led to a rise in water level and a decrease in water salinity in some places to 25 ppm. These actions have become a significant factor that may affect the water area in the estuary and its ecosystem in the future.

The results of Table 1 demonstrate the high accuracy of the proposed information technology compared to existing methods, emphasizing its effectiveness for recognizing and monitoring water bodies based on satellite images.

In 2023, the obtained RMSE results for different methods indicate the accuracy and differences in their effectiveness. The low RMSE value (11.35) indicates the high accuracy of the proposed method compared to the actual data for 2023. The RMSE value for the NDSI method (202.80) indicates a difference between the predicted and actual values. This indicates the low accuracy of this method.

The resulting PDF highlights that the pixel values corresponding to the 'land' class are concentrated around positive values. The pixels representing the 'water' class have negative values. The Otsu algorithm is used to determine the threshold between the 'land' and 'water' classes. This algorithm maximizes the inter-class variance between the 'land' and 'water' distributions by pre-excluding pixels that belong to the 'water' and 'other land features' classes. This approach helps to effectively determine the threshold for classifying the coastal zone in the image.

Analyzing the results confusion matrix for the proposed method and comparing it with the others, it is noticeable that the proposed method and K-means are more effective, having fewer false classifications and a significant number of correctly classified pixels as water or land. It indicates the high accuracy and reliability of the proposed method in identifying water and land regions in images.

© Kashan V. Yu., Hnatushenko V. V., 2024  
DOI 10.15588/1607-3274-2024-1-11

## CONCLUSIONS

The developed technology for automatic delineation of water bodies effectively addresses the challenges of precise and timely determination of the dynamics of water surfaces in digital optical satellite imagery. Compared to traditional methods requiring substantial effort and time for processing and analyzing large datasets, the proposed technology employs machine learning and image analysis methods to automatically extract water bodies. It accelerates and enhances the accuracy of the monitoring process, reducing resource expenditures for data processing and interpretation.

**The scientific novelty** of the developed technology is to improve the methods of identifying and monitoring water bodies based on digital optical satellite images using machine learning. To use of modern algorithms and deep learning models allows for achieving high accuracy and sub-pixel resolution in the classification of surface water bodies. The developed approach demonstrates efficiency in comparison with traditional methods such as water indices and K-means, ensuring the stability of results even under variable research conditions. The obtained high accuracy and stability indicators, as a high Kappa coefficient, confirm the advantages and prospects of the developed method for application in the area of urban ecosystems and water management. This approach opens up new opportunities for more accurate and automated analysis of water bodies, contributing to the further development of research in the area of urban geographic information systems and environmental monitoring.

The proposed technology holds **practical significance** as it enables systematic monitoring of water resources and their changes in urban ecosystems. It makes it possible to accurately determine the volume of water bodies, monitor their changes over time, and predict possible environmental challenges.

**Prospects for further research** involve exploring seasonality and enhancing robustness in the water surface mapping.

## ACKNOWLEDGEMENTS

The work is supported by the state budget scientific research project of Dnipro University of Technology "Models and information technologies of data processing and analysis in complex computer systems and networks" (state registration number 0121U114523).

## REFERENCES

1. Xiang X., Li Q., Khan S., Khalaf O. Urban water resource management for sustainable environment planning using artificial intelligence techniques, *Environmental Impact Assessment Review*, 2021, Vol. 86, pp. 106515. DOI: 10.1016/j.eiar.2020.106515.
2. Bierbaum R., Leonard S., Rejeski D., Whaley C.r., Barra R., Libre C. Novel entities and technologies: Environmental benefits and risks, *Environmental Science & Policy*, 2020, Vol. 105, pp. 134–143. DOI: 10.1016/j.envsci.2019.11.002.
3. Ivanov D., Hnatushenko V., Kashtan V., Garkusha I. Computer modeling of territory flooding in the event of an emergency at Sredniodniprovsk Hydroelectric Power Plant,



- Naukovyi Visnyk Natsionalnoho Hirnychoho Universytetu*, 2022, № 6, pp. 158–163. DOI:10.33271/nvngu/2022-6/123.
4. Mozgovoy D., Hnatushenko V., Vasyliov V. Automated recognition of vegetation and water bodies on the territory of megacities in satellite images of visible and IR bands, *ISPRS Ann. Photogramm. Remote Sens. Spatial Inf. Sci.*, 2018, IV-3, pp. 167–172. DOI: 10.5194/isprs-annals-IV-3-167-2018.
  5. Xie H., Luo X., Xu X., Pan H., Tong X. Automated Sub-pixel Surface Water Mapping from Heterogeneous Urban Environments Using Landsat 8 OLI Imagery, *Remote Sens*, 2016, No. 8(7), P. 584. DOI:10.3390/rs8070584.
  6. Ruppen D., Runnalls J., Tshimanga R., Wehrli B., Odermatt D. Optical remote sensing of large-scale water pollution in Angola and DR Congo caused by the Catoca mine tailings spill, *International Journal of Applied Earth Observation and Geoinformation*, 2023, Vol. 118, P. 103237. DOI: 10.1016/j.jag.2023.103237.
  7. Palomar-Vázquez J., Pardo-Pascual J., Almonacid-Caballer J., Cabezas-Rabadán C. Shoreline Analysis and Extraction Tool (SAET): A New Tool for the Automatic Extraction of Satellite-Derived Shorelines with Subpixel Accuracy, *Remote Sensing*, 2023, No. 15(12), P. 3198. DOI: 10.3390/rs15123198.
  8. Zhiwei Li. and Shen, Huanfeng and Weng, Qihao and Zhang, Yuzhuo and Dou, Peng and Zhang Cloud and cloud shadow detection for optical satellite imagery: Features, algorithms, validation, and prospects, *ISPRS Journal of Photogrammetry and Remote Sensing*, 2022, No. 188, pp. 89–108. DOI: 10.1016/j.isprsjprs.2022.03.020.
  9. Mao T., Fan Y., Zhi S., Tang J. A Morphological Feature-Oriented Algorithm for Extracting Impervious Surface Areas Obscured by Vegetation in Collaboration with OSM Road Networks in Urban Areas, *A Remote Sensing*, 2022, No. 14(10), P. 2493. DOI: 10.3390/rs14102493.
  10. Nardini A., Salas F., Carrasco Z., Valenzuela N., Rojas R., Vargas-Baecheler J., Yépez S. Automatic River Planform Recognition Tested on Chilean Rivers, *Water*, 2023, No. 15(14), P. 2539. DOI: 10.3390/w15142539.
  11. Wenbo Li. Ying Qin, Youqiang Sun, Huang He, Ling Feng, Tian Liqiao, Ding Yulin Estimating the relationship between dam water level and surface water area for the Danjiangkou Reservoir using Landsat remote sensing images, *Remote Sensing Letters*, 2016, Vol. 7, pp. 121–130. DOI: 10.1080/2150704X.2015.1117151.
  12. Xie H., Luo X., Xu X., Pan H., Tong X. Automated Sub-pixel Surface Water Mapping from Heterogeneous Urban Environments Using Landsat 8 OLI Imagery, *Remote Sensing*, 2016, No. 8(7), P. 584. DOI: 10.3390/rs8070584.
  13. Fisher A., Flood N., Danaher T. Comparing Landsat water index methods for automated water classification in eastern Australia, *Remote Sensing of Environment*, 2016, Vol. 175, pp. 167–182. DOI: 10.1016/j.rse.2015.12.055.
  14. Wangchuk S., Bolch T. Mapping of glacial lakes using Sentinel-1 and Sentinel-2 data and a random forest classifier: Strengths and challenges, *Science of Remote Sensing*, 2020, Vol. 2, P. 100008. DOI: 10.1016/j.srs.2020.100008.
  15. Liu Q., Huang C., Shi Z., Zhang S. Probabilistic River Water Mapping from Landsat-8 Using the Support Vector Machine Method, *Remote Sensing*, 2020, No. 12(9), P. 1374. DOI: 10.3390/rs12091374.
  16. Chatufale A., Abhishek P. Extraction of Waterbody Using Object-Based Image Analysis and XGBoost, *Advanced Machine Intelligence and Signal Processing. Singapore: Springer Nature Singapore*, 2022, pp. 341–350. DOI:10.1007/978-981-19-0840-8\_25.
  17. Feng W., Haigang H., Weiming X., Chuan A., Kaiqiang An. Water Body Extraction From Very High-Resolution Remote Sensing Imagery Using Deep U-Net and a Superpixel-Based Conditional Random Field Model, *IEEE Geoscience and Remote Sensing Letters*, 2018, pp. 1–5. DOI: 10.1109/LGRS.2018.2879492.
  18. Jiang W., He G., Long T., Ni Y., Liu H., Peng Y., Lv K., Wang G. Multilayer Perceptron Neural Network for Surface Water Extraction in Landsat 8 OLI Satellite Images, *Remote Sensing*, 2018, No. 10 (5), P. 755. DOI: 10.3390/rs10050755.
  19. Lu Li, Bing W., Shichao W., Li Fan, Qingjie L. Water Body Extraction from High-resolution Remote Sensing images Based on Scaling EfficientNets, *Journal of Physics: Conference Series*, 2021, pp. 1–5. DOI: 10.1088/1742-6596/1894/1/012100.
  20. Hachiya H., Nagayoshi K., Iwaki A., Maeda T., Ueda N., Fujiwara H. Position-dependent partial convolutions for supervised spatial interpolation, *Machine Learning with Applications*, 2023, Vol. 14. DOI: 10.1016/j.mlwa.2023.100514.
  21. Agarap A. Deep learning using rectified linear units (relu), 2018. DOI: 10.48550/arXiv.1803.08375.
  22. Yang X., Zhao S., Qin X., Zhao N., Liang L. Mapping of Urban Surface Water Bodies from Sentinel-2 MSI Imagery at 10 m Resolution via NDWI-Based Image Sharpening, *Remote Sensing*, 2017, No. 9 (6), P. 596. DOI: 10.3390/rs9060596.
  23. Kashtan V., Hnatushenko V., Zhir S. Information Technology Analysis of Satellite Data for Land Irrigation Monitoring, *2021 IEEE International Conference on Information and Telecommunication Technologies and Radio Electronics (UkrMiCo)*. Kyiv, Ukraine, November 29 – December 3, 2021, pp. 12–15. DOI: 10.1109/UkrMiCo52950.2021.9716592.
  24. Kashtan V., Hnatushenko V. Automated pansharpening information technology of satellite images, *Radio Electronics, Computer Science, Control*, 2021, №2 (57), pp. 123–133. DOI: 10.15588/1607-3274-2021-2-13.
  25. Sajib A., Diganta Mir T., Rahman A., Dabrowski T., Olbert A., Uddin M. Developing a novel tool for assessing the groundwater incorporating water quality index and machine learning approach, *Groundwater for Sustainable Development*, 2023, Vol. 23. DOI: 10.1016/j.gsd.2023.101049.

Received 26.12.2023.  
Accepted 31.01.2024.

УДК 004.93

## МАШИННЕ НАВЧАННЯ ДЛЯ АВТОМАТИЧНОГО ВИДІЛЕННЯ ВОДНИХ ОБ'ЄКТІВ ЗА ЗНІМКАМИ SENTINEL-2

**Каштан В. Ю.** – кан. техн. наук, доцент, доцент кафедри інформаційних технологій та комп'ютерної інженерії, Національний технічний університет «Дніпровська політехніка», Дніпро, Україна.

© Kashtan V. Yu., Hnatushenko V. V., 2024  
DOI 10.15588/1607-3274-2024-1-11



**Гнатушенко В. В.** – д-р техн. наук, професор, завідувач кафедри інформаційних технологій та комп'ютерної інженерії, Національний технічний університет «Дніпровська політехніка», Дніпро, Україна.

#### АНОТАЦІЯ

**Актуальність.** Враховуючи загострення екологічних та водних проблем, виникає необхідність у вдосконаленні автоматизованих методів визначення та моніторингу водних об'єктів у міських екосистемах. З врахуванням великого обсягу даних, отриманих від супутникових систем, проблема ефективного та автоматизованого вилучення водних об'єктів стає актуальною. Об'єктом дослідження є водні об'єкти, які автоматично виділяються з оптичних космічних знімків Sentinel-2 за допомогою методів машинного навчання.

**Мета роботи** – підвищення ефективності процесу виділення границь водних об'єктів на цифрових оптичних космічних знімках за допомогою використання методів машинного навчання.

**Метод.** Запропоновано автоматизовану інформаційну технологію виділення границь водних об'єктів на цифрових оптичних супутникових знімках Sentinel-2. Процес включає вісім етапів, починаючи з завантаження даних та використання топографічних карт для отримання базової інформації про предметну область. Після цього відбувається попередня обробка даних, включаючи калібрування зображень, видалення атмосферного шуму та підвищення контрастності. Далі застосовується архітектура EfficientNet-B0 для ідентифікації водних об'єктів, сприяючи оптимальному масштабуванню ширини мережі, глибини та роздільної здатності зображення. Використані ResNet блоки для стиснення та розширення каналів, що дозволяє оптимальне з'єднання великомасштабних та багатоканальних зв'язків у шарах. Після цього Regional Proposal Network визначає області інтересу (ROI), а ROI alignment забезпечує однорідність даних. Застосування Fully connected layer допомагає в сегментації областей, а Fully connected network створює бінарні маски для точної ідентифікації водних об'єктів. Заключним етапом методу є аналіз просторових та часових змін на зображеннях для виявлення різниць, змін та тенденцій, що можуть свідчити про конкретні явища чи події. Такий підхід дозволяє автоматизувати та точно визначити водні об'єкти на супутникових знімках з використанням машинного навчання.

**Результати.** Розроблено програмне забезпечення мовою Python, що реалізує запропонований підхід. Оцінка точності технології, проведена шляхом порівняльного аналізу з існуючими методами, такими як водні індекси та K-means, підтверджує високий рівень точності в період з 2017 по 2023 роки (досягає 98%). Коефіцієнт Каппа, який враховує ступінь узгодженості між реальною та передбачуваною класифікацією, підтверджує стабільність та достовірність нашого підходу, досягаючи значення 0.96.

**Висновки.** Проведені експерименти підтверджують ефективність запропонованої автоматизованої інформаційної технології та дозволяють рекомендувати її для використання в дослідженнях змін на прибережних територіях, прийняття рішень у сфері управління прибережними ресурсами та земельним використанням. Перспективи подальших досліджень можуть включати створення нових методів, які враховують сезонні зміни та забезпечують робастність при виділенні та картографуванні водних поверхонь.

**КЛЮЧОВІ СЛОВА:** виділення, водні об'єкти, оптичні супутникові знімки, водні індекси, машинне навчання, коефіцієнт Каппа, коефіцієнт Пірсона, матриця помилок.

#### ЛІТЕРАТУРА

1. Xiang X. Urban water resource management for sustainable environment planning using artificial intelligence techniques / X. Xiang, Q. Li, S. Khan, O. Khalaf // *Environmental Impact Assessment Review*, 2021. – Vol. 86, P. 106515. DOI: 10.1016/j.eiar.2020.106515.
2. Novel entities and technologies: Environmental benefits and risks / [R. Bierbaum, S. Leonard, D. Rejeski et al.] // *Environmental Science & Policy*. – 2020. – Vol. 105. – P. 134–143. DOI: 10.1016/j.envsci.2019.11.002.
3. Computer modeling of territory flooding in the event of an emergency at Seredniodniprovska Hydroelectric Power Plant / [D. Ivanov, V. Hnatushenko, V. Kashtan, I. Garkusha] // *Naukovyi Visnyk Natsionalnoho Hirnychoho Universytetu*. – 2022. – № 6. – P. 158–163. DOI:10.33271/nvngu/2022-6/123.
4. Mozgovoy D. Automated recognition of vegetation and water bodies on the territory of megacities in satellite images of visible and IR bands / D. Mozgovoy, V. Hnatushenko, V. Vasylyev // *ISPRS Ann. Photogramm. Remote Sens. Spatial Inf. Sci.* – 2018. – IV-3. – P. 167–172, DOI: 10.5194/isprs-annals-IV-3-167-2018.
5. Xie H. Automated Subpixel Surface Water Mapping from Heterogeneous Urban Environments Using Landsat 8 OLI Imagery / [H. Xie, X. Luo, X. Xu et al.] // *Remote Sens.* – 2016. – No. 8(7). – P. 584. DOI:10.3390/rs8070584.
6. Optical remote sensing of large-scale water pollution in Angola and DR Congo caused by the Catoca mine tailings spill / [D. Ruppen, J. Runnalls, R. Tshimanga et al.] // *International Journal of Applied Earth Observation and Geoinformation*. – 2023. – Vol. 118. – P. 103237. DOI: 10.1016/j.jag.2023.103237.
7. Shoreline Analysis and Extraction Tool (SAET): A New Tool for the Automatic Extraction of Satellite-Derived Shorelines with Subpixel Accuracy / [J. Palomar-Vázquez, J. Pardo-Pascual, J. Almonacid-Caballer, C. Cabezas-Rabadán] // *Remote Sensing*. – 2023. – No. 15(12). – P. 3198. DOI: 10.3390/rs15123198.
8. Cloud and cloud shadow detection for optical satellite imagery: Features, algorithms, validation, and prospects / [Li Zhiwei and Shen, Huanfeng and Weng, Qihao and Zhang, Yuzhuo and Dou, Peng and Zhang] // *ISPRS Journal of Photogrammetry and Remote Sensing*. – 2022. – No. 188. – P. 89–108. DOI: 10.1016/j.isprsjprs.2022.03.020.
9. A Morphological Feature-Oriented Algorithm for Extracting Impervious Surface Areas Obscured by Vegetation in Collaboration with OSM Road Networks in Urban Areas / [T. Mao, Y. Fan, S. Zhi, J. Tang] // *A Remote Sensing*. – 2022. – No. 14(10). – P. 2493. DOI: 10.3390/rs14102493.
10. Automatic River Planform Recognition Tested on Chilean Rivers / [A. Nardini, F. Salas, Z. Carrasco et al.] // *Water*. – 2023. – No. 15(14). – P. 2539. DOI: 10.3390/w15142539.
11. Estimating the relationship between dam water level and surface water area for the Danjiangkou Reservoir using Landsat remote sensing images / [Li Wenbo, Qin Ying, Sun Youqiang et al.] // *Remote Sensing Letters*. – 2016. – Vol. 7. P. 121–130. DOI: 10.1080/2150704X.2015.1117151.

12. Automated Subpixel Surface Water Mapping from Heterogeneous Urban Environments Using Landsat 8 OLI Imagery / [H. Xie, X. Luo, X. Xu et al.] // *Remote Sensing*. – 2016. – No. 8(7). – P. 584. DOI: 10.3390/rs8070584.
13. Fisher A. Comparing Landsat water index methods for automated water classification in eastern Australia // A. Fisher, N. Flood, T. Danaher // *Remote Sensing of Environment*. – 2016. – Vol. 175. – P. 167–182. DOI: 10.1016/j.rse.2015.12.055.
14. Wangchuk S. Mapping of glacial lakes using Sentinel-1 and Sentinel-2 data and a random forest classifier: Strengths and challenges / S. Wangchuk, T. Bolch // *Science of Remote Sensing*. – 2020. – Vol. 2. – P. 100008. DOI: 10.1016/j.srs.2020.100008.
15. Liu Q. Probabilistic River Water Mapping from Landsat-8 Using the Support Vector Machine Method / [Q. Liu, C. Huang, Z. Shi, S. Zhang] // *Remote Sensing*. – 2020. – No. 12(9). P. 1374. DOI: 10.3390/rs12091374.
16. Chatufale A. Extraction of Waterbody Using Object-Based Image Analysis and XGBoost / A. Chatufale, P. Abhishek // *Advanced Machine Intelligence and Signal Processing*. Singapore: Springer Nature Singapore – 2022. – P. 341–350. DOI:10.1007/978-981-19-0840-8\_25.
17. Water Body Extraction From Very High-Resolution Remote Sensing Imagery Using Deep U-Net and a Superpixel-Based Conditional Random Field Model / [W. Feng, H. Haigang, X. Weiming et al.] // *IEEE Geoscience and Remote Sensing Letters*. – 2018. – P. 1–5. DOI: 10.1109/LGRS.2018.2879492.
18. Jiang W. Multilayer Perceptron Neural Network for Surface Water Extraction in Landsat 8 OLI Satellite Images / [W. Jiang, G. He, T. Long et al.] // *Remote Sensing*. – 2018. – No. 10(5). P. 755. DOI: 10.3390/rs10050755.
19. Lu Li. Water Body Extraction from High-resolution Remote Sensing images Based on Scaling EfficientNets / Li Lu, W. Bing, W. Shichao et al.] // *Journal of Physics: Conference Series*. – 2021. – P. 1–5. DOI: 10.1088/1742-6596/1894/1/012100.
20. Position-dependent partial convolutions for supervised spatial interpolation / [H. Hachiya, K. Nagayoshi, A. Iwaki et al.] // *Machine Learning with Applications*. – 2023. – Vol. 14. DOI: 10.1016/j.mlwa.2023.100514.
21. Agarap A. Deep learning using rectified linear units (relu) / A. Agarap. – 2018. DOI: 10.48550/arXiv.1803.08375.
22. Mapping of Urban Surface Water Bodies from Sentinel-2 MSI Imagery at 10 m Resolution via NDWI-Based Image Sharpening / [X. Yang, S. Zhao, X. Qin et al.] // *Remote Sensing*. – 2017. – No. 9 (6). – P. 596. DOI: 10.3390/rs9060596.
23. Kashtan V. Information Technology Analysis of Satellite Data for Land Irrigation Monitoring / V. Kashtan, V. Hnatushenko, S. Zhir // 2021 IEEE International Conference on Information and Telecommunication Technologies and Radio Electronics (UkrMiCo), Kyiv, Ukraine, November 29 – December 3. – 2021. – P. 12–15. DOI: 10.1109/UkrMiCo52950.2021.9716592.
24. Kashtan V. Automated pansharpening information technology of satellite images / V. Kashtan, V. Hnatushenko // *Radio Electronics, Computer Science, Control*. – 2021. – №2 (57). – P. 123–133. DOI: 10.15588/1607-3274-2021-2-13.
25. Sajib A. Developing a novel tool for assessing the groundwater incorporating water quality index and machine learning approach / [A. Sajib, Mir T. Diganta, A. Rahman et al.], // *Groundwater for Sustainable Development*. – 2023. – Vol. 23. DOI: 10.1016/j.gsd.2023.101049.